Title
Analysis of organic molecules using the Mars Organic Analyzer, a portable, automated microfabricated capillary electrophoresis instrument

Author
Stockton, Amanda Michelle

Publication Date
2010

Peer reviewed|Thesis/dissertation

Analysis of organic molecules using the Mars Organic Analyzer, a portable, automated microfabricated capillary electrophoresis instrument

by

Amanda M. Stockton

A dissertation submitted in partial satisfaction of the

requirements for the degree of

Doctor of Philosophy

in

Chemistry

in the

GRADUATE DIVISION

of the

UNIVERSITY OF CALIFORNIA, BERKELEY

Committee in charge:

Professor Richard A. Mathies, Chair

Professor Evan R. Williams

Professor Ronald Amundson

Fall 2010

Analysis of organic molecules using the Mars Organic Analyzer, a portable, automated microfabricated capillary electrophoresis instrument

by

Amanda M. Stockton

Abstract

Analysis of organic molecules using the Mars Organic Analyzer, a portable, automated microfabricated capillary electrophoresis instrument

by

Amanda M. Stockton
Doctor of Philosophy in Chemistry
University of California, Berkeley
Professor Richard A. Mathies, Chair

The search for signs of past or present extraterrestrial life requires autonomous instrumentation capable of robust and highly sensitive *in situ* analysis of a broad range of organic compound classes. The Mars Organic Analyzer (MOA) is a portable microchip capillary electrophoresis (μCE) instrument developed for highly sensitive chemical biomarker analysis. This thesis expands the capabilities of the MOA to highly-sensitive analysis of PAHs, aldehydes, ketones, and carboxylic acids in conventional and extremely acidic and saline samples, and demonstrates proof-of-principle for using programmable valve arrays for autonomous sample processing.

A μCE separation and analysis method for PAHs is optimized, resulting in baseline separation of a nine-PAH standard with limits of detection (LODs) ranging from 2000 ppm to 6 ppb. Analysis of an environmental contamination standard from Lake Erie and a hydrothermal vent chimney sample agree with published composition; analysis of a Martian analogue sample from the Yungay Hills (Atacama Desert) is found to contain several PAHs at ppm levels.

Pacific Blue succinimidyl ester is used as an improved fluorescent label for amines and amino acids enabling sub-pptr LODs, and a micellar electrokinetic chromatography (MEKC) method is developed for enhanced compositional analysis. These methods are applied to the analysis of samples from the Murchison meteorite and the Yungay hills (Atacama Desert).

Previous MOA analysis methods suffer from artificially low signal and resolution when samples are acidic, saline, or contain polyvalent cations. To address this challenge, new analysis, labeling, and dilution buffers are developed. Higher ionic strength buffer systems provide better buffering capacity and salt tolerance, and addition of ethylamine-diaminetetraacetic (EDTA) acid effectively neutralizes deleterious effects of multivalent cations. These optimized methods enable analysis of amino acids in a brine sample from Saline Valley, California, and a subcritical water extract of a highly acidic sample from the Rio Tinto, Spain.

MOA analysis methods for oxidized organic carbon are developed and optimized using the fluorescent probe Cascade Blue hydrazide (CB). Hydrazone formation of CB with aldehydes and ketones requires pH 5-6, CB-labeling of 1-ethyl-3[3-dimethylaminopropyl]carbodiimide (EDC) activated carboxylic acids is optimized to pH 3, and separations are optimized at pH 9.5, 20 ^{o}C. Standards developed based on oxidized organics detected in the Murchison meteorite are analyzed, with pM - nM LODs. Aldehyde and ketone analyses are validated via the analysis of several fermented beverages and a basaltic Martian simulant sample. Several polycarboxylic derivatives of benzene, including mellitic acid, are analyzed, demonstrating the first analysis of these highly oxidized molecules on a portable instrument. Successful analyses of carboxylic acids in a lava tube cave sample (Mojave Desert, CA) and a Bumpass Hell hydrothermal area sample (Lassen National Park) demonstrate the utility and versatility of this method.

Finally, an autonomous sample processing system based on the programmable microfluidic rectilinear array Automaton is demonstrated at a proof-of-concept level. Prospects for further development of this sample processing system are considered, as are further enhancements of the total analysis system. The methods developed here are also critically compared to other proposed *in situ* life detection instruments.

For my parents,

Keith and Valerie,

my sister Madison,

and in loving memory

of my brother Jacob

Table of Contents

List of Figures

List of Tables

List of Schemes

Acknowledgements

While this thesis is due, in the largest possible part, to the help, guidance, and support of the people in the Mathies lab at the University of California, Berkeley, many others have helped me on this path. For this reason, I will acknowledge those in educational institutions in chronological order, followed by personal acknowledgements.

My first words of thanks go to my seventh grade English teacher, Mrs. Wheeler-Oakey, who, despite having her leg broken while serving jury duty during the April 19th Oklahoma City bombing, continued to pour energy and devotion into our class. You asked us to research where we would be ten years from our class together; that assignment caused me to research exactly how I would reach my goal of getting to Mars. While the path deviated somewhat (I haven't exactly revolutionized the propulsion field yet), I have managed to hit the major points. Thank you for that assignment. I also thank Mr. Russell, my seventh grade math teacher, for believing in me early on, and encouraging me throughout the rest of my high school years. Without your guidance and support I could not have been nearly as successful.

Next, I thank my teachers at the Oklahoma School of Science and Mathematics. Dr. Charles Roberts gave me the stick of knowledge to beat back the bear of chemistry. You trained me well as one of your warriors, and I thank you for all the work you put into me (and asked me to do) to get to the 2000 Rho National Chemistry Olympiad training camp. Without you, I might have never discovered my love for chemistry, and I would be on a very different path today. Dr. Fahzlur Raman, I thank you for your insight on charming the chemistry snake, and I thank you for getting me my first real research position in chemical synthesis. I thank you both for the insightful and memorable chemistry quotes, analogies, and extremely nerdy chemistry jokes. Your teaching styles have also been extremely helpful, and I've received teaching awards for only partially applying them to classes I have assisted in teaching. I also thank Dr. Dorothy Dodd for telling me that I couldn't make it at MIT, I don't know how you reach the right balance of encouragement and cajoling individually with each student, but it works.

At MIT, I thank Har Gobind Khorana for the opportunity to conduct synthesis under your guidance as a freshman, and I apologize for never getting a high vacuum pump working well enough to successfully distill my final product. I thank all the professors of Aerospace Engineering, primarily for the education but also for the entertainment and compassion. I thank Prof. Richard Shrock for advising me, Prof. Dan Nocera for making inorganic chemistry fun, and Prof. Timothy Swager for teaching organic chemistry in a way that made sense to me, even if no one else got it.

I profusely thank Prof. Christopher Seto at Brown University for the encouragement and positive feedback during my deviation into synthetic organic chemistry. Thank you for giving me projects that took advantage of my engineering background instead of pure synthesis, and for your understanding when I finally remembered that synthetic organic chemistry, while a pleasant diversion, was not my primary goal in life. I thank all the people at Brown for restoring my confidence and helping me get where I am today.

Thank you, Prof. Richard Mathies, for taking me on as a graduate student and letting me work on the Mars project. Thank you for hiring Dr. Thomas Chiesl, who was just the mentor I needed that first painful year when I was struggling with the analysis of PAHs. Thank you for the constructive criticism and for always helping me see how I could do things better. You made the words "Good job," something to strive for, and truly meaningful when I get to hear them.

Thank you for pushing me to be my best. Your management style has been perfect for me, and I fully appreciate it. I could not have asked for a better PhD advisor.

To the entire Mars team, I thank you all. I thank Dr. Thomas Chiesl for his sense of humor, his mentorship, and all the support and cajoling over the years. I can directly attribute my survival of the first year in the Mathies lab to your assistance, and I thank you for your continued advice and mentorship throughout the rest of my graduate career at UC Berkeley. I could not have done it without you, and I wish you well in your new career. Dr. Merwan Benhabib built the Multichannel Mars Organic Analyzer, which Prof. Mathies is letting me take to JPL, thank you. Also, thank for learning "your mom" jokes and providing comedic relief that has lasted into the year since you've graduated. I also thank Dr. Alison Skelley, who I had the misfortune of never really getting to know, for building the MOA technology this thesis is based upon and Dr. James Sherer for building the MOA instrument and teaching me how to align it.

Erik Jensen came up with the idea to combine MOA and Automaton technology as an honorary Mars team member. Thank you for reading drafts of this thesis numerous times, and for patiently taking my frantic phone calls when I started forgetting to turn the pump or distillation off in my scatterbrained state near the end. Eric Chu made many chips used in this thesis; for that I am eternally grateful. Mary Hammond has been amazing throughout the entire graduate process, and I'm not sure how I (or anyone else in the Mathies lab, for that matter) would survive without her. Other people I should mention for their help directly with this thesis, and I apologize for not going into more detail about you, include Samantha Cronier, Nadia del Bueno, and Jungkyu Kim. The rest of the Mathies lab people, past and present, also deserve my thanks for making the Mathies lab experience enjoyable and rewarding.

The people on the Urey project have been immensely helpful through conversations and suggestions, including Dr. Frank Grunthaner, Dr. Frank Greer, Dr. Anita Fischer, Dr. Xenia Amashukeli, Dr. Pascale Ehrenfreund, Prof. Jeff Bada, Dr. Andrew Aubrey, Dr. Daniel Glavin, Prof. Ronald Amundson, and Dr. Peter Willis. Dr. Peter Willis also helped guide me through the NASA Postdoctoral Program proposal process, and I am looking forward to joining Team Willis at the Jet Propulsion Labs soon.

Finally, I thank my family, who have put up with and supported me my entire life. My parents are the best parents a kid could ask for. Mom, thank you for supporting my crazy science experiments, even when they went moldy and stank up the house. Dad, thank you for teaching me what instruction manuals are for and that its normal to have leftover screws when you finish putting something back together. Thank you both for always being just a phone call away when I've needed advice, whether a recipe for egg pie or just exactly how to replace a lower intake manifold gasket. Thank you for adopting Madison; Madison, you are the best sister ever and I'm so lucky you're mine. Thank you for sharing my love of science and for doing science experiments with me. I look forward to seeing where your future will take you. Tim, thank you for being my rock through thick and thin, for not minding that we've been eating frozen dinners, and for cooking those frozen dinners (sorry). I look forward to the next chapter of our lives out in the "real world" where I hear they have these things called "evenings" and "weekends." I can't wait to find out what those are!

Chapter 1 : The Search for Extraterrestrial Life:

What to look for, how to look for it,

and how to make sure you see it if it is there!

1.1 The Search for Life on Mars: Motivation and History

"The Universe must be bio-friendly, since we sentient beings have succeeded in arising within its confines and insist on writing books about it."

- Woodruff T. Sullivan III and John A. Baross, in *Planets and Life*, 2007

Early speculation regarding the prospect of life elsewhere in the Universe centered on our two nearest neighboring planets: Mars and Venus. Astronomers observed "canali" on Mars and interpreted them as canals engineered to bring meltwater from the poles to dry equatorial fields.[1] The clouds surrounding Venus were depicted in science fiction in the 1940s and 1950s as hiding a hot tropical jungle.[2-3] These notions were eventually abandoned when Mariner 2 measured Venusian surface temperatures in excess of 490 K,[4] and Mariner 4 imaged a bleak Martian surface in 1965.[5] While both planets may have been transiently habitable in the past, Mars is the more attractive astrobiological target for many reasons. According to planetary models, Venus was capable of supporting life several billion years ago,[6] but evidence of past life would have been destroyed during global resurfacing events approximately 300 million years ago.[7] Additionally, Venusian conditions (93 bar and >490 K) present significant engineering challenges for analytical instrumentation. However, if once prevalent on Mars, life may have been able to adapt to its loss of atmosphere and magnetic shielding (which protects the terrestrial surface from solar ionizing radiation) by adaptations similar to those used by extremophiles found on Earth (*e.g.* in the dry Antarctic deserts). For example, it has been suggested that Martian bacteria may have employed strategies such as moving deeper underground and subsisting on a monolayer of liquid water at a ice-rock interface.[1]

A summary of Martian exploration with astrobiologically significant results is given in Table 1.1. The most astrobiologically relevant results from these missions and the two most exciting missions to date, the Viking landers of 1976 and the Phoenix lander of 2009, will be discussed here. The two identical Viking 1 and Viking 2 landers, which descended to the western Chryse Planitia and Utopia Planitia, respectively, were equipped with a suite of three life detection experiments complemented by a gas chromatagraph - mass spectrometer (GCMS) using pyrolytic sample extraction. Viking returned valuable information on atmospheric conditions, mineralogy, and surface photographs, and the life detection and GC-MS experiments yielded astrobiologically relevant, but ambiguous, results regarding detection of chemical signs of Martian life.

The three life detection experiments, summarized in Table 1.2, consisted of the Gas Exchange (GEX) experiment, the Labeled Release (LR) experiment, and the Pyrolytic Release (PR) experiment. All three experiments used heat-sterilized Martian samples as controls under the assumption that heating the sample to 145-160 ^{o}C would kill any native biota and control for abiotic native regolith chemistry. Each experiment operated as intended, but gave the unexpected results summarized in Table 1.2. The experiments tested different hypotheses about Martian life but all experiments were performed at elevated temperatures and pressures compared to native Mars, which could have inhibited activity from biota evolutionarily acclimated to Martian temperatures and pressures. The GEX returned results definitively negative for life, and the PR returned initially promising results that turned negative upon further

Table 1.1 Summary of Martian Missions and their Astrobiological Significance

Name	Year Launched	Type of Mission	Astrobiologically Significant Results
Mariner 4	1964	Flyby	"Lunar" landscape at km resolution[8] Magnetic field < 1/1000 of Earth's[8] Atmospheric estimates: 5-6 mbar, ~ ½ CO_2[8]
Mariner 6 & 7	1969	Flyby	Polar solid CO_2, potentially surface hydrates[9] Past volcanism,[10] temperatures 250-275 K[11]
Mariner 9	1971	Orbiter	Images of dry riverbeds; complete mapping, discovered Olympus Mons and Tharsis bulge
Mars 5	1973	Orbiter	Max and min T 272, 200 K, higher H_2O vapor level south of Tharsis
Viking 1 & 2	1975	Orbiter Lander	Ambiguous life detection experiments,[12-16] no organics by pyrolysis-GC-MS[17-18]
Phobos 2	1988	Orbiter	
Mars Pathfinder	1996	Lander	Regolith minerals contain metal oxides[19]
Mars Global Surveyor	1997	Orbiter	Gullies formed by liquid water, potentially water glaciers in craters
Mars Odyssey	2001	Orbiter	Indicated water ice at northern pole
Mars Exploration Rovers (Opportunity and Spirit)	2003	Rover	Jarosite (formed in liquid water), potentially acidic and saline regolith[20-21]
Mars Express	2003	Orbiter	
Mars Reconnaissance Orbiter	2005	Orbiter	
Phoenix	2007	Lander	Direct observance of water ice,[22] detection of the oxidant perchlorate[23]

Table 1.2 Summary of Life Detection Experiments on the Viking Landers

Experiment	Assumption	Experimental Description	Summary of Results	Indicates biology?
Gas Exchange (GEX) – humid non-nutrient mode	Limiting factor to Martian metabolism is lack of H_2O[12]	Incubation at 8-15 ^oC for ~ 7 days under Martian atm enriched with CO_2, Kr, He to 200 mbar and H_2O vapor to saturation[15]	Some desorption of gasses and generation of O_2 not inhibited by heating to 145 ^oC[15]	No[12,15]
Gas Exchange (GEX) – wet nutrient mode	Martian life is heterotrophic and metabolizes a concentrated nutrient rich in complex organics and minerals[12]	Same as humid non-nutrient mode, but wetted sample with a concentrated aqueous nutrient solution[15]	Some desorption of gasses and generation of O_2 not inhibited by heating to 145 ^oC[15]	No[12,15]
Pyrolytic Release (PR)	Martian metabolism best detected under native conditions[12]	Exposed sample to light and a ^{14}C-labeled CO and CO_2 Martian analogue atmosphere, incubated several days. Heated to 650 ^oC and measured evolved gas for ^{14}C incorporation.[13]	Incorporation of ^{14}C that was inhibited 90% by heat sterilization at 175 ^oC for 3 hr, but no inhibition after 2 hrs at 90 ^oC[13]	No, based on 90 ^oC heat steriliz-ation.[12-13]
Labeled Release (LR)	Martian life is heterotrophic and metabolizes a dilute nutrient mixture of simple organics[12]	Wetted sample with dilute aqueous ^{14}C-labeled nutrient solution with simple organics generated by Urey-Miller experiment, measured evolved gas for ^{14}C incorporation[14]	Incoporation of ^{14}C that was abolished by heating to 160 ^oC for 3 hrs and severely diminished by heating to 50 ^oC for three hours[14]	Possibly[12,14]

experimentation. The LR repeatedly returned results consistent with biotic metabolism. The GC-MS, surprisingly, detected no organic molecules native to Mars, but did detect terrestrial contaminants (solvents used to clean the instrument) present in the blank analysis, indicating an actual lack of detection of Martian organics as opposed to instrument failure.[18] This, taken in conjunction with the null results for life returned by the GEX and the PR, were enough to override the LR possible-positive result for most scientists (although some continue to interpret the LR positive result as biotic[24-25]).

To explain the contradictory and ambiguous results of the life detection experiments and the GC-MS, many have postulated that the Martian regolith contains a strong oxidant.[26] The GC-MS results could also be explained by an oxidative conversion of native organics to highly oxidized organic acids and CO_2, which would either be invisible to the GC-MS by adhering strongly to the regolith until decomposition during pyrolysis, or by adhering to the GC column and therefore not eluting into the MS detector.[26] While the strong oxidant theory is widely accepted, the (aqueously insoluble) chemical oxidant would need to be stable for days at 18-50 ^{o}C and decompose (within several minutes) partially at 50 ^{o}C and fully by 145 ^{o}C. Studies that attempt to chemically mimic the results of the biological suite in the laboratory have been unable to duplicate the Martian result with known oxidants.[25,27] The Viking experiments, therefore, rather than answering our questions about Martian life and the fate of Martian organic molecules, simply pose new questions and indicate the need for further Martian exploration to search for organic molecules and to understand possible oxidants.

In 1997, the Pathfinder rover Sojourner characterized Martian soil and rocks using X-ray fluorescence[19] and identified and quantified a range of minerals in the regolith, including MgO (8%), CaO (7%), and FeO (17%). In 2004, the Mars Exploration Rover Opportunity discovered jarosite (K, Na)$Fe_3(SO_4)_2(OH)_6$[20] and other minerals known to be formed only by aqueous processes, indicating that surface water or near-surface ground water were once present.[21] The strong acidity and salinity of the ancient ground waters suggested by Opportunity's data does not preclude the potential of extinct life. For example, terrestrial extremophilic organisms thrive in environments ranging from the hypersaline (3-5 M NaCl),[1,28] to the highly acidic (pH < 2),[1,28-29] to the extremely cold (-17 ^{o}C).[29]

Recently, the Phoenix lander explored the Martian polar regolith for chemical oxidants, salts, and water. Phoenix landed within the Martian arctic circle on May 25th, 2009. The light detection and ranging (LIDAR) instrument on the lander observed water-ice clouds and evidence of water ice precipitation.[30] It also detected calcium carbonate in the range of 3-5 weight percent, amounts large enough to indicate an aqueous formation and supporting a history of liquid water on Mars.[31] At the landing site, Phoenix uncovered a shallow (5-18 cm deep) ice table,[22] which was confirmed to be water ice by the Thermal Evolved Gas Analyzer (TEGA).[22] Phoenix also carried a wet chemistry laboratory (WCL) as part of its Microscopy, Electrochemistry, and Conductivity Analyzer (MECA) package. The WCL worked by thawing an aqueous calibration / leaching solution in an analysis beaker lined with ion-selective electrodes (ISEs). Approximately 500 mg of Martian regolith was then added to the analysis beaker, and the ISEs measured soluble ions in the regolith sample. The WCL detected a pH of 7.6-7.7 with a relatively high concentration (~10 mM total) of several ions, including Na^+, K^+, Ca^{2+}, Mg^{2+}, Cl^-, and 0.4-0.6 % perchlorate (ClO_4^-) by weight.[23] The presence of the oxidant perchlorate is extremely interesting in light of the Viking results. However, perchlorate is not a

strong enough oxidant to fully account for the Viking results, and may have actually been formed via oxidation by the same oxidant that yielded the ambiguous Viking data.[23] Like the Viking landers, Phoenix furthered our knowledge of Mars, but left questions about the viability of Martian life, past or present, - the fate of organic molecules on the Martian surface has yet to be resolved.

1.2 The Rest of the Solar System: Promising Targets for Extraterrestrial Chemical Exploration

There is some contention about the prevalence of Earth-like planets in the galaxy. Some, such as Marcy *et al.*[32] predict that water-rich small-mass rocky planets within the habitable zone of Sol-like stars are common. Others have postulated that conditions similar to those found on Earth may be rare in the galaxy, experienced only transiently by planets in the habitable zone, such as Earth, or near it, such as Venus and Mars.[1] However, there are many small icy satellites orbiting Saturn and Jupiter that may be capable of sustaining some forms of life, which potentially makes them the most common ecosystem in the solar system, if not the galaxy. The moons of Saturn and Jupiter range from the larger-than-Mercury water-ice Ganymede to the small and extremely volcanic Io. Of these moons, a few have recently become popular for astrobiological speculation and future exploration, particularly Europa and the two moons studied by the Cassini-Huygens mission: Titan and Enceladus. Icy moons may also be analogues for the early Earth according to the "Snowball Earth" model, which puts the average terran temperature at only ~ 237 K when life first emerged 4 billion years ago.

Europa, the second Gallilean moon of Jupiter, was perhaps the first moon to fall under intense astrobiological speculation. Voyager images showed an absence both of very dark terrain and of significant topographical relief, indicating a covering of water ice of at least several km, which, with enough warming from the moon's core, will undergo viscous relaxation, deforming and flattening on geological timescales.[33] Based on models of its interior, it is suspected that a liquid water ocean ~100 km deep exists beneath a 20 km thick water ice crust.[34] Photographs of the surface of Europa taken by Galileo provide strong evidence for cryovolcanism on Europa, which strengthens the model-based evidence for liquid water beneath the ice crust.[35] While no organics have been detected on Europa, near-IR spectroscopy has detected sulfur dioxide (SO_2), hydrogen peroxide (H_2O_2), and hydrated salts containing predominantly magnesium, sodium, and sulfate.[36-37] Europa's ocean probably lies over a silicate/metal core,[38] which may be able to drive hydrothermal ecosystems similar to those proposed as the origin of terrestrial life beneath Earth's oceans.[39]

Enceladus, the sixth largest moon of Saturn, is also covered with water ice. Like Europa, it is a differentiated satellite with a water ice crust, liquid water subsurface ocean, and a silicate/metal core.[40] Voyager 1 found that Enceladus orbited within the densest part of Saturn's E-ring, indicating a potential common source of the two.[41] Cryovolcanism, which was merely suggested by Voyager and Enceladus's proximity to the E-ring, was spectacularly confirmed by Cassini's imaging and analysis of a massive geyser system shooting water vapor from Enceladus into space, forming the E-ring.[42] Cassini measured significant amounts of CO_2 in the water vapor plume which may be indicative of subsurface chemistry rich in carbonic acid.[42] The high levels of CO_2 may also suggest the possibility of organic chemistry within Enceladus's ocean.[42]

Titan, the largest moon of Saturn, is the only satellite in the system known to have a significant atmosphere. Titan has a meteorogical methane cycle similar to our hydrological cycle, including cloud formation and precipitation, producing its reddish hue.[43] Titan's surface is home to a large distribution of 10-10,000 km^2 lakes of liquid hydrocarbons.[44] Like other nearby icy moons, Titan's crust is also largely water ice, enriched with ammonia, and it is also suspected of having subsurface liquid water and a silicate/metal core.[45] This subsurface liquid water ocean could drive cryovolcanism, which could serve as a surface energy source for biotic chemistries.[45] While Titan's surface may not be a likely target in the search for Earth-like life, its unique surface hydrocarbon chemistry makes it a highly intriguing target for extraterrestrial chemical exploration.

1.3 Organic Molecular Targets for Extraterrestrial Exploration: Polycyclic Aromatic Hydrocarbons, Amino Acids, Ketones, Aldehydes, and Carboxylic Acids

Terrestrial molecules essential for life that have been considered as targets for extraterrestrial exploration include DNA, RNA, proteins, their component molecules (nucleotides, nucleobases, and amino acids), and lipids. However, since extraterrestrial life may not have the same structural and functional chemical structures, our first search for extraterrestrial biomarkers must include a broader range of organic molecules. Instead of looking for specific biomolecules, McKay has suggested searching for patterns in the concentrations of small molecules that are inconsistent with an abiological origin (Figure 1.1A).[46] Abiotic organic synthetic processes produce a broad set of possible organic molecules, with concentrations defined statistically by the synthetic pathway. Biotic processes tend to select a smaller subset of the organic molecules available, and selectively enrich the concentrations of these useful molecules, while destroying the less-useful abiotically produced molecules in the process. Therefore, this thesis focuses the development of analytical methods for a number of molecule classes that provide information about the organic chemistry of a planet, whether abiotic, extant biotic, or extinct biotic.

Polycyclic aromatic hydrocarbons (PAHs, Figure 1.1B) are ubiquitous in space, and have been found in carbonaceous chondrite meteorites,[47] Martian meteorites,[48-50] and interplanetary dust particles,[51] in addition to being observed in interstellar matter.[52] They are particularly enriched in carbonaceous chondrite meteorites; for example, the Murchison meteorite contains PAHs at 330 ppm.[53] Their ubiquity can be attributed to their resonance-based stability towards ionizing radiation and oxidative damage.[54] Terrestrial PAHs are often found in natural geological sources including volcanic ash, hydrothermal vents,[55] and coal deposits,[56] and from many anthropic sources including cigarette smoke[57] and auto exhaust.[58] Three-dimensional distributions of PAHs similar to biotic structures have also been used as evidence of fossilized organisms, for example, in studies of the Martian meteorite ALH 84001.[50] Since PAHs permeate the solar system, and because organic matter is delivered via impact events to the surface of other solar system bodies (organic infall on Mars ~ 10^5 kg / yr),[59] PAHs should be included in any comprehensive examination of the organic chemistry on an extraterrestrial body.

In the search for life, amino acids (Figure 1.1C) may be the most attractive target, as their composition and chirality can indicate whether the chemistry observed is abiotic, recently extant biotic, or extinct biotic. Terrestrial organisms use amino acids to make enzymes and proteins with sequences determined by genetic DNA. On Earth, amino acids have been biologically limited to a set of 20 common amino acids.[60] While other amino acids are produced abiotically

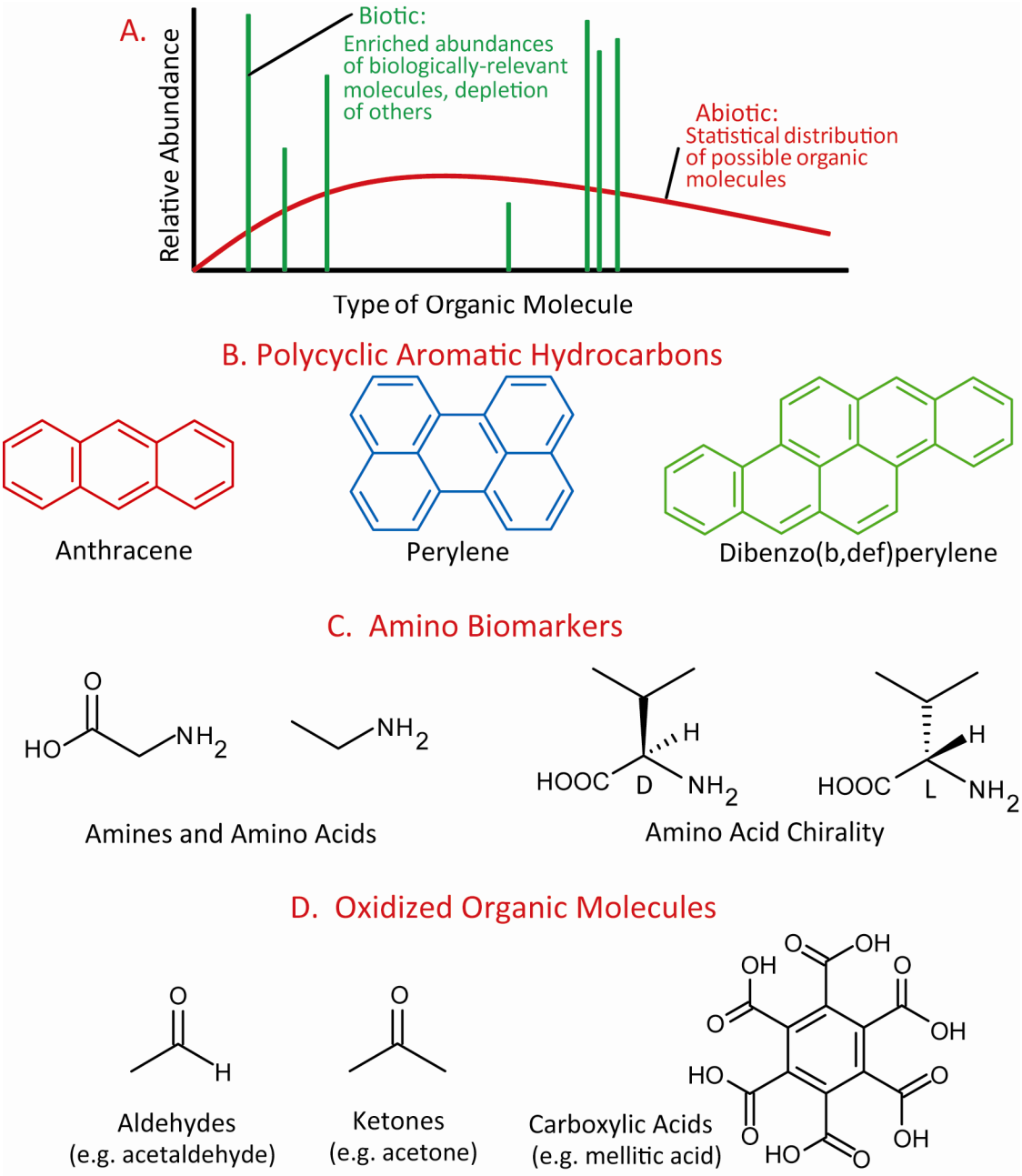

Figure 1.1. Target molecules for extraterrestrial exploration.

(A) Expected distributions of organic molecules of biotic and abiotic origins.[46] (B) Representative PAHs with spectral properties that can be detected by the MOA's 405 nm detection system. (C) Amino-based biomarker amino acids and a depiction of their chirality. (D) Representative oxidized organic molecules, including mellitic acid, which Benner has suggested is the only organic molecule likely to be found on Mars.[26]

and for specific biotic purposes, terrestrial life has depleted other amino acids by focusing on the synthesis of the main 20. Therefore, a statistical distribution of all possible amino acids would indicate an abiotic origin, while a limited subset of amino acids (either common to Earth's subset or unique) significantly enriched over other amino acids would indicate a biotic origin.[46,60]

Homochirality is also a strong indicator of biotic origin. While abiotic chemical reactions produce racemic mixtures of amino acids, biotic processes on Earth produce only homochiral L amino acids. Homochirality of amino acids is important for preservation of the secondary structures of proteins; one D amino acid can significantly alter the structure of an enzyme and render it inactive.[61] While homochirality is an indicator of recently extant life, the slow racemization of amino acids yields a mixture enriched in the biotically-relevant enantiomer. A partial enantiomeric excess (ee) therefore not only indicates an extinct biosphere, but also the age of extinction. Based on continuously dry conditions at temperatures < 250 K, it is expected that a homochiral amino acid sample on Mars would racemize in > 10^{10} years. Since the solar system is only ~ 4.6 x 10^9 years old, if life ever existed on Mars, its homochiral signature should still be present. It has been shown that circularly polarized UV light selectively degrades one amino acid enantiomer over another,[62] and the polarized light we are exposed to in our part of the galaxy is selective for enriching the L enantiomer.[62] Consistent with these facts, mild ees have been found in abiotic alpha-methyl amino acids in the Murchison meteorite.[63] However, these ees are small (5-10%, nearly racemic; terrestrial ee ~100%),[63] and thus any more significant enantiomeric excess can be attributed to biotic processes.

Based on the oxidizing environment suggested by the Viking landers' life detection[14-15] and GC-MS experiments[18] and Phoenix's discovery of Martian perchlorate,[23] a complete survey of organic carbon on Mars must include oxidized compound classes, including aldehydes, ketones, and carboxylic acids (Figure 1.1D). Aldehydes and ketones are partially oxidized organic molecules, and therefore provide information on oxidative processes. This compound class is also represented in space; for example, formaldehyde,[64] propanal, propenal, and propynal[65] have been observed in interstellar matter.

However, if Benner's hypothesis[26] that most organic carbon has been fully oxidized to CO_2 leaving only relatively stable highly oxidized aromatic acids (e.g. mellitic acid) behind is correct, then a survey of Mars must include the capability to analyze these highly oxidized forms of organic carbon. Without the capability to sensitively detect and analyze carboxylic acids, *in situ* chemical analysis experiments may return no viable information on organic chemistry of the Martian surface.

1.4 Fluorescence Detection of Organic Molecular Targets: Labeling Chemistries

The discovery and analysis of the compound classes in Figure 1.1 in extraterrestrial locations will require an extremely sensitive detection method to return any valuable information. Fluorescence is a widely used detection method, particularly for low-pathlength applications, including capillary electrophoresis, due to the ultra-high sensitivity (~pptr) achievable. In order for a chemical species to exhibit fluorescence, it must not only have strong absorbance at the excitation wavelength, but also a relatively long-lifetime excited state with good dipole coupling back to the ground state. For the organic molecules considered in this thesis, these conditions are met only by molecules with extended π systems. Target compound classes that do not have extended π systems or absorbance at the desired excitation wavelength

require chemical derivitization with an appropriate labeling dye. Target analytes are therefore first divided based on whether they are naturally fluorescent, and if not, then by their reactivity with fluorescent dye labels.

Polycyclic aromatic hydrocarbons (PAHs), due to their extended π systems, exhibit natural fluorescence. PAHs have unique absorbance and fluorescence spectra dependent upon their size and structure. The fluorescence spectra of a PAH can therefore be used as an additional degree of species identification during electrophoretic separation on the Mars Organic Analyzer (MOA, Section 1.9) used in this thesis. While all PAHs have significant absorbance in the deep UV, only larger PAHs (3+ rings) have any significant absorbance at the 405 nm excitation wavelength of the MOA. Figure 1.2 shows the absorbance and fluorescence spectra of perylene, a representative PAH detectable by the MOA.

Amines and amino acids are classified together because the amino terminus is the most accessible functional group for derivitization. This is due to the vast array of commercially available amine-reactive fluorescent probes and because the amino group can be targeted directly with no activation. The most common classes of amine-reactive dyes are isothiocyanates, such as FITC, fluorogenic dyes, such as fluorescamine, and activated esters, such as Pacific Blue succinimidyl ester (Figure 1.2). Therefore, in addition to excitation wavelength and quantum yield considerations, labeling dyes are selected for desirable reaction conditions, stability of the dye and labeled amines, and the electrophoretic mobility of fluorescent unreacted dye or fluorescent by-products of reaction with amines or water. FITC labeling of amino acids was first explored for μCE analysis with 488 nm excitation, but the labeling reaction was slow (> 8 hrs) and it was abandoned in favor of fluorescamine labeling.[66] Fluorescamine, a fluorogenic dye that requires 405 nm excitation, has the benefit that there are no unreacted or hydrolyzed dye peaks in the electropherograms.[67] Since only fluorescamine-amine adducts are fluorescent, the bulk solution can be fluorescently screened for the presence of amino analytes prior to μCE analysis, which was desirable in an early proposed version of the Urey instrument package.[68] However, both fluorescamine dye and fluorescamine-labeled amino acids hydrolyze rapidly, and fluorescamine is insoluble in water without an organic co-solvent, which is problematic for use in space-flight applications. Recent developments have used Pacific Blue succinimidyl ester for high quantum yield amino acid labeling with pptr sensitivity.[69] The unreacted and hydrolyzed Pacific Blue molecules have mobilities that differ from the majority of amine and amino acid targets, and thus serve as internal standard peaks confirming the reaction of Pacific Blue and the separation quality.[69]

Ketones and aldehydes can react in aqueous solution with primary amino compounds. In reaction with primary amines, a relatively unstable Schiff base results. Hydrazones, which are formed by the reaction of a carbonyl group with a hydrazide (i.e. Cascade Blue hydrazide), are more stable.[70] Both hydrazones and Schiff bases can be reduced in aqueous solution with sodium borohydride or sodium cyanoborohydride to more stable secondary amines. Both these reducing reagents also reduce aldehydes and ketones, so their utility in producing signal gains must be determined experimentally under the desired conditions.

Carboxylic acids have limited aqueous reactivity. Most conversions used in synthetic organic chemistry, such as conversion to the acid chloride, anhydride, or most active esters, require organic solvents and purification steps. In peptide synthesis, acids are converted to the

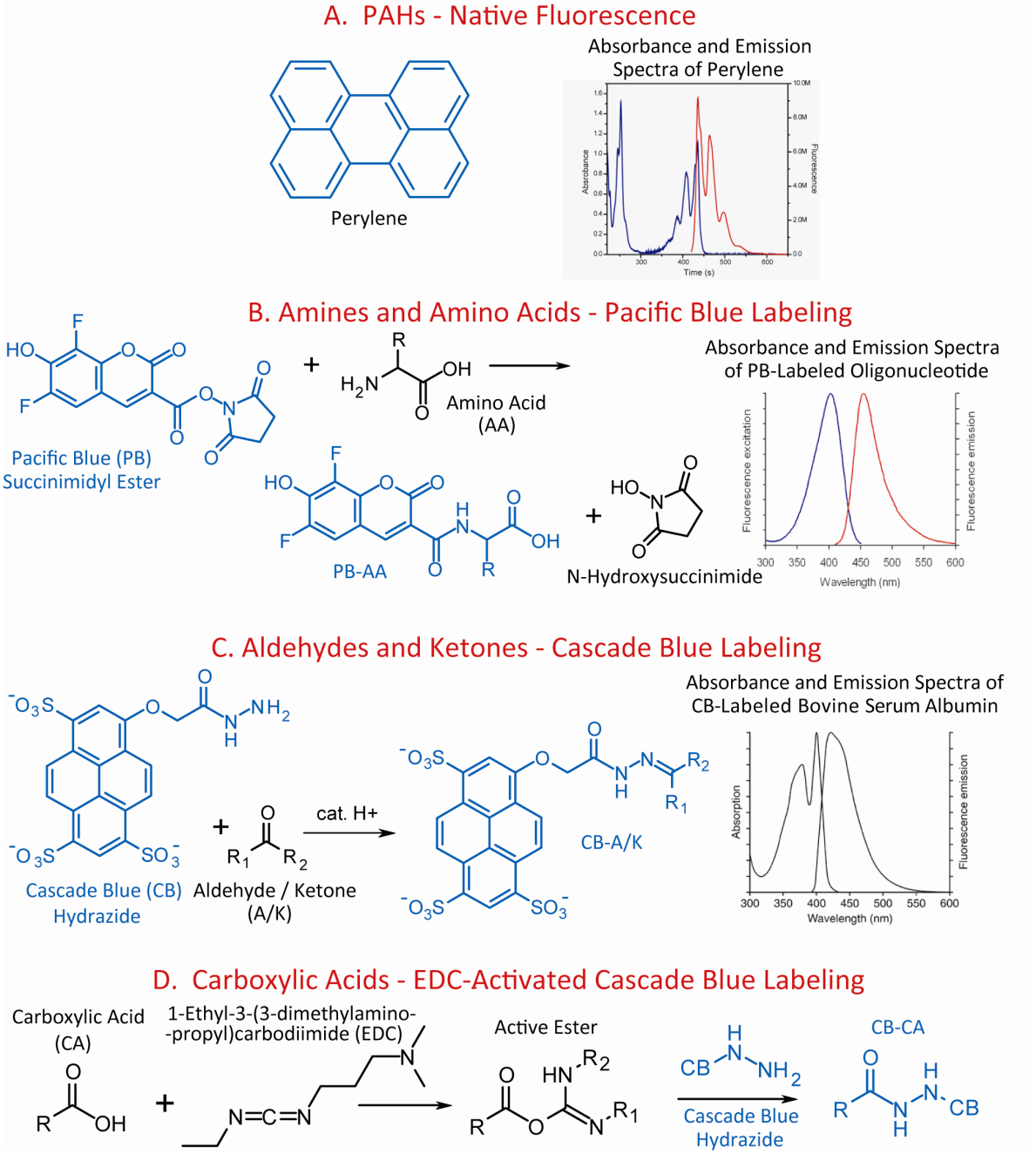

Figure 1.2. Labeling chemistry and spectra of fluorescent derivatives of target molecules.

A) PAHs are naturally fluorescent and require no derivitization, as shown for the representative PAH perylene. (B) Amines are labeled with Pacific Blue succinimidyl ester. Oxidized forms of carbon are labeled with Cascade Blue hydrazide: (C) aldehydes and ketones converted to hydrazones, and (D) acids to hydrazide ester via an active ester. The fluorescent moiety is indicated in blue.

active ester *in situ*, but the conventional triazole-based coupling reagents are only soluble and active in polar non-protic organic solvents. Water soluble carbodiimides, however, are commercially available and can be used for aqueous coupling of amines to acids (Figure 1.2).

1.5 Capillary Electrophoresis

Traditional methods of detecting and analyzing the target compound classes outlined above include high performance liquid chromatography (HPLC), gas chromatography – mass spectrometry (GC-MS), nuclear magnetic resonance spectroscopy (NMR), infrared spectroscopy, capillary electrophoresis, etc. However, most of these methods are not currently suitable for space flight. While advances have been made in miniaturizing HPLC,[71-72] the method still requires a packed column (which may settle or otherwise deform during typical mission operations such as packaging, launch, or flight) and high pressures. Standard HPLC also requires 10-100s mL of solvent; miniaturized HPLC requires much less (1-10 mL), but HPLC systems usually require at least one organic solvent. Advancements are also being made to miniaturize NMR instruments,[73] but miniaturization compatible with a rover or a lander platform is still a distant prospect. IR and other absorbance spectroscopies are facile to implement, but have low sensitivity and only give functional group information for the composite sample with little means to deconvolute the individual contributors. While GC-MS, particularly using pyrolysis extraction, has a legacy of successful space flight operation, it has poor quantitative capabilities and is generally accepted to have sensitivities on the order of ppb for typical (non-polar, volatile) organics. As an alternative, capillary electrophoresis has very low sample and buffer requirements (< 100 μL), low power requirements, and with laser-induced fluorescent detection much greater sensitivity than other methods (low to sub pptr).

In capillary electrophoretic separations, analytes are separated based on their differential velocities induced by an electric field, which are in turn based on the sizes and charges of the analytes. The velocity (v_i) of an analyte under the influence of an applied voltage (V), is directly related to its mobility, μ_i and directly proportional to the electric field (V/L):

$$v_i = \mu_i \frac{V}{L} \qquad \text{(Eq. 1)}$$

The mobility of an analyte is a property of its charge (q) and size according to the following approximation:

$$\mu_i = \frac{q}{6\pi\eta r} \qquad \text{(Eq. 2)}$$

where η is the viscosity of the solution and r is the radius of the analyte. Therefore, the velocity of an analyte in an electric field is directly proportional to its charge, and inversely proportional to its size.[74]

Capillary zone electrophoresis (CZE) relies on the phenomenon of electroosmotic flow (EOF, Figure 1.3A) to mobilize analytes to the detector. EOF arises in glass capillary or microchannel CE columns when the pH of the analysis buffer (typically ~8-9) is raised above the pK_a of the surface silanol groups (~ 3.5). The high pH deprotonates the glass surface nearly completely, resulting in a negatively charged surface. To maintain charge neutrality, positive

ions from the analysis buffer build up near the glass interface, and a double layer of charge, the zeta potential (ζ), is formed. Application of a voltage along the length of the column induces the motion of the mobile layer of positively charged ions toward the negatively charged cathode. The motion of the solvated cations near the surface of the column induces bulk electroosmotic flow (EOF). Unlike the parabolic flow profiles of pressure-driven flows, EOF results in a relatively flat flow profile (Figure 1.3B).[74]

The velocity (v_0, Eq. 3) and the mobility (μ_0, Eq. 4) of EOF depend on the applied field (E) and the zeta potential of the surface:

$$v_0 = \mu_0 E \qquad \text{(Eq. 3)}$$

$$\mu_0 = \frac{E\zeta}{\eta} \qquad \text{(Eq. 4)}$$

The zeta potential depends on the negative charge density of the capillary wall, which is dependent upon the pH of the analysis buffer. The effective mobility (μ_e) of an analyte is a summation of its intrinsic mobility and EOF mobility, and determines the net velocity (v_n) of the analyte towards the detector:

$$\mu_e = \mu_i + \mu_0 \qquad \text{(Eq. 5)}$$

$$v_n = \mu_e E = L/t_{elution} \qquad \text{(Eq. 6)}$$

Positively charged analytes travel with EOF, and thus reach the detector in the shortest amount of time, with the smallest analytes traveling fastest. Negatively charged analytes migrate against EOF and reach the detector later, with the smallest analytes traveling fastest against EOF and arriving last. Neutral analytes travel with EOF and are not separated. Therefore the elution pattern is primarily defined by the charge from highly positive to highly negative, and analytes of the same charge will elute from smallest to largest for positively charged analytes and from largest to smallest for negatively charged analytes (Figure 1.3A).[74]

Analytes that have the same mobility travel together towards the detector in a band that broadens with time. Many factors contribute to band broadening, including temperature, initial sample plug size and shape, interactions between the analyte and other components in the separation and the capillary walls, but contributions from these factors are negligible compared to contributions from channel geometry and diffusion. If the concentration of analytes within a band is taken to be a Gaussian distribution with a standard deviation of σ, then σ^2 may be expressed as the sum of contributions from the factors mentioned above:

$$\sigma^2 = \sigma_D^2 + \sigma_{inj}^2 + \sigma_{temp}^2 + \sigma_{other}^2 \approx \sigma_D^2 \qquad \text{(Eq. 7)}$$

where σ_D^2 is variance due to diffusion, σ_{inj}^2 is variance due to injection plug geometry, σ_{temp}^2 is variance due to temperature, and σ_{other}^2 is variance due to other factors. The analyte zone may be described by a Gaussian with a full-width at half-maximum of

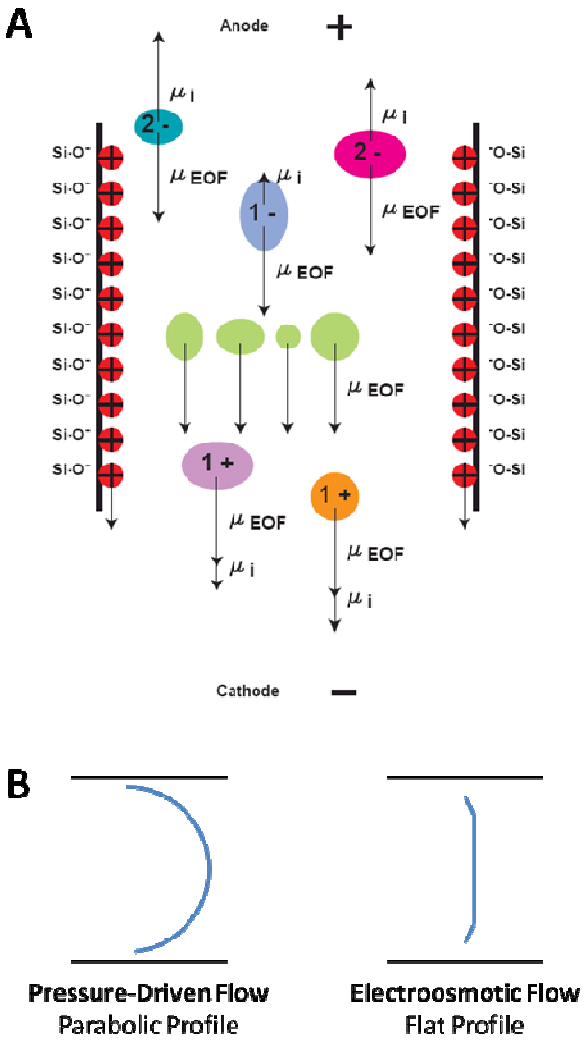

Figure 1.3. Capillary zone electrophoresis and laminar flow profiles.

(A) Capillary zone electrophoresis separation of analytes with different charge and size. All analytes are swept to the detector by electroosmostic flow (EOF); small positively charged ions elute first, while small negatively charged ions elute last. (B) Flow profiles of two laminar flows: the parabolic profile of pressure driven flow, and the flat profile of electroosmotic flow.

$$w_{1/2} = 2.3\sigma = 2.3\sqrt{2D_i t} \qquad \text{(Eq. 8)}$$

where D_i is the diffusion constant of the analyte and t is the elution time.[74]

Separations are mainly characterized by their resolution (R) and peak efficiency (N). Resolution is experimentally determined by the difference in migration time divided by the average full width of the peak at the base:

$$\mathrm{R} = 2\frac{t_2 - t_1}{w_1 - w_2} \qquad \text{(Eq. 9)}$$

where t_1 and t_2 are the elution times and w_1 and w_2 are the full widths at the base of the peaks of the two analytes. Note that the elution times and peak widths used in this equation can either be distance or time measurements, as long as all measurements are consistent. By substituting expressions for mobility and peak width and assuming that the separation length and the true column length are approximately equal, resolution can be expressed as:

$$\mathrm{R} = \frac{1}{\sqrt{32}}(\Delta\mu_i)\sqrt{\frac{V}{D_{avg}(\mu_{avg} + \mu_0)}} \qquad \text{(Eq. 10)}$$

where $\Delta\mu_i$ is the difference in mobilities of the two analytes, V is the potential applied along the channel, D_{avg} is the average diffusion constant of the analytes in the separation medium, μ_{avg} is the average mobility of the two analytes, and μ_0 is the mobility of EOF. The resolution between the two analytes is therefore linearly related to their difference in mobilities, which is due only to their charges and sizes. It is also linearly related to the square root of the applied potential, therefore a 4-fold increase in the applied potential will double the resolution between analytes until Joule heating becomes problematic. High resolution results when EOF and electrophoretic mobility are in opposite directions but similar in magnitude.[74]

Peak efficiency is often quoted in terms of theoretical plates (N) or theoretical plates per meter. If the peak is Gaussian, then N is experimentally determined according to:

$$N = 16\left(\frac{t}{w}\right)^2 \qquad \text{(Eq. 11)}$$

where w is the full width of the peak at the base and t is the elution time. Substituting for w and t gives the equation:[74]

$$N = \frac{\mu V}{2D} \qquad \text{(Eq. 12)}$$

The equations for peak efficiency and resolution above suggest that channel length and separation time are not important for either parameter, indicating that the shortest separation time and the highest applied potential will give the best separation. In practice, however, at extremely high applied potentials and short separation lengths, other factors dominate and these equations become less applicable. At short separation lengths, the diffusive broadening becomes less

important while injection plug width becomes more important, and at high applied potentials broadening from Joule heating dominates. Therefore, while higher field strengths and shorter separations provide better resolution and separation efficiency in theory, there are practical, experimentally based limits on both these parameters.[74]

1.6. Cyclodextrin Assisted Capillary Electrophoresis

Polycyclic aromatic hydrocarbons are neutral, hydrophobic compounds that require additional reagents to solubilize them and separate them in aqueous CZE.[75-78] While work has been done to separate PAHs using micellar electrokinetic chromatography (MEKC)[79-80] and organic solvent enhanced systems,[79] cyclodextrin enhanced CZE separations of PAHs are attractive on the MOA system due to their previous use in amino acid separations and the desire to avoid organic solvents. Cyclodextrins have been previously used with MOA technology to achieve chiral resolution of FITC[66] and fluorescamine[67] labeled amino acids and in successful chiral analysis of extracts of the Murchison meteorite[66] and Atacama desert soils.[81] In PAH separations, a mixture of cyclodextrins is required. A neutral cyclodextrin solubulizes PAHs and travels with EOF, mobilizing analytes to the detector. A negatively charged cyclodextrin moves against EOF and acts as a pseudostationary phase. Separation is therefore achieved via differential partitioning of PAHs between the mobile neutral cyclodextrin and the pseudostationary negatively charged cyclodextrin phases (Figure 1.4B).[75-78]

Cyclodextrins are composed of repeating D-glucose units joined in a ring to form a bucket-like structure (Figure 1.4). The three-dimensional structure of a cyclodextrin can be best described as tapered cylindrical, with the interior cavity being relatively hydrophobic and the exterior being relatively hydrophilic. The radius of the internal cavity of the cyclodextrin is determined by the number of glucose units; α-CD contains 6 D-glucose units with a cavity of 0.5 nm, β-CD contains 7 units with a cavity of 0.7 nm, and γ-CD contains 8 units with a cavity of 0.9 nm. The terminal –OH groups can be modified to other functional groups with relative ease; there are commercially available cyclodextrins modified to the methyl ether, hydroxypropyl ether, sulfobutyl ether, *etc*. These functional group modifications affect the solubility, hydrophobicity, and the charge of the cyclodextrin, so a cyclodextrin can be chosen for desired properties.

The net mobility of a PAH is determined by its complexation constants with the competing cyclodextrin phases according to the equation:

$$\mu_{net}^{i} = \mu_0 + \frac{\mu_0 K_N}{\left(1 + K_N [CD_N]\right)} + \frac{\mu_- K_-}{\left(1 + K_- [CD_-]\right)} \qquad \text{(Eq. 13)}$$

where μ_{net}^{i} is the net mobility of a PAH, μ_0 is the mobility of EOF and hence the neutral PAH and cyclodextrin (CD_N), μ_- is the mobility of the negatively charged CD (CD_-), and K_N and K_- are the complexation constants of the PAH with the neutral and negatively charged CDs, respectively. The equation becomes more complex when considering the separation of two PAHs, even assuming the mobility of the CD are unaffected by PAH complexation:

$$\Delta\mu_{net}^{i,j} = \frac{\mu_0 [CD_N] \Delta K_N^{i,j}}{\left(1 + \left(K_N^i + K_N^j\right)[CD_N] + K_N^i K_N^j [CD_N]^2\right)} + \frac{\mu_- [CD_-] \Delta K_-^{i,j}}{\left(1 + \left(K_-^i + K_-^j\right)[CD_-] + K_-^i K_-^j [CD_-]^2\right)} \qquad \text{(Eq. 14)}$$

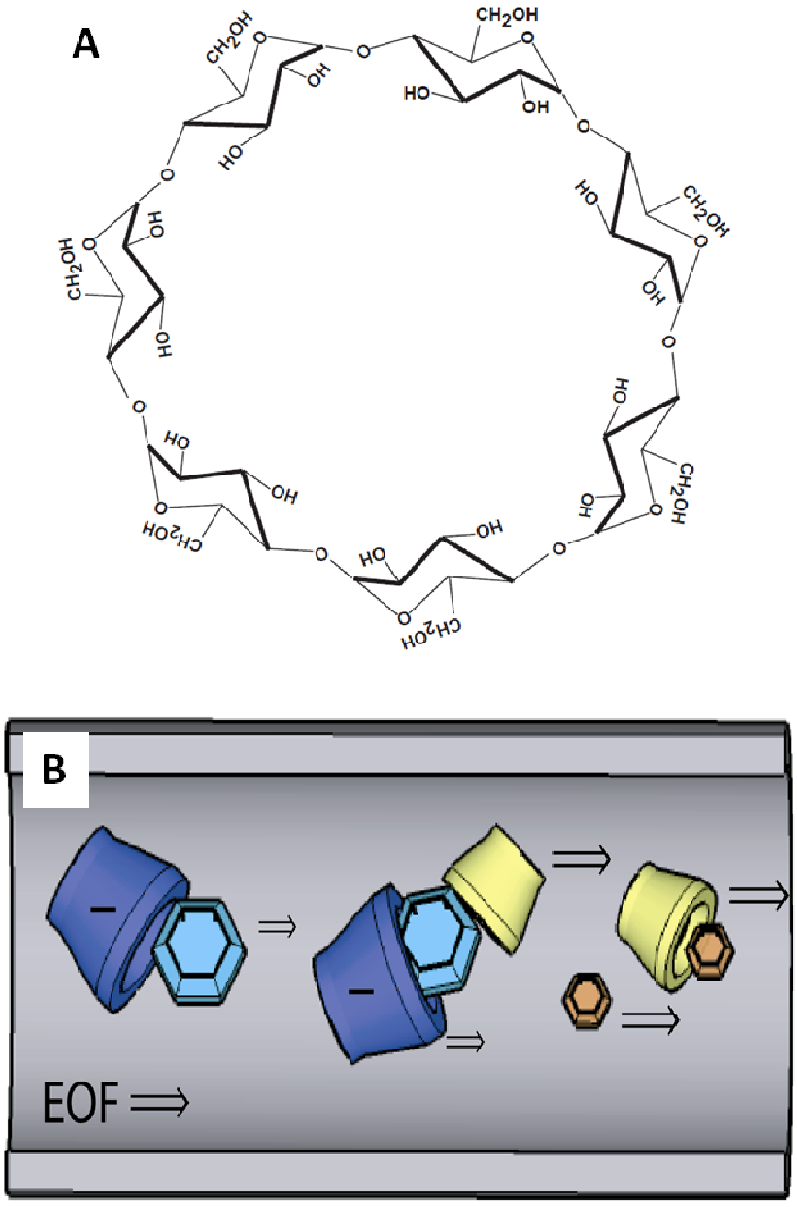

Figure 1.4. (A) Structure of β-cyclodextrin, composed of 7 units of linked D-glucose and (B) cartoon of cyclodextrin-assisted PAH separation.

Neutral and charged cyclodextrins are shown in yellow and blue, respectively. PAHs are represented by hexagonal structures with colors indicating relative binding constants. The neutral cyclodextrin moves with EOF and acts as a mobile phase, the negatively charged cyclodextrin moves against EOF and acts as a pseudostationary phase. PAHs are separated based on their differential binding constants with these cyclodextrin phases.

Substitution into Equation 10 gives an expression for the resolution, which is once again independent of separation time and column length and increases with increasing applied potential. However, due to the viscosity of high concentration CD solutions, Joule heating increases rapidly with increased applied potential, and there can be an additional loss of resolution due to slow complexation constants.[82] Equation 14 additionally indicates that unless all parameters (complexation constants of all target analytes with the CDs, the mobilities of the CDs, and the mobilities of the CD-PAH complexes) are known; CD-assisted PAH separations must be experimentally optimized for CD concentrations and ratios.

1.7 Challenges to Capillary Electrophoresis Analyses from Potential Extraterrestrial Sample Matrices

Exploration of Mars and other Solar System bodies for chemical signatures of life has revealed that preparation for diverse and unexpected chemistries is required, as discussed previously in Sections 1.1 and 1.2, and briefly here. Results from Viking[26] and Phoenix[23] indicate oxidizing chemistry in the Martian regolith, while Sojourner[19] and Opportunity[20-21] revealed potential past ground waters high in salinity and acidity. Sojourner, Opportunity, and Phoenix yielded complimentary results indicating high levels of multivalent metal cations.[19-21,23] Evidence of saline and acidic environments have also been found on astrobiological targets Europa[36-37] and Enceladus.[42]

The application of capillary electrophoresis separations to these extraterrestrial samples requires robustness of the assay to varying sample characteristics. For example, samples with extreme salinity cause dispersive effects during electrophoretic injection and lead to poor resolution and signal loss.[74] Extremely acidic samples provide challenges to labeling chemistry; if the buffer is overwhelmed, the labeling reactions will be inhibited by improper pH,[83] leading to reduced signal. High acidity also leads to cessation of the electro-osmotic flow (EOF) in the separation channels that contributes to a dramatic reduction in signal.[74] Furthermore, multivalent metal cations can alter the surface chemistry of the glass electrophoretic separation columns and also lead to dispersive effects and EOF inhibition.[84] Since the concentrations of organic biomarkers expected in samples from Mars and other extraterrestrial targets may be low, it is crucial for the analytical method to be very tolerant of highly saline, acidic, and metallic samples.

1.8 Miniaturized Capillary Electrophoresis on Microfabricated Devices

As discussed in Section 1.6, capillary electrophoresis (CE) separations offer the benefits of rapid, efficient, high resolution analysis of microliter volume samples with low (mL) use of reagents.[74] Another benefit is its miniaturizability via microfabrication of short small-bore separation columns on a planar glass "chip" surface.[74] The first analytical device miniaturized via microfabrication was a gas chromatographic analyzer fabricated on silicon over 25 years ago, coincidentally also with extraterrestrial exploration as one of the proposed applications.[85-86] Although this device demonstrated some of the inherent advantages of microfabricated analytical systems, including reduced sample and reagent consumption and decreased analysis times, it was

over a decade before the technology was fully developed by other researchers and the concept of a "miniaturized total chemical analysis system" was proposed.[85]

Capillary electrophoresis, traditionally conducted in long (~ 30-50 cm), narrow-bore (~ 50 micron inner diameter), fused silica capillaries, was first successfully conducted in microfabricated amorphous glass in 1992.[87] Microfabricated glass channels have since been used for microcapillary electrophoresis (μCE) separations of multiple targets by multiple separation techniques, including amino acids by capillary zone electrophoresis,[66] DNA by capillary gel electrophoresis,[88] polycyclic aromatic hydrocarbons by cyclodextrin-assisted CE,[78] *etc*… Microfabricated capillary electrophoresis uses short length (~ 20 cm), narrow (~ 100 microns), shallow (~ 35 microns) microfabricated channels, and thus achieves high resolution separations with shorter analysis times and reduced reagent and sample consumption than traditional CE.[85,87] Microchip capillaries and conventional capillaries, while functionally similar, differ in a number of ways, particularly in sample injection, coupling of the electrophoresis device to the detection system, and the ease of coupling the electrophoresis device to a fully automated sample handling system.

Traditional capillaries rely on one of two injection methods: electrokinetic injection, where the capillary is placed in the sample and electrophoresed for several seconds to introduce sample, or hydrodynamic injection, where the capillary is placed in the sample and then elevated relative to the detector to introduce a sample plug into the end of the column. During the injection step, analytes diffuse and broaden the injection plug, making precise plug size difficult to control. On chip, electrokinetic injection is the most attractive option. While there are a number of potential injection structures, the cross-injection structure (Figure 1.5) allows for the most facile control of small sample plug sizes. A cross-injection structure is operated by applying a voltage (~ 1.5 kV) across the sample/waste arm, inducing EOF from the sample to waste and driving sample into the cross channel. After a brief (~10-30 s) equilibration time, the voltages are switched so that the main flow is from the anode towards the detector and a small, repeatable sample plug is introduced into the separation column. Generally "back-biasing" is performed to prevent leakage of additional sample from the cross channel into the separation channel. Back-biasing is a low voltage (~ 1.5 kV) applied during separation to drive flow from the anode towards the sample and waste wells. By applying a ground to the anode and cathode during the initial filling of the cross channel, flow is induced from these wells to the waste well, resulting in a smaller sample plug or a "pinched" injection. Additionally, the size of the sample plug can be increased, after filling the cross-channel with sample, by applying a voltage across the sample/cathode wells, inducing flow directly from the sample well into the separation column. After the required plug size is obtained (< 10 s), the normal separation mode with back-biasing is instated, giving a well defined larger plug size.

Coupling of a laser-induced fluorescence detector is facile when using microfabricated devices for electrophoresis. In confocal laser-induced fluorescence detection, the laser is focused through an objective to a spot (~20 μm) within the separation column, and that same objective collects emitted fluorescence and passes it to the rest of the detection system. With conventional capillaries, the laser beam and the emitted fluorescence must pass through the curved surface of the capillary, which distorts the beam waist. While sheath flow cuvettes with flat windows have been used to make detection in conventional capillaries simpler,[89] microfabricated CE devices

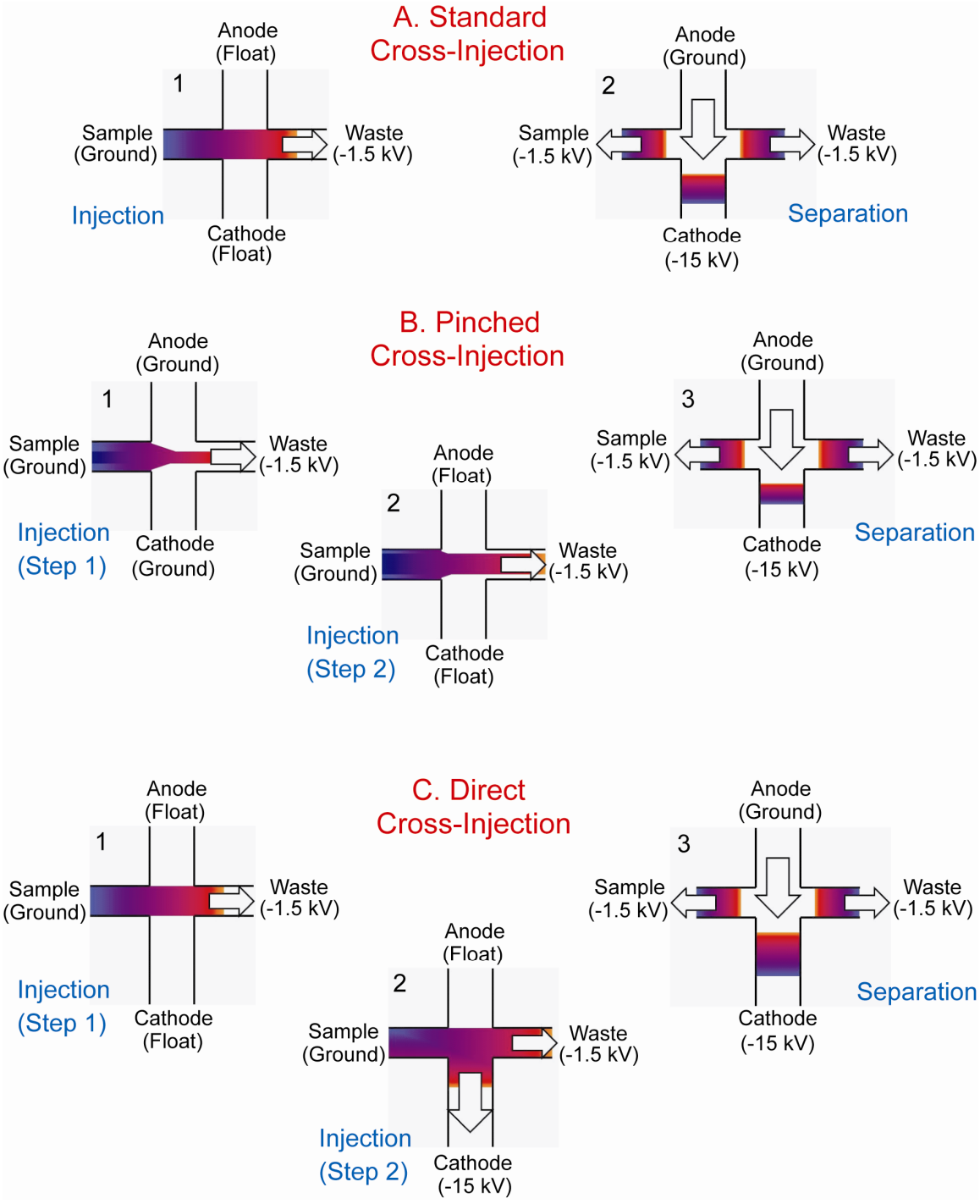

Figure 1.5. Standard cross injection and off-set T injection structures for injection into microchannel separation columns.

The cross injection structure is solely utilized in this thesis.

avoid the problem altogether with their flat air-glass interface at the detection side and a flat glass-fluid interface on the analyte side.

The most advantageous aspect to microfabricated CE is the capability to integrate multiple components into a single chip with relative ease. In the Mathies lab alone, integrated microfluidic components implemented have included multiple μCE channels,[90-91] monolithic membrane valves and self-priming pumps based on these valves,[90-95] dilution circuits,[92,94-95] pH sensitive electrodes,[96] PCR reactors,[88,90,93,97-99] microfabricated heaters,[88,90,93,97-99] resistive temperature detectors,[88,90,93,97-99] thermally-switchable and photopolymerized affinity-capture gels for sample preconcentration and clean-up,[88,98-99] *etc*… Integration of these components allows for automated sample handling systems integrated with the microcapillary analysis column. Integrated devices have been used in many applications, including DNA sequencing,[88,97,100] STR typing for forensics analysis,[88,100] and droplet generation for stochastic studies of cellular populations.[101] For extraterrestrial analysis of organics via μCE, an integrated device that autonomously performs labeling reactions, serial dilutions prior to and after labeling, introduction of standards, and electrophoretic separation will be required.

1.9 Microfabricated Devices for Fluidic Manipulation and Sample Processing

A fully autonomous microdevice incorporating μCE separation methods for extraterrestrial exploration will require sample processing capabilities for on-chip microfluidic manipulations, including labeling reactions, serial dilutions, spiking sample with standards, and transfer of sample and buffer to the μCE channel. Monolithic membrane microvalves fabricated in hybrid three-layer devices have been used to control fluids on the nL to μL volume scale.[94,102-103] Microvalve structures are produced by sandwiching a flexible elastomer membrane between two glass layers, each etched with features corresponding to pneumatic inputs and fluidic channels (Figure 1.6).[94,102-103] Within a microvalve, the fluidic feature is an etched discontinuous fluidic channel, and the pneumatic feature is an etched displacement chamber. When a vacuum is applied to the pneumatic feature, the membrane deflects into the displacement chamber, enabling fluidic flow across the channel discontinuity. Microfabricated valves have small dead volumes (<20 nL), and remain sealed against fluidic pressure up to 75 kPa when pressure is applied to the pneumatic feature.[102] Three valves in series can be operated in sequence to form a peristaltic pump that can move fluid at a rate of nL to μL per cycle with average rates between 1 to 100 nL/s.[102]

For full functionality of a microfluidic device for extraterrestrial exploration, the device must be capable of successful and rapid mixing of fluidic inputs for labeling reactions and dilutions. However, since microfluidic devices operate at low Reynolds number, flow profiles are normally laminar and turbulent flow conducive to rapid (*i.e.* not diffusion limited) mixing is more challenging to access. Additionally, high Schmidt numbers are encountered by these systems, with analytes having low molecular diffusivity compared to viscous momentum. Therefore, micromixers must be utilized for efficient on-chip mixing of fluids. A number of micromixers utilizing monolithic membrane valves have been demonstrated, including continuous flow micromixers[92,104] and rotary pump micromixers that accomplish fixed-volume

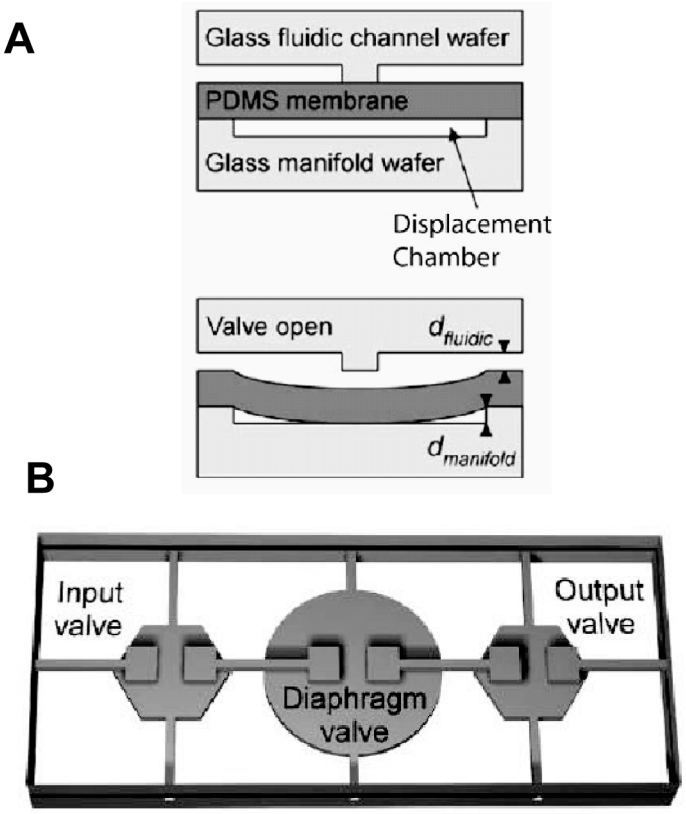

Figure 1.6. Monolithic membrane valve (A) and corresponding peristaltic pump (B).[102]

mixing via pumping in a circular loop.[94] Recently, Jensen *et al.* have developed methods based on asynchronous pumping or a "flutter valve" to induce rapid continuous mixing.[104]

The final MOA system for extraterrestrial analyses will also require a programmable microfluidic processor capable of implementing different assay procedures. The Automaton (Figure 1.7) is a programmable microfluidic platform based on an 8x8 rectilinear array of pneumatically actuated monolithic membrane microvalves.[95,105] This device was originally developed for automated nL-scale multi-step quantitative biomolecular assays. Basic operations are achieved by digital transfer of fluid between microvalves in the array. These operations can be implemented combinatorially, enabling the automation of diverse assay protocols. The Automaton has a high degree of flexibility and programmability with 2^{64} possible valve configurations available for each step in an operation. Precise metering of small volumes (~14 nL) and serial dilution protocols were demonstrated with linearity over a 1000-fold dilution range.[95] The Automaton device was initially demonstrated on a small-volume hydrogen peroxide assay with a sub-μM detection limit,[95] and has more recently been characterized for the automated processing of larger volumes.[104] Because the Automaton can process large sample volumes (10-30 μL) on a microfluidic format compatible with MOA technology, it can provide the microfluidic sample processing required for autonomous MOA analysis, as is discussed and demonstrated as part of this thesis in Chapter 7.

1.10 Instrumentation: the Mars Organic Analyzer (MOA)

The Mars Organic Analyzer (MOA, Figure 1.6)[103] is a portable lab-on-a-chip microcapillary electrophoresis (μCE) instrument that contains all the necessary microfluidics, optics, electronics, and high voltage power supplies for μCE analysis with 405 nm laser-induced fluorescence detection. It has been used to detect fluorescamine-labeled primary amines, amino acids,[81,103] and nucleobases.[106] With cyclodextrin-assisted CE[67] it has been used to determine the chirality of amino acids.[81,103]

The MOA's capability for high resolution separations with highly sensitive detection has been demonstrated by a number of successful analyses both in the laboratory and in the field. In the laboratory, the MOA was used to analyze fluorescamine-labeled amino acids present in samples from the the Yungay Hills region of the Atacama Desert[103] and nucleobases directly sublimed from *E. coli* cells.[106] In 2004, the MOA was field tested in the jarosite-rich Panoche Desert, successfully analyzing amino acids sublimed from a jarosite sample down to sub ppb levels.[103] In 2005, the MOA was successfully tested in the Atacama Desert, analyzing subcritical water extracts of samples taken from the Yungay Hills region, detecting amino acids down to 4 ppb and identifying the age of the organics in the sample as 2×10^3 to 1×10^5 years, consistent with the known El Nino precipitation events 1×10^4 to 1.6×10^4 years ago.[81]

The Mars Organic Analyzer inherently requires low power (15 W) and reagent consumption (~ 90 μL buffer / analysis). Even laboratory prototypes using off-the-shelf parts and standard electronics boards, have low mass (~11 kg) and low volume (< 14,000 cm^3). With an effort towards further miniaturization and optimization, these instruments could easily be much smaller, lighter, and possibly require even less power. These instruments clearly

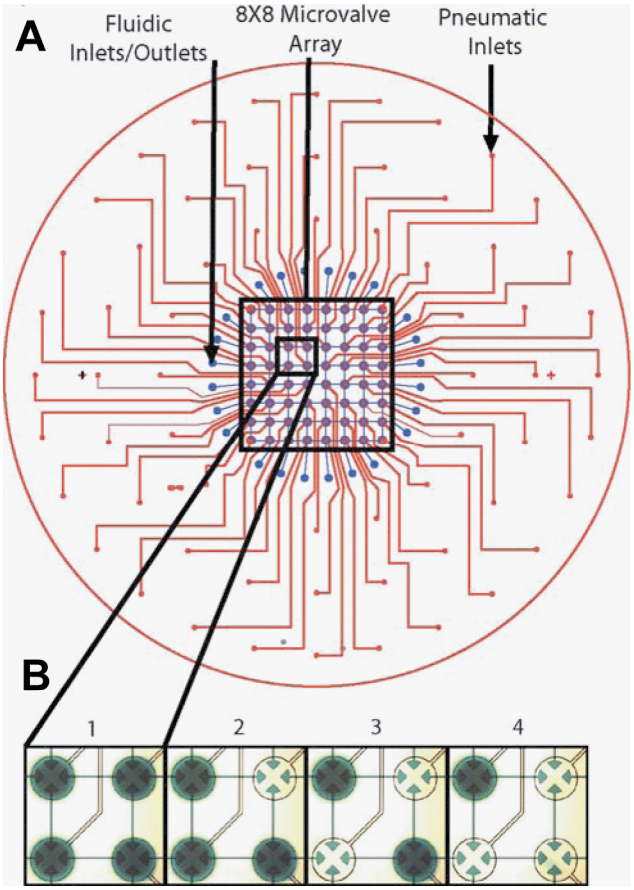

Figure 1.7. Layout of the digital microfluidic platform or Automaton.

(A) Pneumatic channels (red) transmit pneumatic actuation signals to the central array of microvalves. The 4-way microvalves control fluid flow through a rectilinear grid of discontinuous fluidic channels (blue). Close up images of a portion of this array (B) show the programmable loading of a dye into actuated microvalves.[95]

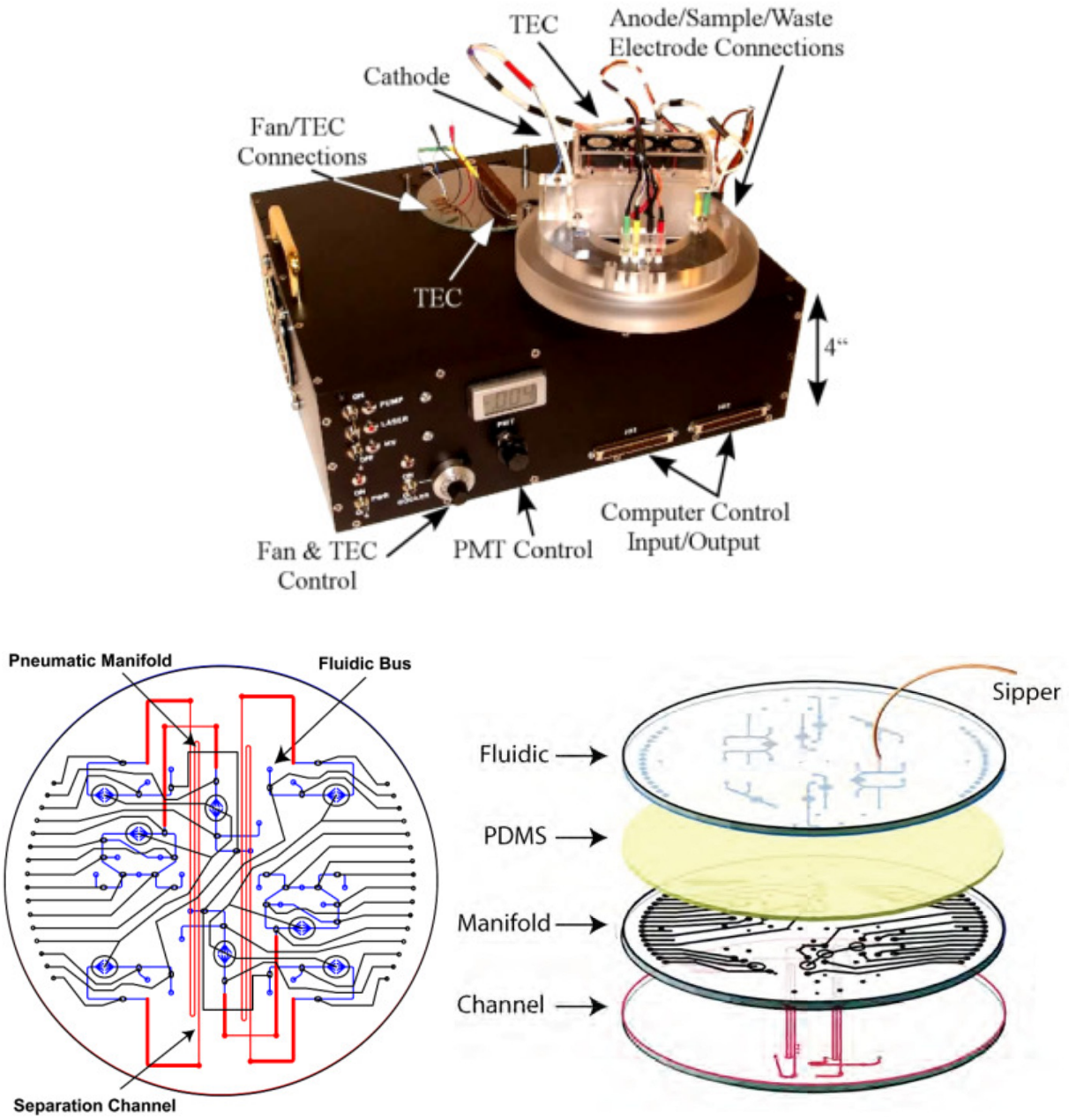

Figure 1.8. The Mars Organic Analyzer (MOA, top) and an example multilayer microdevice (bottom) it can operate.[103]

1.11 Scope of the Thesis

The goals of the work presented in this thesis are (1) the expansion of MOA target analytes to include polycyclic aromatic hydrocarbons (2) the exploitation of Pacific Blue succinimidyl ester labeling for more highly sensitive amino acid analyses, (3) the extension of advanced labeling methods for detection of oxidized forms of carbon including aldehydes, ketones, and carboxylic acids, (4) the development of more robust μCE analyses suited for extraterrestrial extremes of salinity and acidity, and (5) the development of integrated automated methods for performing these assays.

Chapter 2 presents the development of methods for cyclodextrin-assisted μCE analysis of polycyclic aromatic hydrocarbons (PAHs). A mixture of cyclodextrins is used; separation is affected via the differential partitioning of PAHs between a mobile neutral cyclodextrin phase and a pseudostationary charged cyclodextrin phase. Detection is achieved through the native PAH fluorescence at the MOA's 405 nm excitation. Cyclodextrin concentration and ratios are optimized, and samples of astrobiological and environmental interest are analyzed, demonstrating the first analyses of this compound class on a portable μCE platform.

Chapter 3 shows how Pacific Blue succinimidyl ester (PB) can be used for highly sensitive amine and amino acid analysis. Limits of detection are achieved in the sub-pptr levels, allowing detection of amines and amino acids at ~1-10 cells per gram of soil. PB-labeling was used to analyze samples from the Murchison meteorite and the Yungay hills region of the Atacama Desert, demonstrating the utility of this method for highly sensitive analyses of astrobiologically relevant samples.

Chapter 4 presents the necessary modifications to MOA amino acid analytical protocols for successful analysis of samples high in salinity, acidity, and/or divalent cations. Several buffering options are explored, and 30 mM borate, pH 9.5 is chosen as both the separation and labeling buffers. The high ionic strength enhances tolerance high salinity, and the large buffering capacity enhances tolerance to acidity. Ethylenediamine tetraacetic acid (EDTA) is added to the sample after labeling to bind divalent cations that adhere to the surface of the channel walls and interfere with EOF. Using this enhanced analysis system, the MOA successfully analyzes samples that would have been impossible to analyze using the previous protocol: a saturated brine from the Saline Valley, CA, and a sample from the highly acidic and metallic Rio Tinto, Spain.

Chapter 5 presents the development of MOA μCE analysis methods for oxidized carbon classes including aldehydes and ketones. Carbonyl-containing molecules are labeled with Cascade Blue hydrazide through the formation of hydrazones. Labeling conditions and separation conditions are optimized in aqueous media using no organic solvents, leading to the first successful μCE analysis of these partially oxidized organic compounds. The utility of this method is demonstrated through the analysis of several complex fermented beverage samples.

Chapter 6 presents the development of MOA μCE analysis methods for carboxylic acids. Acid functional groups are labeled by converting the acid to an active ester through reaction with water soluble 1-ethyl-3-(3-dimethylaminopropyl)carbodiimide (EDC). The active ester, generated *in situ*, is then reacted with Cascade Blue hydrazide to form the hydrazide ester. Labeling chemistry is optimized in aqueous solution using no organic solvents. The successful

MOA μCE analysis of carboxylic acids is demonstrated by the analysis of a variety of carboxylic acids, including mellitic acid, and carboxylic acids in samples from a Mojave Desert, CA, lava tube cave and the Bumpass Hell hydrothermal area in Lassen National Park, CA.

Chapter 7 presents the initial application of the Automaton microfluidic device to automated sample handling, including the performance of on-chip labeling reactions for amino acids, aldehydes and ketones, and carboxylic acids. The device performs dilutions after labeling, has on-chip storage capability, and loads the MOA μCE sample well via a PEEK tubing fluidic interface. This device represents a significant step toward autonomous portable sample handling and analysis system using MOA technology.

Finally, Chapter 8 presents prospects for the analysis chemistries I developed and the microfluidics technology. Further developments towards an even more comprehensive autonomous miniaturized device are considered. Possible incorporation of further analytical capability including microchip capillary electrochromatography (μCEC) and nanospray ionization (nSI) for coupling to a MS detector for parallel LIF and MS detection are discussed. Terrestrial applications of this technology are considered, and this device is critically compared to other platforms for extraterrestrial organic chemistry exploration.

Chapter 2 : Polycyclic Aromatic Hydrocarbon (PAH) Analysis with the Mars Organic Analyzer Microchip Capillary Electrophoresis System

2.1 Abstract

The Mars Organic Analyzer (MOA), a portable microchip capillary electrophoresis (CE) instrument developed for sensitive amino acid analysis on Mars, is used to analyze laboratory standards and real-world samples for polycyclic aromatic hydrocarbons (PAHs). The microfabricated CE separation and analysis method for these hydrophobic analytes is optimized, resulting in a separation buffer consisting of 10 mM sulfobutylether-β-cyclodextrin, 40 mM methyl-β-cyclodextrin, 5 mM carbonate buffer at pH 10, 5 ^{o}C. A PAH standard consisting of seven PAHs found in extraterrestrial matter and two terrestrial PAHs is successfully baseline separated. Limits of detection for the components of the standard ranged from 2000 ppm to 6 ppb. Analysis of an environmental contamination standard from Lake Erie and of a hydrothermal vent chimney sample from the Guaymas Basin agreed with published composition. A Martian analogue sample from the Yungay Hills region of the Atacama Desert was analyzed and found to contain 9,10-diphenylanthracene, anthracene, anthanthrene, fluoranthene, perylene, and benzo[ghi]fluoranthene at ppm levels. This work establishes the viability of the MOA for studying PAHs as part of the Urey instrument package on the 2013 ESA ExoMars mission.

2.2 Introduction

The analysis of polycyclic aromatic hydrocarbons (PAHs) in terrestrial and extraterrestrial environments is particularly pertinent because of their resistance to oxidative and photochemical degradation.[54] Terrestrial PAHs are predominantly formed via the pyrolysis, dehydrogenation, and incomplete combustion of biogenic material.[54] PAHs can also be produced via abiotic reactions, both in space and through planetary geological activity.[52,54] PAHs have been found throughout the universe, specifically in carbonaceous chondrite meteorites,[47] Martian meteorites,[48-50] and interplanetary dust particles,[51] and radioastronomers have observed PAHs in interstellar matter.[52] Given these extraterrestrial PAH sources, an infall-rate of organic matter onto the Martian surface of approximately 10^5 kg per year,[59] and arguments for abiotic syntheses of PAHs directly on the Martian surface,[54] it is important to probe for PAHs in any survey for organic carbon on its surface.

The Viking landers in 1976 and 1977 probed for but did not detect any organic molecules on the Mars.[17] This result led to the widely held postulate that the Martian regolith contains a strong oxidant.[26] Since Mars has no protective magnetic field and a minimal atmosphere, it has also been postulated that organic molecules on the uppermost surface of the Martian regolith have been destroyed by irradiative sterilization.[26] These concerns indicate how critical it is to improve the sensitivity of PAH detection in such planetary exploration.

Terrestrial analysis for PAHs is of interest in health and environmental studies, due to the carcinogenicity of these molecules. While PAHs can be found in a number of natural geological sources including volcanic ash, hydrothermal vents,[55] coal[56] and petroleum deposits, and oil shales,[107] there are a number of anthropomorphic contributions to PAH prevalence. PAH pollution stems from auto exhaust,[58] wood and cigarette smoke,[57] lumber processing plants,[75] etc., leading to PAH contamination in, for example, marine environments[108] and in the air over major cities.[109] Currently, terrestrial sampling and analysis is focused on the clean-up of environmental contamination sites.[110-111] While there have been recent advances in the analysis of PAHs from these samples including micellar electrokinetic chromatography and supercritical fluid chromatography,[110-112] reverse-phase HPLC remains one of the most commonly used methods.[112] Due to the long analysis times, high cost, and sample blending and destruction of

these methods, it would be useful to have inexpensive, rapid, non-destructive, *in situ* techniques for the measurement of PAH contamination in sediments.[110]

The European Space Agency (ESA) has planned the 2013 ExoMars rover as a part of its Aurora program to search for evidence of past or present life on Mars via the analysis of organic molecules. While Viking was confined to a single sampling site, ExoMars will be able to transit to promising sampling sites. Furthermore, ExoMars will have drilling capability down to 2 m depth, where organics have increased survival.[113] ExoMars will carry a suite of experiments targeting organic molecules, specifically those indicative of life. In particular, ExoMars will carry the Urey instrument,[68] which utilizes subcritical water extraction and the Mars Organic Analyzer (MOA) microchip CE separation system for high sensitivity organic molecule detection.

The MOA contains the electrical, optical, and microfluidic systems required for high performance analysis of amino acid composition and chirality. The core processor is a four-layer microfluidic chip that performs CE separations and analyses. We have previously demonstrated MOA analysis of amino acids and their chirality,[67] bioamines, and nucleobases,[106] and have analyzed a variety of Martian analogue samples with high sensitivity.[103] Successful field tests of the MOA have been conducted in the Panoche Valley, California,[103] and in the Atacama Desert, Chile.[81] Recent work using improved fluorescence labeling reagents has increased our ability to detect amines and amino acids to < 10 cells per gram of soil.[69] However, since the organic carbon found on Mars could be in the form of PAHs we also need the capability to detect these compounds and their derivatives.

In this study we have extended the original MOA amino acid analysis system to the CE separation and analysis of PAHs. To perform separations of hydrophobic PAHs in aqueous solutions, we adapted a previous separation method to the microchip CE format.[75-78] This method employs an aqueous charge-neutral cyclodextrin as a solubilizing agent for the PAHs. A negatively charged cyclodextrin, moving against electroosmotic flow, serves as a pseudostationary phase so that the PAH separation is achieved via differential partitioning between the charged pseudostationary and uncharged mobile cyclodextrin phases. The cyclodextrin ratio, buffer, and temperature conditions are optimized for CE based PAH separations. A standard composed primarily of PAHs found in extraterrestrial matter is used to determine limits of detection for PAHs. Finally, we apply this method to the analysis of environmental and Martian analogue samples, to evaluate the real-world utility of this analytical technique.

2.3 Materials and Methods

Buffer and sample preparation. Methyl-β-cyclodextrin (M-β-CD) with a mean degree of substitution (ds) per cyclodextrin of 1.6-2.0 was obtained from TCI America (M1356; Portland, OR). Sulfobutylether-β-cyclodextrin (SB-β-CD) with a mean ds per cyclodextrin of 5.5 was obtained under the label Advasep 4 from Cydex, Inc. (AR-04A; Lenexa, KS). Hydroxypropyl-β-cyclodextrin (HP-β-CD, 389145) with a mean ds of 1.0 and sulfated-β-cyclodextrin (S-β-CD, 38915-3) with a mean ds of 7-11 were obtained from Sigma-Aldrich (St. Louis, MO). Stock solutions of 100 mM cyclodextrin were prepared and stored at -20 ^{o}C for up to one month. A 100 mM carbonate buffer solution was also prepared and adjusted to pH 10, then stored at room

temperature. Buffers used for analysis were prepared by diluting appropriate combinations of cyclodextrin and buffer stock.

Anthracene (14106-2), fluoranthene (F807), perylene (77340), 9,10-diphenylanthracene (42785), and benzo[a]pyrene (B1760) were obtained from Sigma-Aldrich. Anthanthrene (BCR-091), benzo[ghi]fluoranthene (BCR-139), and benzo[j]fluoranthene (BCR-049) were obtained as the Community Bureau of Reference (BCR) reference materials through Sigma-Aldrich. Dibenzo[b,def]chrysene was obtained from TCI America (D1005; Portland, OR). All PAHs were used as received. Concentrated stock solutions of PAHs were prepared in electrophoresis grade acetonitrile (MeCN) or dimethylsulfoxide (DMSO) in the 50 μM to 10 mM range depending on the solubilities and optical properties. Sample stock solutions 20-100 times more concentrated than the desired final sample concentration were prepared by combining appropriate volumes of PAH stock solutions and diluting with MeCN. The final sample was prepared by diluting the stock solutions with analysis buffer to a final organic solvent composition of 1-5 %.

Limits of detection (LODs) for PAHs were determined using two injection techniques: the standard cross injection and a 10 s gated injection. Each molar LOD was calculated from the average of triplicate experiments. Each dilution series consisted of 10 samples prepared from a high concentration solution in MeCN or DMSO, ranging over at least two decades. The LOD was determined as the extrapolation of a power law fit to a signal-to-noise ratio of 3. LOD samples were prepared in 1-5 % MeCN or DMSO, 95-99 % running buffer, depending on the solubility of each PAH.

Three samples of relevance either to the environmental or astrobiological community were also analyzed. EC-6 is a certified reference sample for organic contaminants from Canada's National Water Research Institute (NWRI). This sample was collected in 1984 from Lake Erie, and serves as one of the NWRI's reference sediments with the lowest levels of toxic organic contaminants. A hydrothermal vent chimney (HVC) sample collected from the Guaymas Basin, Gulf of California, was obtained by researchers at Scripps Institution for Oceanographic Studies, La Jolla, CA.[114] Finally, a sample collected from uppermost duracrust of the Yungay Hills region of the Atacama Desert, AT45A1,[81] provided an analogue to Martian regolith.

These samples were processed first either by subcritical water extraction[115] or by sublimation[116-117] to extract PAHs from the sample matrix. Freeze-dried subcritical water extracts (SCWE) were obtained from collaborators on the Urey project at the Jet Propulsion Laboratories, Pasadena, CA. Sublimation samples were obtained from collaborators at the Scripps Institution for Oceanographic Studies, La Jolla, CA. Both processes were conducted as previously reported.[115,117] Briefly, SCWE samples were obtained by extracting 1 g of sample with 8 mL of water at 200 ^{o}C and 17.2 MPa, and sublimation samples were obtained by heating the sample at 500 ^{o}C and collecting sublimate on a disk attached to a cold finger. SCWE samples obtained were resuspended in 3 mL water and extracted with 4 x 2 mL portions of dichloromethane. Sublimation disks obtained were rinsed 10 times with 100 μL portions of dichloromethane. In both cases, the dichloromethane portions were combined and evaporated, and the residue resuspended in 100 μL running buffer. The hydrothermal vent chimney sample was diluted 1:5 with running buffer, the EC-6 sample was diluted 1:60 with running buffer, and

the Atacama samples were run without dilution. Spiking experiments were conducted by adding 0.5 μL of a standard PAH solution in MeCN to 49.5 μL concentrated or diluted sample to identify and quantify PAHs in the sample.

Microdevice fabrication. The microchip devices were prepared as previously described.[67,103,106,109] Briefly, a sacrificial layer of polysilicon is evaporatively deposited on a 10 cm borofloat wafer (Precision Glass & Optics, Santa Ana, CA). A layer of photoresist is spin-coated onto the polysilicon surface and patterned through a chrome mask using a contact aligner. The photoresist is developed and the exposed polysilicon is removed via an SF_6 plasma etch. The glass is then etched in a buffered 49 % HF bath for 3 minutes. The pattern provides 23.6 cm long folded separation channels 100 μm wide etched 25 μm deep, with a 1.2 cm long cross-channel located 0.6 cm from the anode end of the channel. The remaining photoresist is removed, and reservoir holes are drilled using 1.2 mm diamond-tipped drill bits. The polysilicon layer is removed via plasma etch and the wafer is bonded to a blank wafer to form completed channels. A 3 mm deep PDMS gasket with 4 mm diameter wells is placed over the reservoir holes to allow for larger volume storage at the reservoirs. A schematic of the microdevice design can be found in Appendix A.

Mars Organic Analyzer. The Mars Organic Analyzer[69,81,103,106] was used with modifications to perform the PAH CE separations. The 404 nm laser is passed through a dichroic (Z405tranDCXR, Chroma, Rockingham, VT) and focused to a 10-20 μm spot in the channel approximately 0.6 cm from the cathode reservoir. Fluorescence is collected by the objective and reflected by the dichroic through a long pass filter (50 % T at 425 nm, HQ425lp, Chroma, Rockingham, VT) onto a PMT, which was read at 50 Hz using LabView on an IBM ThinkPad laptop.

Separation and injection procedures. The microchip separation channel was prepared by first filling the sample, waste, and anode wells with running buffer. A vacuum was applied to the cathode well, drawing running buffer into the separation channel and filling it with buffer. The cathode well was then filled with running buffer, and the buffer in the sample well was drawn out and replaced with sample.

Two injection techniques were used in this study. The standard cross injection was accomplished by first applying a potential across the sample (ground) and waste (-750 V) wells for 45 s, thus filling the cross channel. The anode is floated for this step, and the cathode grounded. The potentials are then switched so that the main potential is applied across the anode (ground) and cathode (-15 kV) wells. A back bias of -1200 V is applied at the sample and waste wells. The gated injection, which gives a longer sample plug, is performed by first filling the cross channel by applying -750 V at the waste, floating the anode, and grounding the sample and cathode for 45 s. Then a sample plug is injected into the column by applying -750 V at the waste, floating the anode, grounding the sample, and applying -15 kV at the cathode for 10 s. After the injection, the cathode remains at -15 kV, the anode is grounded, and a back-bias of -1200 V is again applied at the sample and waste wells.

Safety. Several PAHs have been identified as or are suspected of being carcinogens. PAH solids and stock solutions were handled in a ventilated hood and stored in closed containers. Disposable nitrile gloves were worn while working with PAHs.

2.4 Results and Discussion

Effect of charged cyclodextrin on PAH separations. To explore the dependence of PAH separation quality on the identity and concentration of the charged CD, sulfated-β-cyclodextrin (S-β-CD) and sulfobutylether-β-cyclodextrin (SB-β-CD) were used in varying concentrations in a constant 40 mM methyl-β-cyclodextrin (M-β-CD), 5 mM carbonate buffer, pH 10. Sample containing 40 μM 9,10-diphenylanthracene, 600 μM anthracene, and 20 μM perylene in 5 % MeCN, 95 % running buffer was injected via a cross-injection. No separation was observed at any concentration of S-β-CD. Figure B.1 in Appendix B presents electropherograms of PAH separations at concentrations of SB-β-CD varying from 0 to 10 mM. With no SB-β-CD, there is no separation of PAH components and they emerge as a single peak. This is expected, since all PAHs elute with the mobile M-β-CD phase. As the concentration of SB-β-CD is increased, PAH separation is accomplished and average migration time is increased. This migration time increase is due to enhanced partitioning of the PAHs into the negatively charged SB-β-CD at higher concentrations of this CD. Larger SB-β-CD concentrations also increase the signal-to-noise ratio because more PAHs are solubilized. The highest resolution and signal-to-noise was observed at the highest 10 mM concentration of SB-β-CD. Increasing the SB-β-CD concentration also increased currents during the separation, which imposed a maximum practical limit to the SB-β-CD concentration at ~10 mM and ~100 μA. Above this concentration, electrolysis and bubble formation led to separation failures.

Effect of neutral cyclodextrin on PAH separations. To choose the optimal neutral CD and concentration, two uncharged cyclodextrins, M-β-CD and hydroxypropyl-β-cyclodextrin (HP-β-CD), were used in varying amounts in a constant 10 mM SB-β-CD, 5 mM carbonate buffer, pH 10 (Figure 2.2). Sample containing 9,10-diphenylanthracene, anthracene, fluoranthene, and perylene in 5 % MeCN, 95 % running buffer was cross-injected. Separations using HP-β-CD produced co-elution of 9,10-diphenylanthracene and anthracene peaks at some concentrations of HP-β-CD, and overall lower resolution than M-β-CD, so this combination was not explored further. Figure 2.1 shows electropherograms of PAH separations at concentrations of M-β-CD varying from 10 to 70 mM.

Higher resolution between peaks and an overall average longer migration time is observed at lower concentrations of M-β-CD, while higher signal strength and hence signal-to-noise ratios are observed at higher concentrations of M-β-CD. The resolution between the anthracene and fluoranthene peaks and between the fluoranthene and perylene peaks is plotted in Figure B.2 in Appendix B at the concentrations of M-β-CD tested, and a general downward trend in resolution with increasing M-β-CD is seen. This trend is expected, since as the concentration of M-β-CD is increased, PAHs become more likely to associate with M-β-CD over SB-β-CD, thus the effectiveness of the pseudostationary phase is decreased. Signal-to-noise ratios for anthracene and perylene are also plotted, and a general upward trend in signal-to-noise ratio with increasing M-β-CD is seen. This trend is due to the increased total PAH concentration that can be solubilized in higher total CD concentration. The crossing point of these two trends occurs at approximately 40 mM M-β-CD. The cyclodextrin mixture chosen for further parameter optimization was 10 mM SB-β-CD and 50 mM M-β-CD to give better signal strength of all PAH peaks during optimization experiments while showing similar separation characteristics to the optimal 40 mM M-β-CD.

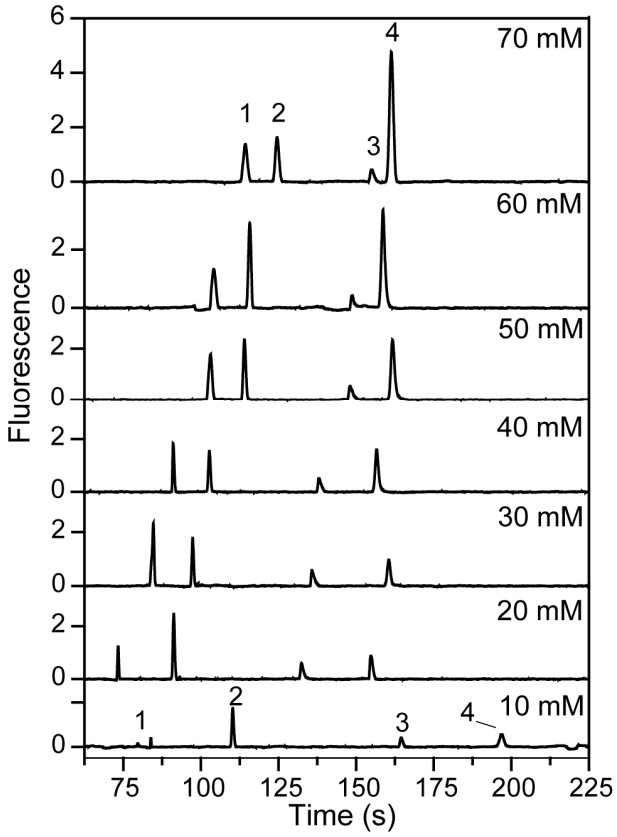

Figure 2.1. Dependence of PAH separation on the concentration of M-β-CD.

Each sample contains 9,10-diphenylanthracene (1, 33 μM), anthracene (2, 500 μM), fluoranthene (3, 160 μM), and perylene (4, 17 μM). In addition to the indicated concentration of M-β-CD, the running buffer contains 10 mM SB-β-CD, 5 mM carbonate buffer, pH 10.

Effect of temperature on PAH separation. Many parameters were examined for their effects on the PAH separation, including separation field strength, injection parameters, addition of organic solvents, carbonate buffer concentration, and temperature. The only parameter to show desirable effects on separation was temperature. Samples containing 1.2 μM 9,10-diphenylanthracene, 600 nM dibenzo[b,ef]chrysene, and 24 μM anthracene in 5 % MeCN, 95 % running buffer were cross injected. Figure 2.2 presents electropherograms of the PAH separations at temperatures from 5 ^{o}C (bottom) to room temperature (top) in 5 ^{o}C increments. At room temperature (~23 ^{o}C), all peaks emerge after about 120 s, and the 9,10-diphenylanthracene and dibenzo[b,def]chrysene peaks are quite close (resolution ≈ 1). At about 5 ^{o}C, the retention times are increased, and there is significantly increased resolution between all three peaks. This trend is shown in the insert (top right), which plots the resolution between the 9,10-diphenyl--anthracene and the dibenzo[b,def]chrysene peaks at each temperature tested. The data show a clear increase in resolution at 5 ^{o}C, but relatively similar resolution at 10 ^{o}C and higher. At temperatures less than about 15 ^{o}C, however, late-migrating PAHs such as fluoranthene, perylene, and benzo[ghi]fluoranthene, occasionally fail to elute (not shown). Current Urey operation protocol calls for regulation of the chip separation temperature at 4 ^{o}C.

Separation of the Mars 9 PAH standard. Figure 2.3 presents an electropherogram of the separation of the Mars 9 PAH standard (M9PAH). The PAHs in this standard were chosen based on their optical properties, specifically absorbance at 404 nm, and their presence in extraterrestrial matter. Seven of the PAHs in the standard are found in significant amounts in extraterrestrial matter, including Martian and non-Martian meteorites, while the remaining two PAHs are found predominantly as terrestrial contaminants. M9PAH was injected via a cross injection in 5 % MeCN, 95 % running buffer. The concentrations of PAHs used in this separation range from 20 nM for anthanthrene and perylene to 300 μM for anthracene. Average peak efficiency for this separation is around 3×10^{5} plates per meter, and the high resolutions (> 1) reflect the lack of overlapping peaks. The concentrations, identities, and sources of PAHs in this standard are given in Table 2.1, along with the characterization of this separation, including the peak efficiencies and resolutions.

Limits of detection. Limits of detection (LODs) for the studied PAHs are listed in Table 2.1. Cross injection LODs range from 100 μM (2 parts per thousand) for anthracene down to 290 pM (7 ppb) for perylene. Gated injection LODs are around one tenth to one half those determined using the cross injection, and range from 20 μM (400 ppm) for anthracene to 260 pM (6 ppb) for perylene. These LODs are dependent on individual PAH spectral properties, and would be expected to improve upon transitioning to a shorter-wavelength excitation laser. Also, due to competitive and cooperative binding effects that occur when there are multiple PAHs in solution, these LODs may not be representative of true detection limits in a complex mixture. The signal for anthracene, in particular, is extremely sensitive to the presence of other PAHs. Although its calculated LOD is in the hundreds of μM range, it is easily detectable at lower concentrations if other PAHs are present. For example, the anthracene signals in Figure 2.2 are quite strong despite its only 24 μM concentration. However, perylene, which has a LOD in the hundreds of pM range, shows a relatively weak signal in Figure 2.3 at 20 nM. These effects are likely due to competitive and cooperative binding, respectively. Despite these effects, these LOD results indicate the usefulness of this method for highly sensitive *in situ* PAH detection.

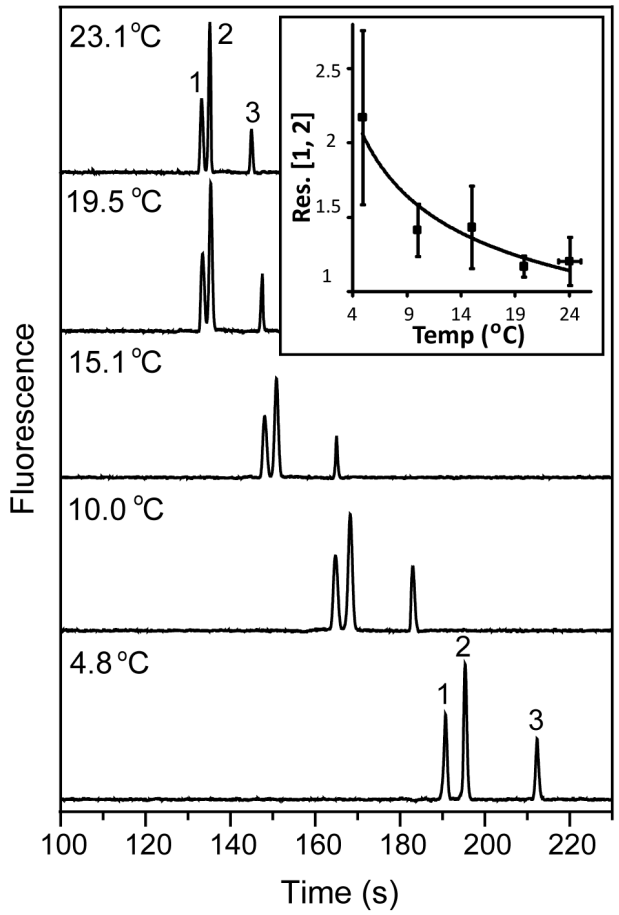

Figure 2.2. Dependence of PAH separation on temperature.

Sample contains 9,10-diphenylanthracene (1, 1.2 μM), dibenzo[b,def]chrysene (2, 600 nM), and anthracene (3, 24 μM). Running buffer contains 10 mM SB-β-CD, 50 mM M-β-CD, 5 mM carbonate buffer, pH 10. Each data point represents the average of triplicate experiments; the error bars are calculated from the standard deviation of those experiments.

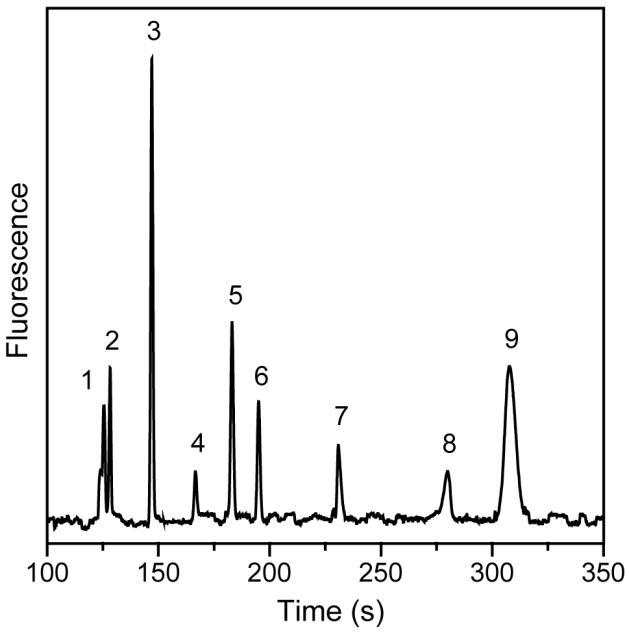

Figure 2.3. Separation of the Mars 9 PAH standard (M9PAH).

The M9PAH standard consists of 9,10-diphenylanthracene (1, 800 nM), dibenzo[b,def]chrysene (2, 200 nM), anthracene (3, 300 μM), anthanthrene (4, 20 nM), benzo[a]pyrene (5, 1 μM), benzo[j]fluoranthene (6, 4 μM), fluoranthene (7, 20 μM), perylene (8, 20 nM), and benzo[ghi]fluoranthene (9, 2.5 μM). Running buffer contains 10 mM SB-β-CD, 40 mM M-β-CD, 5 mM carbonate buffer, pH 10, 20 ^{o}C.

Table 2.1 Separation characteristics of PAHs with the Mars Organic Analyzer.[a]

PAH	Peak No.	Conc. (μM)	Peak Efficiency (plates per m)	Res.	Limits of Detection[b,c]		Sources
					Cross Injection	10 s Gated Injection	
9,10-diphenylanthracene	1	0.8	2.7×10^5	NA	4.4 ± 0.9 nM (150 ± 30 ppb)	2.3 ± 0.3 nM (80 ± 10 ppb)	None in literature
Dibenzo[b,def]chrysene	2	0.2	4.1×10^5	1.2	1.9 ± 0.6 nM (60 ± 20 ppb)	800 ± 200 pM (24 ± 3 ppb)	None in literature
Anthracene	3	300	4.9×10^5	8.5	100 ± 100 μM (2000 ± 2000 ppm)	20 ± 20 μM (400 ± 400 ppm)	Non-Martian meteorites
Anthanthrene	4	0.02	4.1×10^5	8.0	2 ± 1 nM (60 ± 30 ppb)	1.1 ± 0.5 nM (30 ± 10 ppb)	Martian and other meteorites
Benzo[a]pyrene	5	1	5.1×10^5	6.1	5 ± 4 nM (130 ± 100 ppb)	3.2 ± 0.8 nM (80 ± 20 ppb)	Martian and other meteorites
Benzo[j]fluoranthene	6	4	5.3×10^5	4.3	150 ± 20 nM (3.8 ± 0.5 ppm)	50 ± 10 nM (1.3 ± 0.3 ppm)	Martian and other meteorites
Fluoranthene	7	20	1.7×10^5	10	500 ± 200 nM (10 ± 4 ppm)	60 ± 9 nM (1.2 ± 0.2 ppm)	Martian and other meteorites
Perylene	8	0.02	1.6×10^5	8.7	290 ± 40 pM (7 ± 1 ppb)	260 pM (6.6 ppb)	Martian and other meteorites
Benzo[ghi]fluoranthene	9	2.5	8.4×10^4	3.1	1.7 ± 0.9 μM (40 ± 20 ppm)	800 ± 300 nM (18 ± 7 ppm)	Martian and other meteorites

[a] Separation shown in Figure 5.
[b] Molar limit of detection and uncertainty calculated from triplicate 10-sample experiments.
[c] Parts per million / billion limit of detection calculated assuming 100% PAH recovery from 1 g soil dissolved in 100 μL running buffer.

Complex samples. In order to validate the MOA for the detection and separation of PAHs, a number of samples of environmental and astrobiological interest were examined. Figure 2.4A shows the analysis of a SCWE of EC-6, Canada's National Water Research Institute's (NWRI's) sediment standard for low level PAH contamination. The peaks corresponding to the PAH contaminants anthracene (3), benzo[a]pyrene (6), fluoranthene (8), and benzo[ghi]fluoranthene (9) are readily observed and identified via spiking experiments. This identification agreed with that determined by NWRI laboratories, according to NWRI product literature. Quantification yields sediment contamination of 118 ± 9, 20 ± 10, 831 ± 10, and 86 ± 1 ppb for anthracene, benzo[a]pyrene, fluoranthene, and benzo[ghi]fluoranthene, respectively, as compared to the NWRI values of 37, 250, 297, and 175 ppb. These results are summarized in Table 2.2. The MOA-determined values are 3 to 12-fold lower than those determined by the NWRI for benzo[a]pyrene and for benzo[ghi]fluoranthene. This difference is most likely due to the SCWE protocol, which was optimized for amino acid extraction with a subcritical water dielectric constant of ~35. Since PAHs are more hydrophobic than amino acids, extraction efficiency of these molecules would be expected to dramatically increase upon raising the temperature of the SCWE to produce dielectric constants < 15.[115] The MOA-determined values for anthracene and fluoranthene are larger than the NWRI values by a factor of approximately three. According to NWRI product literature, the sample contains PAHs and PCBs invisible to the 404 nm detection system. The cooperative binding effect of PAHs to cyclodextrins noticed during the determination of the limits of detection may account for the three-fold enhancement.

Figure 2.4B presents the analysis of a sublimate of a hydrothermal chimney vent from the Guaymas Basin, Gulf of California.[114] Peaks are seen for a number of components, including 9,10-diphenylanthracene dibenzo[b,def]chrysene, anthracene, pentacene, anthanthrene, benzo[a]pyrene, benzo[j]fluoranthene, and fluoranthene. While the total PAH concentration in this sample is large, the number of components makes quantification of the concentration of a single component difficult due to the strong background signal. Due to these difficulties, ranges of PAH concentrations are estimated, and are listed in Table 2.2. The maximum concentration was determined by using the baseline-to-peak height to determine the PAH signal (i.e. no non-PAH background contribution to detected signal), the minimum was determined by subtracting the large background profile to expose only the PAH spikes (i.e. no PAH signal buried in background). A large concentration and variety of PAHs is expected in HVCs, and our results agree with those published in other HVC samples.[55]

Figure 2.5 presents the analysis of the SCWE of sample AT45A1[81] from the top 1 cm of the duracrust in the Yungay Hills region of the Atacama Desert (Atacama) compared to a subcritical water system flush (Blank). Six PAH components are found in this sample, including 9,10-diphenylanthracene (400 ± 100 ppb), anthracene (9000 ± 6000 ppm), anthanthrene (180 ± 80 ppb), fluoranthene (400 ± 300 ppb), perylene (2 ± 1 ppb above background), and benzo[ghi]fluoranthene (70 ± 50 ppm). PAHs in the blank system flush include 9,10-diphenylanthracene (920 ± 20 ppb), anthanthrene (150 ± 60 ppb), and perylene (3 ± 1 ppb), and are probably due to system carryover between samples. These results are summarized in Table 2.2. While there is little information on PAHs in the Yungay Hills region in the literature, the total organic matter has been cited in the 20-40 ppm range.[118] Despite using spiking experiments to calibrate, the quantization of anthracene is not consistent either with this result or the low levels of other PAHs in the sample, and is probably an overestimate due to cooperative binding effects. The Yungay Hills region of the Atacama Desert is the driest in the world, receiving only

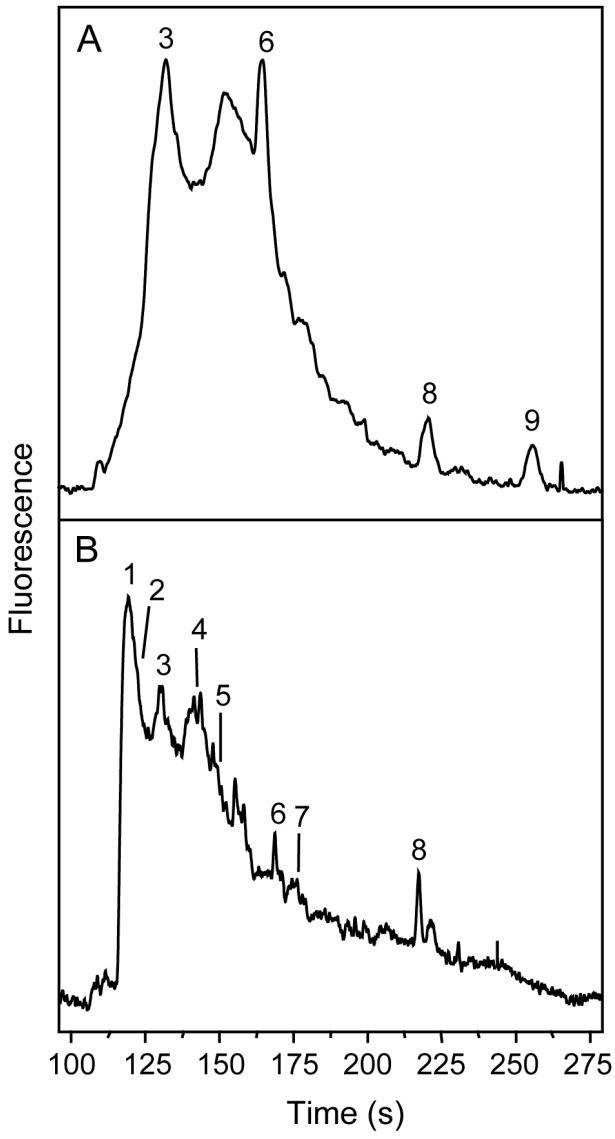

Figure 2.4. Separation of a subcritical water extract of NWRI certified reference sediment EC-6 (A) and a sublimed component of a hydrothermal chimney vent (HVC, B).

PAHs in the EC-6 sample are anthracene (1, 118 ± 9 ppb), benzo[a]pyrene (2, 20 ± 10 ppb), fluoranthene (3, 831 ± 10 ppb), and benzo[ghi]fluoranthene (4, 86 ± 1 ppb). PAHs identified in the HVC sample include 9,10-diphenylanthracene (1), dibenzo[b,def]chrysene (2), anthracene (3), pentacene (4), anthanthrene (5), benzo[a]pyrene (6), benzo[j]fluoranthene (7), and fluoranthene (8).

Table 2.2 PAH analysis of environmental and Martian analogue samples.[a]

PAH	Hydrothermal Vent Chimney[b]	EC-6 (NWRI)[c]	EC-6 (MOA)[d]	Atacama Blank[d]	Atacama Sample (above blank)[d]
9,10-diphenylanthracene	7 (-2) – 17 (+3) ppb[e]	--	--	920 ± 20 ppb	400 ± 100 ppb
Dibenzo[b,def]chrysene	0.12 (-0.04) – 5 (+2) ppb	--	--	--	--
Anthracene	50 (-50) – 100 (+100) ppb	37 ppb	118 ± 9 ppb	--	9000 ± 6000 ppm
Pentacene		--	--	--	--
Anthanthrene	0.3 (-0.3) – 4 (+2) ppb	--	--	150 ± 60 ppb	180 ± 80 ppb
Benzo[a]pyrene	2 (-2) – 6 (+6) ppb	250 ppb	20 ± 10 ppb	--	--
Benzo[j]fluoranthene	200 (-100) – 1000 (+400) ppb	--	--	--	--
Fluoranthene	220 (-70) – 400 (+100) ppb	297 ppb	831 ± 10 ppb	--	400 ± 300 ppb
Perylene	--	--	--	3 ± 1 ppb	2 ± 1 ppb
Benzo[ghi]fluoranthene	--	175 ppb	86 ± 1 ppb	--	70 ± 50 ppm

[a] Composition calculated for initial sample assuming 100 % recovery during subcritical water and dichloromethane extraction.
[b] Analysis conducted of dichloromethane soluble portion of sublimate.
[c] Non-certified values as quoted by the National Water Research Institute, Environment Canada, Burlington, Ontario, CA.
[d] Analysis conducted of dichloromethane soluble portion of SCWE.
[e] Ranges determined by assuming no baseline obscuring of peak for the lower value and no baseline contribution to peak for the larger value. Errors are calculated for each assumption to give the ranges and errors listed.

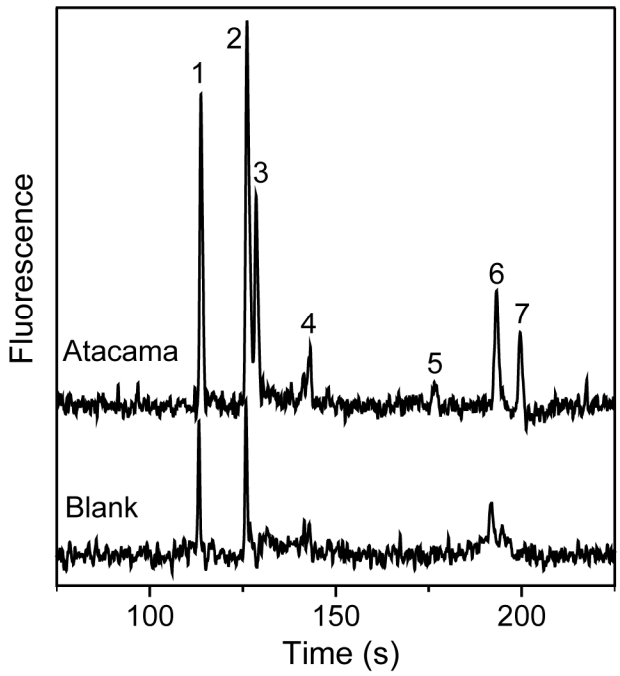

Figure 2.5. Separation of subcritical water extract of Atacama duracrust surface sample AT45A1 and instrumental blank.

Atacama sample was taken from the top 1 cm of duracrust in the Yungay Hills region of the Atacama Desert, Chile.[25] The blank is a subcritical water flush of the extraction system between samples. PAH quantities in the sample adjusted for blank composition are 400 ± 100 ppb 9,10-diphenylanthracene (1, 920 ± 20 ppb Blank), 9000 ± 6000 ppm anthracene (3), 180 ± 80 ppb anthanthrene (4, 150 ± 60 ppb Blank), 400 ± 300 ppb fluoranthene, 2 ± 1 ppb perylene (6, 3 ± 1 ppb Blank), and 70 ± 50 ppm benzo[ghi]fluoranthene (7).

one significant rain event of 2.3 mm over a four-year observation period.[119] Due to the perpetually dry conditions and prolonged UV exposure on the surface of this 1 million-year-old-desert, the Atacama duracrust serves as the best possible terrestrial model for soil conditions and composition and amounts of organic molecules on the Martian surface. The success of the MOA in detecting and analyzing PAHs in this sample indicates that the MOA is technically competent to detect PAHs on or below the Martian surface if they are present.

2.5 Concluding Remarks

The method for PAH analysis developed here significantly advances the capabilities of the MOA for organic carbon detection and may also prove useful for environmental monitoring. This method exploits a mixture of charged and uncharged CDs to solubilize and mobilize the hydrophobic PAHs in an aqueous solution for convenient CE analysis without organic solvents. Resolutions >1 are achieved between PAHs of the same molecular weight and of similar structures. Excellent limits of detection are observed for some PAHs, down to 7 ppb or 260 pM, which is comparable to other currently used laboratory methods. We have demonstrated the utility of this method for the analysis of samples of interest to the environmental community and to the astrobiology community with the analysis of the Mars analogue sample from the Atacama Desert.

Improvements to the MOA analysis system to enable the detection of additional PAHs are also possible. Based on the absorbance spectra of PAHs found in extraterrestrial sources, the number of detectable PAHs could be expanded by moving to a shorter wavelength excitation laser. Meteoric PAHs pyrene, benzo[ghi]perylene, and coronene are undetectable with the 404 nm detection system, but would be detectable on a system that uses a 350 nm excitation laser. Excitation at 350 nm would also significantly increase the sensitivity of the MOA for many of the PAHs observed with the current system. Even shorter wavelength lasers may enable the detection of the highly oxidized mellitic acid[26] as well. The MOA is part of the Urey instrument, has been selected for the 2013 ExoMars Mission (see http://astrobiology.berkeley.edu).

2.6 Acknowledgements

We thank the Urey Instrument team for support and comments, and especially Xenia Amashukeli for providing SCWE samples, Andrew Aubrey for providing sublimation samples, and Pascale Ehrenfreund for informative discussion. Microdevices were constructed in the Berkeley Microfabrication Laboratory by Eric Chu. This research was supported by NASA grant number NNX08AR09G and by Jet Propulsion Laboratory contract number 1297596.

Chapter 3 : Enhanced Amine and Amino Acid Analysis Using Pacific Blue and the Mars Organic Analyzer Microchip Capillary Electrophoresis System

3.1 Abstract

The fluorescent amine reactive probe Pacific Blue succinimidyl ester (PB) is used for the detection of trace amounts of amines and amino acids by microchip capillary electrophoresis on the Mars Organic Analyzer (MOA). The spectral and chemical properties of PB provide a 200-fold increase in sensitivity and improved resolution compared to fluorescamine derivatization. With the use of cross injection and PB labeling, the MOA detected amino acids at concentrations as low as 75 pM (sub-parts-per trillion). Micellar electrokinetic chromatography (MEKC) which separates PB-labeled amino acids by their hydrophobicity is also demonstrated. The optimized MEKC conditions (45 mM CHAPSO, pH 6 at 5 °C) effectively separated amines and 25 amino acids with enantiomeric resolution of alanine, serine, and citrulline. Samples from the Yungay Hills region in the Atacama Desert, Chile, and from the Murchison meteorite are successfully analyzed using both techniques, and amino acids are found in the parts-per-billion range. Abiotic amino acids such as β-alanine and ε-aminocaprioc acid are detected along with several neutral and acidic amino acids in the Murchison sample. The Atacama Desert sample is found to contain homochiral L-alanine and L-serine indicating the presence of extant or recently extinct life.

3.2 Introduction

Exploration of our solar system has been fundamentally motivated by the search for organic signatures of extant or extinct life.[120-121] Amino acids are excellent biomarkers in this quest because they have been detected in meteorites[53,122] and comet particles[123] and because of their universal presence in terrestrial biology. Most importantly, the observation of an enantiomeric excess of either the D or L optical isomers and a biologically selected subset of amino acids is viewed to be indicative of life processes.[60] Mars is an excellent candidate to probe for extraterrestrial life because of its proximity to Earth and the multiple lines of evidence indicating the presence of liquid water on its surface at one time.[124-127] However, it is expected that only trace amounts of organics would be found in the topmost accessible layers of soil because of radiative damage.[128] Viking, the only spacecraft to thus far probe Mars for biomarkers, was not able to detect any organics in the Martian regolith using GC/MS technology.[17] Therefore, the ability to sample at depths significantly below the surface and flying an instrument with the highest possible sensitivity is of utmost importance for biomarker detection.

The European Space Agency is developing the ExoMars mission with a primary goal to study the biological environment of the Martian surface and to search for possible Martian life. The Urey instrument, which has been selected to fly on this mission, will utilize the Mars Organic Analyzer (MOA), a portable microfabricated capillary electrophoresis (CE) instrument to detect primary amines and amino acids as well as amino acid chirality. Microfluidic systems, such as the MOA, are excellent for *in situ* analysis because of their small size and mass, their low sample volumes and reagent consumption, their ability to analyze multiple types of analytes, and their integrated automated analysis format.[99,129-130] The MOA has been field-tested in the Panoche Valley, California, and in the Atacama Desert, Chile, successfully analyzing fluorescamine-labeled amino acids at parts-per-billion levels with enantiomeric resolution.[81,103] In further work we have shown that fluorescamine derivatization can also be used to label organic amines, amino sugars, and two of the four nucleobases. The MOA is sensitive enough to

detect amines derived from only 103-104 bacterial cells per gram of soil.[106] These detection capabilities are 3 orders of magnitude better than the GC/MS system used on the Viking missions.

To explore whether even better reagents and methods can be used to enhance the capabilities of the MOA, we explore here the use of a highly fluorescent amine reactive probe, Pacific Blue succinimidyl ester (PB). Pacific Blue has superior optical and chemical properties for detection of bioamines compared to fluorescamine and thus may provide a significant advance. In addition, we wanted to see if improved CE methods like micellar electrokinetic chromatography (MEKC) can improve compositional analysis for complex amino acid mixtures. For real-world testing of PB labeling we have used these two separation formats to analyze standards and two samples thought to be representative of Mars: a sample from the Yungay Hills region of the Atacama Desert and a sample from the Murchison meteorite.

3.3 Materials and Methods

Instrumentation and Microdevice Fabrication. Capillary zone electrophoresis (CZE) and MEKC experiments were conducted on the MOA, a portable microchip CE system with fully integrated optics, high-voltage power supplies, and pneumatics that has been previously described in detail.[103] The instrument includes a 405 nm diode laser with an excitation intensity of 8 mW in the channel. Fluorescence is collected through the excitation objective and directed to a photomultiplier tube (PMT). The optics subsystem has been optimized for the optical properties of Pacific Blue by exchanging the dichroic and replacing the bandpass filter with a 50% T at 425 nm long-pass filter (z405tranDCXR and HQ425lp, respectively, Chroma Technology Corp., Rockingham, VT). Temperature was controlled via a modification to the stage allowing for an externally controlled recirculation bath.

Photolithography and etching was performed using standard wet chemical fabrication technologies.[66-67,131-133] Briefly, a sacrificial amorphous silicon layer was deposited on a 10 cm diameter Borofloat glass wafer by low-pressure chemical vapor deposition. Photoresist was spun-coat and soft-baked at 90 °C for 30 min. Channels were patterned by UV light through a chrome mask with similar layout to previous designs[66-67,81,103,106,134-135] with the exception that the turn geometry has been replaced with tapered or "hyperturns" to reduce band broadening and increase resolution.[136] The microchip design can be seen in Appendix A Figure A.1. Amorphous silicon was removed using a CF_4 plasma etch, and the wafers were isotropically etched with concentrated HF to ultimately produce channels 100 μm wide and 25 μm deep. The effective separation length was 22.6 cm with a total distance of 23.4 cm. Hyperturn sections used a thinner 55 μm channel width with a 2:1 aspect ratio triangle transition at the entrance and exit. Access holes were drilled, and then the wafer was thermally bonded to a blank wafer. Well expanders with 40 μL capacity were fabricated from 3 mm thick poly(dimethylsiloxane) (PDMS) to ameliorate evaporative and hydrodynamic balancing effects.

Electrophoresis Conditions. The microfluidic chip is prepared daily by first cleaning the PDMS well expanders with isopropyl alcohol followed by flowing 150 mM NaOH through the channels. The chip is filled with separation buffer, and a buffer blank is used to further clean the chip via electroosmotic flow. Electrophoresis channels were filled with 4 mM Li_2CO_3 pH 8.5 buffer for analysis. Samples were injected by grounding the sample and cathode, floating the

anode, and applying -1000 V to the waste for 30 s. The potentials were then switched to separation mode by grounding the anode and applying -15 kV to the cathode and -1500 V on the sample and sample waste well for a separation field strength of 650 V/cm. A standard was made up to include amino acids, amines, and diamines that are either signatures of life or bioamines that span the range of possible electrophoretic mobilities for most amine-containing compounds. Resulting electropherograms were baseline-corrected and then filtered using a 0.3% Loess filter via Peakfit (Systat, San Jose).

Sample Preparation. Standards were created from 20 mM stock solutions of amines and amino acids. A 20 mM stock solution of PB (Invitrogen, Carlsbad, CA) dissolved in dimethylformamide (DMF) was prepared and kept frozen (-20 °C) when not in use. Typically, 0.5 μL of the desired amine or amino acid components was pipetted into an Eppendorf tube mixed with 20 μL 4 mM Li_2CO_3 pH 8.5 buffer and a 100% molar ratio excess of Pacific Blue. Amino acids were reacted for 3-4 h and then diluted for analysis in pH 8.5 buffer. Peaks were identified by spiking with the desired amino acid at 4× concentration. For limit of detection (LOD) measurements, sterile procedures were used in a laminar flow hood and serial dilutions were prepared from three independent valine stock solutions. Pacific Blue stock solution (1 μL) was added to a 100 μL aliquot of each concentration of valine and allowed to react overnight (dilution then reaction). All water and buffer solutions were irradiated in Falcon tubes placed directly on the surface of a 4 W UV handheld lamp (UVP, Upland, CA) for at least 24 h to degrade background amino acids prior to reaction. All reaction vessels were thoroughly rinsed with the irradiated water.

Subcritical Water Extraction / Reaction Protocol. A 500 mg sample of Murchison meteorite (USNM6650,2) was provided via collaboration through the Astrobiology Sample Analysis Program at NASA Goddard.[137] Amino acids were extracted via subcritical water extraction as previously described.[115] Briefly, the sample was loaded into a cell and the amino acids were extracted with 8 mL of subcritical water at 200 °C and 3000 MPa with a 5 min equilibration time. The sample was subdivided and freeze-dried. One-sixteenth of the sample extract, corresponding to only 31 mg of meteorite extract, was sent to UC Berkeley for analysis on the MOA. The sample was then rehydrated in 50 μL of 4 mM Li_2CO_3 pH 8.5 buffer and frozen when not in use. For the Atacama sample, amino acids were extracted from 1 g of soil previously collected (AT45_A1) from the Yungay Hills region in the Atacama Desert, Chile,[81,103] via the same subcritical water extraction protocol. The samples were then freeze-dried and resuspended in 500 μL of 4 mM Li_2CO_3 pH 8.5 buffer. This resuspension (200 μL) was then centrifuged and the supernatant used for analysis.

For both the Murchison sample and the Atacama extracts, 7 μL aliquots of the stock were used for analysis. The first aliquot was used to perform a raw sample analysis, whereas the second included a prereaction spike of citrulline (1 μL of 250 μM citrulline) in order to normalize for the degree of reaction, and the third included a post-reaction spike to aid in peak identification. To each 7 μL of subcritical water extract, 7 μL of pH 8.5 buffer and 7 μL of the Pacific Blue stock solution were added and allowed to react for 2 h. The solution was then brought to a final volume of 100 μL and further diluted as needed with buffer for analysis. A 7-fold dilution was used on both samples for amino acid quantification, and dilutions of 20-80-fold were used to quantify amine concentration.

3.4 Results and Discussion

Pacific Blue Chemistry. The MOA was originally developed for the analysis of fluorescamine derivatized amino acids[103] and for the detection of organics with naturally occurring fluorescence such as polycyclic aromatic hydrocarbons (PAHs).[138] Although the MOA has demonstrated high sensitivity for organic amine detection, enhancing the sensitivity with an improved derivitization agent is essential given the low levels of organics expected on Mars.[113] Pacific Blue succinimidyl ester is expected to be a brighter amine reactive probe than fluorescamine because it has a larger extinction coefficient (46 000 vs 7800 cm/mol), a higher fluorescence quantum yield (0.78 vs 0.11), and improved NHS (N-hydroxy succinimide) reaction chemistry.[139] Reactions are performed at a pH of 8.5 and occur by nucleophilic addition of a deprotonated amine nitrogen to the carbonyl group of the dye (see Scheme 3.1). N-Hydroxy succinimide is a good leaving group, and a molar excess of dye enables pseudo-first-order kinetics which pushes the reaction kinetics to the product side. Amino acid derivatization by PB reaches 90% completion in approximately 15 min, and the amide reaction products are very stable. For these reasons, the performance of PB for enhanced bioamine detection with the MOA was explored.

Capillary Zone Electrophoresis. A microchip electropherogram of a Pacific Blue labeled standard is presented in Figure 3.1A. Glutamic and aspartic acid have a net charge of -2 after labeling and elute last, while most neutral amino acids (net charge -1 after labeling) elute in the middle grouping and are separated by the size/shape of the different side chains. Amines and basic amino acids are neutral and elute first. Peak efficiencies are on average ~1,000,000 plates per meter, and nearly all peaks are baseline-resolved. The enhanced resolution and peak efficiencies are derived from the chemical nature of Pacific Blue. Pacific Blue contains two fluorines, a hydroxyl group, and a carbonyl making it very hydrophilic. These chemical properties reduce interactions between labeled amino acids and the surfaces inside the microchip thereby reducing band broadening and increasing peak efficiencies. Separation parameters (e.g., salt concentration, buffer pH, temperature) were optimized and found to follow separation trends previously observed for fluorescamine.[67,103,106,134] Lowering the temperature to a practical terrestrial limit (4-10 °C) yielded the most significant improvement in resolution. Lithium carbonate was used instead of sodium carbonate because of its decreased electrophoretic mobility and smaller separation currents.

Pacific Blue and its hydrolysis products are naturally fluorescent and appear as unique peaks in the electropherogram at 109 and 116 s. These peaks do not coelute with standard amino acids and are used as an internal reference to monitor changes in electroosmotic flow and as an internal standard. Because the effective electrophoretic mobility (elution time) of an amino acid is relative to that of the electroosmotic flow, amino acid peaks can be calibrated to the known standard by compressing or expanding the time scale based on the PB standard peaks. The unreacted Pacific Blue peak (which coelutes with propylamine) also serves as a reference for the degree of reaction.

Micellar Electrokinetic Chromatography. Standard microchip electrophoresis has the ability to separate amino acids (or amines) based on a single methyl unit difference in optimal cases; however, as the size of the amino acid side chain increases, the differential resolving power of this technique diminishes. Additionally, functional groups such as alcohols, thiols, guanidinium can induce similar charge/friction ratios, and thus many amino acids intrinsically

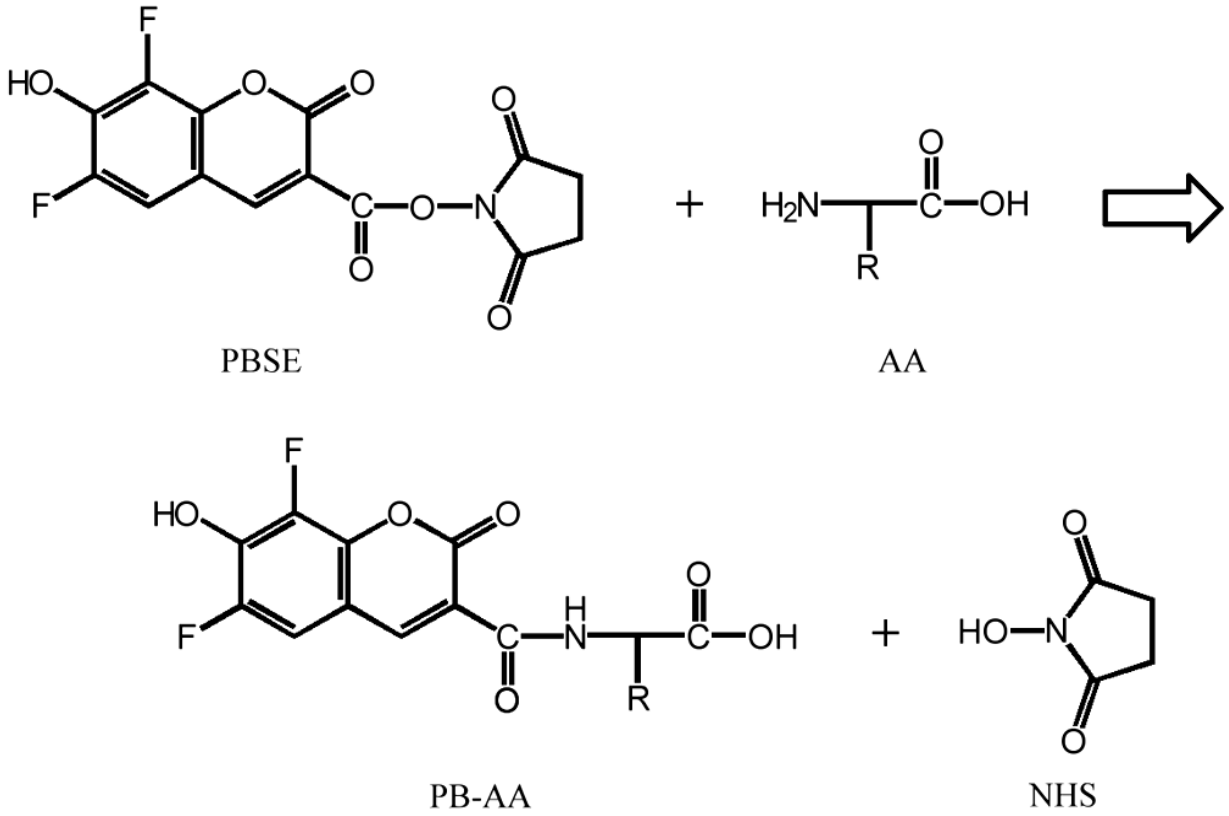
F
HO
O
O
F
C
O
N
O
O
O
+
H2N
C
OH
R
PBSE
AA
F
HO
O
O
F
C
H
N
O
C
OH
O
R
+
HO
N
O
O
PB-AA
NHS

Scheme 3.1

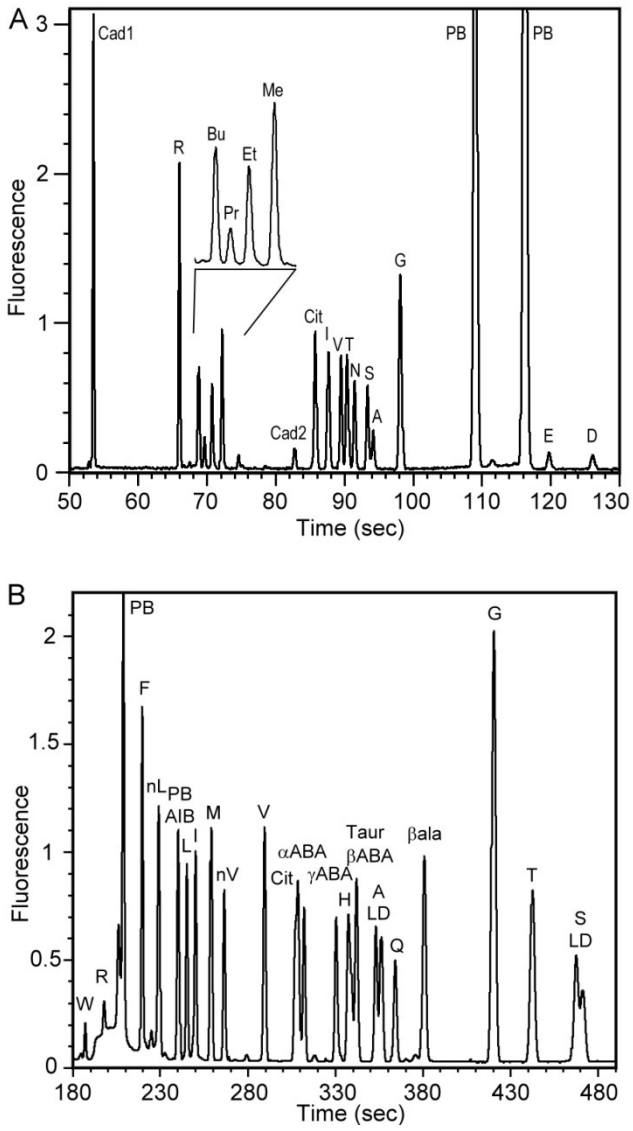

Figure 3.1. Optimized separations of the Pacific Blue labeled Mars 16 standard.

(A) Microchip electrophoresis separation of the Pacific Blue labeled Mars 16 standard by zone electrophoresis in 4 mM Li_2CO_3 pH 8.5 buffer at 10 ^oC and 650 V/cm. Amino acids are designated by their one letter abbreviation. Citrulline, a urea cycle intermediate, is designated Cit. The separation of methyl, ethyl, propyl, and butyl amine (Me, Et, Pr, Bu) are shown in the inset for clarity. Cadaverine, a representative biological diamine, has two peaks labeled Cad1 and Cad2. Pacific Blue related peaks (PB), act as an internal mobility standard. (B) Optimized MEKC separation of Pacific Blue labeled amino acids in 4 mM Li_2CO_3 45 mM CHAPSO pH 6.5 at 10 ^oC. Several non-proteogenic amino acids (norleucine, norvaline, aminoisobutyric acid, γ-aminobutyric acid, β-aminobutyric acid, α-aminobutyric acid, and β-alanine) are well separated from their proteogenic counterparts. Enantiomeric separation is achieved for citrulline, alanine and serine.

have similar electrophoretic mobility. To address this issue, we explored separation technologies based on micellar elecktrokinetic chromatography (MEKC).[132,140-141] MEKC uses a pseudostationary phase composed of running buffer and a surfactant above its critical micelle concentration (cmc). MEKC is advantageous because it separates amino acids based on differential hydrophobicity. During electrophoresis each amino acid partitions into and out of the hydrophobic core of the micelle based on the net interaction between the Pacific Blue labeled amino acid reaction product and the micelle. Amino acids with a larger degree of hydrophobicity preferentially partition into the hydrophobic core of the micelle and migrate with electroosmotic flow compared to hydrophilic amino acids that are excluded from the micelle and migrate according to their intrinsic electrophoretic mobility.

A variety of surfactants were examined to determine that most effective for MEKC separations; several were found to be ineffective such as the ionic sodium dodecyl sulfate (SDS), and neutral Tween, and Triton. A zwitterionic surfactant, such as CHAPSO, is evidently needed in order to create the proper interaction with the PB amino acid complex. This observation is consistent with previous MEKC studies where a zwitterionic label (TRITC) was used with a negatively charged surfactant (SDS).[132] Cationic surfactants were not tested to avoid fouling of microchannel surfaces via ionic attraction to the negatively charged glass walls.

CHAPSO was optimized for the separation of amino acids above the cmc (8 mM at 20 °C and 50 mM Na^+). Low concentrations of CHAPSO (near the cmc) had reduced ability to distinguish between hydrophobic amino acids such as isoleucine and leucine, whereas extremely high concentrations yielded slower separations, over-resolved hydrophobic amino acids, and the loss of hydrophilic amino acid resolution. An intermediate concentration of 45 mM CHAPSO was used for subsequent MEKC separations. Electropherograms showing the effects of running buffer pH are shown in Appendix C Figure C.1A. The speed of the separation is highly dependent on pH (because of the dependence of electroosmotic flow on pH), and a more basic running buffer leads to faster separations. The separation is complete in ~200 s at pH 9 and 600 s at pH 6. The resolution of the separation increases over all hydrophobicity ranges with decreasing pH because of the increased effective separation length. The analysis time is a strong function of temperature and increases with decreasing temperature (Appendix C Figure C.1B). However, resolution and peak efficiencies dramatically improve with decreasing temperature such that all amino acids with hydrophobicity below that of glycine are baseline-resolved at 5 °C. At 20 °C cysteine elutes prior to alanine, coelutes with D/L-alanine at 10 and 15 °C, respectively, and elutes after alanine at 5 °C. Glutamic and aspartic acid have much longer migration times and are best analyzed by the standard zone electrophoresis method.

The conditions that yield the best separation for amino acids by MEKC (including chirality, see below) are therefore achieved at 5 °C using the 4 mM Li_2CO_3 pH 6 running buffer containing 45 mM CHAPSO. However, as a matter of practicality, a pH 6.5 running buffer is used to decrease analysis time and an analysis temperature of 10 °C is used to avoid condensation and resulting arcing problems that hamper terrestrial operations. These conditions still yield over one million plates/meter and do not impact resolution significantly. A separation performed using the conditions optimized for terrestrial analysis is presented in Figure 3.1B. Most amino acids are baseline-resolved or better, and the peak capacity of MEKC separations is much greater than that of CZE techniques. Several nonproteogenic amino acids (norleucine, norvaline, aminoisobutyric acid, γ-aminobutyric acid, β-aminobutyric acid, α-aminobutyric acid,

and β-alanine) are well separated from their proteogenic counterparts. Clearly resolved enantiomeric peaks for L-alanine from D-alanine can be seen at 350 s and those for L-serine and D-serine at 470 (resolution 0.73 and 0.58, respectively). The chiral separations result from the differential interaction between the L- and D-forms of amino acids and the chiral center on the CHAPSO surfactant used to create the micelles. MEKC provides a separation with higher peak capacity, the ability to distinguish between proteogenic and nonproteogenic amino acids, and can give an indication of biotic or abiotic origin based on the chirality ratio of a limited set of amino acids.

Pacific Blue Limit of Detection Analysis. The overall sensitivity of the MOA with Pacific Blue labeling was tested with valine. Figure 3.2 presents measurements made from a series of independent serially diluted valine stock solutions (dilution followed by reaction) for both CZE and MEKC separations. Both the detector settings of the PMT and the background noise level were constant. The upper bound of the dynamic range of the MOA was ~3 μM valine (the largest concentration measurable without dilution). The LOD at a signal-to-noise ratio (S/N) of 3 for PB-valine is 75 pM for separations performed by zone electrophoresis and 80 pM for MEKC. This represents sub-parts-per-trillion analysis capabilities and a 200-fold increase in sensitivity compared to previous methods utilizing fluorescamine (LOD = 13 nM). This increase in sensitivity is attributed to both the enhanced optical and chemical properties of Pacific Blue. The sublinear dependency of S/N on concentration is most likely due to PB reagent depletion at the higher amino acid concentrations convolved with the partial hydrolysis of the active PB reagent. The labeling efficiency is nearly independent of amino acid side chain except for those with steric hindrances such as aminoisobutyric acid (AIB). The reduced labeling efficiency of AIB relative to other amino acids such as valine follows previously observed trends. An injection bias exists in both separation formats: In CZE, net neutral analytes are preferentially injected, whereas glutamic and aspartic acid are poorly injected and need ~5× the concentration for equivalent signals. MEKC has a less severe injection bias compared to CZE but preferentially injects hydrophobic amino acids. Relative to valine, phenylalanine peaks are 150% more intense and serine signals are half as intense. In previous work, Skelley et al. detected 500 attomol of valine extracted via acid hydrolysis per *E. coli* cell on the MOA. By collecting the sample in a 10 μL volume and using Pacific Blue, the performance reported here should enable the detection of valine from as few as 10 *E. coli* cells per gram of soil.

The ability to perform two orthogonal separations on the same sample enables the use of pseudo-two-dimensional (2D) analysis techniques to improve our ability to identify components. The CZE and MEKC electrophoretic mobility was determined for the common set of 20 biotic amino acids along with some abiotic amino acids. The relative electrophoretic mobility of 29 different amino acids in an optimized MEKC separation has been plotted as a function of its relative mobility in CZE in Figure 3.3. The subset of neutral amino acids that would otherwise coelute using CZE are well resolved using MEKC. Additionally, the identity and concentrations of a peak or peak set can be determined by crosscorrelating the peak heights and elution profiles from the two separation methods. This result demonstrates the well-known enhanced analysis power that is provided by performing two orthogonal separations.[142]

Analysis of Astrobiological Samples. Two samples of interest to the astrobiology community were tested to explore the efficacy of our analysis techniques using Pacific Blue. The Murchison meteorite (USNM6650,2) is of interest because of its nonterrestrial origin and

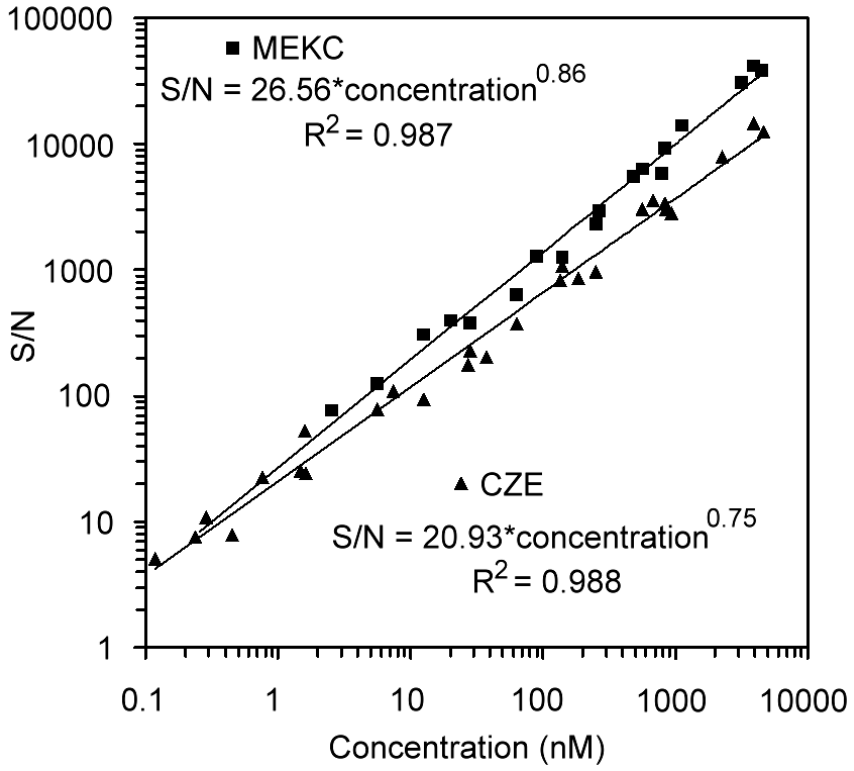

Figure 3.2. Signal to noise ratio as a function of valine concentration for capillary zone electrophoresis (triangles) and micellar electrokinetic chromatography separations (squares).

The limit of detection was calculated to be 75 pM and 80 pM at a signal to noise ratio of 3 for CZE and MEKC, respectively.

because it has been previously analyzed and found to contain many nonproteogenic amino acids such as β-alanine and 2-aminoisobutyric acid.[53,143-144] The second sample is a Martian analogue sample from the duracrust of the Yungay Hills region of the Atacama Desert, Chile (AT45_A1). The Yungay Hills region of the Atacama Desert is one of the driest regions on Earth receiving less than 1 mm of precipitation per year and represents the dry limit of microbial life on Earth.[145] Both CZE and MEKC analysis were performed on subcritical water extracts prepared at JPL.

Figure 3.4A presents the CZE analysis of the Murchison meteorite extract. Even though the analysis was performed on the equivalent of only 31 mg of meteorite, the sample required significant dilution in order to bring most peaks on scale. The sample has a significant amount of complexity and contains ammonia, amines, diamines, and amino acids. Peaks were identified in independent experiments by spiking a standard and calibration to Pacific Blue elution times. The acidic amino acids aspartic and glutamic acid elute at 118 and 124 s along with an additional peak at 128 s that may be amino malonic acid (R group = COOH) due to its mobility relative to glutamic and aspartic acid and previous reports of malonic acids in Murchison;[146] however, this was unverified because of the lack of a commercial comparison. The peaks from 64-66 s appear in the time range expected for lysine; however, because of the large background signal in this region a conclusive identification cannot be made. An unlabeled peak at 85 s is most likely due to several coeluting amino acids with electrophoretic drag greater than isoleucine but less than citrulline.

The MEKC analysis of the Murchison extract is shown in Figure 3.4B. Peaks that showed no significant increase in signal over those from the instrumental blank are marked with an asterisk. The instrumental blank is an analysis performed on a subcritical water extraction of an empty extraction cell (no soil) to monitor differential sample carryover. The hydrophilic amino acids serine, threonine, and glycine are easily identified between 390 and 490 s. Several nonproteogenic amino acids (norleucine, ε-aminocaprioc acid, aminoisobutyric acid, γ-aminobutyric acid, β-aminobutyric acid, α-aminobutyric acid, and β-alanine) are identified. As a result of both the increased sensitivity and enhanced separation power afforded by Pacific Blue, there are several small peaks that are detected but not identified. Extraction of amino acids from a larger starting mass of meteorite and the use of a more encompassing amino acid standard set will help to identify these peaks in the future. A significant chiral excess of the L-forms of alanine and serine is seen. Although some of this excess can be attributed to the background levels of L amino acids found in the instrumental blank, it is likely the primary contributor to the excess L-amino acids is the unavoidable terrestrial contamination that is significant compared to the amino acids extracted from the equivalent of only 31 mg of sample source.[147-148] A separate portion of the same subcritical water extract was analyzed in parallel at NASA Goddard by LC/MS and found to have similar amino acid composition and D/L ratios as observed here. This demonstrates that the putative terrestrial contamination was introduced upstream of the MOA analysis process and that the MOA is equivalent to the current recognized laboratory standards. Table 3.1 summarizes the results from the Murchison sample.

Figure 3.5A presents the CZE analysis of soil extract taken from top 3 cm of site 45 in the Yungay Hills region of the Atacama Desert.[81] Previous fluorescamine-based analysis was only able to detect methyl and ethyl amines above the blank in the duracrust from this region. However, the increased sensitivity provided by Pacific Blue based analysis now allows the identification of many additional amino acid components in this sample. This analysis (both

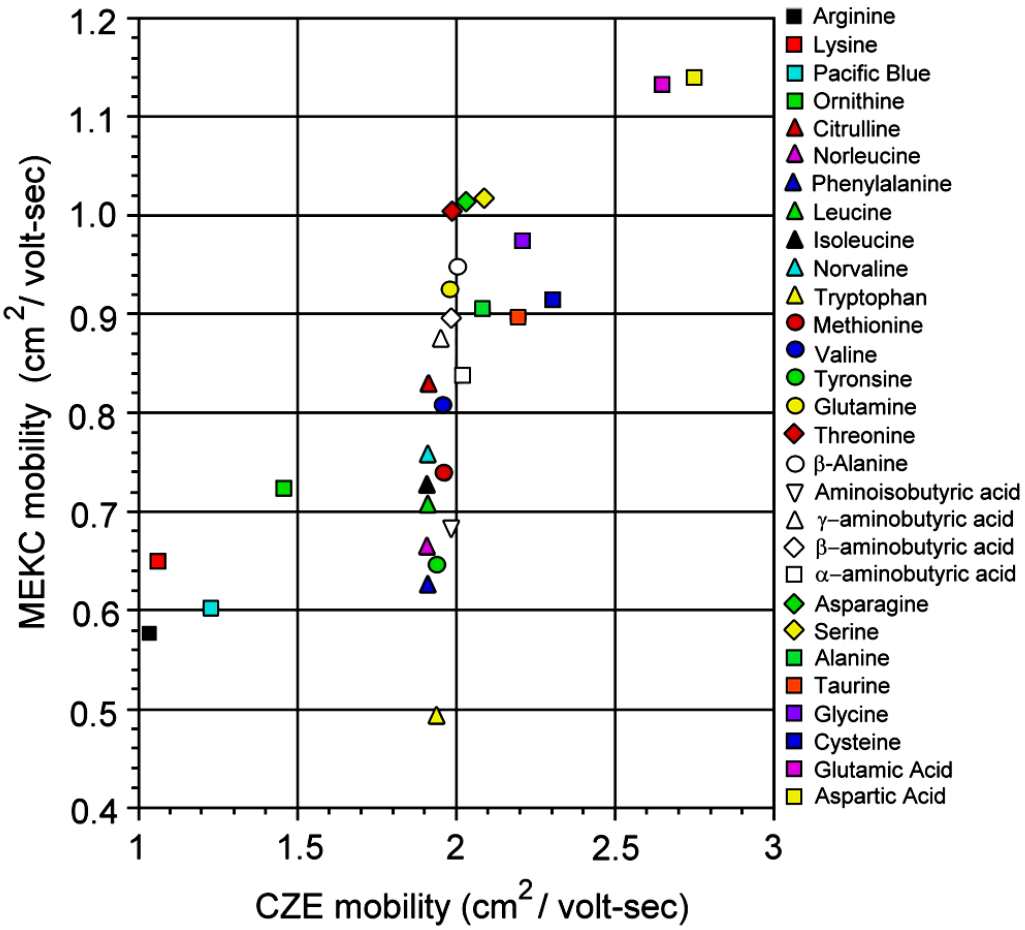

Figure 3.3. Psuedo 2D mobility diagram of 29 representative biotic and abiotic amino acids.

Many of the neutral amino acids co-elute in CZE but are well separated by MEKC in the vertical dimension.

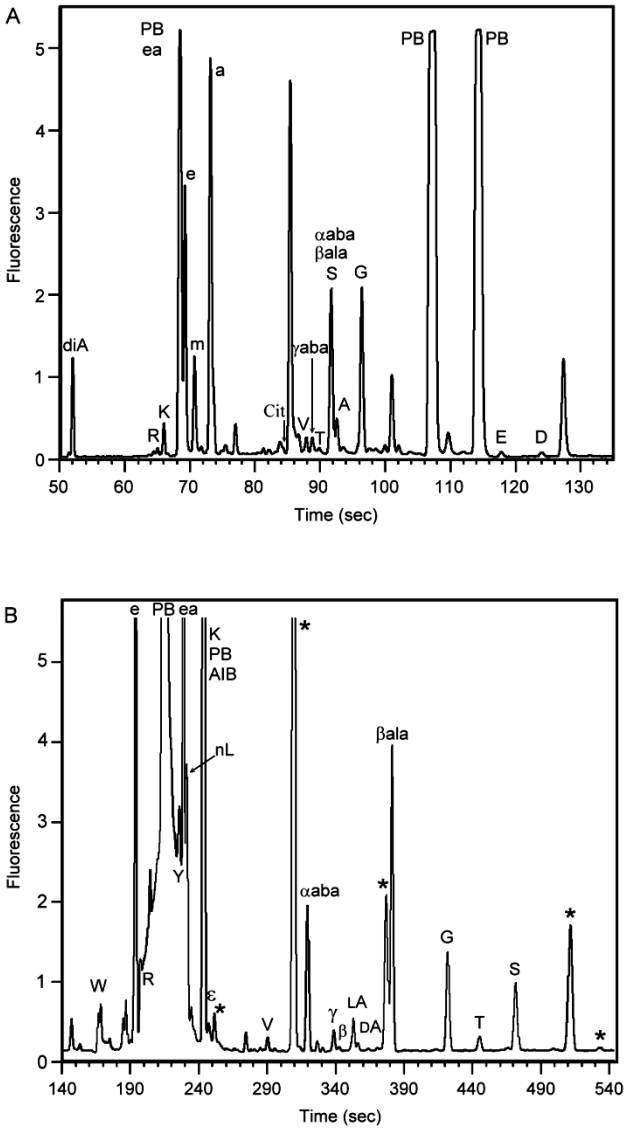

Figure 3.4. Microchip electrophoretic analysis of the sub-critical water extract from 6.25 mg of the Murchison Meteorite USNM6650,2 by (A) capillary zone electrophoresis and (B) MEKC.

Peaks having signals equivalent to the blank are marked with asterisks. The reaction product was diluted seven-fold for analysis. Amino acids are designated by their one-letter designations. Ammonia, methylamine, ethylamine, and ethanolamine are designated a, m, e, ea respectively. Peaks were identified by their mobility relative to the Pacific Blue peaks (PB) and by spiking.

resolution and limits of detection) was hindered by the presence of a high concentration of salt in the sample that caused dispersion of the peaks. The high salt concentration also led to poor injection efficiency under standard injection conditions. A longer 150 s cross injection was used (instead of the standard 30 s step) to bias the injection to lower mobility amino acid species. Concentrations of amino acids for this modified injection scheme were calculated based on experiments including an internal citrulline standard of known concentration and postreaction spikes of an amino acid standard. The dispersion effects can be diminished by further diluting the sample; however, the amino acids are proportionally diluted. In this sample, alanine appears as a shoulder on the serine peak because of salt effects, but its calculated concentration is consistent with the MEKC results which are less affected by the presence of salt. Several amino acids coelute before valine at 84 s and are tentatively identified as leucine, isoleucine, and phenylalanine. A large peak nearly comigrating with serine at 89 s is β-alanine.

The MEKC analysis of the Atacama Desert sample is shown in Figure 3.5B. The extended injection was used for this analysis, and peaks that have the same magnitude in the blank are marked with an asterisk. Several proteogenic amino acids are detected such as serine, threonine, glycine, glutamine, alanine, valine, isoleucine, and phenylalanine. Other amino acids detected are β-alanine, and ε-aminocaprioc acid and unidentified peaks at 215, 220, 316, and 320s. Glutamine is normally converted to glutamic acid during the subcritical water extraction process so its presence either indicates a large abundance in the sample or an extraction anomaly. The insets of this electropherogram show a magnified view of the alanine and serine peaks in the sample along with the sample spiked with an amino acid standard including a 1:1 ratio of LD alanine and serine. Comparison of these two traces indicates that the sample is nearly homochiral L alanine and L serine. The D/L ratio of alanine and serine was calculated to be 0.014 and 0.008, respectively, indicating that this sample is derived from recent extinct or extant terrestrial organisms. Skelley et al. determined that there is 500 attomol of valine per *E. coli* cell.[106] This value was used to calculate an equivalent of ~850,000 *E. coli* cells/gram of soil in this sample which is consistent with cell culture experiments.[149] Table 3.1 summarizes the results from the Atacama sample.

3.5 Conclusions

The search for organic compounds in our solar system that are derived from life requires the ability to detect molecules with the highest possible sensitivity. We show here that Pacific Blue derivatized amino acids offer superior optical and chemical properties for amine biomarker detection yielding sub-parts-per trillion analysis capabilities, or a 200-fold increase in sensitivity, compared to fluorescamine. MEKC separations provide an orthogonal method for the enhanced identification of amino acids with minimal loss in sensitivity and a minimal increase in analysis complexity. A variety of biotic and abiotic amino acids have been analyzed in two samples thought to be representative of Mars: the extraterrestrial Murchison meteorite and a Martian analogue sample from the Atacama Desert. Analysis of the Murchison meteorite demonstrates the ability of the MOA with PB labeling to successfully analyze amines and amino acids from an extraterrestrial object. The analysis of the Atacama soil sample using PB successfully detected chiral amino acids indicative of life at a level 850K cell equivalents per gram of soil. Given that information on the chemical nature of Martian soil is very limited and that concentrations of organics are likely to be low, the parallel and orthogonal detection technologies presented here

Table 3.1 Amines and Amino Acids in Astrobiological Samples

		Murchison (ppb)[a,b]	Atacama (ppb)[a,c]
amino acids common to both samples	glycine	1273.9	28.5
	threonine	211.4	260.4
	valine	208.8	42.3
	β-alanine	1859.5	775.9
	ε-aminocaprioc acid	295.4	384.6
chiral analysis	L-alanine	659.8	95.9
	D-alanine	174.8	1.3
	L-serine	838.6	231.6
	D-serine	75.6	1.9
amino acids found in only one sample	norleucine	808.7	
	α-aminobutyric acid	1394.7	
	β-aminobutyric acid	443.3	
	tyrosine	286.2	
	tryptophan	525.4	
	citrulline		68.0
	lysine		59.8
	arginine		235.3
	isoleucine		21.0
	phenylalanine		173.7
	glutamine		4.7
	taurine		6.0
acidic amino acids	aspartic acid	123.71	376.1
	glutamic acid	117.83	
	aminomalonic acid	576.76	
amines	ammonia	667.9	103.6
	methylamine	231.6	40.8
	ethylamine	940.0	182.7

[a] Concentration calculated by CZE and MEKC assuming 100% recovery during subcritical water extraction. [b] Analysis completed from the equivalent of 31 mg of the Murchison meteorite—extracted from USNM6650,2. [c] Analysis performed on 1 g of duracrust from Yungay Hills Atacama Desert, Chile, AT45_A1.

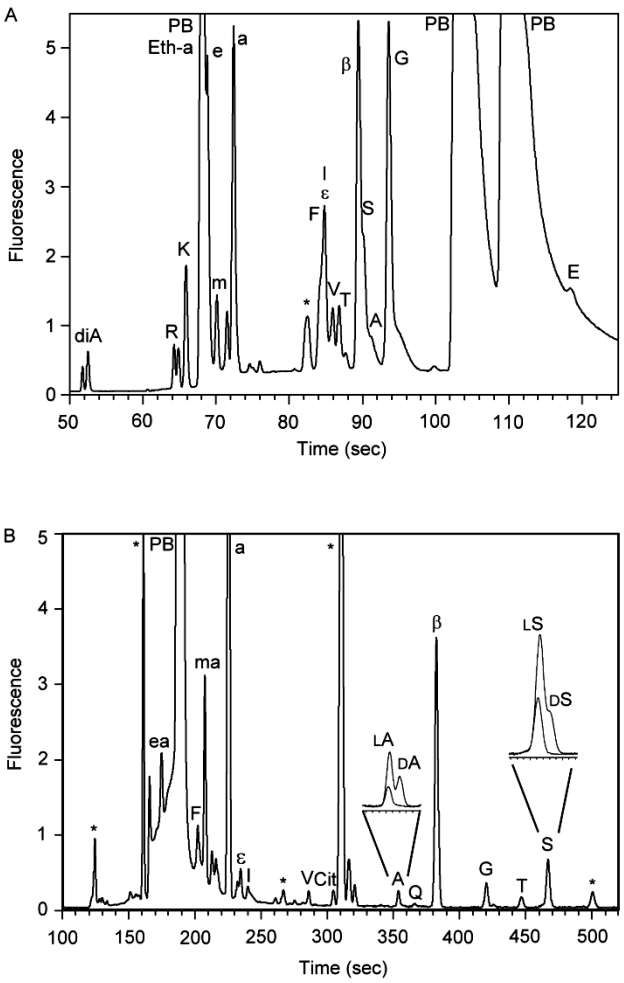

Figure 3.5. Microchip electrophoretic analysis of the sub-critical water extract from 1 g of duracrust from the Yungay Hills region of the Atacama Desert, Chile, AT45_A1 by (A) capillary zone electrophoresis and (B) MEKC.

Peaks having signals equivalent to the blank are marked with asterisks. The reaction product was diluted seven-fold for analysis. Standard amino acids are designated by their one-letter designations. Ammonia, methylamine, ethylamine, and ethanolamine are designated a, m, e, ea respectively. Peaks were identified by their mobility relative to the Pacific Blue peaks (PB) and by spiking. The inset of (B) shows a magnified view of the sample and sample spiked with a 1:1 ratio of LD alanine and serine.

together with high-sensitivity PB labeling will be advantageous for unambiguous bioamine detection and identification on Mars and on other planets in our solar system. For more information on the development of the MOA for planetary exploration see http://astrobiology.berkeley.edu.

3.6 Acknowledgements

We acknowledge the assistance of the international Urey Instrument Team as well as the ASAP participants in the course of this research. Microfabrication was carried out at the University of California, Berkeley, Microfabrication Laboratory. This research was supported by NASA Grants NNG04GB75G and NNX08AR09G and by the Jet Propulsion Laboratory at Cal Tech under contract no. 1297596.

Chapter 4 : Capillary Electrophoresis Analysis of Organic Amines and Amino Acids in Saline and Acidic Samples Using the Mars Organic Analyzer

Reprinted with permission from "Capillary Elelctrophoresis Analysis of Organic Amines and Amino Acids in Saline and Acidic Samples Using the Mars Organic Analyzer," by Amanda M. Stockton, Thomas N. Chiesl, Tim K. Lowenstein, Xenia Amashukeli, Frank Grunthaner, and Richard A. Mathies (2009) *Astrobiology* **9**(9), 823-831.

4.1 Abstract

The Mars Organic Analyzer (MOA) has enabled the sensitive detection of amino acid and amine biomarkers in laboratory standards and in a variety of field sample tests. However, the MOA is challenged when samples are extremely acidic and saline or contain polyvalent cations. Here, we optimize the MOA analysis, sample labeling, and sample dilution buffers to more robustly handle such challenging samples. Higher ionic strength buffer systems with pK_a's near pH 9 are developed to provide better buffering capacity and salt tolerance. The addition of ethylaminediaminetetraacetic acid (EDTA) is shown to effectively neutralize the negative effects of multivalent cations. The optimized protocol utilizes a 75 mM borate buffer (pH 9.5) for Pacific Blue labeling of amines and amino acids. After labeling, 50 mM (final concentration) EDTA is added to samples containing divalent cations to ameliorate their effects. This optimized protocol is used to successfully analyze amino acids in a saturated brine sample from Saline Valley, California, and a subcritical water extract of a highly acidic sample from the Rio Tinto, Spain. This work expands the analytical capabilities of the MOA and increases its sensitivity and robustness for samples from extraterrestrial environments that may exhibit pH and salt extremes as well as metal ions.

4.2 Introduction

Exploration of Mars and other Solar System bodies for chemical signatures of life requires that we prepare for diverse and unexpected chemistries. In 1976, the Viking landers performed the first experiments to detect signs of past or present Martian life. No organic molecules of Martian origin were detected by its gas chromatograph – mass spectrometer (GC-MS)[18], and the biology experiments were considered ambiguous.[14-15] These observations have been attributed to sterilizing radiation,[26] the presence of a strong oxidant in the regolith[15,150] and the conversion of organic molecules to acids and amines during the pyrolysis extraction.[26,151] In 1997, the Pathfinder rover Sojourner characterized Martian soil and rocks using X-ray fluorescence[19] and identified and quantified a range of minerals in the regolith, including MgO (8 %), CaO (7 %), and FeO (17 %). In 2004, the Mars Exploration Rover Opportunity discovered jarosite (K, Na)$Fe_3(SO_4)_2(OH)_6$[20] and other mineralogical evidence of ancient near surface ground water.[21] The strong acidity and salinity of the ancient ground waters suggested by Opportunity's data does not preclude the potential of extinct life. For example, terrestrial extremophilic organisms thrive in environments ranging from the hypersaline (3-5 M NaCl),[28] to the highly acidic (pH < 2),[28-29] to the extremely cold (-17 ^{o}C).[29] Furthermore, Phoenix recently observed extant Martian water ice near the northern Martian pole.

Evidence of saline and acidic environments has also been found on other astrobiological targets. The significant amounts of CO_2 measured by Cassini in Enceladus's water vapor plume[42] may be indicative of subsurface chemistry rich in carbonic acid. Spectra taken by Galileo's near-infrared mapping spectrometer of Europa's surface have suggested that it is paved in areas with hydrated salts[37] and that sulfuric acid is a major component of its surface.[36] These challenging environments suggest that organic molecules and potential biomarkers, if present, will be at very low concentrations, making it critical that future planetary exploration instruments be as sensitive as possible while remaining independent of the input sample chemistry.

In the search for extraterrestrial life, amino acids are well justified target molecules due to their ubiquity in life on Earth and the large amount of information that can be obtained from measurement of their concentration, composition and chirality.[60] Racemic mixtures of amino acids have also been found in a number of extraterrestrial sources, including Martian meteorites,[48] and carbonaceous chondrite meteorites.[53] Racemic mixtures indicate an abiological source, while homochiral amino acid composition provides strong evidence of extant or recently extinct life;[60] the degree of their racemization provides a measure of the age of extinct biota.[152] However, it is important not to limit our search to a single compound class. Amines,[81] nucleobases,[106] polycyclic aromatic hydrocarbons (PAHs),[138] and other organic molecules[67] are also important chemical markers and help to define whether the chemistry of an extraterrestrial sample is prebiotic, extant biotic, or extinct biotic.

The Mars Organic Analyzer (MOA)[103] is a portable lab-on-a-chip microcapillary electrophoresis (μCE) instrument that contains all the necessary microfluidics, optics and electronics for CE analysis. We have previously used the MOA to detect fluorescamine-labeled primary amines, amino acids,[103] nucleobases,[106] and PAHs,[138] and to determine the chirality of amino acids.[67] The MOA was successfully field tested in the Panoche Valley, CA,[103] and in the Atacama Desert.[81] Recent work using Pacific Blue succinimidyl ester (PB) as the labeling reagent has enhanced MOA sensitivity to the parts-per-trillion (pptr) level.[69] PB labeling also enables the performance of micellar electrokinetic chromatography (MEKC) for pseudo-2D separations and thus dramatically enhances compositional analysis.[69]

The application of the MOA to real-world samples requires that we enhance the robustness of the assay to varying sample characteristics. For example, samples with extreme salinity cause dispersive effects during μCE injection and lead to poor resolution and signal loss.[74] Extremely acidic samples provide challenges due to inhibition of the labeling reaction[83] and cessation of the electro-osmotic flow (EOF) in the separation channels, both of which dramatically reduce signal. Furthermore, multivalent cations can alter the surface chemistry of the μCE channels and also lead to dispersive effects and EOF inhibition.[84] Since the concentrations of organic biomarkers expected on Mars may be low, it is crucial to enhance the MOA's tolerance to highly saline, acidic, or ionic samples. Here we explore the assay conditions and buffers that are necessary to analyze samples containing high levels of acid, salts and multivalent cations, and determine optimal labeling and analysis protocols. These optimized formats are then used to successfully analyze two samples from representative extreme environments: saturated brine from Saline Valley, CA, and a subcritical water extract from the acidic Rio Tinto in Spain.

4.3 Materials and Methods

Buffer and sample preparation. Lithium carbonate, sodium tetraborate, and sodium phosphate were obtained from Sigma-Aldrich (St. Louis, MO). Stock solutions of 100 mM carbonate, 100 mM phosphate, and 400 mM borate were prepared. The carbonate stock was adjusted to pH 8.5 using 100 mM HCl. Phosphate (pH 9.0) and borate (pH 9.5) were used without pH adjustment. Both the disodium and tetrasodium salts of ethylamine diamine tetraacetic acid (EDTA) were obtained from Fischer Scientific (Pittsburgh, PA), and combined to produce a 250 mM, pH 7.0 aqueous stock solution. Racemic stock solutions (20 mM in water)

were prepared for each amino acid (Sigma-Aldrich), and combined in appropriate volumes. Pacific Blue succinimidyl ester (PB) (ex. 405 nm, em. 425 nm) was obtained from Invitrogen (Carlsbad, CA) and dissolved to 20 mM in N,N-dimethylformamide and stored at -20 ^{o}C. Fluorescamine (Sigma Aldrich) stock solution (20 mM) was prepared in dimethylsulfoxide (DMSO, Sigma Aldrich).

A stock solution of an amino acid standard containing equal 40 μM concentrations of citrulline, valine, serine, alanine, glycine, aspartic acid, and glutamic acid was prepared. Labeling reactions were conducted by combining one part each of the amino acid stock and buffer, then adding two parts PB stock solution. The labeling mixture was allowed to react overnight at room temperature before dilution for analysis. This standard was diluted to 400 nM of each amino acid with the appropriate buffers for each experiment. Analysis was conducted by filling the separation column and wells with the analysis buffer, then replacing the solution in the sample well with the diluted, labeled amino acid standard. Electropherograms were analyzed using Peak Fit to determine the signal-to-noise, resolution, and peak efficiency in theoretical plates per meter for each amino acid peak.

To determine the effect of EDTA on labeling reaction, buffer solutions were prepared containing EDTA concentrations ranging from 0 to 200 mM in 30 mM borate buffer (pH 9.5). Reactions containing 20 μM glycine and 400 μM fluorescamine were conducted in these buffer solutions. After a five minute reaction, each sample was diluted to a final concentration of 133 nM glycine, 2.7 μM fluorescamine in its respective buffer. Fluorescence intensity measurements were then taken on a Jasco FP-750 spectrofluorometer.

Saline Valley and Rio Tinto samples were labeled by a standard protocol and an optimized protocol. The optimized protocol consisted of combining 5 μL of the sample with 20 μL 75 mM borate (pH 9.5) and adding 10 μL PB stock. After an overnight reaction at room temperature, water and 250 mM EDTA were added to the labeled Rio Tinto sample to provide a final 10-fold dilution with final EDTA and borate concentrations of 50 mM and 30 mM, respectively. The Saline Valley sample was allowed to react for 30 min; water was then added to provide a final 10-fold dilution of the sample with borate concentration of 30 mM. The standard method was conducted in an identical manner, using 4 mM carbonate buffer (pH 8.5) in place of all borate and borate/EDTA buffers. Samples labeled via the optimized method were analyzed with 30 mM borate in the separation column, and samples labeled via the standard method were analyzed using 4 mM carbonate in the separation column.

Salt sample SV07-4 was obtained from the Saline Valley, California[153-154] and was labeled according to both the standard method and the optimized protocol. A sediment sample from the Rio Tinto, KF03-136,[155] was obtained as part of the Astrobiology Sample Analysis Program (ASAP).[137] A subcritical water extraction (SCWE) was performed by collaborators at the Jet Propulsion Laboratory (JPL) on 500 mg of sample.[115] One sixteenth of the total extract was freeze-dried and resuspended in 400 μL 4 mM carbonate, pH 8.5 for analysis.

Microdevice fabrication. The microdevices were prepared as previously described.[67,103,106,138] In summary, a sacrificial layer of polysilicon was deposited via chemical vapor deposition on a 10-cm borofloat glass wafer. A layer of photoresist was then spin-coated onto the wafer and patterned through a chrome mask using a contact aligner. After the

photoresist was developed, the exposed polysilicon was removed by plasma etching. Etching in buffered HF produced 23.6 cm long folded separation channels 100 μm wide and 25 μm deep. After removing photoresist, reservoir holes were drilled, the polysilicon layer was removed, and the wafer was bonded to a blank wafer to form completed channels. Injections were performed via a 1.2-cm long cross-channel located 0.6 cm from the anode end of the channel. A 3-mm deep PDMS gasket with 4-mm diameter wells is placed over the reservoir holes to allow for larger volume. A schematic of the microdevice has been published and is presented in Appendix A.[69,138]

Mars Organic Analyzer. The Mars Organic Analyzer[103] was used with minor modifications to the optical subsystem that allow for more sensitive analysis of amino acids.[69,138] The 404 nm laser was passed through a dichroic and focused to a 10-20 μm spot in the channel approximately 0.6 cm from the cathode reservoir. Fluorescence was collected by the objective and reflected by the dichroic through a long pass filter onto a PMT, which was digitized at 50 Hz.

Separation and injection procedures. The microchip separation channel was prepared by first filling the sample, waste, and anode wells with running buffer. A vacuum was applied to the cathode well, drawing running buffer into the separation channel. The cathode well was then filled with running buffer, and the buffer in the sample well was drawn out and replaced with sample. Cross injection was accomplished by first applying a potential across the sample (ground) and waste (-1000 V) wells for 30 s with the anode and cathode grounded. This was followed by a 200-ms step where the anode is floated. The separation was performed by applying -15 kV at the cathode, -1.4 kV at the sample and waste, and ground at the anode.

4.4 Results

Initial buffer system selection. The fluorescamine labeling reaction has an optimal pH range between 8.0 and 10.0.[83] Since PB labeling proceeds via a similar reaction mechanism, the reaction buffers chosen for study have pK_a values near the same range. Phosphoric acid has a pK_a at 7.21 associated with the equilibrium between its diprotonated anion and monoprotonated anion. Borate has a pK_a value of 9.23 due to its interaction with water. Each of these options provides a more suitable choice than carbonate (pK_as 6.37, 10.25). Unacceptably high separation currents were observed with buffers containing greater than 50 mM borate or 10 mM phosphate concentrations. The following three buffer systems were chosen for study: 30 mM borate in both the sample and the separation channel, 30 mM borate in the separation channel with 5 mM borate in the sample, and 5 mM phosphate in the separation channel with 30 mM borate in the sample.

Effects of NaCl in the sample. Electropherograms shown in Figure 4.1 reveal the effect of high concentrations of salt in the sample. The high-salt sample exhibits lower signal, broader peaks, and reduced resolution compared to the experiment performed with no NaCl in the sample solution. The signal-to-noise ratios, resolutions, and peak efficiencies for the amino acids were then determined for each NaCl concentration and buffer system and summarized in Figure 4.2. All four buffer systems showed a significant decline in all three parameters with increasing sample NaCl, with the 5 mM borate system (Buffer D) displaying the most significant decline. While the buffer system containing 5 mM phosphate in the separation channel and 30 mM borate

in the sample (Buffer B) retained the best signal-to-noise ratio with increasing sample NaCl, the buffer system containing 30 mM borate in both the separation channel and the sample (Buffer C) retained the best resolution and peak efficiencies. Because of its operational simplicity, the latter buffer system was chosen for further optimization.

Effects of multivalent cations and EDTA. Studies of samples containing additional contaminating salts, including Na_2SO_4, $MgCl_2$, $NaClO_4$, $FeCl_3$, and $CaCl_2$, indicated that the anion has a negligible effect on the separation quality. However, multivalent cations were found to reduce the signal significantly even at concentrations as low as 5 mM. We therefore added EDTA to the sample buffer to chelate these cations and counteract their effect, as illustrated using Mg^{2+} as a model cation in Figure 4.3. The sample used for the top electropherogram (A) contains both 5 mM $MgCl_2$ and 10 mM EDTA; full signal strength and high separation quality is observed. The 5 mM $MgCl_2$ sample used for the bottom trace (B) does not contain EDTA; therefore, signal is not obtained. An optimization experiment was conducted varying the EDTA and $MgCl_2$ concentration (Figure 4.4). When the $MgCl_2$ concentration is higher than the EDTA concentration, no signal is observed, as expected. When the $MgCl_2$ concentration is equal to the EDTA concentration, some peaks are observed, but with lower signals and reduced resolution and peak efficiency. When the EDTA concentration is greater than the $MgCl_2$ concentration, signal, peak efficiency, and resolution are restored. However, the signal and other performance characteristics tend to decrease as the EDTA concentration is further increased. Experiments using $FeCl_3$ (Appendix D Figure D.2) exhibit similar trends. Based on these results, an EDTA concentration of 50 mM was chosen as the optimal concentration for further studies.

Effects of EDTA on labeling. The fluorescent signal of a solution of an amino acid and fluorescamine provides a convenient measure of the extent of the amino acid labeling reaction. Fluorescence measurements were made in buffers containing 30 mM borate and EDTA concentrations ranging from 0 to 200 mM (Appendix D Figure D.3). There is a significant decline in labeling efficiency in samples containing EDTA; the higher the concentration of EDTA, the stronger the inhibition. While exploring the reason for EDTA inhibition of the labeling reaction is beyond the scope of this work, it may be due to decreased cationic species available to stabilize the negatively charged tetrahedral intermediate formed when an amino compound attacks the carbonyl carbon in the first step of the labeling reaction mechanism. We conclude that the optimal labeling buffer should not contain EDTA because the positive effects of EDTA can be achieved by dilution after reaction.

Analysis of Saline Valley and Rio Tinto samples. Two samples exhibiting extreme salinity and acidity were chosen to test the robustness of the optimized buffer system. The high salinity sample is a halite saturated brine, SV07-4, from Saline Valley, California (Figure 4.5). conclude that the optimal labeling buffer should not contain EDTA because the positive effects of EDTA can be achieved by dilution after reaction.

Analysis of Saline Valley and Rio Tinto samples. Two samples exhibiting extreme salinity and acidity were chosen to test the robustness of the optimized buffer system. The high salinity sample is a halite saturated brine, SV07-4, from Saline Valley, California (Figure 4.5). This sample is of particular interest, because it contains halophilic *Archaea* and *Bacteria*.[153] An image of the brine taken using a 100X oil-immersion lens shows several prokaryote cells (rod and coccoid shapes) accompanying cubic halite (NaCl) crystals and a mirabilite ($MgCl_2$) needle (Figure 4.5A). Despite the abundance of prokaryote cells, MOA analysis of these Na-Cl-SO_4-

rich brines via the standard protocol (Figure 4.5A) exhibits extremely low signal amino acid peaks because of the high salt concentration (saturated with halite and mirabilite). Analysis via the optimized protocol shows significantly increased peak intensities (Figure 4.5B), allowing for the identification and quantification of multiple amino acids in the brine solution. The amino acid composition and concentrations in this sample are shown in Table 4.1.

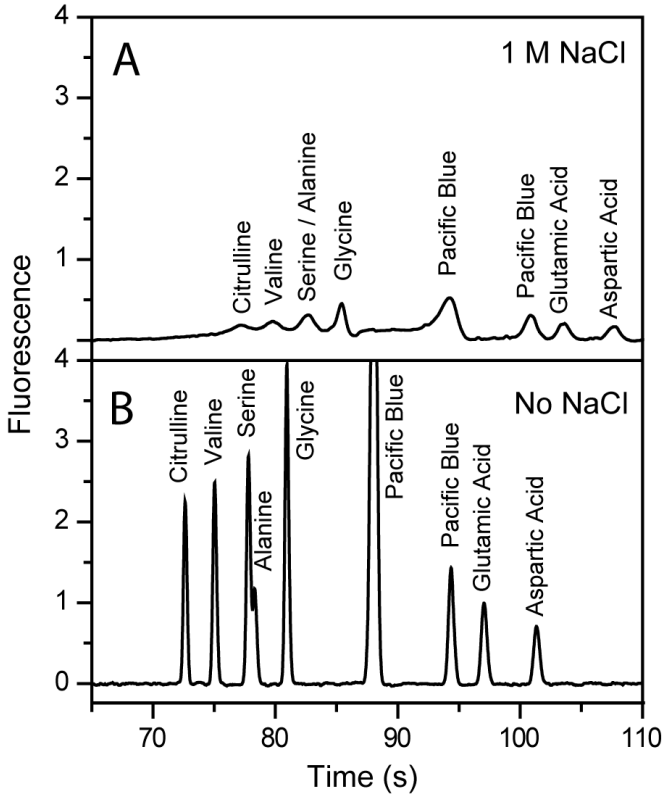

Figure 4.1. Electropherograms of an amino acid standard with (A) and without (B) 1 M NaCl.

The separation channel and sample buffer contain 5 mM borate buffer, pH 9.5. The standard contains 2 μM each citrulline, valine, serine, alanine, glycine, aspartic acid, and glutamic acid labeled with Pacific Blue.

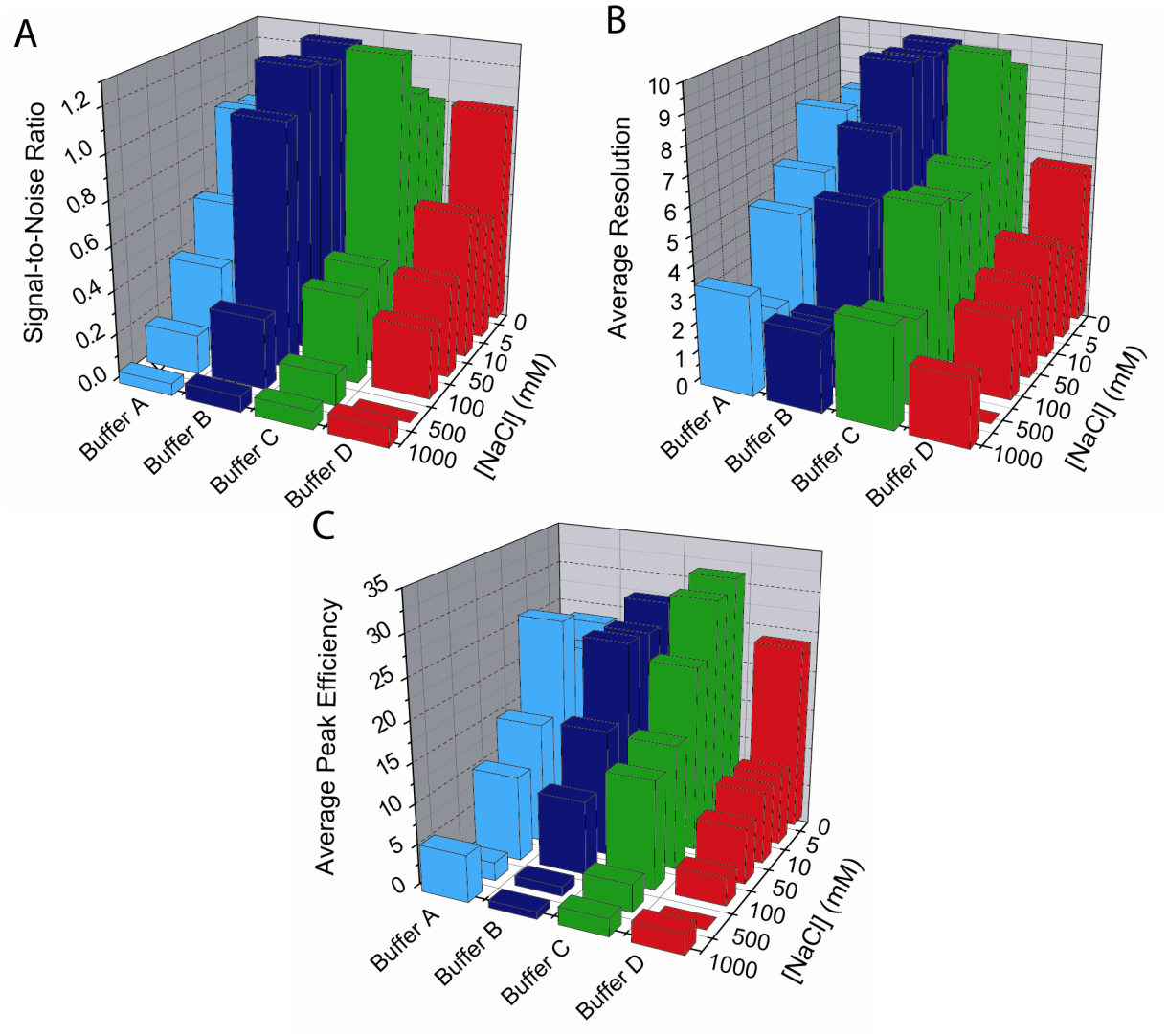

Figure 4.2. Effects of sample salt content on separation performance using selected buffering systems.

Buffer A consists of 30 mM borate in the separation channel and 5 mM borate in the sample. Buffer B consists of 5 mM phosphate in the separation channel and 30 mM borate in the sample. Buffer C consists of 30 mM borate in both the separation channel and the sample. Buffer D consists of 5 mM borate in both the separation channel and the sample. (A) Average signal-to-noise of all amino acid peaks normalized to the no-salt case for each buffer. (B) Average resolution between amino acid peaks for each buffer system at the indicated concentrations of NaCl. (C) Average amino acid peak efficiency in theoretical plates-per-meter (x 10^{-4}) for each buffer system at the indicated concentrations of NaCl. The sample is the same as Figure 4.1.

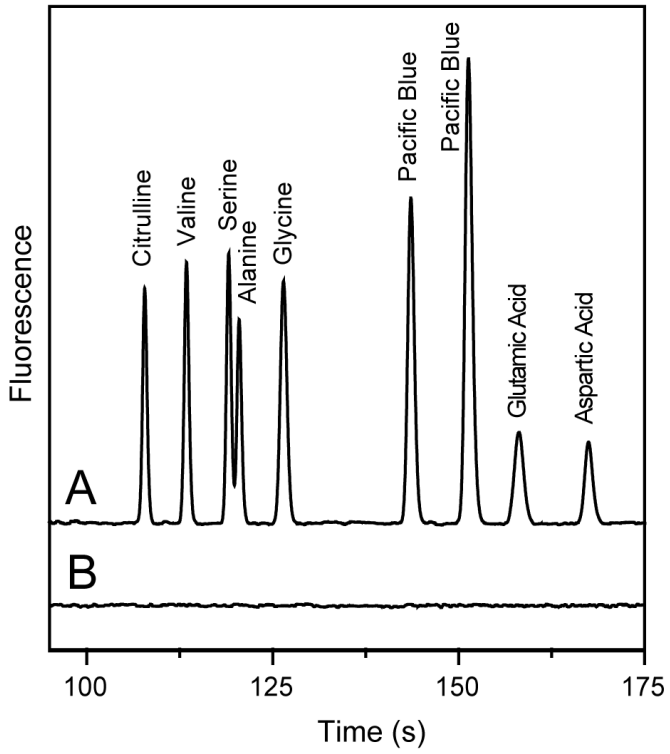

Figure 4.3. Electropherograms of a standard containing 5 mM $MgCl_2$ with 10 mM EDTA (A) and without EDTA (B).

The separation column and sample contain 30 mM borate buffer, pH 9.5. The sample contains 2 μM each citrulline, valine, serine, alanine, glycine, aspartic acid, and glutamic acid labeled with Pacific Blue.

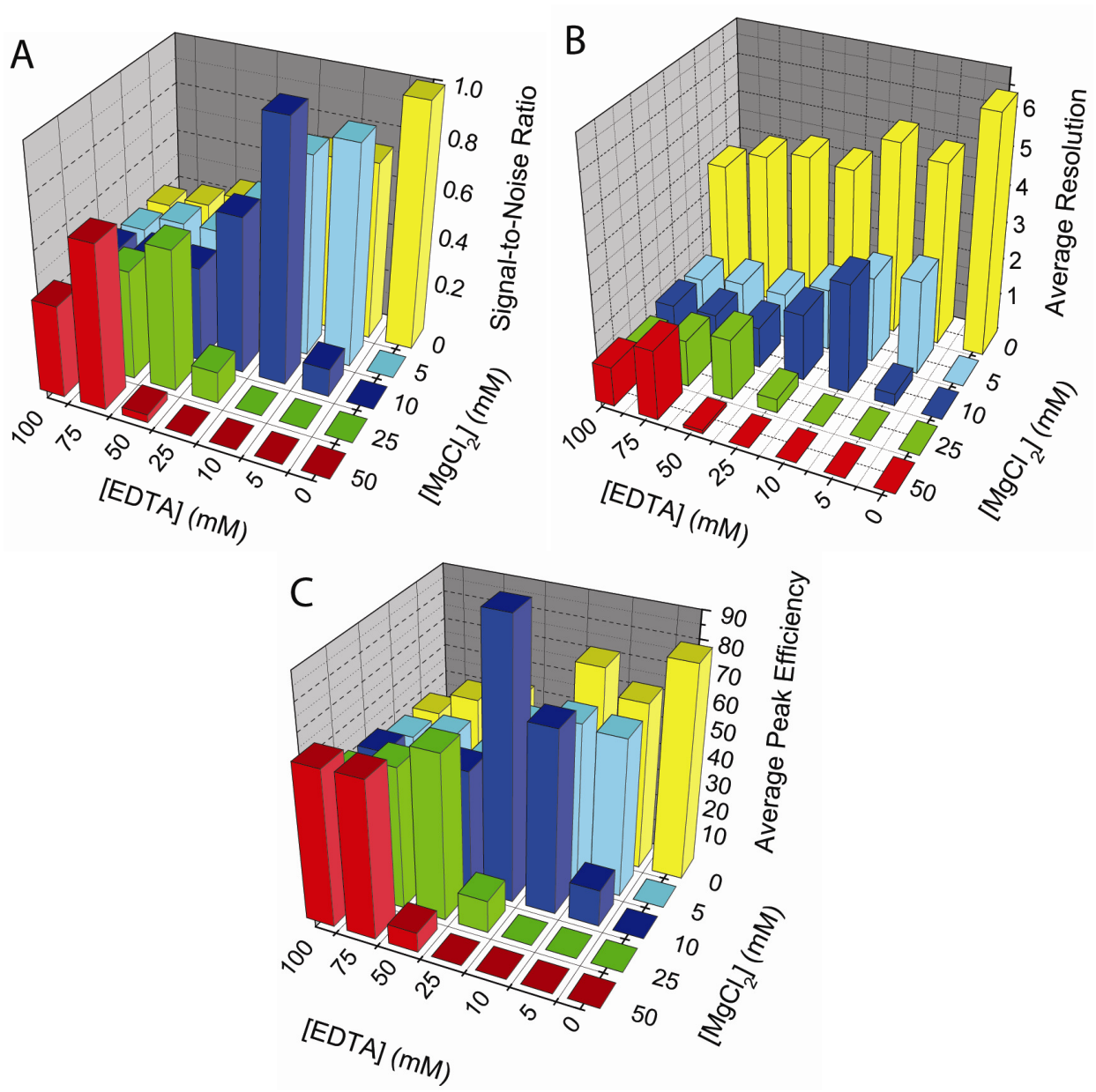

Figure 4.4. Effects of different EDTA and $MgCl_2$ concentrations in the sample buffer on separation performance.

The separation channel and sample contain 30 mM borate buffer, pH 9.5. (A) Average signal-to-noise of all amino acid peaks normalized to the no-salt, no-EDTA case. (B) Average resolution between amino acid peaks for each concentration of EDTA and $MgCl_2$. (C) Average peak efficiency in theoretical plates-per-meter (x 10^{-4}) of amino acid peaks for each concentration of EDTA and $MgCl_2$. The sample is the same as in Figure 4.3.

rich brines via the standard protocol (Figure 4.5A) exhibits extremely low signal amino acid peaks because of the high salt concentration (saturated with halite and mirabilite). Analysis via the optimized protocol shows significantly increased peak intensities (Figure 4.5B), allowing for the identification and quantification of multiple amino acids in the brine solution. The amino acid composition and concentrations in this sample are shown in Table 4.1.

The Rio Tinto in Spain provides an example of both high salinity and extreme acidity. The sample pH is less than 2 and it contains high iron, magnesium, and general salts with concentrations greater than 500 mM,[155] making μCE amino acid analysis challenging. A subcritical water extract of the Rio Tinto sample KF03-136 was analyzed with the standard and optimized assays. Analysis with the standard protocol (Figure 4.6B) exhibited low signal and an absence of peaks eluting after ~150 s. However, analysis using the optimized buffer system (Figure 4.6A) showed much stronger amine and amino acid signals, allowing for substrate identification and quantification (Table 4.1). In KF03-136, ammonia, ethylamine, serine, and glycine are present in pptr levels, while methylamine, valine, alanine, and aspartic acid are present in high ppb. The complexity of the trace and the large levels of amines and amino acids in this sample are likely derived from a thriving acidophile population. This improvement in analytical capability was due to improved buffering against the high acid concentration, chelation by EDTA of multivalent cations (*e.g.* Mg^{2+}, Fe^{3+}), and increased resistance to deleterious salt effects in the injection and separation.

4.5 Discussion

The optimized MOA analysis protocol developed here provides several benefits over our previous methods. The 5 mM borate buffer system used in the salt experiments is most similar to the previously used 4 mM carbonate buffering system.[69] With no NaCl present in the sample, there is no mismatch in ionic strength between the sample matrix and the separation buffer, so there is little difference between the 5 mM borate buffer and the other buffer systems tested. However, at higher sample NaCl concentrations, the mismatch in ionic strengths of the sample and separation column produce intense dispersive effects when using the 5 mM borate system. Because the ionic strength of the separation buffer is higher for the 30 mM borate system, the mismatch is reduced and dispersive band broadening is less pronounced.

The 30 mM borate system has a larger capacity than the 4 mM carbonate system, so it can buffer a significantly larger concentration of acid or base present in a sample. The larger buffer capacity is partly due to the higher concentration of buffer salt: 30 mM borate in the optimized system compared to 4 mM carbonate in the previous system. However, it also arises from a better choice of the buffer pK_a values relative to the operating pH. The carbonate buffer was used at pH 8.5, which is well out of its effective buffering range (pK_a 6.4). The borate buffer has a pK_a (9.23) that is significantly closer to the operating pH of 9.5.

To ensure that the analysis is not compromised by the presence of divalent cations, it is essential to have some EDTA in the sample buffer. While the presence of EDTA reduces signal, the complete loss of signal seen with even a 5 mM addition of Mg^{2+} makes the 10-50% EDTA-induced loss in signal and separation quality acceptable. It is also interesting to note that divalent cations appear to counter the deleterious effect of EDTA on the separation, as nearly full signal, resolution, and peak efficiency are restored when the EDTA concentration is just higher

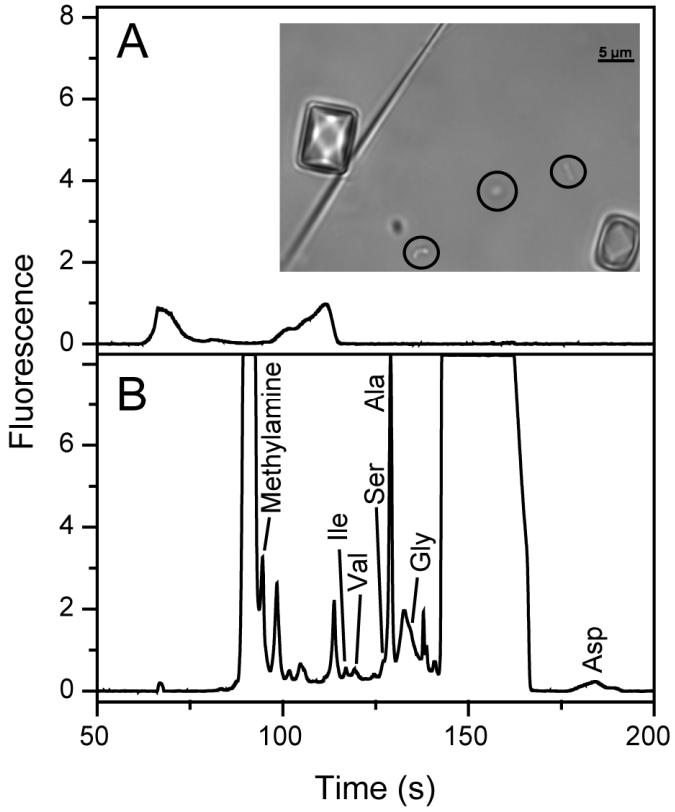

Figure 4.5. Analysis of Saline Valley brine SV07-4.

(A) Electropherogram of Pacific Blue labeled sample with the separation channel and sample containing 4 mM carbonate, pH 8.5. The inset presents a photomicrograph of a wet mount viewed using a 100X oil immersion lens. Prokaryote cells occur as rod and coccoid shapes (circled); halite (cube) and mirabilite (needle) crystallized from the Na-Cl-SO_4-rich brine after collection. Scale bar is 5 µM. (B) Electropherogram of Pacific Blue labeled sample, where the separation channel contains 30 mM borate, pH 9.5, and the sample contains 30 mM borate, 50 mM EDTA, pH 9.5.

Table 4.1 Amino Acid Analysis of Challenging Samples

Amine / Amino Acid	Rio Tinto[a] (KF03-136, ppb)	Saline Valley[b] (SV07-4, μM)
Ammonia	9,520	ND[c]
Methylamine	809	200
Ethylamine	3,640	ND[c]
Leucine + Isoleucine	136	ND[c]
Valine	418	4.3
Serine	19,800	11
Alanine	855	210
Glycine	6,200	0.48
Aspartic Acid	717	27

[a] Composition calculated as a fraction of initial sample assuming 100% recovery during the subcritical water extraction and subsequent processing.
[b] Concentrations of detected species in the received saturated brine solution.
[c] Species not reported because either they were not observed or they were observed with signal at or below that in a buffer blank.

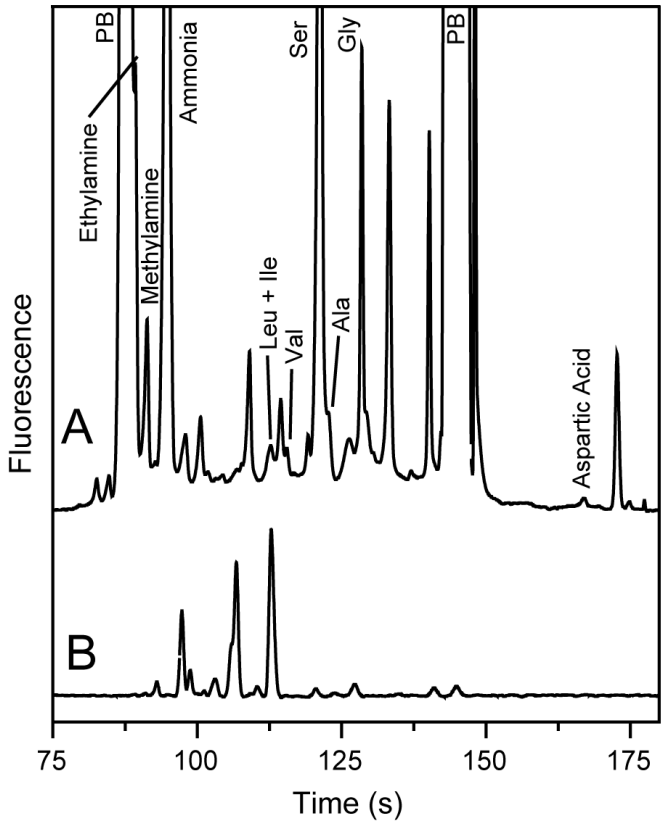

Figure 4.6. Electropherograms of a pacific Blue labeled subcritical water extract of the Rio Tinto sample KF03-136 (Fernández-Remolar, 2005).

The sample was diluted five-fold with sample buffer before labeling, then analyzed at a total dilution factor of 10-fold. (A) Separation channel contains 30 mM borate, pH 9.5. The sample was diluted with 30 mM borate before labeling, then brought to a final sample buffer composition of 30 mM borate, 50 mM EDTA for injection. (B) Separation and sample buffer are both 4 mM carbonate, pH 8.5.

than the $MgCl_2$ concentration. Although EDTA also has an inhibitory effect on sample labeling, it is easy to circumvent this problem by adding EDTA to the sample after the labeling reaction is complete.

The net benefits of the optimized method over the standard method are best demonstrated by the analysis of terrestrial samples with extremes of salinity and pH. The high salt sample is brine taken from the saline pan of Saline Valley. The sampling site hosts a diverse community of single-celled halophilic algae (genus *Dunaliella*) and halophilic *bacteria* and *archaea*, and thus we would expect large concentrations of amino acids.[153-154] This sample is pH neutral and does not contain significant levels of divalent cations, so high salt concentrations (Na^+, Cl^-, and SO_4^{2-} at halite and mirabilite saturation) are the major concern. Analysis with our previous method shows low signal and peak broadening which makes amino acid identification and quantitation impossible. The analysis via the optimized protocol, however, allows for identification of several amino acids and quantitation of total amino acid content at 450 μM. This result is a significant advance in the MOA capabilities, because it demonstrates the potential for the direct analysis of aqueous extracts, without extensive preprocessing.[115,117]

The Rio Tinto river in Spain has a pH less than 2 and contains high concentrations of metal salts.[156] Despite these seemingly hostile characteristics, the Rio Tinto hosts a rich ecosystem, with a surprising degree of eukaryotic diversity,[156] and thus high levels of amino acids and organic amines are expected.[137] The extreme acidity of this concentrated ASAP[137] sample severely inhibited labeling via the previous protocol, and the high metal content severely limited the injection, resulting in low signal. In our Rio Tinto extract analysis for the ASAP,[137] the sample was manually neutralized before labeling and analyzed via the standard protocol, but the electropherogram still showed low signal strength, because of the high salt concentration resulting from neutralization and the high metal content.

In contrast, the optimized method employed here to analyze the Rio Tinto sample required no neutralization before labeling and produced traces with high signal strength. This improvement is seen because of the much larger buffering capacity of the optimized buffering system, and the addition of EDTA to the sample buffer after labeling to negate effects of the sample's exceptionally high metal content. The unusually high abundance of serine in this sample raises the question whether the SCWE method, salts, a co-eluting amine, or an analytical artifact may increase the intensity of this peak. While this assignment was confirmed by coelution of a serine spike, additional 2-dimensional CE separations using MEKC[69] and mass spectrometry would provide valuable confirmation.

The optimized buffer system developed here should also be useful for chiral separations of labeled amino acids. The improved buffering system should facilitate separation of fluorescamine labeled amino acids in cyclodextrin buffers that have been shown to provide chiral resolution.[67] Chiral separations of Pacific Blue labeled amino acids conducted with micellar electrokinetic chromatography (MEKC)[69] should also exhibit decreased sensitivity to sample salt and pH once the detailed conditions are optimized.

4.6 Conclusions

This work demonstrates that proper buffering is critical for successful sample analysis, and that amino acid extracts obtained from samples from extreme environments can be directly injected into the MOA μCE instrument and analyzed. These new methods critically advance the development of our analytical system for biomarker detection providing broad applicability and versatility for planetary exploration. For more information on MOA development, see http://astrobiology.berkeley.edu.

4.7 Acknowledgements

We thank Daniel Glavin (NASA Goddard Space Flight Center) and Mary Sue Bell (NASA Johnson Space Center) for providing ASAP sample KF03-136 from the Rio Tinto. Microdevices were fabricated in the UC Berkeley Microfabrication Laboratory by Wai K. Chu. This research was supported by NASA grants NNG04GB75G and NNX08AR09G, NSF grant EAR 0433802 (T. K. L.), and by the Jet Propulsion Laboratory and the California Institute of Technology under contract 1297596.

Chapter 5 : Analysis of Carbonaceous Biomarkers with the Mars Organic Analyzer Microchip Capillary Electrophoresis System: Aldehydes and Ketones

5.1 Abstract

A microchip capillary electrophoresis method is developed for the analysis of two oxidized forms of carbon, aldehydes and ketones, with the Mars Organic Analyzer (MOA). Fluorescent derivitization is achieved in ~ 15 min by hydrazone formation with Cascade Blue hydrazide in 30 mM borate pH 5-6. The microchip CE separation and analysis method is optimized via separation in 30 mM borate buffer, pH 9.5, at 20 ^{o}C. A carbonyl standard consisting of ten aldehydes and ketones found in extraterrestrial matter is successfully separated; the resulting limits of detection depend on the reactivity of the compound and range from 70 pM for formaldehyde to 2 μM for benzophenone. To explore the utility of this method for analyzing complex samples, analyses of several fermented beverages are conducted, identifying 10 aldehydes and ketones ranging from 30 nM to 5 mM. A Martian regolith simulant sample, consisting of a basalt matrix spiked with soluble ions and acetone, is designed and analyzed, but acetone is found to have a limited detectable lifetime under simulant Martian conditions. This work establishes the capability of the MOA for studying aldehydes and ketones, a critical class of oxidized organic molecules of interest in planetary and in terrestrial environmental and health studies.

5.2 Introduction

The search for direct chemical evidence of extraterrestrial life began in 1975, when NASA launched the Viking landers that carried a suite of biological experiments[14-15] and a pyrolysis gas chromatograph–mass spectrometer (GC-MS).[17] The biological experiments yielded what appeared to be ambiguous results,[14-15] and the GC-MS detected no organic molecules of non-terrestrial origin.[17] Since the delivery of organic matter from space is calculated at 10^5 kg/year,[59] this negative result has been attributed to the presence of a strong oxidant in the Martian regolith that produced acids indetectable via GC-MS,[15,150] sterilizing radiation that degraded organics in the unprotected regolith,[26] and the degradation of organic molecules during the GC-MS pyrolysis extraction.[26,151] More recently, the Mars Exploration Rover Opportunity discovered jarosite[20] and other mineralogical evidence of transient ancient liquid water[21] and the Phoenix lander directly observed water ice,[22] increasing the possibility of life at some time on Mars. The hypothesis that Viking's results can be attributed to a strong oxidant in the regolith is strengthened by the fact that Phoenix discovered the oxidant perchlorate.[23] The combined evidence strongly suggests that future *in situ* life detection instrumentation must have the capability to very sensitively detect oxidized organic molecules.

In the search for molecular signatures of life on Mars the chances of successful detection are dramatically improved if oxidized organic molecules can be detected with high sensitivity. Aldehydes and ketones have been found in a number of extraterrestrial sources. Aldehydes in the C_1 to C_4 range and ketones in the C_3 to C_5 range were detected in the Murchison meteorite.[53] Formaldehyde was the first polyatomic organic molecule observed in interstellar media,[157] and propionaldehyde, propenal and propynal were observed in interstellar space in 2004.[65] The proven presence of aldehydes and ketones in extraterrestrial sources together with the oxidizing soil chemistry on Mars argue strongly that a comprehensive molecular examination of Mars must include the ability to detect and analyze aldehydes and ketones.

Ketones and aldehydes are also highly prevalent analytes on Earth. Formaldehyde's toxicity has made news due to its contamination in a range of building materials.[64] Other aldehydes and ketones are predominant in fermented beverages; acetaldehyde contributes to hangover[158] and diacetyl and acetoin give a buttery aroma to wine.[159] Methylethylketone is used in dry erase markers, acetone is used in nail polish remover, 2-pentanone is used as a flavoring food additive, and p-anisaldehyde is found naturally in anise and used for perfumes. Interest in determining levels of ketones and aldehydes stems from the health hazards related to many of them: acetaldehyde has been linked to Alzheimer's,[160] formaldehyde is a toxic carcinogen,[161] and methylethylketone is an irritant. Based on these observations, it would be valuable to develop new methods to probe aldehyde and ketone concentrations in samples of health and environmental significance.

The Mars Organic Analyzer (MOA)[103] is a portable lab-on-a-chip microcapillary electrophoresis (μCE) instrument that includes all the necessary microfluidics, optics, and electronics for in situ capillary electrophoresis analysis of a variety of organic molecules. We have previously used the MOA and fluorescamine derivitization to analyze primary amines,[103] nucleobases,[106] and amino acids[103] and their chirality.[67] The use of Pacific Blue (PB) as an amine-reactive derivitization agent increased the amino acid sensitivity of the MOA to the low parts-per-trillion level,[69] and the development of a micellar electrokinetic chromatography (MEKC) separation method allows for pseudo-2D amino acid separations and enhanced compositional analysis capabilities.[69] Using mixtures of charged and uncharged cyclodextrins, we also developed methods to analyze polycyclic aromatic hydrocarbons (PAHs) on the MOA.[138] The MOA's robustness for the analysis of analytes in samples containing high salinity, acidity, and high concentrations of multi-valent metallic salts was enhanced through careful buffer selection and the use of ethylaminediaminetetraacetic acid (EDTA).[162] Successful field tests of the MOA were conducted in the Panoche Valley, CA,[103] and in the Atacama Desert, Chile.[81] Recently, a second generation multichannel MOA prototype has been developed with a CCD spectrometer to enhance species identification through fluorescence spectra collection.[91]

Here we show that aldehydes and ketones, an important subset within the larger class of oxidized organic molecules, can be labeled using Cascade Blue hydrazide (CB) and analyzed using capillary electrophoresis on the MOA. CB is a fluorescent probe that reacts with the carbonyl of ketones and aldehydes to form hydrazone linkages (inset Figure 5.1). We optimize the CB labeling reaction and separation of CB-labeled aldehydes and ketones, and then analyze a standard containing aldehydes and ketones found in the Murchison meteorites and several fermented beverages. A Mars simulant is developed by spiking soluble ions quantified by Phoenix[23] and acetone into a clean basalt matrix, and exposing this simulant to ambient conditions and UV irradiation to measure the expected lifetime of acetone under putative Martian chemical and irradiative conditions. This work expands the demonstrated capability of the MOA to perform highly sensitive analyses of a critical class of oxidized organic molecules.

5.3 Materials and Methods

Buffer and sample preparation. Sodium tetraborate and boric acid were obtained from Sigma-Aldrich (St. Louis, MO) and used to prepare 400 mM borate stock solutions. These stocks were diluted to 30 mM borate and adjusted to the desired pH using NaOH or HCl. Ketone and aldehyde standards were prepared as aqueous 20 mM stock solutions using p-anisaldehyde,

3-methyl-2-butanone, butyraldehyde, diethylketone, methylethylketone, propionaldehyde, acetone, and acetaldehyde (all Sigma-Aldrich), and formaldehyde (EMD Chemicals). A 20 mM stock solution of benzophenone (Sigma-Aldrich) was prepared in dimethylsulfoxide (DMSO, Sigma-Aldrich). These ketone and aldehyde stocks were combined in appropriate volumes to create the carbonyl standard. Cascade Blue hydrazide trisodium salt (CB, Ex. 396, Em. 410) was obtained from Invitrogen (Carlsbad, CA) and dissolved to 20 mM in water and stored at -20 ^{o}C.

Labeling reactions were conducted by combining 4 μL of the standard with 12 μL CB stock and 34 μL 30 mM borate buffer. The labeling mixture was allowed to react at room temperature for 15 minutes to overnight before 1:10 dilution for analysis. Unless otherwise indicated, separations were conducted at 20 ^{o}C. Electropherograms were analyzed using PeakFit (Systat Software, San Jose, CA) to determine the signal-to-noise, resolution, and peak efficiency in theoretical plates per meter for each aldehyde and ketone peak.

To determine the effect of the labeling buffer pH on the labeling reaction and separation, 30 mM borate buffer solutions were prepared at pH ranging from 2 to 12. These buffers were used for the labeling reaction, then diluted and analyzed with 30 mM borate pH 9.5. To explore the pH dependence of the separation, labeling was conducted using 30 mM borate, pH 5-6, then diluted and analyzed with each of the buffers. Time-course experiments were conducted by preparing labeled aldehyde and ketone standard using 30 mM borate, pH 5-6, and were diluted at various times into 30 mM borate, pH 9.5, for immediate analysis.

Limits of detection were determined by preparing 10 to 12 concentrations of the indicated ketone or aldehyde in 30 mM borate, pH 5, from each of three independently prepared 20 mM stock solutions. CB (1 μL) was added to 20 μL of each concentration and allowed to react overnight. Immediately before analysis 79 μL 30 mM borate, pH 9.5, was added to each reaction.

Wine samples were obtained from local retailers and included Toasted Head Chardonnay (2007, Woodbridge, CA), Charles Shaw White Zinfandel (2008, Napa and Sonoma, CA), Bears' Lair Merlot (2007, Napa, CA), Bears' Lair Cabernet Sauvignon (2007, Napa, CA), Beringer Cabernet Sauvignon (2008, Napa, CA), Real Tesoro Cream Sherry (Spain, imported by Plume Ridge Wine Negotiants Industry, CA) and Gekkeikan Sake (Folsom, CA). Wine samples were labeled by combining 10 μL sample with 4 μL CB stock and 26 μL 30 mM borate buffer, pH 5-6. After an overnight reaction, these reactions were diluted either 1:5 or 1:50 with 30 mM borate buffer, pH 9.5. Labeled aldehyde and ketone standard was combined with the labeled samples for identification of aldehyde and ketone components. Quantitation was conducted by diluting the wine 1:10 with buffer spiked with appropriate concentrations of aldehyde / ketone components prior to labeling and analysis as above.

A Mars simulant sample was created by spiking into a washed and sterilized basalt matrix soluble ions of the identity and concentrations measured by the Phoenix lander.[23] Basalt, which has been suggested to be an adequate matrix simulant of Martian regolith,[163-164] was collected from the Mojave Desert in a region near the Pisgah lava flows at GPS UTM coordinates Zone 11S 557603 mE 3843054 mN. The top cm of basalt was removed from the desert lawn and samples collected from the 1-3 cm directly below. The basalt was then run through a wire mesh with holes 515 x 575 μm to remove basalt gravel. The resulting dust was washed with ten 100

mL portions of isopropanol, acetone, and Millipore water, and baked at 110 °C overnight. To create the soluble ion component measured by Phoenix, the following were added to 100 g of the clean, dry basalt: 423.7 mg $NaClO_4 \cdot H_2O$ (Sigma-Aldrich), 59.3 mg KCl (Sigma-Aldrich), 312.8 mg $Ca(ClO_4)_2 \cdot H_2O$ (Sigma-Aldrich), 24.6 mg $CaCl_2 \cdot 2H_2O$, and 1.704 g $MgSO_4 \cdot 7H_2O$. Triply-distilled Millipore water (100 mL) was added to create a slurry and evenly distribute the soluble ions, then desiccated during a two-day bake at 110 °C.

Acetone degradation experiments were conducted by adding acetone at 10x the total aldehyde and ketone content observed in the Murchison meteorite (270 ppm)[53] to the Mars simulant. The acetone-containing simulant was measured into Petri dishes (2 g each) which were placed under a UV lamp (Mineralight Model UVGL-25, long-wave, ~ 365 nm) or under aluminum foil at ambient conditions. Samples of 50-150 mg were removed immediately and at 5 min intervals. Acetone was extracted by adding 30 mM borate buffer pH 5-6 to the samples at 1 µL per mg, vortexing briefly (~ 15 s), and then centrifuging for ~ 30 s. Within 1 min of the introduction of buffer, 10 µL of the sample supernatant was removed and combined with 5 µL 10 mM CB and allowed to react for 15 min. Immediately prior to analysis on the MOA, the reaction mixture was diluted to a final buffer of 30 mM borate, 12.5 mM EDTA, pH 9.5.

Microdevice fabrication. The microdevices were prepared as previously described.[67,69,81,103,106,138,162] Briefly, a sacrificial layer of polysilicon was deposited on a 10-cm borofloat glass wafer and photoresist was spin-coated onto the wafer. The photoresist was patterned through a chrome mask using a contact aligner. After developing the photoresist, the exposed polysilicon was removed by plasma etching and the glass was etched in buffered HF. Reservoir holes were drilled after the photoresist was removed. The polysilicon layer was then removed, and the wafer was thermally bonded to a blank wafer to form completed channels. The fabrication produces 23.6 cm long folded separation channels 110 µm wide and 30 µm deep. Injections were performed via a 1.2-cm long cross-channel located 0.6 cm from the anode end of the channel. A 3-mm deep PDMS gasket with 4-mm diameter wells placed over the reservoir holes allows for larger volumes, alleviating evaporative and hydrodynamic imbalance issues. A schematic of the microdevice can be found in prior publications and Appendix A.[69,138,162]

Mars Organic Analyzer. The Mars Organic Analyzer (MOA)[103] was used with minor modifications previously made to the optical subsystem that allow for more sensitive analysis of amino acids and polycyclic aromatic hydrocarbons.[69,138,162] The 404 nm laser was passed through a dichroic and focused to a 10-20 µm spot in the channel approximately 0.6 cm from the cathode reservoir. Fluorescence was collected by the objective and reflected by the dichroic through a long pass filter (50 % T at 425 nm) onto a PMT, which was digitized at 50 Hz.

Separation and injection procedures. Microchip separation and injection channels were first filled with 1 N NaOH for cleaning, rinsed with water, then filled with running buffer for analysis. Buffer in the sample well was drawn out and replaced with sample. Cross injection was accomplished by applying a potential across the sample (ground) and waste (-1000 V) wells for 30 s with the anode and cathode grounded. This was followed by a 200-ms step where the anode is floated. The separation was performed by applying -15 kV at the cathode, -1.4 kV at the sample and waste, and ground at the anode.

5.4 Results

Labeling reaction pH optimization. The effectiveness of the labeling reaction, measured by the sum of the area of all peaks in the carbonyl standard, is plotted against the pH of the labeling reaction in Figure 5.1A. The values and error bars are calculated from the average and standard deviation of triplicate experiments. Aldehydes are more reactive than ketones, and the signal observed between pH 9-11 can be attributed solely to aldehyde peaks (Appendix E Figure E.1 provides complete electropherograms). As shown in Figure 5.1A, the optimal pH for reaction is between 4 and 8, but the reaction is not hampered significantly by pH as low as 2. An acidic environment provides a slight degree of protonation to the aldehyde / ketone carbonyl (pK_a ~ -7) that allows for a stable intermediate. The acidic environment also encourages a water molecule leaving group, which is kinetically favorable over a hydroxide leaving group. Scheme E.1 (in Appendix E) shows the mechanism for acid-catalyzed hydrazone formation. At pH below 3, protonation of the CB-hydrazide (pK_a ~3) reduces its reactivity. Between pH 9 and 11 the overall labeling is low, which is expected because basic pH disallows a water molecule leaving group. Some signal is restored by moving to pH 12 and higher, perhaps due to the presence of small amounts of highly reactive deprotonated CB-hydrazide (pK_a ~ 18). Based on these results and the natural pH of a 30 mM borate solution prepared from boric acid, we selected a labeling buffer of 30 mM borate, pH 5-6.

Analysis buffer pH optimization. The average resolution between the methylisopropylketone peak, the co-elution peak of butyraldehyde, diethylketone, and methylisopropylketone, and the methylethylketone peak is used as a measure of separation quality and plotted against the pH of the 30 mM borate analysis buffer in Figure 5.1B. (See Figure 5.2 for a representative separation.) The values and error bars are calculated from the average and standard deviation of triplicate experiments. Below pH 7, electrophoresis is unsuccessful, and no peaks reach the detector. Above pH 11, peaks experience significant broadening and are not resolvable (average resolution < 0.5). The optimal pH is 10 yielding an average resolution > 2.5 with low run-to-run variability. The decrease in average resolution is similar when the pH is reduced or increased; however, pH 9 gives lower run-to-run variability compared to pH 11. Based on these results, 30 mM borate, pH 9.5, is selected as the analysis buffer.

Other conditions were explored, including ionic strength of the buffer, temperature of analysis, and labeling reaction time. The buffer ionic strength (30 mM) was optimized as previously described to provide high resolution and tolerance to variations in sample composition while maintaining low enough operating currents to consistently avoid instrument electrical overloads[162]. The average resolution was measured as a function of analysis temperature from 5 to 35 ^{o}C and found to vary less than the run-to-run variation. The typical analysis temperature was 20 ^{o}C. The labeling reaction is very fast and no discernable difference in signal is obtained with reaction times ranging from 15 minutes to several days. Samples were analyzed after a 30 min reaction for immediate use or overnight when convenient.

Optimal analysis of the carbonyl standard. The carbonyl standard was labeled overnight at pH 5, then diluted into the pH 9.5 analysis buffer for analysis at 20 ^{o}C using the MOA. The electropherogram of this separation is shown in Figure 5.2, and the resolutions and peak efficiencies are given in Table E.2 in the Appendix E. The larger aromatic species p-

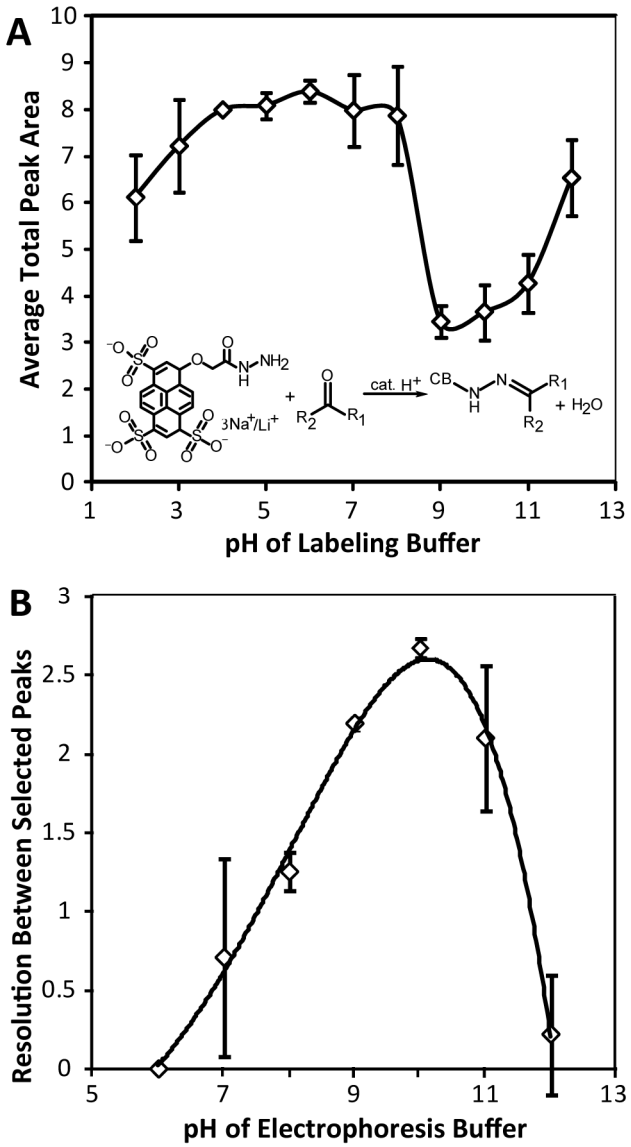

Figure 5.1. Labeling efficiency (A) and separation quality (B) dependence on pH.

(A) pH dependence of the sum of the areas of all peaks resulting from the Cascade Blue hydrazide labeling of 10 representative aldehydes and ketones followed by MOA CE analysis. Labeling is conducted at the indicated pH, then diluted with 30 mM borate pH 9.5 for immediate analysis. (B) Dependence of the average resolution between the methylisopropylketone, the butyraldehyde, diethylketone, methylisopropylketone, and the methylethylketone peaks on the pH of separation buffer. Peaks selected from a separation of the carbonyl standard labeled with Cascade Blue hydrazide. Labeling is conducted at pH 5, then diluted and analyzed with 30 mM borate at the indicated pH.

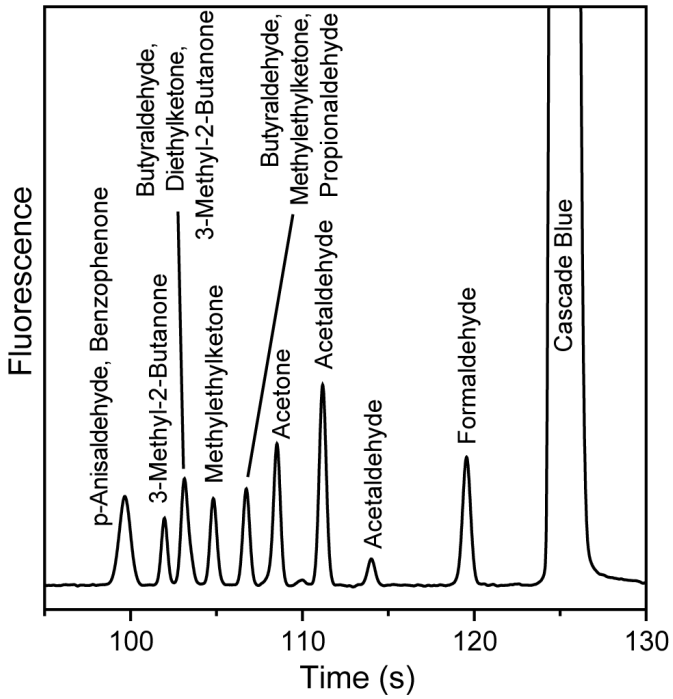

Figure 5.2. The optimized MOA CE separation of the carbonyl standard.

Separation was conducted using 30 mM borate pH 9.5. Concentrations are 1.6 μM formaldehyde (Limit of Detection 70 ± 30 pM), 3.2 μM acetaldehyde (LOD 700 ± 200 pM), propionaldehyde, and butyraldehyde, 16 μM acetone (LOD 5 ± 2 nM), p-anisaldehyde, and benzophenone (LOD 1.6 ± 0.6 μM), and 32 μM methylethylketone, diethylketone, and 3-methyl-2-butanone. Aldehydes and ketones with asymmetry about the carbonyl group are resolved into two peaks, due to slow isomerization between the cis-like and trans-like isomers at the hydrazone linkage.

anisaldehyde and benzophenone co-elute, but unique peaks are seen for 3-methyl-2-butanone, methylethylketone, acetone, acetaldehyde, and formaldehyde. Aldehydes and ketones that have asymmetry about the carbonyl give rise to two peaks, presumably due to slow interconversion between the cis-like and trans-like isomers at the hydrazone linkage. Resolution of cis/trans isomers into two peaks has also been reported for rapid (~100 s) CZE separations of the interconverting isomers of proline peptides.[165-166] Aldehydes and ketones have varying degrees of reactivity, therefore different concentrations (1.6 to 32 μM) were required to produce peaks of equal magnitude.

Limits of detection were determined for selected aldehydes and ketones in the carbonyl standard. Formaldehyde, which is the most reactive species studied, has the lowest limit of detection at 70 ± 30 pM. Acetaldehyde, which has a reactivity similar to that of other aliphatic aldehydes, was found to have a limit of detection about 10 times that of formaldehyde at 700 ± 200 pM. Acetone, representative of the reactivity of aliphatic ketones, has a limit of detection another order of magnitude higher at 5 ± 2 nM. The aromatic ketones and aldehydes have dramatically higher limits of detection; the benzophenone limit of detection is almost 1000x higher at 1.6 ± 0.6 μM. The limits of detection report on the true concentration of the analyte prior to labeling, thus low-concentration experiments were labeled at the low concentration and were not formed by post-labeling dilution.

Wine and fermented beverage analysis. To explore the utility of the MOA to examine samples of environmental and health interest we performed analyses of a variety of fermented beverages (Figure 5.3). Fermented beverages were analyzed for aldehydes and ketones in the carbonyl standard and for aldehydes and ketones commonly found in fermented beverages,[159] especially diacetyl and acetoin, which are responsible for buttery flavor and aroma. Results are summarized in Table 5.1. The wines made by traditional fermentation processes (chardonnay, white zinfandel, and cabernet sauvignon) have the highest concentrations of aromatic ketones and aldehydes and diacetyl, with the cabernet sauvignon containing the highest (~5 mM and ~2 mM respectively). The highest level of acetoin (~1 mM) was observed in cream sherry, where fermentation is halted early by fortification with distilled ethanol. The cream sherry, along with the sake, also were found to have the highest levels of formaldehyde (14-27 μM). The cream sherry and sake were found to have an order of magnitude more acetaldehyde (400-600 μM) than traditional wines (30-50 μM). The traditional wines fermented from red grapes (white zinfandel and cabernet sauvignon) as well as the sake were found to have 3-methyl-2-butanone in the 0.9 to 18 μM range, while the cream sherry (also fermented from red grapes) had no detectable levels of this ketone. The wines fermented from red grapes with their skins (cabernet sauvignon, and cream sherry) were found to have high nM to low μM concentrations of methylethylketone. The chardonnay (fermented from white grapes), the white zinfandel (fermented from red grapes without their skins), and the sake (fermented from rice) contain no detectable levels of this ketone. Pyruvic acid was found in the hundreds of μM range for cabernet sauvignon, sherry, and sake, and elevated to the mM range for the chardonnay and white zinfandel. Millimolar quantities of a-ketoglutaric acid were found in the chardonnay and cabernet sauvignon, which decreased to the hundreds of μM range in the white zinfandel and the sake, and to below detectable levels in the sherry.

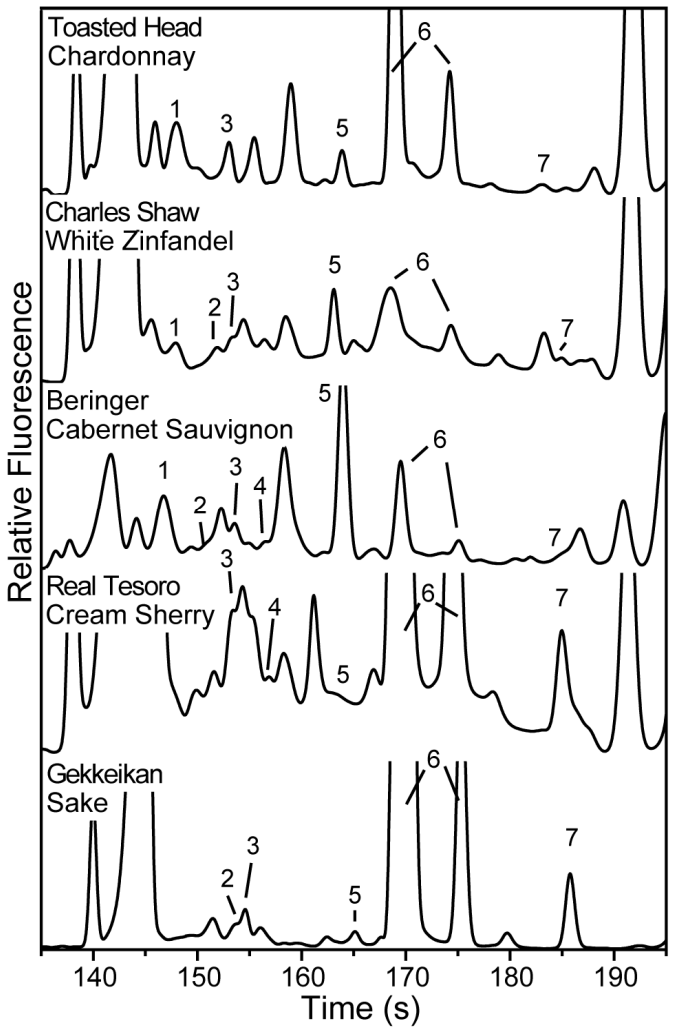

Figure 5.3. Analysis of Cascade Blue labeled fermented beverages.

Benzophenone and p-anisaldehyde (1), 3-methyl-2-butanone (2), acetoin (3), methylethylketone (4), diacetyl (5), acetaldehyde (6), and formaldehyde (7) are readily identified and quantitated concentrations are summarized in Table 5.1. All electropherograms are of samples of equal beverage volumes and are displayed offset on the same scale. Samples are labeled at pH 5, then diluted to pH 9.5 for analysis on the MOA.

Table 5.1 Aldehyde and ketone content of selected fermented beverages

Ketone or Aldehyde	Fermented Beverage				
	Toasted Head Chardonnay	**Charles Shaw White Zinfandel**	**Beringer Cabernet Sauvignon**	**Real Tesoro Cream Sherry**	**Gekkeikan Sake**
Benzophenone / p-Anisaldehyde	3.3 ± 0.7 mM	840 ± 90 µM	5 ± 1 mM	---	--
3-Methyl-2-butanone	--	18 ± 4 µM	900 ± 2 nM	--	14 ± 3 µM
Acetoin	120 ± 30 µM	30 ± 7 µM	70 ± 10 µM	1.1 ± 0.2 mM	70 ± 10 µM
Methylethyl-ketone	---	--	1.3 ± 0.4 µM	300 ± 100 nM	--
Diacetyl	80 ± 20 µM	300 ± 60 µM	1.9 ± 0.4 mM	30 ± 15 nM	17 ± 4 µM
Acetaldehyde	28 ± 4 µM	49 ± 9 µM	50 ± 10 µM	600 ± 100 µM	380 ± 20 µM
Formaldehyde	170 ± 40 nM	230 ± 50 nM	90 ± 10 nM	27 ± 8 µM	14 ± 4 µM
Pyruvic Acid	1.0 ± 0.3 mM	1.0 ± 0.6 mM	110 ± 50 µM	270 ± 40 µM	160 ± 70 µM
α-Ketoglutaric Acid	1.5 ± 0.3 mM	500 ± 300 µM	1.2 ± 0.2 mM	--	300 ± 100 µM

Analysis of acetone in a Martian simulant sample. Given that we now know some information about the soil chemistry on Mars[23] it is of interest to examine the detectability of carbonyl compounds in these samples. The Mars simulant sample with soluble ions spiked into a clean basalt matrix at concentrations measured by Phoenix was designed to mimic the Martian regolith[23]. Acetone was spiked into this Mars simulant sample as a model carbonyl-containing compound, and the sample was either exposed to darkened ambient conditions or UV irradiation to simulate potential Martian conditions. The acetone concentration was chosen at 10x that found in the Murchison meteorite for ease of tracking its rapid decay in the Mars simulant. The normalized, blank-corrected area of the acetone peak at various exposure times is shown in Figure 5.4. Values and error bars reported are calculated from the average and standard deviation of triplicate experiments. Under ambient conditions in the dark, the acetone peak area drops significantly within 25 min. When exposed to UV irradiation, the acetone content drops precipitously within 5 min and to blank levels within 20 min.

5.5 Discussion

The differences in concentrations required to obtain roughly equal peak heights in Figure 5.2 for the various ketones and aldehydes reflect the relative reactivities of the compounds studied. Formaldehyde has the most cationic character at the carbonyl carbon, and thus is the most reactive compound studied, as indicated by its 70 pM LOD. Alkyl aldehydes and then alkyl ketones constitute the next most reactive compound classes. The electron-donating alkyl groups provide some stability to the carbonyl carbon, reducing its electrophilicity. Aryl aldehydes and ketones are least reactive due to resonance stabilization, which dramatically reduces the electrophilic reactivity of the carbonyl carbon. The lower reactivity of these species are best illustrated by the dramatically higher 1.6 μM LOD obtained for benzophenone. Nevertheless, these results demonstrate that CB-labeling followed by CE analysis is a robust method for aldehyde and ketone analysis.

With the labeling method developed here, the MOA can be used for a wide variety of practical food and environmental analyses. As an example, we have performed quantitative analysis of several ketones and aldehydes found in fermented beverages. Acetoin is produced during the fermentation process, reaching a peak of approximately 1.1 mM[159] then decreasing to approximately 50-230 μM;[159] all table wines studied are within this range except for the cabernet sauvignon, which exhibits a slightly higher acetoin concentration (300 ± 60 μM). When fermentation is halted early by ethanol fortification, acetoin is locked in a higher concentration, as in the sherry (1.1 ± 0.2 mM). Acetaldehyde is formed during the fermentation process in large quantities that vary significantly based on wine type.[167] White wines have been reported to contain 250 μM to 11 mM acetaldehyde, red wines 90 μM to 5 mM acetaldehyde, sake 300 μM to 2 mM, and sherry 2 to 11 mM.[167] Despite using freshly opened bottles for each analysis and spiking acetaldehyde prior to labeling for quantitation, the values determined here are significantly lower than those reported elsewhere.[167] This probably stems from two causes: (1) the wines analyzed here contain sulfites; the bisulfite ion reacts reversibly with carbonyl compounds, lowering their available concentration for reaction with the CB-hydrazide, and (2) the very alkaline conditions used in prior analyses[168] to hydrolyze sulfite-bound carbonyls have been shown to generate acetaldehyde from other wine components.[168] Pyruvic acid in wine is reported in the literature to be in the 60-600 μM range.[159] All wines studied fell within this range

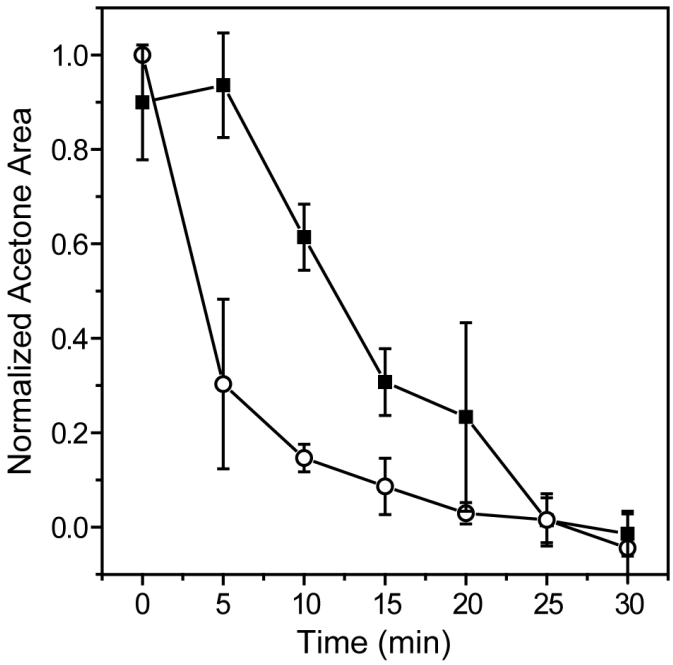

Figure 5.4. Measured concentration of acetone in the Mars simulant held in the dark (filled squares) and exposed to UV irradiation (open circles).

Acetone peak areas and error bars are calculated from the averages and standard deviations of data that has been blank corrected and normalized.

except for slightly elevated levels in the white wine (chardonnay) and the blush (white zinfandel). α-Ketoglutaric acid is reported in the 30-400 μM range in wines;[159] our analyses of chardonnay and cabernet sauvignon suggest the range extends up to the low mM level. Despite our inability to rule out contributions to peaks from unidentified aldehydes and ketones due to comigration, and a peak capacity within the region of interest of only ~ 30 (see Supplemental Appendix E for peak capacity calculations), this method is able to quantify all wine components but acetaldehyde to within comparable values reported by previous researchers.[159,167-168]

Although the presence of formaldehyde in fermented beverages is a concern, the highest levels of formaldehyde observed in the fermented beverage samples examined are below the U.S. health advisory limit for formaldehyde contamination of drinking water (33 μM);[169] a 60 kg person would need to consume approximately 17 L of cream sherry (~30 μM) to reach the World Health Organization Tolerable Daily Intake for formaldehyde in drinking water (150 μg/kg body weight),[170] which would correspond to an ethanol dose of ~ 3x LD_{50} (rat, 10.3 g/kg body weight).[171] In fact, all levels are at least an order of magnitude lower than those reported by the Environmental Working Group's National Assessment of Tap Water Quality in South Lake Tahoe's public drinking water in 2002 (170 μM).[172]

The successful analysis of acetone in the Mars simulant sample demonstrates our capability to analyze aldehydes and ketones in samples having significant concentrations of multivalent cations, oxidants, and other salts. Because these experiments indicate a limited lifetime of aldehydes and ketones in Martian soil, detection of these molecules on Mars would require a recent biological generation or recent exposure to ambient conditions and rapid analysis. Since little is known about the organic chemistry of Mars or other extraterrestrial bodies, any comprehensive organic chemical analysis suite should include the capability to detect and quantify these partially oxidized organic molecules with high sensitivity. Our technique has additional capabilities required for *in situ* astrobiological analysis, including the absence of organic solvents, a highly fluorescent probe yielding high sensitivity to aldehydes and ketones (2 parts-per-trillion for formaldehyde), portability, and ease of automation as demonstrated previously[91]. The versatility and robustness of this system for successful aldehyde and ketone analysis from very different matrices and analyte compositions is demonstrated by the ease at which we were able to handle both wine samples with high concentrations of a large number of aldehydes and ketones and the Mars simulant sample with low concentrations of a single ketone component. However, the rapid disappearance of acetone under simulated Martian conditions and the oxidation of Martian organic molecules to their carboxylic acid derivatives proposed in the literature[26] indicates the further need for an analytical method capable of detection and quantification of organic acids. We are developing techniques to label carboxylic acids using CB and a coupling reagent; this work will be published separately. For more information, visit http://astrobiology.berkeley.edu.

5.6 Acknowledgements

Microdevices were fabricated in the UC Berkeley Microfabrication Laboratory. This research was supported by NASA grant NNX08AR09G.

Chapter 6 : Analysis of Carbonaceous Biomarkers with the Mars Organic Analyzer Microchip Capillary Electrophoresis System: Carboxylic Acids

In preparation for submission to *Astrobiology*. Co-authors are Caroline Chandra Tjin, who conducted and analyzed part of the limit of detection experiments, and Thomas N. Chiesl and Richard A. Mathies, who provided invaluable advice, guidance, leadership, and editing.

6.1 Abstract

The evidence for oxidizing surface chemistry on Mars suggests that any comprehensive search for organic compounds indicative of life requires methods to sensitively analyze higher oxidation states of carbon. To address this goal, microchip capillary electrophoresis methods are developed for analysis of carboxylic acids with the Mars Organic Analyzer (MOA). Fluorescent derivitization is achieved by activation with the water soluble 1-ethyl-3-(3-dimethylaminopropyl)carbodiimide (EDC) followed by reaction with Cascade Blue hydrazide in 30 mM borate, pH 3. A standard containing twelve carboxylic acids found in terrestrial life is successfully labeled and separated in 30 mM borate, pH 9.5, 20 ^{o}C using the MOA CE system. Limits of detection are 5-10 nM for monoacids, 20 nM for malic acid, and 230 nM for citric acid. Polyacid benzene derivatives containing 2, 3, 4, and 6 carboxyl groups are also analyzed. Mellitic acid was successfully labeled and analyzed with a LOD of 300 nM (5 ppb). Successful analyses of carboxylic acids sampled from a lava tube cave and a hydrothermal area demonstrate the versatility and robustness of our method. This work establishes that MOA technology can be used for sensitive analyses of a wide range of carboxylic acids in the search for extraterrestrial organic molecules.

6.2 Introduction

In 1976, the Viking landers explored the Martian surface for signs of life and organic carbon.[12-15,17] The two landers each carried a suite of life detection experiments[12-16] and a GC-MS instrument for organic molecule detection.[17-18] While the labeled release experiment in the life detection suite returned evidence consistent with a biotic metabolism,[14] the GC-MS detected no organic molecules of Martian origin.[15] The prevalent explanation for these seemingly contradictory results is that the organic nutrient media introduced in the labeled release experiment was oxidized by a strong oxidant native to the Martian regolith[26] which would also account for the GC-MS results.[12,17-18] The strong oxidant theory is further strengthened by the recent Phoenix lander observations of the oxidant perchlorate in the polar Martian regolith.[23] The oxidizing conditions on Mars suggest that organic carbon, if it is present, will be found in an oxidized form such as carboxylic acids. In fact, Benner *et al.*[26] proposed that aromatically stabilized highly oxidized species, such as the hexacarboxylate benzene derivative mellitic acid, are the only surviving organic molecules on Mars.[26]

Carboxylic acids are ubiquitous in extraterrestrial material. They have been found in meteorites, including the Murchison meteorite, which contains several carboxylic acids including all possible isomers C_1-C_5.[53] In interstellar space, carboxylic acids including formic acid[157,173] and acetic acid[174] have been observed by microwave spectroscopy. Carboxylic acids, including formic acid, have also been found in Earth's troposphere.[175] With an average organic carbon in-fall rate to Mars of 10^8 kg/yr,[59] it is highly likely that organic acids are present on Mars. Thus, any survey for the presence of organic carbon on Mars must consider organic acids.

The Mars Organic Analyzer (MOA) microchip capillary electrophoresis system[103] has demonstrated exceptionally high sensitivity for a variety of compound classes. The MOA was originally designed and built for highly sensitive detection and analysis of fluorescamine-labeled amino acids,[103] and it was used to successfully analyze these targets in samples of jarosite from

the Panoche Valley, CA, and the Atacama Desert, Chile, with pptr limits of detection.[103] The use of Pacific Blue succinimidyl ester labeling of amines and amino acids enabled even more sensitive analyses of samples from the Murchison meteorite and the Atacama desert.[69] Enhanced labeling and analytical protocols enabled analyses of samples high in salinity, acidity, and polyvalent metal cation content, including saturated brines from the Saline Valley, CA, and the acidic and metallic Rio Tinto in Spain.[162] Cyclodextrin-assisted CE separations were used by Stockton *et al.*[138] to detect ppb levels of polycyclic aromatic hydrocarbons in a variety of environmental and Mars simulant samples.[138] The use of Cascade Blue hydrazide (CB) derivitization enabled MOA detection of aldehydes and ketones from samples ranging from fermented beverages to a basaltic Martian regolith simulant.[176] This raises the question as to whether new methods can be developed to analyze carboxylic acids using the MOA.

Several CE methods have been reported for the separation and detection of carboxylic acids.[177-181] Most methods take advantage of the high mobilities of underivatized organic acids and operate under reversed polarity,[178-179] requiring the use of coated capillaries or a surfactant to suppress or reverse EOF. These methods typically use indirect absorbance or fluorescence detection or direct absorbance targeting the carboxyl group at 200 nm, with limits of detection ranging from 0.5-1000 μM.[177-179] Fluorescent derivitization of organic acids has also been employed for CE separations,[178] but has been more commonly employed for HPLC separations.[182] Water soluble carbodiimides, particularly 1-ethyl-3-(3-dimethylaminopropyl) carbodiimide (EDC), have been used for efficient aqueous carboxylic acid activation[182-183] for fluorescent derivitization.

In this paper, we utilize EDC activation to enable Cascade Blue hydrazide (CB) labeling of carboxylic acids (Scheme 6.1) for capillary electrophoresis analysis on the MOA. One-pot activation and derivitization is conducted in aqueous solution with no organic solvents. The EDC-activated CB labeling reaction and separation of CB-labeled carboxylic acids is optimized as a function of reaction pH and reaction time. We analyze a standard containing carboxylic acids found in the Murchison meteorite, typical terrestrial carboxylic acids, and several polycarboxylic acid derivatives of benzene, including mellitic acid. Samples from a lava tube cave and a hydrothermal area are analyzed for their organic acid content. This work expands the capability of the MOA to the highly sensitive analysis of carboxylic acids, a critical class of oxidized organic molecules.

6.3 Materials and Methods

Buffer, reagent, and sample preparation. Sodium tetraborate and boric acid were obtained from Sigma-Aldrich (St. Louis, MO) and used to prepare 400 mM borate stock solutions that were diluted to 30 mM borate and adjusted to the desired pH using NaOH or HCl. Carboxylic acid standards were prepared as aqueous 20 mM stock solutions using octanoic, heptanoic, hexanoic, pentanoic, butanoic, propionic, acetic, formic, pyruvic, α-ketoglutaric, malic, citric, and mellitic acids (all Sigma-Aldrich). These carboxylic acid stocks were combined in appropriate volumes to create the acid standards. Cascade Blue hydrazide trisodium salt (CB, Ex. 396, Em. 410) was obtained from Invitrogen (Carlsbad, CA) and dissolved to 10 mM in water and stored at -20 ^{o}C. The activating reagents 2-(7-aza-1H-benzotriazole-1-yl)-

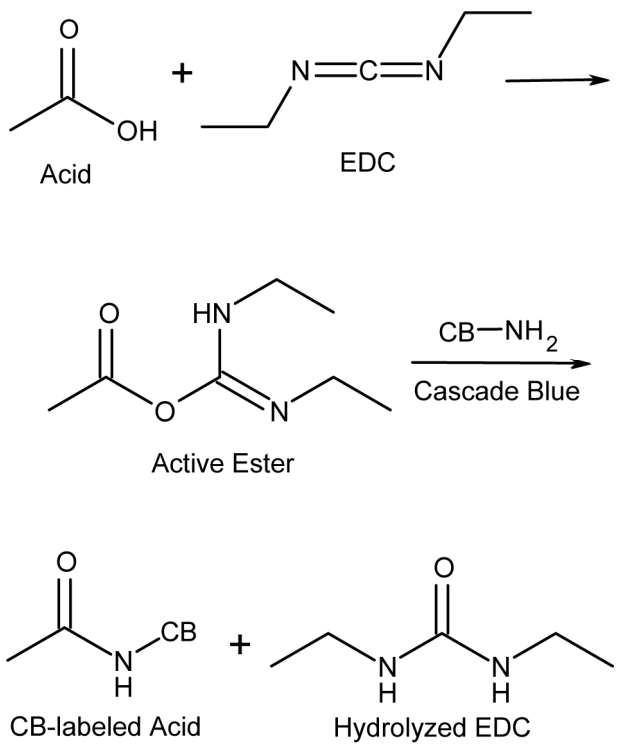

Scheme 6.1. EDC-activated labeling of carboxylic acids.

1,1,3,3-tetramethyluronium hexafluorophosphate (HATU, Sigma), 2-(1H-benzotriazol-1-yl)-1,1,3,3-tetramethyluronium hexafluorophosphate (HBTU, Sigma), 2-(6-chloro-1H-benzotriazole-1-yl)-1,1,3,3-tetramethylaminium hexafluorophosphate (HCTU, Novabiochem), and 1-ethyl-3-(3-dimethylaminopropyl)carbodiimide (EDC, Sigma) were dissolved to 20 mM in acetonitrile. The coupling catalysts 1-hydroxy-7-azabenzotriazole (HOAt, Sigma), hydroxylbenzo-triazole (HOBt, Sigma), and N-hydroxysuccinimide (NHS, Sigma) were also dissolved to 20 mM in acetonitrile. The 20 mM solutions of activating reagents and catalysts were divided into 100 μL aliquots, evaporated to remove solvent, and stored at -20 ^{o}C. Just prior to use, the aliquots were resuspended to the desired concentration with 30 mM borate buffer, pH 3.

Labeling reactions were conducted by combining 1 μL of standard with 3 μL CB stock, 36 μL 30 mM borate buffer, and 10 μL EDC in 30 mM borate buffer. The labeling mixture was allowed to react at room temperature overnight before 1:100 dilution for analysis. Unless otherwise indicated, separations were conducted at 20 ^{o}C. Electropherograms were analyzed using PeakFit (Systat Software, San Jose, CA) to determine the signal-to-noise, resolution, and peak efficiency in theoretical plates per meter for each aldehyde and ketone peak.

To determine the effect of the labeling buffer pH on the labeling reaction and separation, 30 mM borate solutions were prepared at pH ranging from 2 to 12. This range of pH range put some stock solutions at a pH outside the buffering regimes of borate, so a large volume (46 μL out of 50 μL total) of the pH adjusted solution was used to preserve the pH. These buffers were used for the labeling reaction, then diluted and analyzed with 30 mM borate pH 9.5. To explore the pH dependence of the separation, labeling was conducted using 30 mM borate, pH 3, then diluted and analyzed with each of the buffers. Time-course experiments were conducted by preparing labeled carboxylic acid standard using 30 mM borate, pH 3, and were diluted at various times into 30 mM borate, pH 9.5, for immediate analysis.

Limits of detection were determined by preparing 10 to 12 concentrations of the indicated carboxylic acid in 30 mM borate, pH 3, from each of three independently prepared 20 mM stock solutions. For the aliphatic acids and malic acid, 1 μL CB and 4 μL 20 mM EDC was added to 50 μL of each concentration of acid and allowed to react for 18 or 48 hrs. For citric acid, 2 μL CB and 3 μL 40 mM EDC was added to 50 μL of each concentration of acid, and for mellitic acid, 5 μL CB and 5 μL 40 mM EDC was added to 50 μL of each concentration of acid. Immediately before analysis, each reaction was diluted 1/3 with 30 mM borate, pH 9.5.

The Bumpass Hell samples were collected in clean, individually wrapped 1.5 mL Eppendorf tubes from the outflow channel draining the entire Bumpass Hell hydrothermal area near the base of the boardwalk (40.457346 ^{o}N, -121.502266 ^{o}W) at Lassen National Park, CA. The samples were stored at -20 ^{o}C, and were labeled by combining 30 μL sample with 2 μL CB stock, 10 μL 80 mM EDC in 30 mM borate buffer, pH 3, and 8 μL 30 mM borate buffer, pH 3. After an overnight reaction, these solutions were diluted 1:5 with 30 mM borate buffer, pH 9.5, immediately prior to analysis. Labeled carboxylic acid standard was combined with the labeled samples for identification of carboxylic acid components. Quantitation was conducted by spiking with appropriate concentrations of carboxylic acid components prior to labeling and analysis.

The Yurtle cave samples were collected from the floor of Yurtle cave (mouth GPS UTM coordinates Zone 11S 557603 mE 3843054 mN) in the Pisgah lava flows in the Mojave Desert, CA. For sampling, the top 1 cm of particulate basalt sediment was removed and the sample collected from the lower 1-3 cm of sediment. The sample was run through a wire mesh with 515 x 575 μm holes to remove basalt gravel before extraction for analysis by combining H_2O with the sample at a ratio of 1 μL H_2O per 1 mg sediment. This extract was labeled by combining 1 μL sample with 1 μL CB stock, 1 μL HCl, 10 μL 20 mM EDC in 30 mM borate buffer, pH 3, and 7 μL 30 mM borate buffer, pH 9.5. After an overnight reaction, these reactions were diluted 1:10 with 30 mM borate buffer, pH 9.5, immediately prior to analysis. As with the Bumpass Hell samples, labeled carboxylic acid standard was combined with the labeled samples for identification of carboxylic acid components and quantitation was conducted by spiking with appropriate concentrations of carboxylic acid components prior to labeling and analysis.

Microdevice fabrication. The microdevices were prepared as previously described[67,69,81,103,106,138,162,176] and will be briefly discussed here. A sacrificial layer of polysilicon was deposited on a 10-cm borofloat glass wafer. Photoresist was spin-coated onto the wafer and patterned through a chrome mask using a contact aligner. The photoresist was developed and the exposed polysilicon was removed by plasma etching. After the glass was etched in buffered HF, the photoresist was stripped and reservoir holes were drilled. The polysilicon layer was then removed, and the wafer was thermally bonded to a blank wafer to form completed folding channels (23.6 cm long, 110 μm wide, 30 μm deep). Injections were performed via a cross-channel (1.2-cm long) located 0.6 cm from the anode end of the channel. A 3-mm deep PDMS gasket with 4-mm diameter wells placed over the reservoir holes alleviates evaporative and hydrodynamic imbalance issues by allowing for loading of sample and buffer volumes up to 50 μL. A schematic of the microdevice can be found in previous publications.[69,138,162]

Mars Organic Analyzer. The Mars Organic Analyzer (MOA)[103] was used with the previously published minor modifications to the optical subsystem that allow for more sensitive analysis of amino acids and polycyclic aromatic hydrocarbons.[69,138,162] The 404 nm laser was passed through a dichroic and focused to a 10-20 μm spot in the channel approximately 0.6 cm from the cathode reservoir. Fluorescence was collected by the objective and reflected by the dichroic through a long pass filter (50 % T at 425 nm) onto a PMT, which was digitized at 50 Hz.

Separation and injection procedures. Separations and injections were conducted as previously described.[176] Microchip separation and injection channels were first filled with 1 N NaOH for cleaning, rinsed with water, then filled with running buffer for analysis and the sample well replaced with sample. Cross injection was accomplished by applying a potential across the sample (ground) and waste (-1500 V) wells for 30 s with the anode and cathode grounded. This was followed by a 200-ms step where the anode is floated. The separation was performed by applying -15 kV at the cathode, -1.5 kV at the sample and waste, and ground at the anode.

6.4 Results

Labeling optimization experiments. The one-pot labeling method is shown in Scheme 6.1. The carboxylic acid is activated *in situ* with the EDC activating reagent; the activated ester then reacts with Cascade Blue hydrazide (CB) to form the hydrazide amide. This amide-like product is stable against hydrolysis and further reaction. Several activating reagents were evaluated at different pHs in aqueous solution, including HATU, HBTU, HCTU, and EDC. Of these, only EDC gave significant coupling of carboxylic acids with CB in aqueous solution. Potential catalytic reagents were also explored for their use in increasing the efficiency of EDC-activated coupling, including HOAt, HOBt, and NHS, but none produced higher labeling efficiencies than EDC alone.

The pH dependence of the EDC-activated reaction of carboxylic acids with CB is shown in Figure 6.1 A. In this experiment, a standard containing straight-chain aliphatic acids C_1-C_8 was reacted with CB and EDC at various pHs and analyzed with the MOA. No reaction is seen at any basic pH. The reaction extent rises with lower pH and an optimal reaction efficiency is seen at pH 3. This observation is due to the necessity of protonation of one of the EDC nitrogens to increase the electrophilicity at the central carbon which increases its reactivity towards nucleophilic attack by a lone pair on the carboxylic oxygen. The kinetics of labeling at pH 3 were also examined (Figure 6.1 B). At room temperature, the reaction proceeds to ~ 50 % in 1 hr, and to ~ 80 % in 18-20 hrs. Increased temperature was found to decreases the reaction efficiency (Figure F.1 in Appendix F).

Separation optimization experiments. The dependence of separation quality upon pH and temperature was explored and found to be similar to that previously observed for separations of aldehydes and ketones.[176] This is expected because in both separations the -3 charged CB moiety is the dominating factor determining the mobility of the labeled analytes. The average resolution between peaks in the C_1-C_8 aliphatic acid standard labeled at pH 3 (Figure F.2 A in Appendix F) does not depend on the temperature of separation. However, the peak amplitudes decrease with decreasing temperature (Figure F.2 B in Appendix F). The pH dependence was also explored, with the aliphatic standard labeled at pH 3 and then diluted into analytical buffer of the desired pH. Optimal separation is achieved at pH 9 - 10 (Figure F.3 in Appendix F), so further separations were conducted at pH 9.5.

Optimal labeling and separation of a carboxylic acid standard and limits of detection. A standard was created containing the C_1-C_8 normal aliphatic acid standard and several keto- and poly-acids including pyruvic, α-ketoglutaric, malic, and citric acids. The standard was labeled at pH 3 and diluted to pH 9.5 for analysis (Figure 6.2). Polyacids are derivatized multiple times and thus give rise to multiple peaks. Limits of detection (LOD, Table 6.1) were determined for two aliphatic monoacids (propionic and butyric acids) and for the polyacids malic, citric, and mellitic acid. LODs represent the labeling detection limit; they are calculated from solutions diluted to low concentration prior to labeling. The aliphatic acid LODs were determined after 18 and 36 hrs of labeling, but no major differences in LOD were seen either between the two acids or the two reaction times (~ 5 nM), so further LOD experiments were conducted only at 18 hr reaction times. Polyacids had higher LODs: the di-carboxylic malic acid LOD was 20 nM, the tri-carboxylic citric acid was 230 nM, and the hexa-carboxylic mellitic acid was 300 nM.

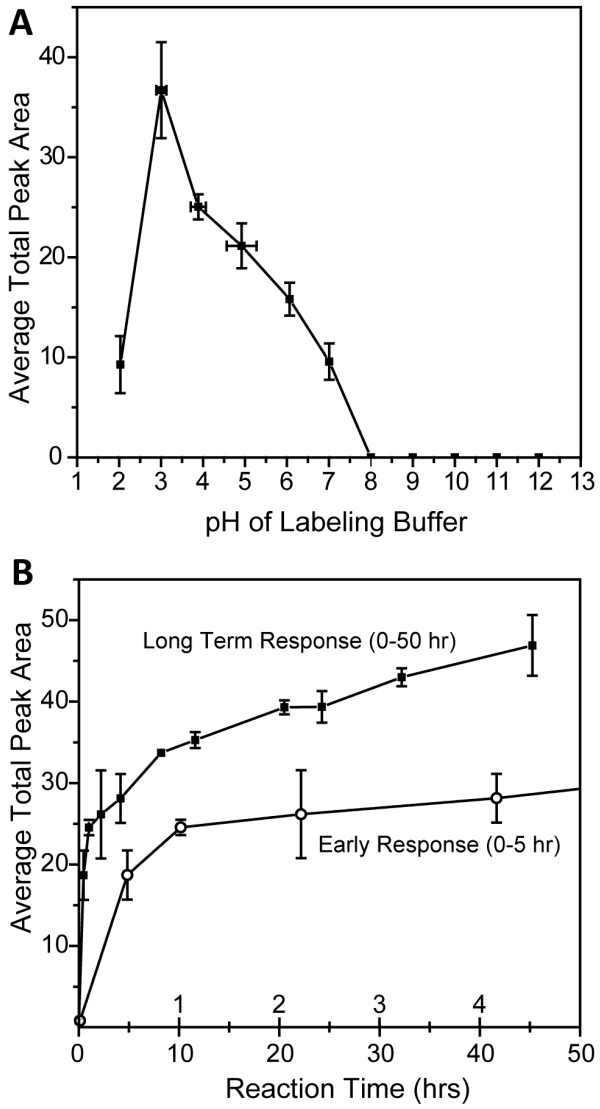

Figure 6.1. Optimization of 1-ethyl-3-(3-dimethylamineopropyl) carbodiimide (EDC)-activated Cascade Blue hydrazide (CB) labeling of carboxylic acids.

(A) Dependence of the total peak area of a standard on labeling pH with overnight reaction (> 18 hr). (B) Dependence of the total peak area of the acid standard on labeling reaction time at pH 3. The acid standard contains 2.7 mM formic acid and heptanoic acid, 1.3 mM acetic acid, propionic acid, butyric acid, pentanoic acid, and hexanoic acid, and 4 mM octanoic acid. Labeling reactions contained 1 µL standard, 36 µL 30 mM borate, at indicated pH, 3 µL 20 mM CB, and 10 µL 20 mM EDC. Reactions were diluted 1:5 with 30 mM borate, pH 9.5, prior to analysis. The peak areas for each acid were determined and summed; the average of triplicate experiments is plotted with error bars determined from the standard deviation.

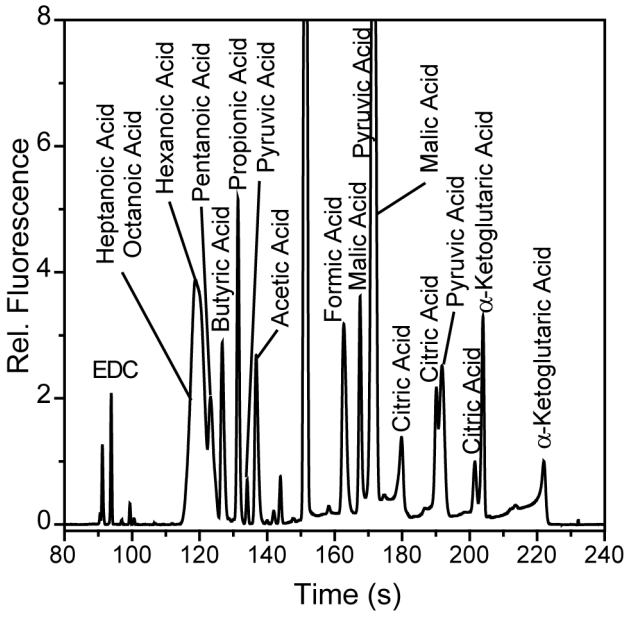

Figure 6.2. Optimized separation of a Cascade Blue labeled carboxylic acid standard.

The standard contains 2 μM formic acid and heptanoic acid, 1 μM acetic acid, propionic acid, butyric acid, pentanoic acid, hexanoic acid, 3 μM octanoic acid, and 5 μM malic acid, pyruvic acid, α-ketoglutaric acid, and citric acid. The 30-hr labeling reaction used EDC activation in 30 mM borate, pH 3. The labeled standard was diluted with 30 mM borate, pH 9.5, before analysis at 20 ^{o}C in the same buffer.

Table 6.1. Carboxylic acid limits of detection

Carboxylic Acid	Limit of Detection[a]	
	(18 hr Reaction)	(48 hr Reaction)
Propionic Acid	6 ± 5 nM	2 ± 1 nM
Butyric Acid	7.3 ± 0.5 nM	16 ± 6 nM
Malic Acid	20 ± 3 nM	--[b]
Citric Acid	230 ± 80 nM	--[b]
Mellitic Acid	300 ± 200 nM	--[b]

[a] LOD and uncertainty calculated from triplicate experiments at twelve concentrations.

[b] No significant difference seen between 18 and 48 hr reactions for propionic and butyric acids, so further LODs conducted only at 18 hrs.

Mobilities and peak assignments of polyacidic benzene derivatives. In capillary zone electrophoresis (CZE), two factors determine the elution time of analytes: their inherent mobility and the induced electroosmotic flow (EOF) in an electric field. EOF mobilizes all analytes to the detector; negatively charged analytes migrate against EOF, reducing their net velocity. The inherent mobility of an analyte is given by the first-order approximation Eq. 1:

$$\mu_i = \frac{q}{6\pi\eta r} = C\frac{q}{r} \qquad \text{Eq. 1}$$

where μ_i is the analyte mobility, q is the analyte charge, η is the viscosity of the solution, r is the analyte solvated radius and C is $1/6\pi\eta$.

In the case of malic acid, the charge of the labeled acid is the sum of the charges of CB (-3) and the underivatized carboxyl groups (-1 per underivatized carboxyl). Based on the relative sizes of CB and malic acid, a reasonable assumption is that the radius of the singly labeled acid approximates the radius of a CB molecule, and the radius of the doubly labeled acid is approximately twice the CB radius. Eqn. 1 gives $-4C/r_{CB}$ for the mobility of the singly labeled acid and $-3C/r_{CB}$ for the mobility of the doubly labeled acid. These simplified mobility calculations indicate that the singly labeled species migrates faster against EOF and thus elutes later than the doubly labeled acid due to its considerably smaller effective radius.

The separation pattern for malic acid is supported by labeling experiments performed at different acid-to-CB ratios (Figure F.4 in Appendix F). When CB >> acid, the dominant product is the doubly labeled acid which is the more intense earlier peak. When CB < acid, the dominant product is the singly labeled amino acid which appears later.

This treatment extends to the evaluation of highly oxidized polyacid derivatives of benzene (Figure 6.3). Separations of polyacid benzene derivatives terephthalic (di-acid), trimesic (tri-acid), pyromellitic (tetra-acid), and mellitic (hexa-acid) acids are shown in Figure 6.3A. The peak assignments were used to calculate individual mobilities μ_i in Figure 6.3B according to the equation:

$$\mu_i = \mu_{net} - \mu_{EOF} = \frac{L_{channel}}{V}(v_i - v_{EOF}) = \frac{L_{separation}L_{channel}}{V}\left(\frac{1}{t_i} - \frac{1}{t_{EOF}}\right) \qquad \text{Eq. 2}$$

where μ_{net} is the analyte net mobility, μ_i is the inherent mobility, μ_{EOF} is the induced EOF mobility, v_i is the velocity of the analyte in an applied potential V along a channel of length $L_{channel}$, $L_{separation}$ is the separation column length, t_i is the analyte elution time, t_{EOF} is the elution time of neutral markers of EOF, and v_{EOF} is the velocity of EOF. For the separations in Figure 3A, typical t_{EOF} are ~ 75 s, $L_{separation}$ = 22.6 cm, $L_{channel}$ = 23.4 cm, and V = 15 kV.

The mobilities are plotted in Figure 6.3B. For each polyacid (dash-dotted lines indicated by the polyacid name), the singly labeled derivative has the most negative mobility and elutes last, the doubly labeled next to last, and so on. The acids can be divided into size groups based on the number of CB molecules in the derivatized polyacid (dashed lines indicated by number of CB). Within these size groups, mobilities increase in absolute value with increasing charge, confirming prior assumptions and peak assignments. The slopes of lines fit to each size group

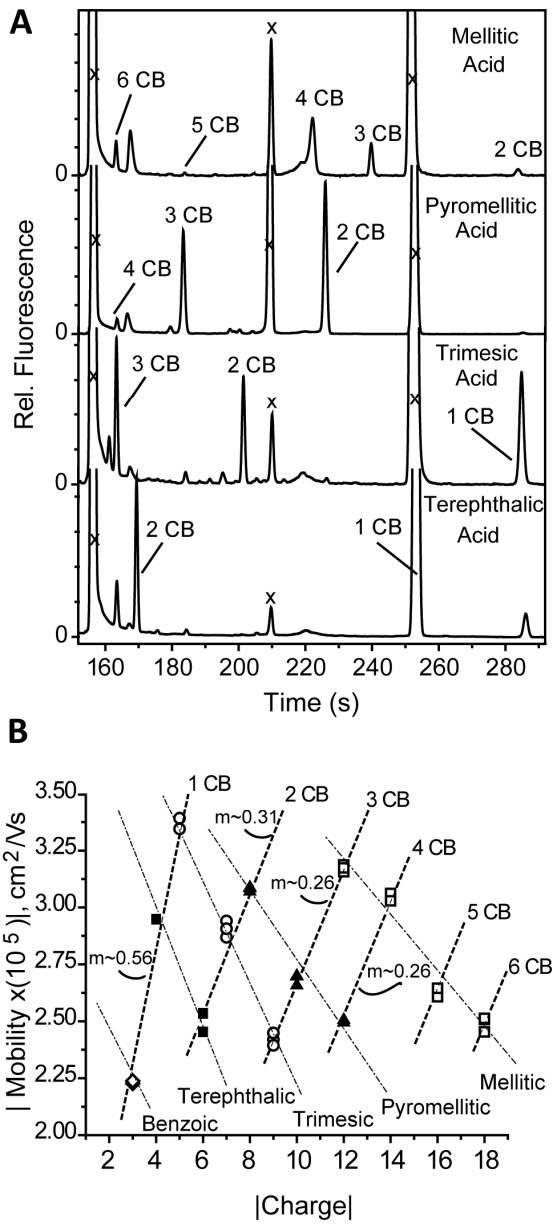

Figure 6.3. (A) Electropherograms of polycarboxylic acid derivatives of benzene with peak assignments indicated, and (B) Plot of mobilities of polycarboxylic acid derivatives of benzene vs. nominal charge.

For ease of visualization, the absolute values were taken of the charge and the mobility so that positive values could be plotted on both axes. Degree of labeling is indicated by 1 CB for reaction with one CB molecule, 2CB for reaction with 2 CB molecules, etc. Slopes of the linear fit to each size group are indicated. System peaks are labeled with "x." Chemical species is identified by icon: benzoic acid by diamonds, terephthalic acid by filled squares, trimesic acid by circles, pyromellitic acid by triangles, and mellitic acid by open squares. Labeling reactions used EDC activation in 30 mM borate, pH 3. Labeled acids were diluted with 30 mM borate, pH 9.5, before analysis at 20 ^{o}C in the same buffer.

are inversely related to the analyte size, revealing that r_{2CB} is $1.8r_{1CB}$, r_{3CB} and r_{4CB} are similar at ~ $2.1r_{1CB}$.

Of note is the lack of observance of a singly-labeled mellitic acid peak. This relatively small and highly negatively charged (-8) molecule is expected to travel faster than the EOF and is not mobilized to the detector. Also of note is the extremely small peak observed for the penta-labeled mellitic acid. The low signal of this peak is presumably due to activation of the underivatized site (positive ρ values) associated with either EDC activation or CB derivitization that increases the rate of conversion of the penta-labeled acid to the hexa-labeled derivative.

Real-world sample analysis. In complex samples containing amines, EDC-activated acids react with amines as well as CB, reducing the yield of labeled product and thus the carboxylic acid signal. To counteract this problem, we tested protocols to cap amines with Boc-OSu (Scheme F.1 in Appendix F) and Pacific Blue succinimidyl ester. Simple amine capping with these reagents did not show any improvement in acid labeling efficiency (Figure F.5 in Appendix F), so they were not used for complex sample analysis.

Figure 6.4 presents electropherograms with peak assignments of two astrobiologically relevant samples, an aqueous extract of a Yurtle Cave sediment (top) and Bumpass Hell (bottom). The Yurtle Cave sample, collected from a lava tube cave in the Pisgah Lava flows in the Mojave Desert, was extracted with water to solubilize carboxylic acids for reaction. The extract required the addition of HCl for pH adjustment to avoid excessive dilution with buffer because its initial pH was ~10. The pH of the Bumpass Hell sample, collected from the outflow channel draining the Bumpass Hell hydrothermal area in Lassen National Park, CA, was 1.9. Due to its low pH, the Bumpass Hell sample was labeled at high concentration with little to no pH adjustment.

The carboxylic acids in both samples were quantitated by the addition of carboxylic acid standard spikes prior to labeling. The numerical results for these samples are given in Table 6.2. The Yurtle Cave sample contains a diverse set of monoacids with a total concentration of ~ 2 ppm, and has peaks corresponding to all of the C_1-C_8 straight-chain aliphatic acids in the standard in Figure 6.2. The Bumpass Hell sample contains fewer aliphatic acids but has several significant polyacid peaks, including those identifiable as pyruvic, malic, citric, and α-ketoglutaric acids. The total carboxylic acid content in this sample is > 16 μM.

6.5 Discussion

Limits of detection. The reactivities of the single carboxylic acids studied here are relatively unaffected by the structure of the individual acid. The benzoic acids exhibited somewhat reduced reactivity that was not studied in detail; the primary contribution to LOD variation is from mild CB self-quenching. The LODs of malic and citric acid were evaluated for the peak most visible at the lowest concentration; for malic this was the twice-labeled acid and for citric this was the thrice-labeled acid. The self-quenching of CB is evident from the higher LODs of these acids (20 nM for malic and 230 nM for citric) than their mono-labeled counterparts (5-10 nM for propionic and butyric). This conclusion was independently verified with bulk fluorescence measurements. The LOD for mellitic acid was calculated for the tetra-labeled peak because the 6-labeled peak co-elutes with formic acid and the 5-labeled peak is

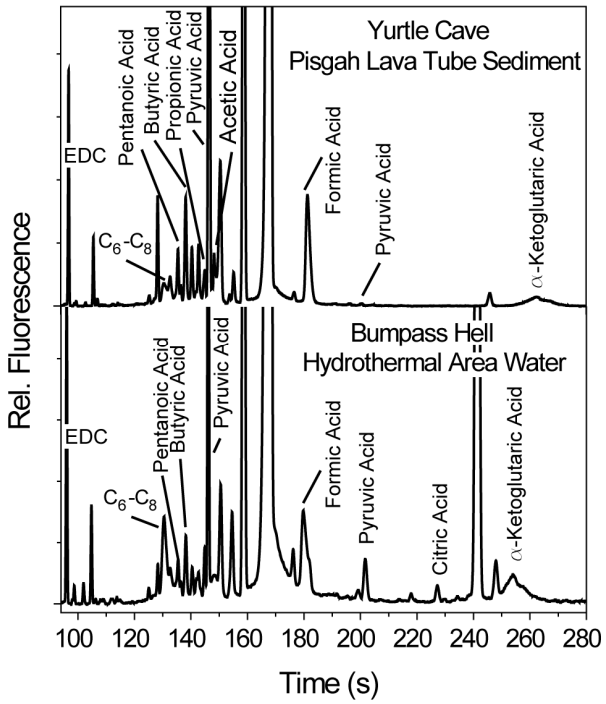

Figure 6.4. Cascade Blue labeled extracts of a sediment from the floor of a lava tube cave in the Pisgah lava flows in the Mojave Desert, CA, (top) and a water sample taken from the outflow channel of Bumpass Hell, a hydrothermal area in Lassen National Park, CA (bottom).

The sediment sample was extracted with water. Both samples were labeled using CB with EDC activation in 30 mM pH 3 borate. Samples were analyzed in 30 mM borate, pH 9.5.

barely visible. The calculated mellitic acid LOD is highest of the acids (300 nM), translating to a 5 ppb limit of detection in a sediment sample, assuming 100 % extraction efficiency from 1 g sample dissolved to 50 μL volume (after lyophilization and rehydration). This sensitivity represents a dramatic improvement over previous flight instrumentation, since mellitic acid would have been virtually invisible to Viking's pyrolysis-GC-MS.[26] Salts of higher benzenecarboxylic acids are not volatile and do not yield volatile pyrolysis products, as confirmed by laboratory thermolysis MS experiments.[26] These experiments demonstrated that benzenecarboxylic acids are not detectable by MS using Viking extraction methods, even using higher pyrolytic temperatures and injecting directly into the MS (no GC).[26] Thus, the MOA's ability to detect these molecules with high sensitivity represents a significant advantage over the heritage pyrolysis-GC-MS methods used by Viking.

Astrobiological sample analysis. The successful analysis of samples from a lava tube cave in the Pisgah lava flows in the Mojave Desert, CA, and the Bumpass Hell geothermal area in Lassen National Park, CA, demonstrate the versatility of this analytical method and its robustness to varying sample extremes. The successful extraction and analysis of carboxylic acids from the fine basalt of the lava tube cave sediment demonstrate analytical robustness to similar Martian basalts.[184] Since Phoenix measured a slightly basic pH (~8) in the regolith at its polar landing site, the successful analysis from this pH 10 sample further validates the analytical protocol's robustness to potential Martian conditions.

The Mars Exploration Rover results suggest that the equatorial regions may be highly acidic, with sulfuric acid dominant.[20] The sulfurous[185] and acidic (pH < 2) Bumpass Hell sample, therefore, provides an analogue to this extreme sample matrix. The successful analysis of carboxylic acids from this sample demonstrates the versatility of our method to the variety of pH and salinity conditions that Mars may pose.

Comparison with instruments for organic chemical exploration on Mars. For comparison with other instrumental approaches, we consider the detection limit of the Sample Analysis at Mars (SAM) instrumental suite quoted at 10^{-11} mol.[186] Given the same 1 g sample and 100 % extraction efficiency assumed in our detection limit calculation, SAM would be able to detect ~ 32 ppb mellitic acid. While SAM is a GC-MS instrument, it will potentially carry a Sample Processing System (SPS) in 2-4 of its sample cups for derivitization of acids with a silylating reagent, such as N-methyl-N-(tert.-butyldimethylsilyl)trifluoroacetamide (MTBSTFA) to facilitate the detection of oxidized species including acids.[187] The most recently reported SPS protocol for extraction and derivitization of acids requires a separate system for derivitization and the use of an organic solvent, such as DMF, with recovery and derivitization rates for amino acids ranging from 30-100 %.[187] The method presented here requires no organic solvents, can be used with aqueous extraction techniques like subcritical water extraction (SCWE),[115] and the derivitization reaction can be performed on the same microfluidic device used for separations. With a 5 ppb LOD for mellitic acid, the MOA method presented here is 6-7 times more sensitive than SAM.

Another issue facing future instrumentation on Mars is robustness to varying sample matrices. Phoenix[23] indicated that robustness to a basic pH is required, while the Mars Exploration Rovers[20] indicate that robustness to extremely low pH is required. Both observations indicate that robustness to high salinity is required. It has been argued that if active

Table 6.2. Carboxylic acids in environmental samples

Carboxylic Acid	Concentration in Sample	
	Bumpass Hell	Yurtle Cave
Propionic Acid	--	61 ppb
Butyric Acid	7.5 µM	30 ppb
Acetic Acid	--	130 ppb
Formic Acid	6.8 µM	200 ppb
Pyruvic Acid	0.41 µM	1500 ppb
Citric Acid	1.5 µM	--

geothermal hot springs exist on Mars, these could provide an environment for Martian organisms[1]; terrestrial acidic hot springs are home to extremophilic ecosystems[29] and deep sea hydrothermal systems have been proposed as sites for the origin of life.[39] Therefore, it is important to have analytical protocols capable of delivering highly sensitive analyses of oxidized organic carbon from all possible relevant sample matrices. The true lesson of Viking may well be the need to fly robust analytical protocols with very high sensitivity for trace oxidized organic carbon. The methods for analysis of carboxylic acids developed here provides the robust and highly sensitive analyses required, making it ideal for use in *in situ* extraterrestrial chemical exploration. For more information on the MOA, visit http://astrobiology.berkeley.edu.

6.6 Acknowledgements

Microdevices were fabricated in the UC Berkeley Microfabrication Laboratory. This research was supported in part by NASA grant NNX08AR09G.

Chapter 7 : Autonomous Sample Processing and Analysis Using a Programmable Microfluidic Automaton and the Mars Organic Analyzer

This work is a collaborative effort between Amanda Stockton and Erik Jensen. Jensen conceived of the initial idea and fabricated, programmed, and operated the Automaton. Stockton prepared the chemistry and labeling protocols, operated the MOA, and wrote the text of this chapter. Thomas Chiesl provided advice and mentorship. This, along with further work, is in preparation for publication in *Lab on a Chip*.

7.1 Abstract

The Mars Organic Analyzer (MOA) provides highly sensitive assays for the target organic molecule classes indicative of life. The next critical step in the development of this system is autonomous sample processing. Here, we exploit the programmable capability of a microfluidic Automaton to integrate sample labeling, dilution, and loading with the MOA microchip capillary electrophoresis device. Three different chemistries are automated: amines and amino acids are labeled with Pacific Blue succinimidyl ester (PB), aldehydes and ketones are labeled via hydazone formation with Cascade Blue hydrazide (CB), and carboxylic acids are labeled with CB via EDC (1-ethyl-3-(3-dimethylaminopropyl) carbodiimide) activation (CB-EDC). The autonomous microfluidic process exhibits labeling efficiencies for PB and CB-EDC that were comparable to manual labeling. CB labeling of aldehydes and ketones is less efficient due to the extended transfer time between the Automaton sample processing system and the MOA microchip. The peak efficiencies decline with increased transfer time due to diffusion from the sample well into the separation column. Alternative device formats with faster transfer times are discussed which should result in higher peak efficiencies. This work demonstrates that Automaton-based sample processing is a promising technology for performing autonomous MOA analyses.

7.2 Introduction

The Mars Organic Analyzer (MOA)[81,103,106,134] is a highly sensitive microchip capillary electrophoresis instrument designed for *in situ* extraterrestrial organic chemical analyses. It has been used for highly sensitive analyses of polycyclic aromatic hydrocarbons (Chapter 2),[138] amines and amino acids (Chapters 3 and 4),[69,162] aldehydes and ketones (Chapter 5),[188] and carboxylic acids (Chapter 6).[189] Even as a laboratory prototype it has low mass (~ 10 kg), low volume (12”x12”x4”), low power requirements, and low reagent consumption and requires no organic solvents. The instrument was field tested in the Atacama desert[81] and the Panoche Valley, CA,[103] fully demonstrating its portability and applicability to Mars-analogue environments. However, the current MOA lacks an autonomous sample processing system capable of conducting labeling derivitizations, spiking of standards, dilutions, and analysis.

Several microchip formats have been developed for integrated sample processing. Passive micromixing devices require large microdevice footprints and rely on channel geometry or diffusion to induce mixing.[190-191] Active micromixers usually rely on an external perturbation to induce mixing, including ultrasonic, magnetic, and pressure field disturbances.[191] Active mixing structures based on microvalve technology range from circular dilution circuits[94,129] to a series of mixing microvalves actuated in sequence.[92,95,105] For continuous mixing operations, Benhabib developed a device utilizing a single combining valve with multiple, addressable fluidic inputs.[92] Mixing was then achieved either by serial transfer of the combined fluid through three downstream mixing valves, or by rapid (100 ms) alternating actuation (fluttering) of two downstream valves.[92] For precise metering and mixing of nL scale fluids, Jensen *et al.*[95,104-105] developed the most promising device - the microfluidic Automaton described in more detail below.

The Automaton is a programmable microfluidic sample processing system based on an 8x8 rectilinear array of microvalves.[95] It was developed for automated nanoliter-scale

quantitative, multi-step biomolecular assays. Protocols developed using this device for on-chip reagent mixing and serial dilution were optimized, achieving linearity over a 1000-fold dilution range. This device was initially demonstrated on a small-volume hydrogen peroxide assay with a sub-μM detection limit,[95] and has more recently been characterized for combinatorial processing operations involving larger (10-30 μL) volume samples.[104] Because the Automaton can process large sample volumes on a microfluidic format, we decided to explore its utility for microfluidic sample processing for MOA analysis. In this chapter, we explore Automaton operational methods for amine labeling with Pacific Blue succinimidyl ester, aldehyde and ketone labeling with Cascade Blue hydrazide (CB), and carboxylic acid labeling with CB using EDC (1-ethyl-3-(3-dimethylaminopropyl)carbodiimide) activation. We also explore a modular interface using PEEK tubing for integration of the Automaton sample processing system with the MOA μCE device. This work demonstrates proof-of-principle autonomous labeling, dilution, and analysis protocols using the Automaton as a front-end sample processing device for MOA analysis.

7.3 Materials and Methods

Sample and reagent preparation. Samples and reagents were prepared as previously described.[69,162,188-189] Briefly, all amino acid, aldehyde, ketone, and carboxylic acid standards were obtained from Sigma-Aldrich and prepared as 20 mM stock solutions in Millipore filtered water, except for benzophenone which was prepared in dimethylsulfoxide (DMSO). Standard solutions were prepared by combining appropriate amounts of these stock solutions with the indicated buffer solutions. Sodium tetraborate and boric acid were obtained from Sigma-Aldrich and used to prepare 400 mM aqueous stock solutions of buffer without pH adjustment. From these stock solutions, 30 mM aqueous borate solutions pH 9.5, pH 6, and pH 3 were prepared. The 30 mM borate stocks at pH 9.5 and pH 6 required no pH adjustment; pH 3 was obtained via the addition of 100 mM HCl (Sigma-Aldrich). Cascade Blue hydrazide (CB, Invitrogen) was dissolved in triply-distilled Millipore water to 10 mM. Pacific Blue succinimidyl ester (PB, Invitrogen) was dissolved in dimethyl formamide (DMF, Sigma-Aldrich) to 20 mM. EDC (1-ethyl-3-(3-dimethylaminopropyl) carbodiimide, Sigma-Aldrich) was dissolved to 20 mM in triply-distilled acetonitrile (MeCN, Sigma-Aldrich), divided into 100 μL aliquots, dried down to residue, and stored at -20 ^{o}C until rehydration to the appropriate concentration in 30 mM borate, pH 3.

Labeling reactions and dilutions. Labeling reactions and subsequent dilutions for electrophoretic separations were conducted as previously described,[69,162,188-189] except that some were conducted manually using Eppendorf pippetters in 500 μL Eppendorf tubes and others were conducted autonomously within the Automaton chip. For amino acid labeling, an amino acid standard in 30 mM borate, pH 9.5 (2 μM each citrulline, valine, serine, alanine, and glycine and 8 μM each aspartic acid and glutamic acid) was combined 1:1 with 40 μM PB in 30 mM borate, pH 5-6. No dilution of labeled amino acids was conducted prior to electrophoresis. Aldehyde and ketone labeling was conducted by combining an aldehyde and ketone standard in 30 mM borate, pH 5-6 (80 μM 3-pentanone and methylethylketone, 40 μM benzophenone and p-anisaldehyde, 8 μM butyraldehyde, propionaldehyde, and acetaldehyde, and 4 μM formaldehyde) with 1 mM CB in 30 mM borate, pH 5-6, in a 1:1 ratio. After a 15 minute incubation, the reaction mixture was combined 1:1 with 30 mM borate, pH 9.5. Carboxylic acid

labeling was conducted by combining a carboxylic acid standard (200 μM formic acid, 400 μM each acetic, propanoic, butanoic, pentanoic, hexanoic and heptanoic acids, and 600 μM octanoic acid) with 4 mM CB in 30 mM borate and 10 mM EDC, all in 30 mM borate, pH 3, in a 1:1:1 ratio. After a 15 min incubation, the reaction mixture was diluted 1:3 with 30 mM borate, pH 9.5.

Mars Organic Analyzer (MOA) instrumentation. The MOA has been well described in literature and was used without modification.[69,81,103,106,134,138,162,188-189] It houses the necessary high voltage power supplies to drive microcapillary electrophoretic separations and the optics for laser induced fluorescence detection. A 405 nm diode laser is reflected off a dichroic and focused through an objective to a ~20 μm spot within the center of the separation channel. Fluorescence is collected by the objective, passed through the dichroic, and focused into a fiber-optic that feeds into a photomultiplier tube (PMT) that is read by a Labview program.

Automaton and microchip capillary electrophoresis device fabrication and control. The Automaton rectilinear array of monolithic membrane microvalves was fabricated and controlled as previously described[95,104] and briefly described here (Figure 7.1). The device was fabricated by standard glass microfabrication procedures, with isotropic feature etching into 1.1 mm thick borosilicate glass wafers. The pneumatic features were etched to 70 microns, yielding final channel widths of 170 microns, and the fluidic features were etched to 30 microns, yielding final channel widths of 75 microns. After drilling 500 micron and 1.1 mm holes in the pneumatic and fluidic wafer layers, respectively, the wafers were bonded together reversibly using a featureless 254 μm thick PDMS elastomer membrane (HT-6240, Rogers Corp.).

Valves are nominally closed, and a closing pressure of 30 kPa was supplied to all unopened microvalves during the programmed operations. Individual microvalves were opened by the application of an actuation vacuum (-87 kPa) and held in that state for a specified amount of time before proceeding to the next programmatic step; similarly, the valves were closed by applying the closing pressure for a specified amount of time before proceeding. Opening and closing pressures were supplied via a 3/8" thick aluminum manifold and Labview-controlled actuation of solenoid valves (Teco Pneumatic, HV010E1-PSL). The manifold interfaces with the pneumatic inputs via Viton O-rings (Parker, V747 5-197), and a second 3/8" aluminum manifold is placed on the fluidic layer with a central hole that allows access to the microvalve array and fluidic inputs.

Microchip CE devices (Figure 7.1) were fabricated via standard photolithography procedures as previously described[67,81,103,106,134,138,162,188-189] using the design published by Chiesl *et al.*[69] incorporating tapered turn geometry.[136] Channels were etched to 35 μm depth.

Microchip capillary electrophoresis. Electrophoretic separations were conducted as previously described.[69,162,188-189] The electrophoresis channel and all wells are first filled manually with 30 mM borate, pH 9.5. The sample well is then evacuated and refilled with sample. Manual CE chip loading was conducted by pipetting sample into the sample well. Autonomous chip loading was conducted by placing one end of a ~30 cm long 50 μm internal diameter piece of PEEK tubing in the sample well and attaching the other end to an Automaton fluidic output via a snug-fitting hole punched in a 3 mm thick PDMS elastomer gasket. In all instances, cross injection was conducted by applying -1500 V at the waste channel while floating

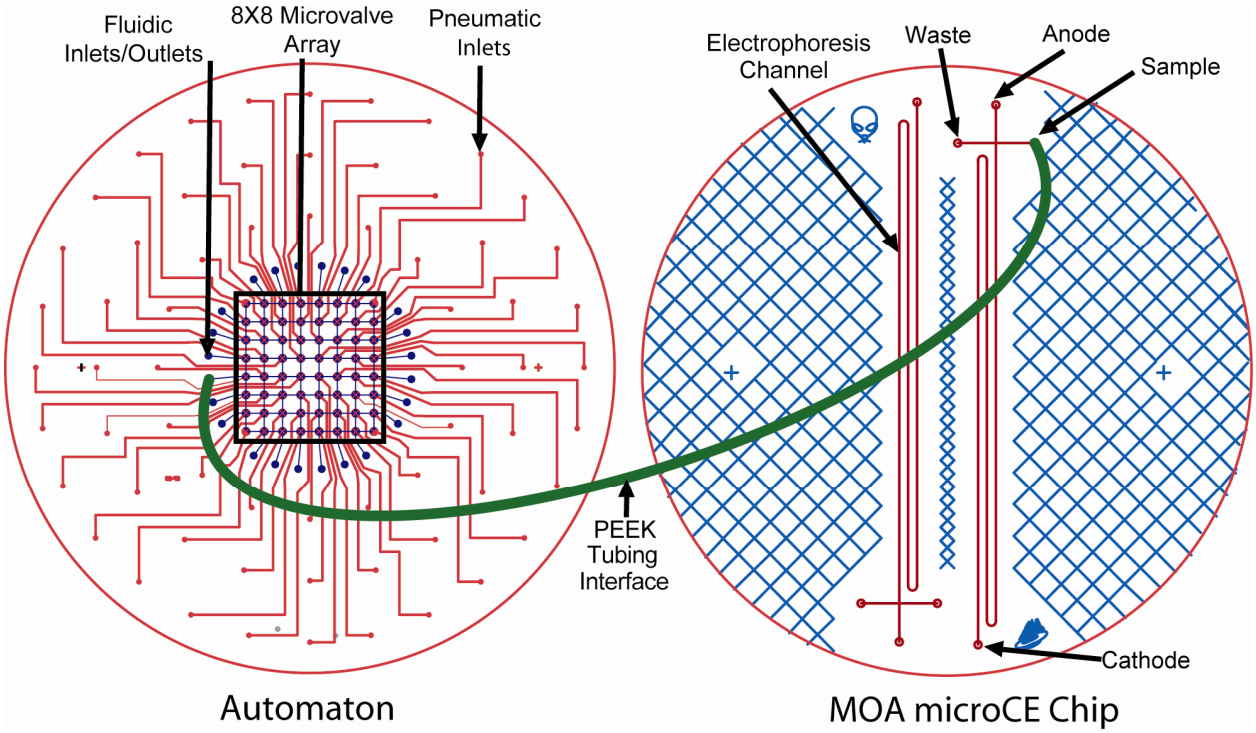

Figure 7.1. Schematic of the Automaton device (left) and the MOA µCE chip (right).

The Automaton pneumatic features are shown in red, the fluidic features in blue. The MOA µCE channels are shown in red, channel identifiers and bonding lines in blue.

the cathode and grounding the sample and anode wells for 30 s. A 200 ms step was then conducted, where the anode was floated and other applied potentials remained the same. Separation was conducted by grounding the anode, applying -15 kV to the cathode, and applying a back-biasing potential of -1500 V to the sample and waste. All separations were completed within 250 s from injection.

Automaton-MOA interfacing and sample processing. The Automaton and the MOA were coupled via a PEEK tubing interface for fluidic transfer. The PEEK tubing (30 cm long, 50 μm i.d.) attached to an Automaton fluidic output through a 3 mm thick PDMS gasket with a tight-fitting punched hole. Gel Slick (BioWhittaker Molecular Applications) was applied to both the Automaton glass surface and the PDMS gasket surface to ensure good PDMS-glass adhesion. The output end of the PEEK tubing was permitted to hang freely just inside the drilled hole of the sample well of the microchip capillary electrophoresis device. This interface is shown in Figures 7.1 and 7.2.

Autonomous sample processing programs, are efficiently described in the text by a fluidic program language developed by Jensen *et al.*[104] Valves are indicated by their position in matrix format, with columns designated by numbers and rows designated by capital letters (Figure 7.3A). Reservoir inputs are labeled with the lowercase letter in italics according to the valve they are attached to; for example, an input reservoir to valve D3 is denoted *d3*. Operations are enclosed in parentheses and can be combined to create a program, which is enclosed in square brackets (Figure 7.3B). A number after a program indicates the number of times a program is repeated. Two types of operations were used in this work: combining operations and transfer operations.

The combining operation receives inputs from two or more fluidic reservoirs and transfers the mixed product to another reservoir. Single letter codes assign valve usage during the performance of this operation, and are listed prior to the valves they apply to. Vertical bars divide the various valve assignments. Combining valve(s) are designated by "c," and receive fluidic input from valves designated by "i" for input. Each cycle of a combining operation delivers one valve volume per combining valve used to the output; an operation that utilizes three combining valves transfers one valve volume per cycle. The combined fluid is then transferred to the output via the mixing valves designated by "m." Occasionally certain valves are held continuously open to provide a direct path from a fluidic reservoir to a location within the grid; these valves are designated by "o."

Transfer operations move fluid from one reservoir to another. For this operation the individual valve usage is trivial and only the input and output reservoirs and the number of valve volumes transferred per cycle need to be specified. Transfer operations are designated with the letter "t," followed by the reservoir from which fluid is being transferred and the receiving reservoir. For example, (t:*c3*,*a1*) is the operation that sends fluid from reservoir *c3* to reservoir *a1*. The number of valve volumes transferred per cycle is listed after the operation (in this case 1), and the number of times the cycle is repeated is listed after the brackets (in this case 20).

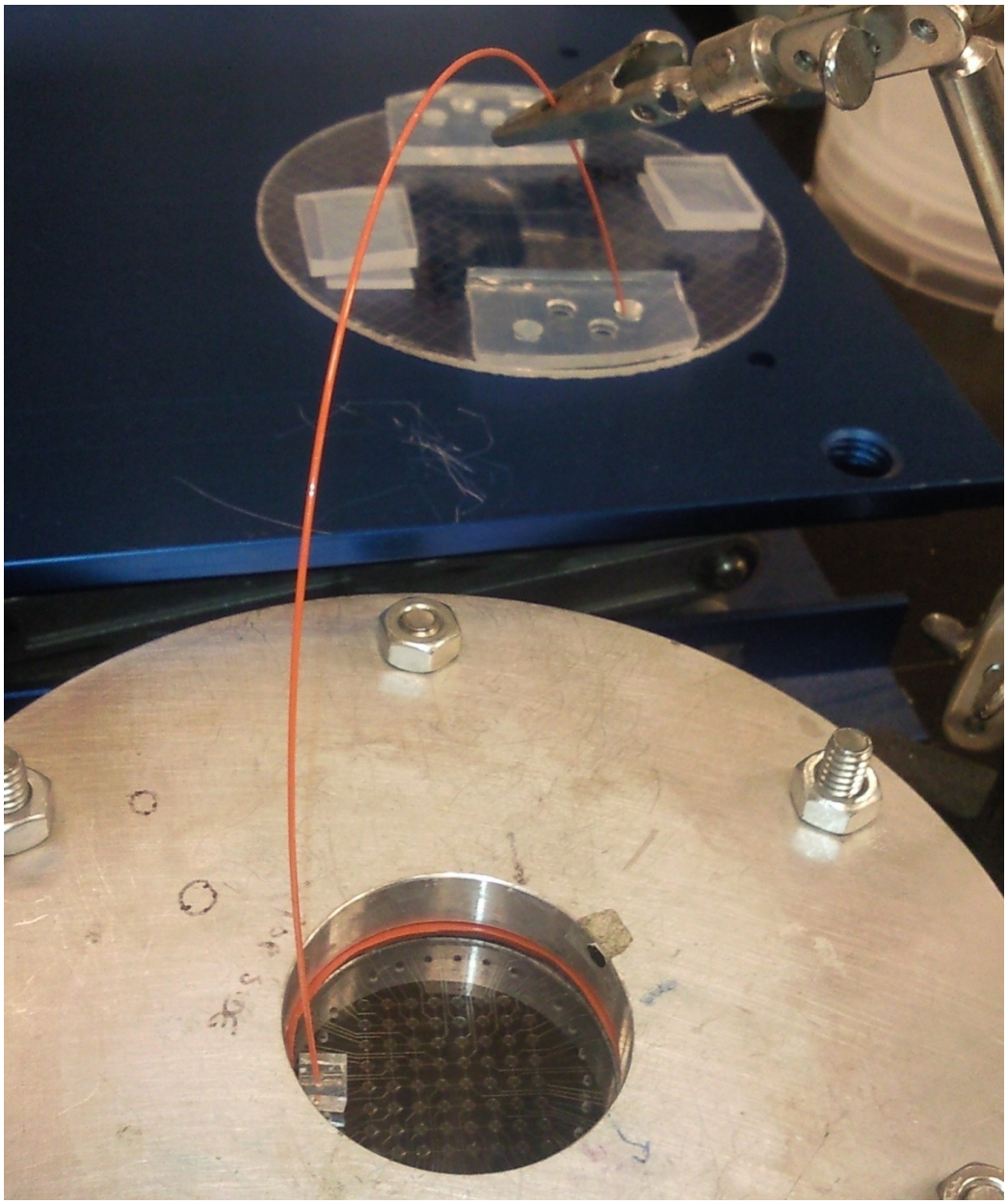

Figure 7.2. The Automaton device (bottom), an 8x8 rectilinear array of valves, and its interface to the Mars Organic Analyzer microchip CE device (top).

The 30 cm long 50 μm internal diameter PEEK tubing interface attaches to the Automaton fluidic outlet via a snug-fitting PDMS gasket, and is freestanding in the 3 mm wide 40 μL capacity well formed by a similar PDMS gasket over the MOA CE chip sample well.

7.4 Results and Discussion

Pacific Blue labeling of amino acids. PB labeling of amino acids was conducted on the Automaton device with automatic transfer to the sample well of the CE microchip as well as manually. The Automaton program depicted in Figure 7.4 A combines the PB from reservoir *c1* and the amino acid standard from reservoir *d2* in combining valve C2. The combined fluid is mixed through serial transfer via B2 and B1 to the Automaton fluidic output interfaced to the MOA microdevice at reservoir *b1*. The fluidic travel time from the Automaton to the MOA was ~ 10 min, and an additional ~ 10 were required to fill the MOA reservoir. The manual reaction was allowed to proceed for 15 min before manual loading and separation. The resulting electropherograms using the two labeling methods are shown in Figure 7.4B.

Comparison of the peak areas resulting from the two methods (Table 7.1) gives a measure of the extent of the derivitization reaction. Autonomous on-chip labeling provided approximately 70% (± 20%) the peak areas of manual off-chip labeling. Preliminary kinetics studies of PB-labeling of amino acids (by Caroline Chandra Tjin) indicate that at 10-20 minutes the PB-AA reaction is still far enough from completion to impose a strong dependence of amino acid peak area on reaction time. This adequately explains the relatively small difference between autonomous on-chip labeling and manual off-chip labeling reaction efficiencies and the relatively large error in both measurements. An optimized autonomous labeling protocol would involve an on-chip storage step before transfer to the microchip CE device to allow for reaction completion, and would possess capabilities for more rapid filling of the sample well as discussed below.

Peak efficiencies allow for comparison of the quality of the separations achieved from manual and autonomous sample transfer. Autonomous sample transfer results in peak efficiencies of 30% of those resulting from manual transfer. Reduced peak efficiencies are also obtained when the sample is manually labeled and loaded and then analyzed 10-15 min later. This indicates that the cause of the decreased separation quality is due primarily to diffusion of sample from the sample well into the injection arm during the 10 min sample transfer and is not inherent to autonomous labeling.

Separation quality of autonomously loaded samples can be increased in a number of ways: the pumping program can be modified to mix and transfer a larger volume per pump cycle, smaller wells can be punched in the microchip CE device fluidic reservoir gasket, permitting 10 μL volumes as opposed to the 40 μL volumes used here, the Automaton sample processing device can be fabricated with larger-volume valves to achieve faster transfer, and the electrophoretic injection program can be modified to include a "push-back" step, where EOF drives fluid from all arms of the chip back into the sample well for several seconds before the usual injection procedure. With these improvements we expect future versions will have autonomous peak efficiencies similar to those obtained manually.

Cascade Blue labeling of aldehydes and ketones. The results of autonomous on-chip aldehyde labeling and dilution and autonomous fluidic transfer of diluted sample to the microchip CE device are compared to the results of manual off-chip labeling and dilution and manual fluidic transfer of diluted sample to the microchip CE device in Figure 7.5B. These electropherograms clearly show that autonomous on-chip labeling is feasible with the Automaton sample processing device, as indicated by the peaks identified in Figure 7.5B. However, a large

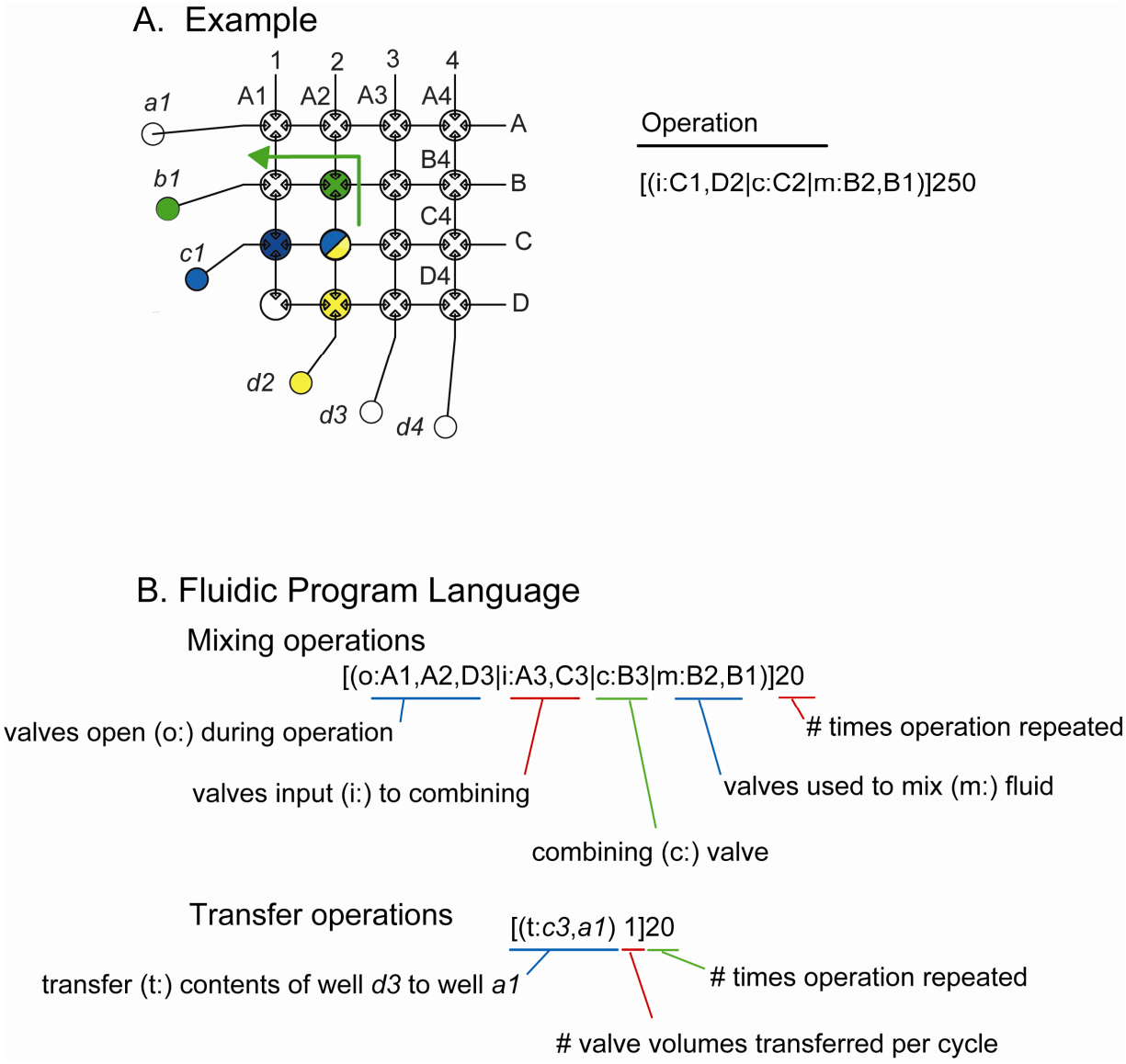

Figure 7.3. Fluidic program language.

(A) Combining operation showing labeling of valve array and inputs. Inputs from wells *c1* and *d2* are drawn in via valves C1 and D2, combined in valve C2, and sent to output well *b1* via mixing valves B2 and B1, with a total fluidic transfer of one valve volume per cycle. The cycle is then repeated 250 times. (B) Fluidic program language. This is the basic notation indicating what fluidic manipulations are accomplished with a mixing or transfer operation.

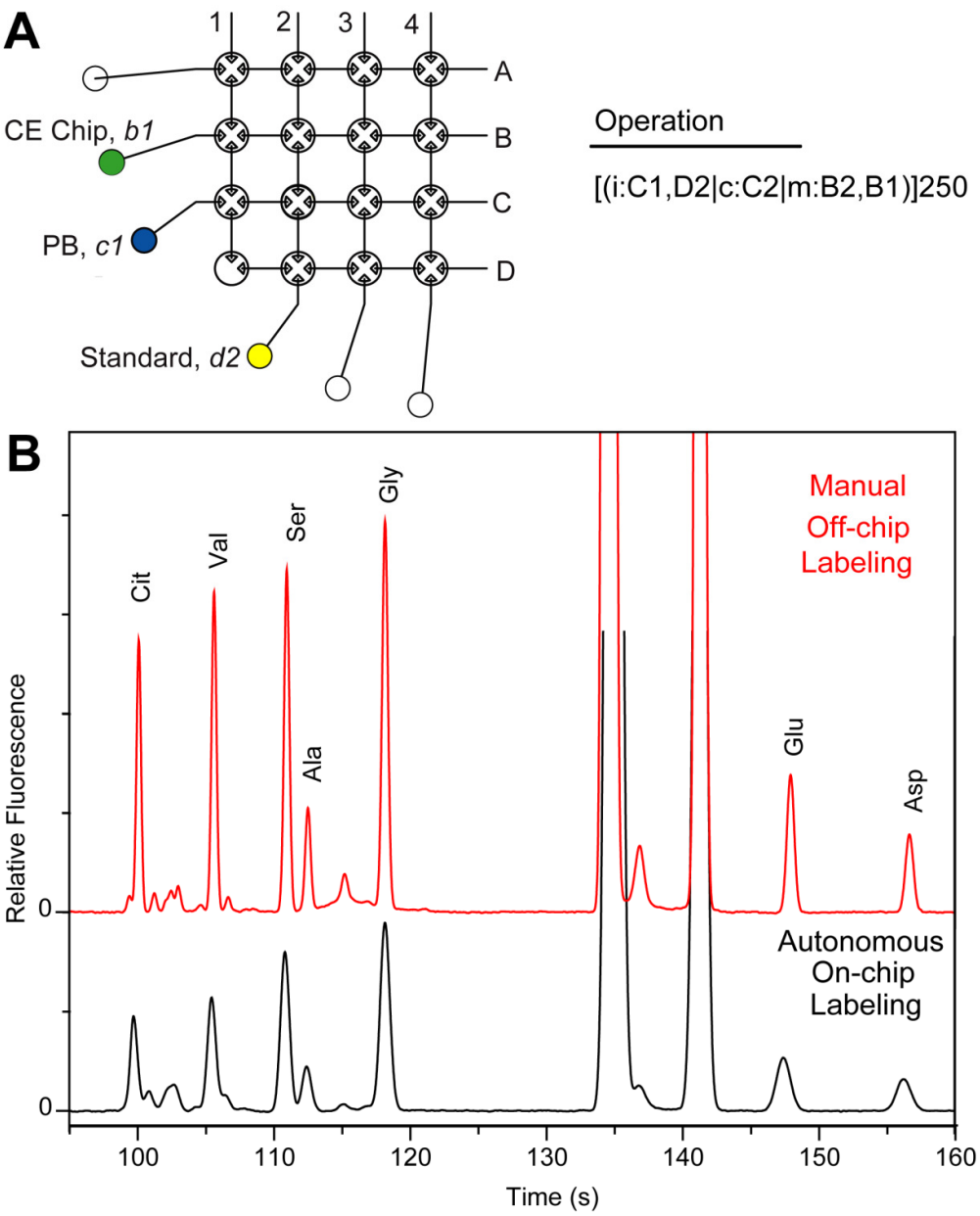

Figure 7.4. Autonomous and manual Pacific Blue succinimidyl ester (PB) labeling of an amino acid standard.

(A) A depiction of the automaton delineating reservoir use and the fluidic program executed here, and (B) electropherograms of autonomous on-chip sample labeling and transfer (bottom) and manual sample labeling and transfer (top). Labeling is conducted by combining equal volumes of 40 µM PB in 30 mM borate, pH 5-6 with an amino acid standard in 30 mM borate, pH 9.5. The standard contains 2 µM each citrulline (Cit), valine (Val), serine (Ser), alanine (Ala), and glycine (Gly) and 8 µM each aspartic acid (Asp) and glutamic acid (Glu).

Table 7.1 Comparison of Manual and Autonomous Handling of PB-Labeled Amino Acids

	Labeling efficiency (Peak area)		**Separation quality (Peak efficiency, N, x 10^5)**	
	Manual off-chip	**Autonomous on-chip**	**Manual off-chip**	**Autonomous on-chip**
Cit	0.7	0.4	3.9	1.4
Val	0.9	0.5	3.7	1.2
Ser	1.0	0.8	3.5	1.2
Ala	0.3	0.2	3.6	1.2
Gly	1.3	1.0	3.2	1.2
Glu	0.5	0.4	3.3	0.4
Asp	0.3	0.3	3.1	0.9
Average	0.7	0.5	3.5	1.1
Normalized	**1**	**0.7**	**1**	**0.3**

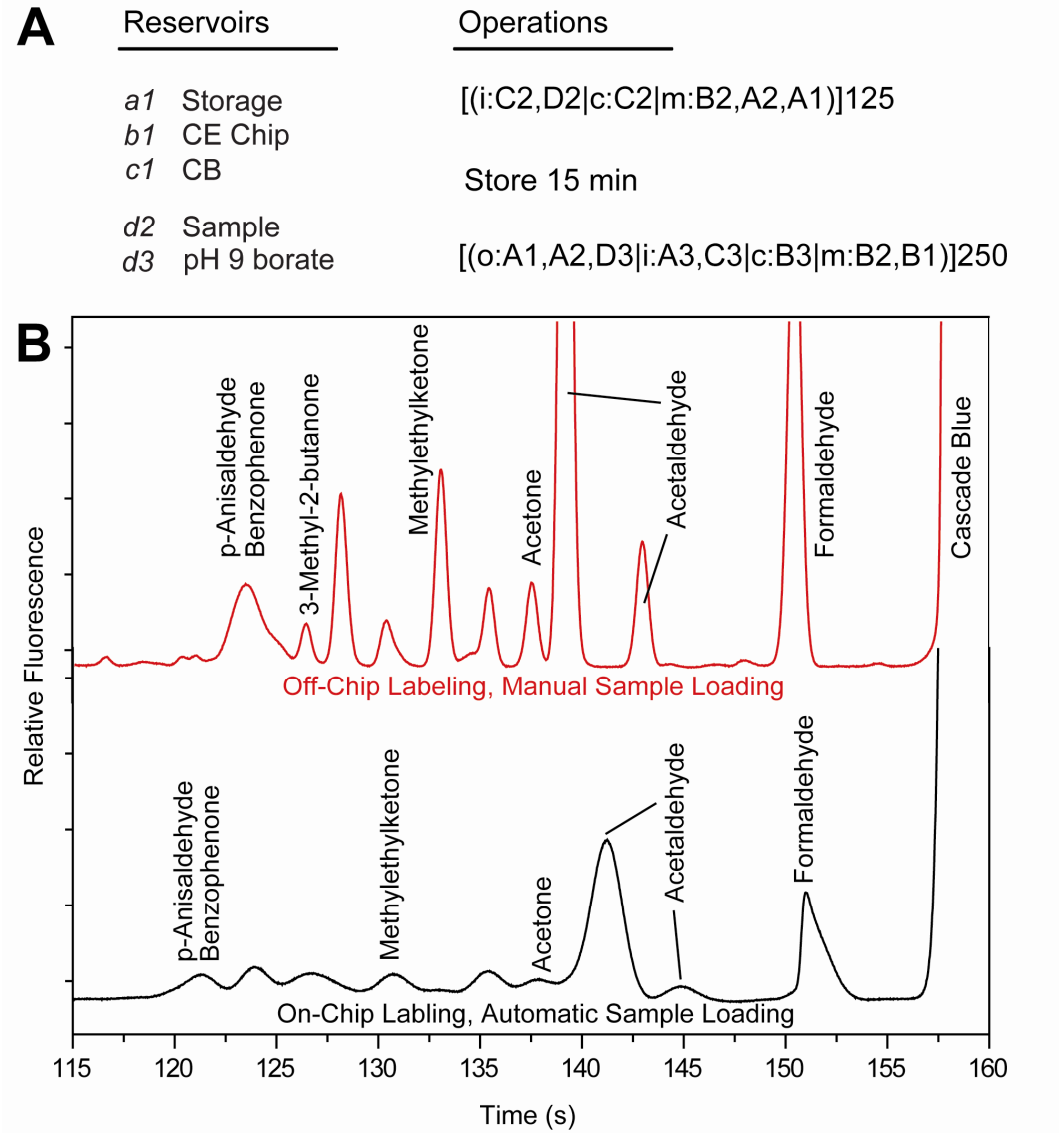

Figure 7.5 Autonomous and manual Cascade Blue hydrazide (CB) labeling of an aldehyde and ketone standard.

(A) Reservoir designations and fluidic program for the operations conducted here, and (B) electropherograms of autonomous on-chip sample labeling, dilution, and transfer (bottom) and manual sample labeling, dilution, and transfer (top). Labeling is conducted by combining equal volumes of 1 mM CB in 30 mM borate, pH 5-6 with a carbonyl standard in 30 mM borate, pH 5-6. Dilution is conducted by combining equal volumes of labeled sample and 30 mM borate, pH 9.5. The standard contains 388 µM total aldehyde and ketone content: 80 µM 3-pentanone and methylethylketone, 40 µM benzophenone and p-anisaldehyde, 8 µM butyraldehyde, propionaldehyde, and acetaldehyde, and 4 µM formaldehyde.

reduction in aldehyde and ketone peak areas are observed in addition to peak broadening. As previously described,[188] the hydrazone products of the aldehyde and ketone reaction with Cascade Blue hydrazide formed in acidic pH decompose rapidly in the basic pH required for sample injection and separation via microchip CE. This fact, combined with the relatively long transfer times (~ 10 min) utilized by this proof-of-principle interfacing of the Automaton and the MOA microchip CE devices, adequately explains the reduction in aldehyde and ketone peak heights and peak areas seen for the autonomous process versus the manual process. Additionally, diffusion of sample into the electrophoresis column during the 10 min transfer contributes to band broadening and thus reduced peak amplitudes. However, despite these concerns, the results indicate that the autonomous labeling chemistry and dilutions proceed as expected.

Cascade Blue labeling of EDC-activated carboxylic acids. Electropherograms of autonomous on-chip carboxylic acid labeling and dilution with automatic sample loading is compared to both autonomous on-chip labeling and dilution with manual sample loading and to a fully manual protocol in Figure 7.6B. These three sample processing conditions were evaluated by comparing reaction efficiency as quantified by the peak areas and separation quality as quantified by the peak efficiencies (Table 7.2).

The peak areas were compared as a measure of relative labeling efficiency (Table 7.2). The peak areas obtained by on-chip reaction are 40-50% larger than those obtained by a similar manual off-chip reaction with a run-to-run error of less than 10%. Due to concerns about evaporation during long-term storage on the current version of the Automaton sample processing device, these reactions were conducted with only a 15 min incubation time. Since it has previously been demonstrated that EDC-activated CB labeling of carboxylic acids requires long times (> 8 hr) to proceed to completion,[189] observed peak areas are expected to be highly dependent on exact reaction times. The manual off-chip reaction was allowed to react for exactly 15 minutes from mixing of reagents to dilution. The on-chip reaction had at least a 15 minute reaction time, with some of the fluid mixed earlier or diluted later than the rest, explaining the observed difference in peak areas.

The peak efficiency calculations reveal that updated programs providing larger volume transfer per microvalve actuation step reduced the transfer time and improved separation qualities from 30% of manual loading for the slower program (PB-labeling) to 96% of manual loading for the faster program (CB-EDC labeling). The program utilized for the sample dilution transferred two valve volumes per cycle, roughly halving the time required to fill the sample well. Manual transfer of manually and autonomously labeled samples results in a 1% difference in peak efficiency, which is within the normal run-to-run variation (1%). Autonomous sample transfer results in efficiencies within 4% of those from manual transfer, a major improvement over the slower program used for PB results. These improved peak efficiencies for autonomous transfer demonstrate how small changes in microfluidic operational programming can improve final results. However, the tailing of later peaks in this separation indicate that further optimizations reducing the time required for sample-filling operations will be necessary.

Interestingly, a new peak appeared at ~120 s for all on-chip autonomous EDC-activated CB labeling of carboxylic acids. A small amount of Gel Slick (1 μL) was combined with a blank simulant of 90 μL total 1:1:1 water / EDC / CB, diluted into pH 9.5 borate buffer and analyzed.

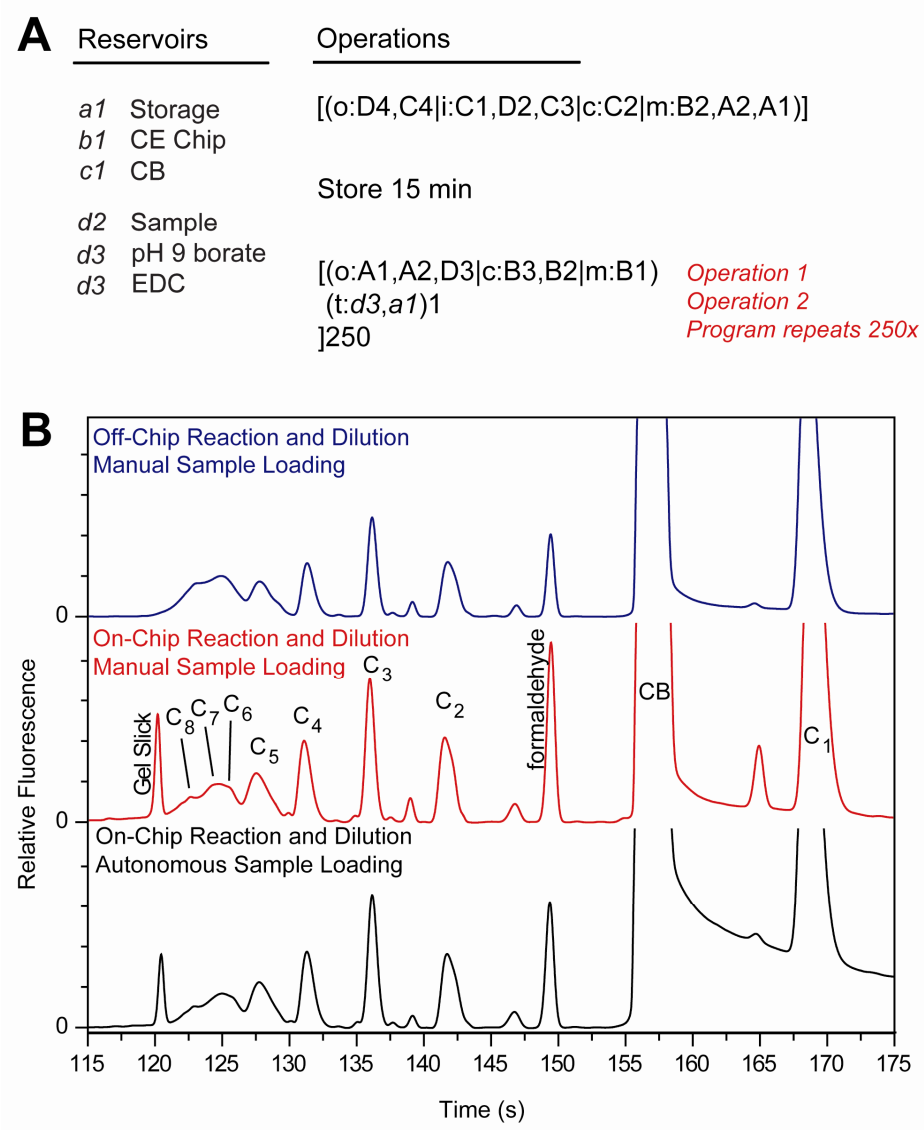

Figure 7.6. Autonomous and manual Cascade Blue hydrazide (CB) labeling of a carboxylic acid standard with 1-ethyl-3-(3-dimethylaminopropyl)carbodiimide (EDC) activation.

(A) Reservoir designations and fluidic program for the operations conducted here, and (B) electropherograms of autonomous on-chip sample labeling, dilution, and transfer (bottom) autonomous on-chip sample labeling and dilution with manual transfer (middle) and manual sample labeling, dilution, and transfer (top). Labeling is conducted by combining equal volumes of 4 mM CB, a carboxylic acid standard, and 10 mM EDC, all in 30 mM borate, pH 3. Dilution is conducted by combining one volume of labeled sample with three volumes of 30 mM borate, pH 9.5. The standard contains 3.2 mM total carboxylic acid content: 200 µM formic acid, 400 µM each acetic, propanoic, butanoic, pentanoic, hexanoic, and heptanoic acids, and 600 µM octanoic acid.

Table 7.2 Comparison of Manual and Autonomous Handling of CB-Labeled Carboxylic Acids

	Labeling efficiency (Relative peak area)			**Separation quality (Peak efficiency, N, x 10^5)**		
	Auto-rxn Auto-loading	**Auto-rxn Manual loading**	**Manual rxn and loading**	**Auto-rxn Auto-loading**	**Auto-rxn Manual loading**	**Manual rxn and loading**
Pentanoic acid	3.3	3.7	2.2	0.31	0.27	0.32
Butanoic acid	3.4	3.6	2.3	0.86	0.88	0.89
Propanoic acid	4.5	4.8	3.2	1.7	1.7	1.7
Acetic acid	2.6	2.6	1.8	1.5	1.8	1.6
Average	3.5	3.7	2.4	1.1	1.2	1.1
Normalized	1.5	1.5	1.0	0.97	1.0	1.0

A large peak was observed at ~ 120 s that overlapped with the unidentified peak when spiked into on-chip labeling reactions, indicating that this peak is directly due to a carboxylic acid component of the Gel Slick used to ensure good adhesion between the Automaton glass surface and the PDMS elastomer gaskets.

7.5 Conclusions

The work presented here demonstrates the proof-of-principle of utilizing the Automaton rectilinear array of microvalves for processing samples at the volumes required for MOA analysis. While the Automaton's use for large volume sample processing has been characterized,[104] these results provide a concrete example of the utility of large volume sample processing for sample labeling and dilution and MOA microchip CE device sample loading.

Further work remains to completely incorporate Automaton technology into a fully autonomous MOA sample processing system. A streamlined Automaton-based device must be designed with the smallest number of valves possible to allow for full MOA analysis of targeted compound classes: CZE of amines, amino acids, aldehydes, ketones, and carboxylic acids, and MEKC of amino acids. It must also possess the capability to spike samples prior to labeling with target class standards and to dilute samples post-labeling with EDTA for tolerance to matrices high in divalent cations.[162] The interface between the MOA microchip CE device and the Automaton-based sample processing system must also allow for cleaning of and replenishing buffer to the channel and reservoir wells.

Finally, the transfer time between Automaton device and microchip CE device must be decreased, to ensure that diffusion of sample in the injector does not lead to reduced efficiency separations. Success in this direction was achieved with the carboxylic acid target class by a simple change in operational programming. Increasing the valve volume, decreasing the MOA well size, and modifying the injection protocol to "push-back" any diffused analyte to the sample well prior to injection and analysis should provide further improvement. The work presented in this chapter demonstrates the proof-of-concept of Automaton sample processing for MOA analysis, and is being continued for future publication as discussed in Chapter 8.

Chapter 8 : Prospects

The preceding chapters have focused on the development of analytical assays using the Mars Organic Analyzer (MOA) for the detection of relevant organic compound classes and the validation of these assays on extraterrestrial sample analogs. Analyses of polycyclic aromatic hydrocarbons, aldehydes, ketones, and carboxylic acids were developed. In addition, methods were developed for the analysis of amines and amino acids in highly acidic, saline, and metal cation laden sample matrices. These science achievements were required to ensure that the MOA technology has the necessary sensitivity, robustness, and analyte diversity for successful extraterrestrial analysis. However, there are also engineering challenges that must be addressed in order to provide a flight-ready MOA instrument: the miniaturization of the MOA volume, weight, and power requirements and the further automation of sample processing and analysis. A flight-ready MOA instrument will also need to be tested on Earth and in simulant Mars conditions to validate its capabilities. In this chapter, the future development of MOA technology including its use in extraterrestrial and potential terrestrial applications is considered. Future extraterrestrial missions with astrobiological goals are discussed, and the potential usefulness of the MOA technologies in these applications is critically evaluated.

8.1 Future developments towards a flight-ready system

Based on the science developments presented in this thesis, the Mars Organic Analyzer technology is ready for the next steps in automation and miniaturization that will lead to a flight-ready instrument. Future automation will need to be accomplished through on-chip sample preparation and handling, and miniaturization will be accomplished by reducing the size, weight, and power requirements of the MOA electronic, mechanical and optical components. Miniaturization steps that are "outside the chip" are beyond the scope of this thesis: using integrated circuits instead of prototyping electronics boards, using better packaging to reduce the size of the 405 nm diode laser, switching to lighter-weight materials than those used in construction of the MOA body, *etc*… On-chip sample preparation and handling systems, however, are directly related to the objectives of this thesis and thus are discussed in more detail here.

During a MOA analysis of an unknown sample for amines, amino acids, aldehydes, ketones, and carboxylic acids, a multitude of analytical steps must be performed, including dilutions prior to labeling, sample derivitization, spiking with a standard, dilutions post-labeling, spiking post-reaction with a pre-labeled standard, and loading buffers and samples into the electrophoresis column. A flow chart of a sample analysis using CZE for amines, amino acids, aldehydes, ketones, and carboxylic acids and MEKC for amines and amino acids is shown in Figure 8.1. Many devices have been demonstrated that have some of the functionality required to perform the operations described in this flow chart. Skelley's MOA chip can retrieve an off-chip sample and load and clean an electrophoresis column,[103] Benhabib's McMOA chip can perform simple mixing operations and serial dilutions,[92] and Jensen's Automaton[95] chip can perform labeling reactions and dilutions as demonstrated in Chapter 7. However, to date, the MOA technology has not reached the level of a fully autonomous chip-based system that performs all the operations necessary for robotic extraterrestrial exploration.

The Automaton,[95] a square grid of monolithic PDMS membrane valves[95] that has been shown to be capable of the basic operations required for MOA sample handling,[95,104] should be

capable of all necessary operations for robotic extraterrestrial exploration with only minor design modifications. The 8 x 8 array used for the original Automaton is more than sufficient for conducting all necessary combining and mixing operations required for a fully autonomous MOA analysis.

Figure 8.2 shows two proposed designs utilizing the Automaton format with combining valve technology for a complete implementation of all operations given in the flow chart in Figure 8.1. Both designs incorporate a basic Automaton with either a 3x3 array of valves or a 4x4 array of valves (Figure 8.2). The valves at the perimeter of these grids can receive fluidic input from multiple reservoirs, each of which is controlled with a "stop" valve to prevent cross-contamination of the reservoirs, which was an issue with earlier designs. The incorporation of multiple inputs at the perimeter of the grid enables the capability of the Automaton grid-based combining and mixing operations while minimizing the total number of valves required. In selecting one of these devices, three main considerations must be evaluated: (A) weight of the final operating system, (B) time required to perform operations, (C) footprint of the device, and (D) redundancy and simplicity of the device.

Weight is an easily identified limiting factor in instrument design for space flight as the payload in any launch is typically on the order of 1% of the entire launch weight, and the instrument only a small percentage of the entire payload (*e.g.* for the Mars Exploration Rovers all the instruments combined accounted for only ~ 0.5 % of the payload mass launched). The weights of the two proposed devices themselves are nearly identical, but since each valve requires a solenoid for operation, the weight of the operating system scales with the number of valves. The 4x4 device uses 36 valves, while the 3x3 device uses 29, giving the 3x3 the advantage of lower operating weight.

In addition, for Martian analysis on a solar powered rover platform, operations must be conducted within typical Martian equatorial daylight hours, or ~12 hrs. Therefore, systems capable of performing operations more rapidly will be able to conduct more sample analyses during the lifetime of the mission. The operating time can be evaluated by counting the number of valve actuations required to conduct a simple operation, such as transferring 30 μL of buffer from a reservoir connected on-chip to an electrophoresis channel well. Based on this metric and 200 nL valve volumes, the 4x4 system (134 actuations) outperforms the 3x3 system (175 actuations). The footprints of the two devices are similar, 1.2x1.2 cm for the 3x3 format and 1.5x1.5 cm for the 4x4 format, thus multiple devices of both types can be incorporated into a single 4-inch diameter wafer stack for essential device redundancy. The 4x4 device is less crowded and is therefore more elegant and visually appealing, and it also provides essential redundancy in that it is more tolerant of isolated valve failure without critically hindering mission performance. This preliminary trade study implies that the 4x4 device would be most desirable, and the 3x3 device provides a necessary alternative should weight considerations dominate.

Both designs can be incorporated into a single multi-layer wafer stack with the electrophoresis channel, or can be fabricated as a separate modular system using a simple PEEK tubing fluidic interface. A fully integrated wafer stack provides the smaller-volume operating system essential for space flight. The modular system allows for facile interchange of both electrophoresis chips and Automaton-based chips, which reduces fabrication complexity and

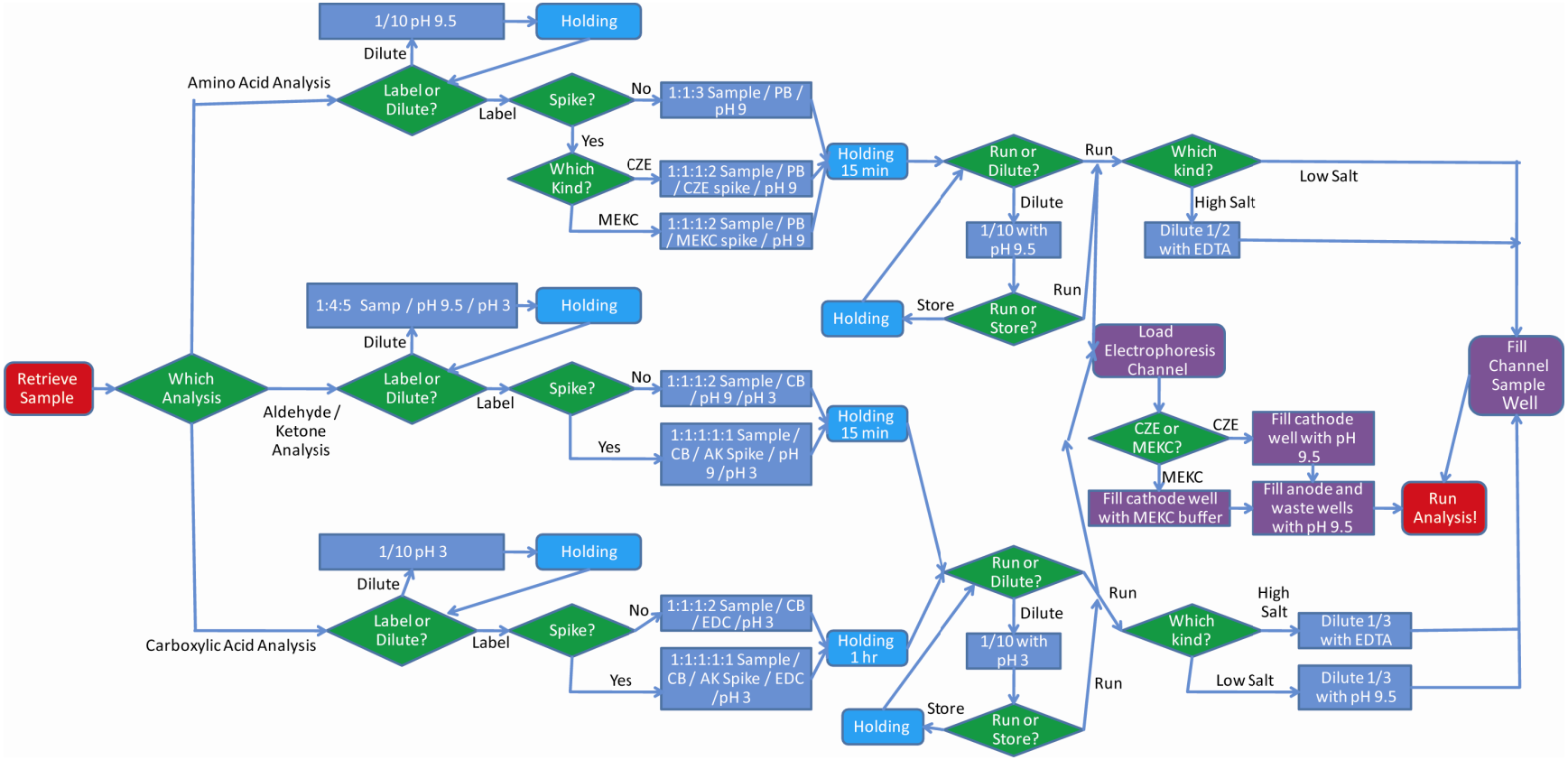

Figure 8.1. Flow chart depicting the full analysis of an unknown sample using CZE for amines, amino acids, aldehydes, ketones, and carboxylic acids, and MEKC for amines and amino acids.

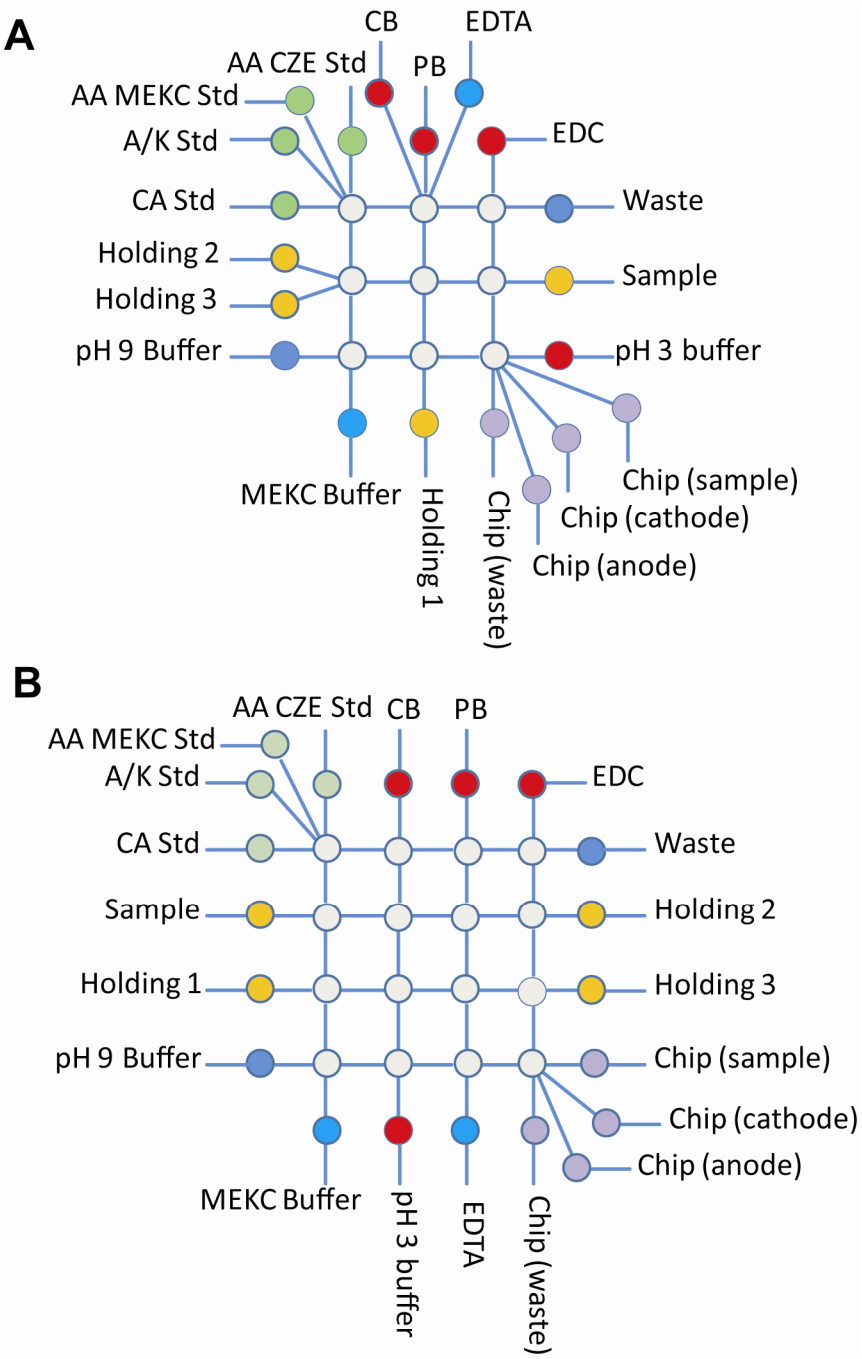

Figure 8.2. Automaton-based designs utilizing a 3x3 grid (A) and a 4x4 grid (B).

Both designs are capable of performing all operations required for full MOA analysis of amines, amino acids, aldehydes, ketones, and carboxylic acids.

increases device yields. For space flight applications, PDMS membranes will be inadequate due to their chemical permeability and intolerance to mission temperature extremes.[192] Replacement of PDMS with membranes of other materials, such as Teflon, has been demonstrated in similar systems[192] and their implementation should be feasible here.

8.2 Mass Spectrometry (MS) Detection for Microcapillary Electrophoretic (μCE) Separations Using Integrated Nanospray Ionization (nSI)

While LIF will remain the detection method of choice for ultra-high sensitive detection, there are benefits to having the additional capability of MS detection. MS detection gives structural information that can potentially resolve ambiguities due to comigration of species in μCE and provides isotopic information on separated species. MS has also been used as a detector for CE systems using a chiral complexation reagent to perform chiral analysis of underivatized amino acids.[193] Therefore, coupling MS detection in parallel with LIF detection for detecting μCE separations has the potential to provide enhanced information on extraterrestrial chemical complexity.

Electrospray ionization (ESI) is the most common method for on-line coupling of chromatographic separations into mass spectrometers.[194] Typically ESI operates in the flow regime of microliters to milliliters per minute requiring an applied potential of 3-5 kV and a heated nebulizing gas to aid in the desolvation process.[194] ESI operating on the order of nanoliters per minute, or nanospray ionization (nSI), uses much smaller nozzles (2-15 μm diameter).[195] Coupling low-flow separation devices, such as μCE or μCEC, with nSI offers advantages inherent to microfluidic systems: lower sample volume requirement, higher sensitivity, and lower power requirements.[195] The commercially available Advion microchip-based nSI device (Figure 8.3 A) produces reproducible, controllable, and robust nSI. The emitters are fabricated on the planar face of a silicon wafer, making their application to the wafer-stack μCE / μCEC devices feasible through direct bonding of the two devices. For example, at Advion, fully integrated high density arrays of glass channels for high performance liquid chromatography (HPLC) were successfully bonded to arrays of corresponding silicon nozzles interfaced to MS. In preliminary work at JPL, Peter Willis has used μCE similar to that presented here with integrated Advion nozzles interfaced to MS for successful detection of μCE separated amino acids (Figure 8.3 B).

Integration of nSI nozzles with the electrophoresis microcapillary devices used in this thesis would allow for enhanced compositional and isotopic analyses of all compound classes explored here. This integration, when coupled with the ultra-high sensitivity available from LIF detection, provides essential redundancy in species identification. Isotopic information obtainable via MS analysis provides redundancy in determination of a biotic or abiotic source of analyzed species. Additionally, since MS is "legacy" technology in space flight due to its successful operation on Viking[17-18] and Cassini,[42] MS instruments are highly likely to be flown on future astrobiological exploration missions. However, incorporating MS detection to μCE systems will necessarily increase the total mass, power, or volume requirements of the instrument payload package and introduce additional integration challenges.

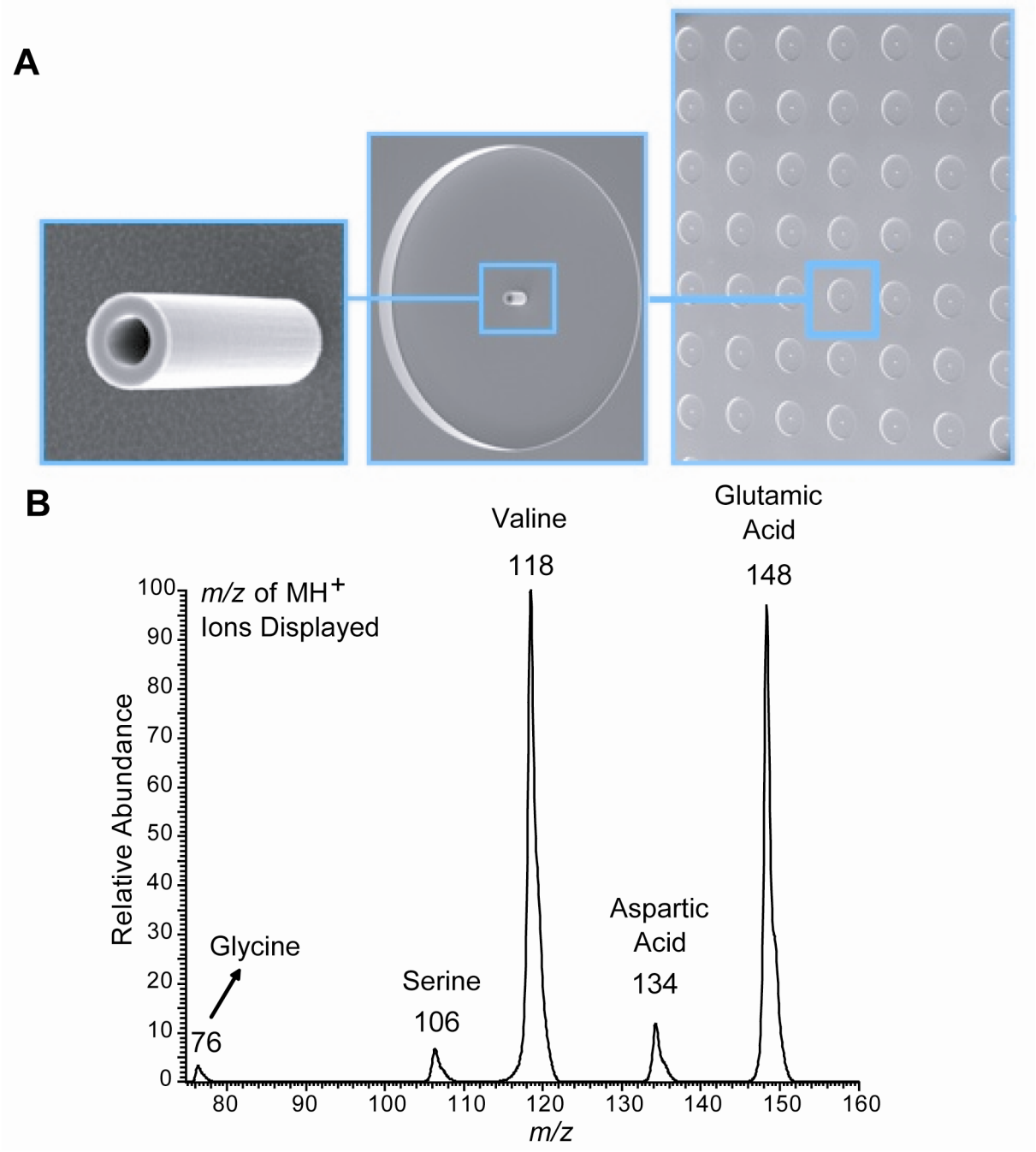

Figure 8.3. (A) Images of Advion micromachined nSI nozzles for coupling MS detection to µCE / µCEC separations, and (B) MS data obtained by Peter Willis at JPL illustrating nanospray ionization and detection of amino acids.

8.3 Microcapillary Electrochromatography Separation of Polycyclic Aromatic Hydrocarbons

Despite the demonstrated success of this analytical system in the analysis of complex environmental and astrobiologically relevant samples for a number of PAHs in Chapter 2, this method is currently limited to the detection and analysis of a subset of this diverse compound class. This limitation stems from two main causes, namely the PAH subset is limited to (A) those PAHs compatible with the MOA LIF detector (absorbance at 405 nm), and (B) those sizes and shapes that have significant affinity for the CDs used. The first limitation can easily be alleviated by using shorter wavelength diode lasers for excitation (260 nm for complete coverage, 350 nm for partial coverage) or, with a loss in sensitivity, by using nanospray ionization (nSI) to couple mass spectrometric (MS) detection to the microcapillary separation device as discussed above in Section 7.2. The second limitation must be alleviated via optimization of separate CD-assisted separations for each size range of PAHs studied or via a separation technology different from the CD-assisted separation method used in Chapter 2. An attractive technology for these separations is microchip capillary electrochromatography (μCEC), which can be used for a much broader range of neutral molecules.

Microchip capillary electrochromatography (μCEC) offers a separation method capable of almost universal coverage of the diverse PAH compound class (Figure 8.4 A).[196-198] CEC combines the separation efficiency, small sample and reagent volumes, and short analysis times of CE with the broad applicability of high performance liquid chromatography (HPLC), typically using a 10-100 μm i.d. CE column filled with a porous solid support (e.g. derivatized silica beads).[196] As in μCE separations, electroosmotic flow drives the flow of solvent and analytes through the column; however, instead of a charge-based separation as in μCE, μCEC relies on the adsorptive interaction of analyte molecules with the solid support. Because the separation is chemical, high resolution separations are possible of a wide array of neutral and charged organic species.[196-201] No mechanical pumping is required, maintaining the low power and volume requirements seen in μCE.[196,201] Porous polymer monoliths (PPMs) are an attractive option for use as the stationary phase in microfluidic devices, as they can be fabricated *in situ* via photopolymerization of casting solutions and covalently linked to the microdevice substrate (Figure 8.4 B). The use of PPMs as the solid substrate gives the user a high degree of control over pore size and chemical properties of the stationary phase[201] and yields highly reproducible results (retention time RSD < 1.7 %).[200] Photopolymerized PPMs are particularly attractive for microdevices, as they can be precisely patterned using photomasks. The incorporation of μCEC capability in one or more channels of a multi-channel device would enhance the analytical capability of the MOA system. However, it would also increase complexity and the number of potential failure modes.

8.4 Terrestrial Applications

While the MOA was designed for extraterrestrial exploration, it has Earth-based applications as well. Because of its portability and the variety of organic analyte classes targeted by the MOA, it is well-suited for point-of-care diagnostics. Metabolic analysis may be the most attractive application of the MOA in this arena, as many metabolic disorders can be diagnosed by

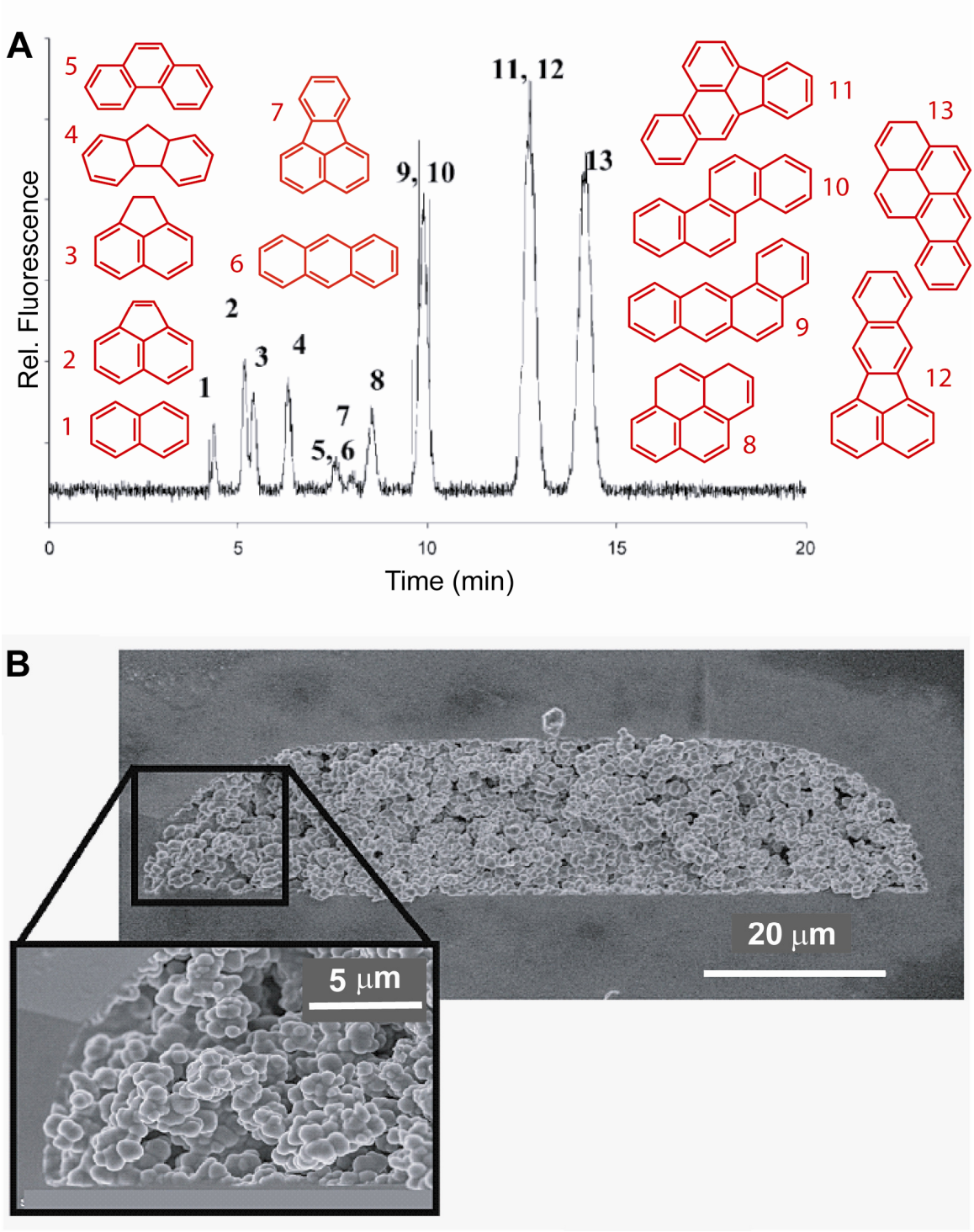

Figure 8.4. (A) PAH standard separation using μCEC.[197] (B) SEM image of a porous polymer monolith (PPM) for μCEC separations.

The PPM is covalently anchored to the wall of the channel.[200]

the presence of unusually high levels of targets such as aldehydes (acid ketodosis), amino acids (phenylketonuria), etc. in the blood or urine.

MOA instrumentation could also be applied to environmental contamination monitoring. A MOA instrument set to autonomously sample from and analyze a busy shipping channel could monitor sediment or water contamination from PAHs or formaldehyde. PAHs and formaldehyde have also been associated with lumber processing,[64,76] indicating that autonomous MOA analysis of these toxic compounds in nearby ground and drinking water would be beneficial. A network of MOA instruments placed near a potential source of contamination, such as a coal mine or oil refinery, could monitor, in real-time, spreading environmental contamination from the source.

However, the MOA may be even more useful for real-time analysis. Due to the wide use of fermentations to produce everything from ethanol to medicines, there could potentially be a significant scientific and financial benefit from a system that could monitor such fermentations in real-time for use of nutrients and production of desired and waste products. For example, the MOA has been used to detect the neuroactive amines histamine and tyramine[135] and aldehydes and ketones (Chapter 4) in fermented beverages. The MOA was also recently used to measure depletion and production of amino acids, aldehydes, and ketones during a typical beer fermentation.[202] This implies that the MOA could have significant use in the real-time monitoring of fermentations for use of key nutrients and the production of toxic and off-flavor compounds.

8.5 Astrobiological Extraterrestrial Exploration in the Next Decade

The Mars Science Laboratory (MSL) rover, named Curiosity, is currently scheduled to launch in late 2011. This rover has the science goal of assessing the environmental conditions at its landing site for the potential of present or past conditions capable of supporting life or preserving life markers. MSL will have a sampling arm that can deliver samples to a suite of instruments. A full list of MSL instruments is given in Table 8.1. The most astrobiologically relevant of those instruments is the Sample Analysis at Mars (SAM) suite, which has GC, MS, and tunable laser spectroscopy capabilities, which combine to allow for identification of a wide range of organics and isotopic ratio determination.

MSL will be only the second mission to Mars to explicitly explore Martian organic chemistry and prospects for present or past life. Since MSL is a rover, it has a significant advantage in sampling capabilities over the stationary Viking landers. MSL will have the capability to collect surface scrapings, like Viking did, and those unearthed by standard operation of its wheels. However, it is very likely that the top several centimeters of Martian regolith have been sterilized of organic molecules by the oxidizing chemistry suggested by Viking[26] and detected by Phoenix[23] and UV and ionizing radiation that bombards the Martian surface and photolytically degrade organics.[26] The lack of capability to collect subsurface samples from any depth could preclude the possibility of SAM's detection of any organic molecules.

In addition, although SAM's pyrolysis extraction can heat samples to 110 ^{o}C, the lack of detection of organic molecules by Viking's pyrolysis-GC-MS-procedure[15-16] suggests that reliance on the same extraction, separation, and detection techniques may lead once again to failure to detect Martian organic molecules. It has been demonstrated that the Viking GC-MS could, at a lower bound, detect the organic content of 10^6 bacteria in a single gram of soil.[17,203]

This means that a null result for this instrument does not return a particularly meaningful lower bound to the amount of organic carbon in a Mars sample. However, MSL may carry a Sample Processing System (SPS) for derivitization of acids with a silylating reagent, such as N-methyl-N-(tert.-butyldimethylsilyl)-trifluoroacetamide (MTBSTFA), which will allow for detection of oxidized species including acids via GC-MS.[187] Given a quoted detection limit of 10^{-11} mol, 1 g of sample, and 100 % extraction and derivitization efficiency, SAM can detect 32 ppb mellitic acid. Given the same assumptions, as discussed in Chapter 5, the MOA can detect 5 ppb mellitic acid, or a 7-fold improvement in sensitivity. Additionally, the latest reported version of the SPS uses the organic solvent DMF for extraction and derivitization,[187] while the MOA analysis method requires no organic solvents. If coupled to an aqueous extraction method such as subcritical water extraction (SCWE),[115] recovery and derivitization rates within the 30-100 % quoted by SAM's SPS[187] should easily be matched. However, it is possible that the SPS will be descoped from the final instrument platform. In this case, if Benner's hypothesis that only highly oxidized species like mellitic acid survive on Mars,[26] then it is highly likely that MSL's SAM will return a similar negative result for Martian organics. The MOA analysis methods presented in Chapter 5 offer a more sensitive analytical method that is robust to varying sample matrices and uses only aqueous solvents, providing a much needed and more reliable alternative to GC-MS technology.

Another mission to Mars with a similar goal of exploring potential present or past habitability and analysis of Martian organic chemistry is the European Space Agency's (ESA's) ExoMars rover, due to launch in 2018. A key difference from MSL's design is that ExoMars will be able to drill to depths of 1 m for sampling. However, like MSL, the ExoMars instrument package (Table 8.2) has deficiencies that may lead to its failure to detect organic molecules. As with Viking and MSL, ExoMars will also carry a GC-MS with pyrolysis volatilization of organic molecules. However, ExoMars will also be able to use laser desorption to inject ions into the MS, and this alternative extraction method may increase its chances of success significantly. At the time of writing this thesis, a viable portable field prototype has yet to be built, leading to questions about science readiness due to potential time and budget constraints.

ExoMars may also carry the Life Marker Chip (LMC), an antibody array-based detector. While antibody binding can be extremely useful for biological assays, many questions about its applicability to extraterrestrial exploration remain. The LMC, by its very nature as an antibody array, has a finite limit to the number and identity of individual biomarkers it can target based on the number of antibodies patterned, their redundancy, and the detection method used. This limitation of the LMC leaves it vulnerable to failure because its success is based on the predictive (or wild guessing) powers of the instrument developers and the dangerous assumption that extraterrestrial life evolved the same structures for data and energy storage as terrestrial organisms. Additionally, the long-term stability of surface-bound antibodies in the proposed format during the long (~1 yr) space flight, to temperatures experienced both in transit (-10 to 50 ^{o}C) and on the Martian surface, and to ionizing radiation exposure outside the protection of the Earth's magnetosphere has yet to be addressed. Surface binding assays are also typically slow (overnight incubations required), which may cause incompatability issues with successful operations in a single Martian equatorial day (~ 12 hrs). While ExoMars will conduct exciting new experiments on the Martian surface and has the potential to discover signs of past or present Martian life, there are still enough questions about the appropriateness and reliability of its

Table 8.1 Mars Science Lab Instruments

Instrument	Description
SAM (Sample Analysis at Mars)	GC, MS, and tunable laser spectroscopy, organic molecule identification and determination of isotopic ratios
CheMin	X-ray diffraction and fluorescence, mineral identification and quantitation
Mars Hand Lens Imager	Micrograph acquisition, positioned on the sampling arm
Alpha Particle X-ray Spectrometer	Determines relative abundance of elements, positioned on sampling arm
MSL Mast Camera	Positioned at roughly human eye height to give an image of Mars as a human explorer might experience it
ChemCam	Laser ablation / spectrometer
Radiation Assessment Detector	Assesses the Martian radiation environment with a focus on implications for human exploration
Rover Environmental Monitoring Station	Measures atmospheric pressure, temperature, humidity, winds, and UV radiation
Dynamic Albedo of Neutrons	Detects hydrogen down to 1 m below surface, could indicate buried ice or hydrated minerals

instrument suite to require continued development of alternative instruments for biomarker detection, including the MOA, for extraterrestrial exploration.

No missions to explore the organic chemistry of the icy moons discussed in Chapter 1.2 have been developed or funded to date. However, two missions in the concept phase are worth mentioning here. ESA has the Europa Jupiter System Mission (EJSM) under consideration for launch in 2020. This mission's primary science objective is to determine whether the Jupiter system harbors environments capable of supporting life, with a focus on Europa and Ganymede. Specific objectives include characterizing ice shells and subsurface oceans, determining global surface compositions and chemistries, and understanding the formation of surface features with a focus on identification and characterization of candidate sites for future *in situ* exploration. While EJSM is mainly proposed as a flyby / orbiter, Russia has proposed a joint lander to explore the Europa surface chemistry *in situ*, and will potentially have some degree of drilling or melting capability to sample subsurface. The MOA, with its aqueous-based chemistry, can measure the organic content in even highly saline and acidic water samples with ease, making it an ideal instrument for this mission.

NASA also has a mission in concept for exploration of the icy moon Titan. The Titan Mare Explorer (TiME), if selected and funded as a Discovery class mission, could launch as early as 2016. This mission could incorporate a lake lander, a submersible, and a balloon to fully examine the chemistry above, on, and beneath the surface of Titan's hydrocarbon lakes. TiME's science objectives include determining the chemistry, physical properties, and depth of Titan's lakes, and the meteorology over the seas and its relationship to the lakes. Potential splashdown sites include Ligeia Mare (~100,000 km^2) and Kraken Mare (~370,000 km^2). While Titan may not be a target site for the search for life, its organic chemistry is exciting enough to be a target for chemical exploration in its own right. It would be particularly interesting to explore the oxidation or amination of hydrocarbons that compose in the atmosphere and surface liquids by the potentially ammonia-rich water ice crust, and the MOA, with its target molecules, would be particularly useful for exploration of this moon. Since very little is known about hydrocarbon chemistry operating at 93.7 K over ammonia-rich water ice on a global scale, exploration of Titan for organic molecules would yield a wealth of exciting information.

8.6 The Future of Astrobiological Exploration

"The more I examine the universe and study its architecture, the more evidence I find that the universe in some sense knew that we were coming."

- Freeman Dyson, 1979

If the previous era was one of small steps for man and giant leaps for mankind in manned and *in situ* exploration of nearby solar system bodies, then the current era is one of large telescopes and the small Earth-like planets they discover in the habitable zones of distant solar systems. While technology and political will continue to progress to allow manned exploration of nearby Mars and potentially the small icy satellites of the more distant gas giants, there will always be those frontiers just out of reach of humankind that must be explored by robotic astrobiologists. If the Drake equation (Eq. 7.1) correctly predicts the number of planets

Table 8.2 Instruments On Board the ExoMars Rover

Instrument	Description
PanCam	Panoramic camera for digital terrain mapping
MOMA	(Mars Organic Molecule Analyzer) MS with two modes: GC with pyrolysis vaporization and laser desorption (LD)
MicrOmega-IR	Infrared imaging spectrometer to identify mineralogical and molecular composition of samples at the grain scale
MARS-XRD	X-ray diffractometer for mineral analysis
Raman Spectrometer	Provides geological and mineralogical context information
WISDOM	(Water Ice and Subsurface Deposit Observation on Mars) ground penetrating radar
MA-MISS	Mars Multispectral Imager for Subsurface Studies, mounted inside drill
CLUPI	Close-UP Imager for high resolution color close-up images
LMC	(Life Marker Chip) Antibody array detection for a limited set of biomarker targets

$$N = R^* \times f_P \times n_e \times f_l \times f_i \times f_C \times L \qquad \text{Eq. 7.1}^{a}$$

inhabited by intelligent communicable life, then a modification of the Drake equation (multiplying by $L_a / f_i f_c L$, where L_a is the average amount of time any form of life survives on a planet) would predict the number of planets hosting chemically detectable life. While the average lifetime of a civilization capable of long-distance communication is debatable, we can assume it is at least 100 years based on our technological progress on Earth. The average time that all life exists on a planet may be assumed to be similar to the amount of time life has existed on Earth, or approximately 4 billion years. The fraction of planets that develop intelligent life is harder to estimate. Based on a statistical analysis of all terrestrial species and those that have developed intelligence, this number is very low. However, it can be argued that, to some extent, evolution proceeds towards more complex and hence more intelligent life forms, making the number ~1. Based on nothing but conjecture, let's assume the actual number is close to 0.5. The fraction of intelligent species that develop long-range communication technology is just as challenging. However, in *Ishmael*, Daniel Quinn makes the compelling argument that societies that tend towards conquering and communication eventually displace competing societies,[204] which is supported by Jared Diamond in *Guns, Germs, and Steel*.[205] Thus, we can assume this number is high, and can arbitrarily choose 0.9, based on just as much data as our previous estimate. Applying these estimates to the Drake equation suggest that our robotic astrobiologists have ~ 10^{10} better probability of discovering extraterrestrial life than the Search for Extraterrestrial Intelligence (SETI) has of communicating with intelligent neighbors. The Drake equation is mere conjecture, highlighting the unnerving fact that our search for our own origins and potential nearest neighbors, whether intelligent civilizations or microbial colonies, relies solely on evidence from one data point, the planet Earth. Until we can obtain at least a second data point on our plot of life-bearing bodies, conjecture is all we have. Even with a second data point, we will need more – science can not draw a straight line between its only two data points and declare a trend. Therefore the search goes on, not just in pursuit of Martian microbes or Europan deep-sea tube worms, but in search of truth about our own origins, future, and place in the Universe. I have every confidence we will find that truth, and am grateful for the opportunity to contribute to the development of an instrument that may help us discover it.

[a] f_p = fraction of stars with planets, n_e = average number of planets capable of supporting life, f_ℓ = fraction of life-supporting planets that evolve life, f_i =fraction of inhabited planets that evolve intelligent life, f_c = fraction of intelligently-inhabited planets that develop communications technology, L = lifetime of an intelligent civilization with communications technology

Appendices:

A. Microchip details

B. Supplemental information for Chapter 2

C. Supplemental information for Chapter 3

D. Supplemental information for Chapter 4

E. Supplemental Information for Chapter 5

F. Supplemental Information for Chapter 6

Appendix A: Microchip details

A.1 Microdevice Details

The MOA instrument was designed to utilize a 4-layer hybrid microchip that has been described in great detail in the references indicated in the main text. This work was conducted using a simpler 2-layer test chip that includes only the electrophoresis channels. The mask design is shown in Figure S01. The electrophoresis channels are shown in red, and are 23.4 cm long and 100 μm wide. The cross channel is located 0.6 cm from the anode end of the channel. The detector is positioned 0.5 cm from the cathode end of the channel. The turn sections are tapered to 55 μm with 2:1 aspect ratio entrance and exit triangle transitions. Features in blue include alignment marks for automated drilling, cartoon channel identifiers, and features to vent trapped air and thus aid in bonding. The entire design is etched to 25 μm depth on a 100 mm diameter borofloat glass wafer.

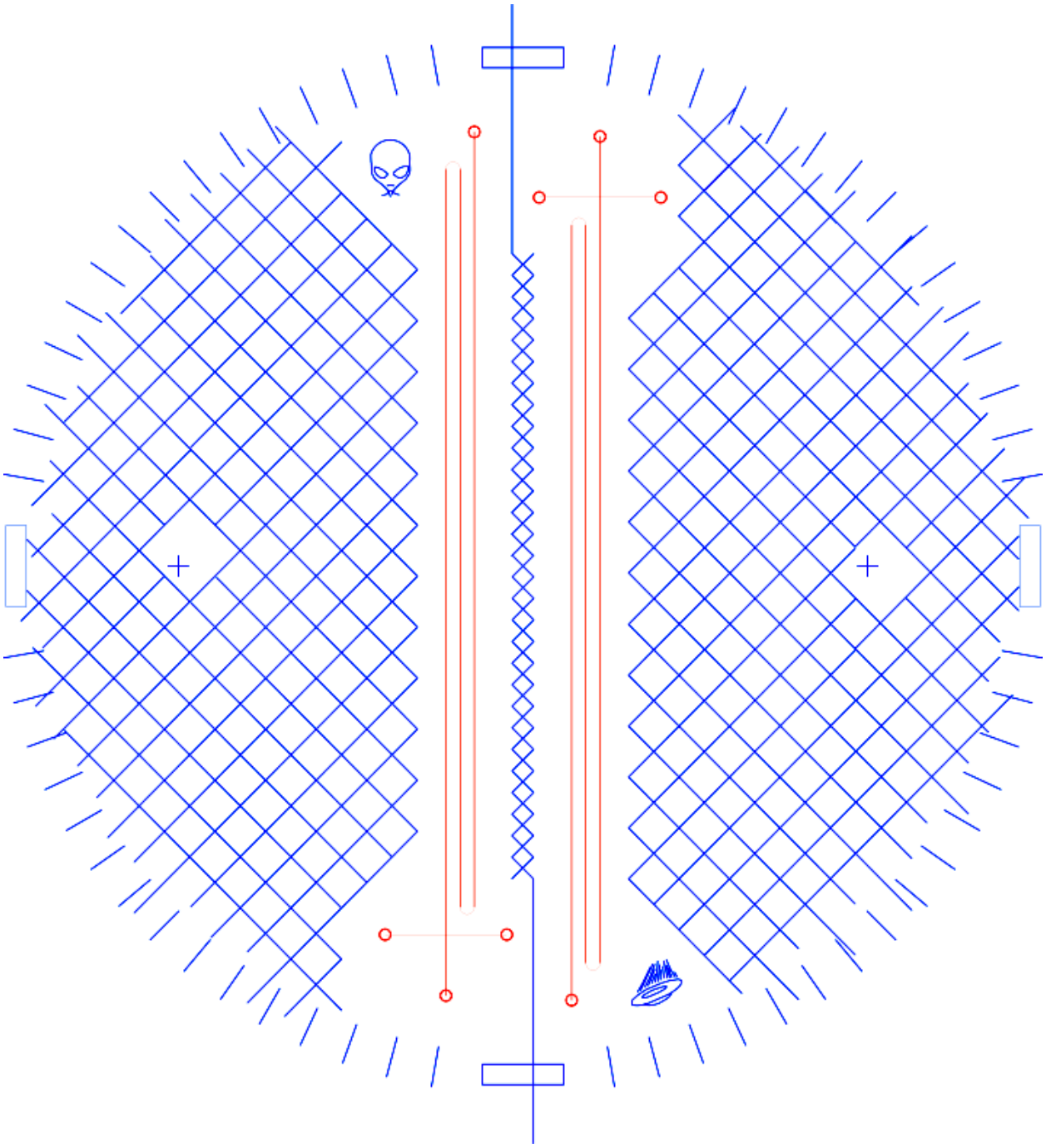

Figure A. 1. MOA test chip mask design.

Electrophoresis channels are in red. The blue features include alignment marks for automated drilling, cartoon identifiers for ease of chip and channel identification, and vents to aid in escape of trapped air during bonding.

Appendix B: Supplemental Information for Chapter 2

Polycyclic Aromatic Hydrocarbon (PAH) Analysis with the Mars Organic Analyzer Microchip Capillary Electrophoresis System

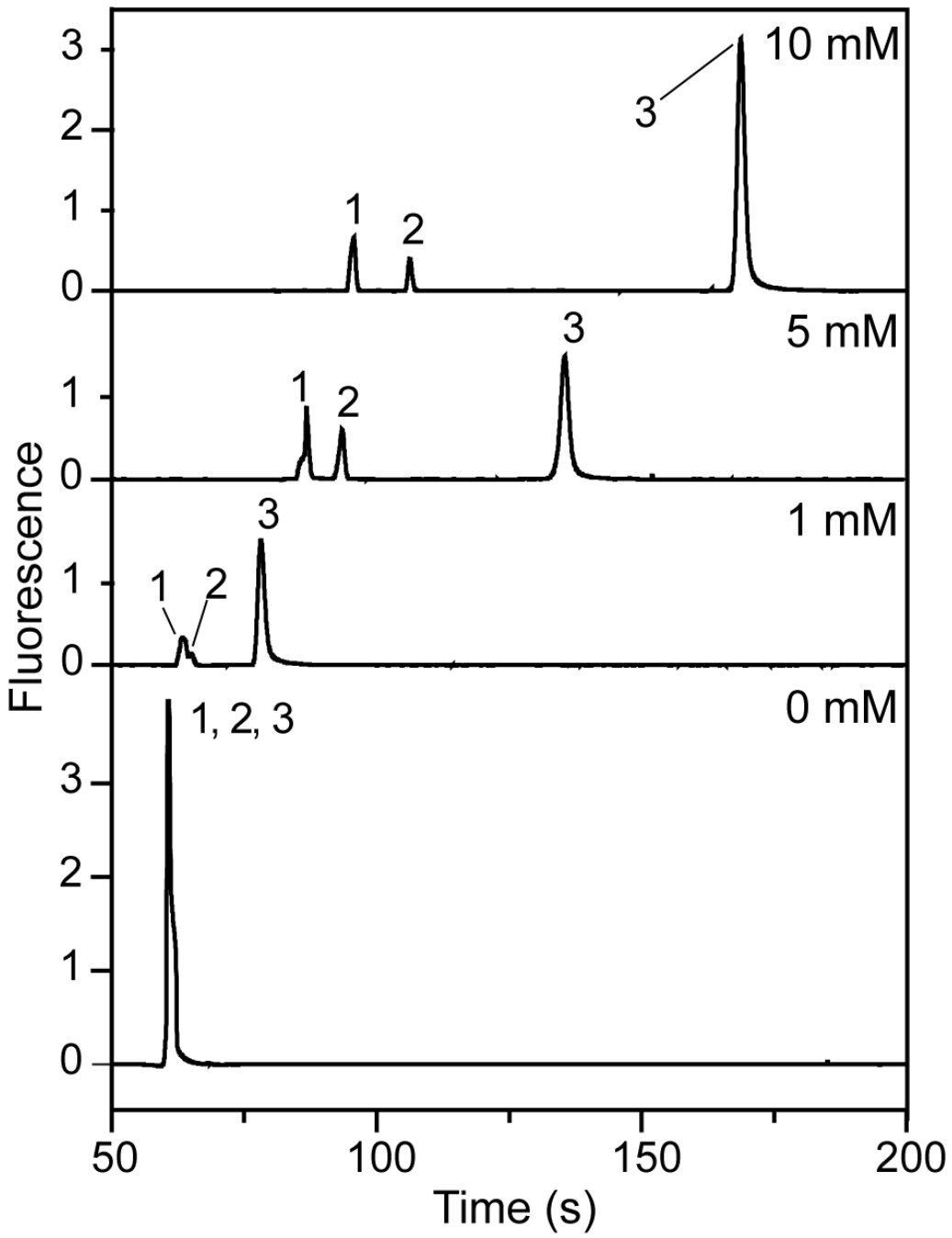

Figure B. 1. Dependence of PAH separation on the concentration of SB-β-CD.

Each sample contains 9,10-diphenylanthracene (1, 40 μM), anthracene (2, 600 μM), and perylene (3, 20 μM). The running buffer contains the indicated concentration of SB-β-CD in addition to 40 mM M-β-CD, 5 mM carbonate buffer, pH 10.

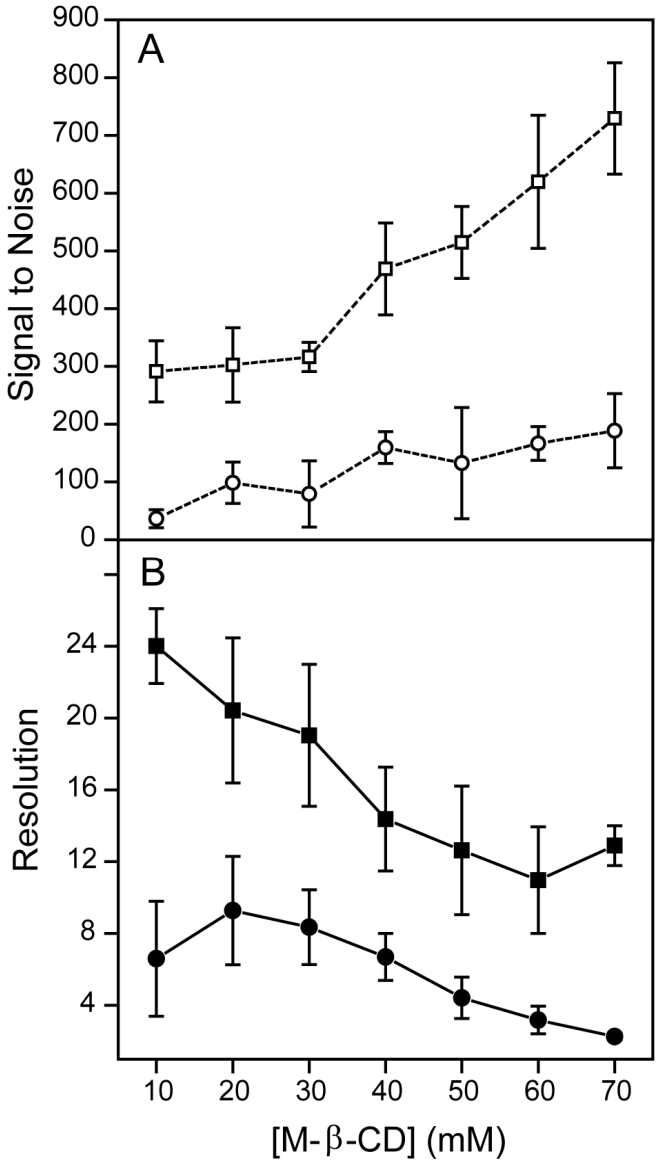

Figure B. 2. Dependence of signal-to-noise ratio (A, dashed lines) and resolution (B, solid lines) of PAH separations on M-β-CD concentration.

Signal-to-noise ratio for anthracene (open circles) and perylene (open squares), as well as the resolution between the anthracene and the fluoranthene peaks (filled squares) and between the fluoranthene and the perylene peaks (filled circles) was calculated from triplicate electropherograms of separations at various concentrations M-β-CD, 10 mM SB-β-CD, 5 mM carbonate buffer, pH 10.

Appendix C: Supplemental Information for Chapter 3

Enhanced Amine and Amino Acid Analysis Using Pacific Blue and the Mars Organic Analyzer Microchip Capillary Electrophoresis System

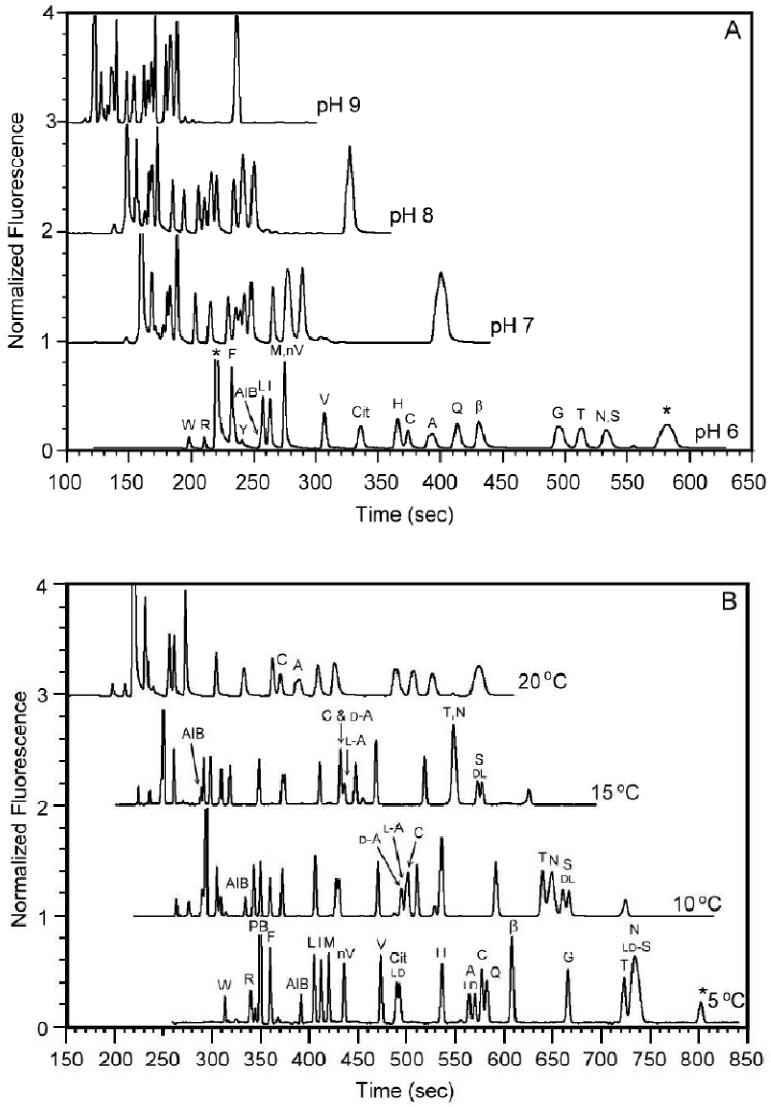

Figure C. 1. Optimization of micellar electrokinetic chromatography separation of PB-labeled amino acids.
(A) Dependence of separation on pH at 20 ^{o}C. (B) Dependence of separation on temperature with pH 6 buffer.

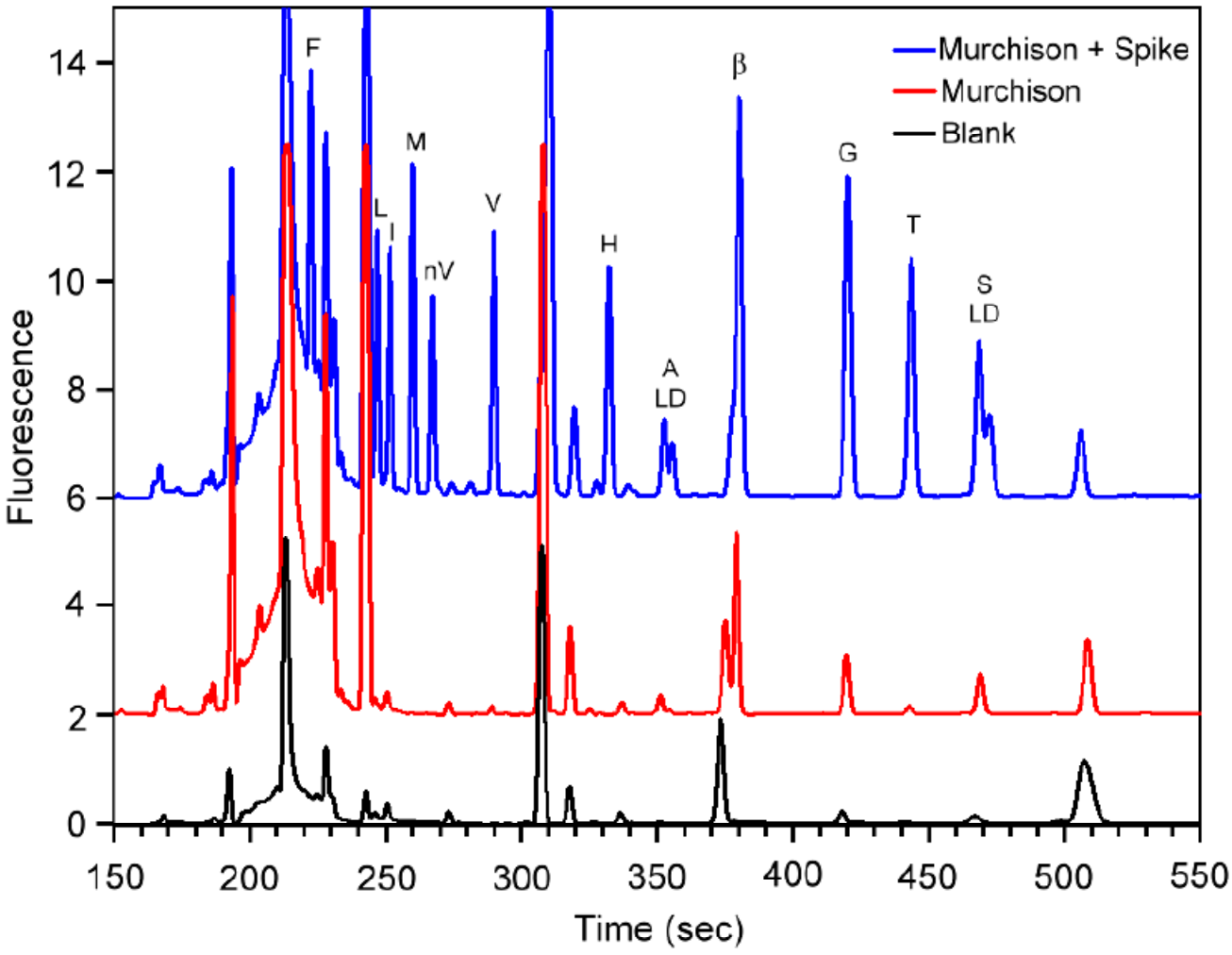

Figure C. 2. Microchip electropherograms of the sub-critical water extracts from the Murchison instrumental blank (black), Murchison sample (red), and Murchison sample + spike (blue) by MEKC.

Amino acids that have been spiked into the sample are designated by their one-letter designations. These traces show the relative background levels of amino acids in a sample and how peaks in a sample can be identified by their relative position to a spiked sample.

Appendix D: Supplemental Information for Chapter 3

Capillary Electrophoresis Analysis of Organic Amines and Amino Acids in Saline and Acidic Samples Using the Mars Organic Analyzer

D.1 Initial Buffer Selection

A screening run was conducted of the buffer systems shown in the matrix in Table D.1. Cells are shaded according to the quality of separation achieved with the indicated buffer system. Green represents a high quality separation, defined by baseline or better resolution of the serine and alanine peaks. White represents a medium quality separation with resolution of the serine and alanine peaks between 0.5 and 1. Yellow represents a low quality separation, defined by an inability to differentiate serine and alanine peaks or run-to-run inconsistency in resolution of these peaks. Red cells represent buffer combinations that resulted in high enough separation currents to cause electrical shorts in the instrument. An example set of electropherograms resulting from this screen is shown Figure D.1. We chose the four buffer systems that showed high separation quality and were likely to span a range of tolerance to salt added to the sample buffer for the further optimization experimentation conducted.

D.2 Effects of Sample EDTA

In addition to the experiments optimizing EDTA concentration for various $MgCl_2$ concentrations discussed in the main manuscript, we conducted a similar study using $FeCl_3$. Electropherograms resulting from this study are shown in Figure D.2. Where the EDTA concentration was less than the $FeCl_3$ concentration, there is either no signal or highly unrepeatable anomalous results.

D.3 EDTA Effects on Labeling

The decrease in labeling efficiency with increasing EDTA concentration is shown in Figure D.3.

D.4 Saline Valley Sample SV07-4

The Saline Valley sample SV07-4 and its associated blanks for both the optimized 30 mM borate, pH 9.5 system and the previously used 4 mM carbonate, pH 8.5 system are shown in Figure D.4. Figure D.5 presents the Saline Valley sample and a comparison to it spiked with arginine, methylamine, citrulline, valine, and glycine.

D.5 Rio Tinto Sample KF03-136

The Rio Tinto sample KF03-136 and its associated blanks for both the optimized 30 mM borate, pH 9.5 system and the previously used 4 mM carbonate, pH 8.5 system are shown in Figure D.6. Figure D.7 presents the Saline Valley sample and a comparison to it spiked with citrulline, valine, serine, alanine, glycine, aspartic acid, and glutamic acid.

Table D. 1 Initial buffer screening experimental results

			Analysis Buffer							
			[Borate]					[Phosphate]		
			5 mM	10 mM	20 mM	50 mM	75 mM	5 mM	10 mM	20 mM
Sample Buffer	[Borate]	5 mM								
		10 mM								
		20 mM								
		50 mM								
		75 mM								
		100 mM								
	[Phosphate]	5 mM	Experiments not conducted.							
		10 mM								
		20 mM								
		50 mM								
		100 mM								

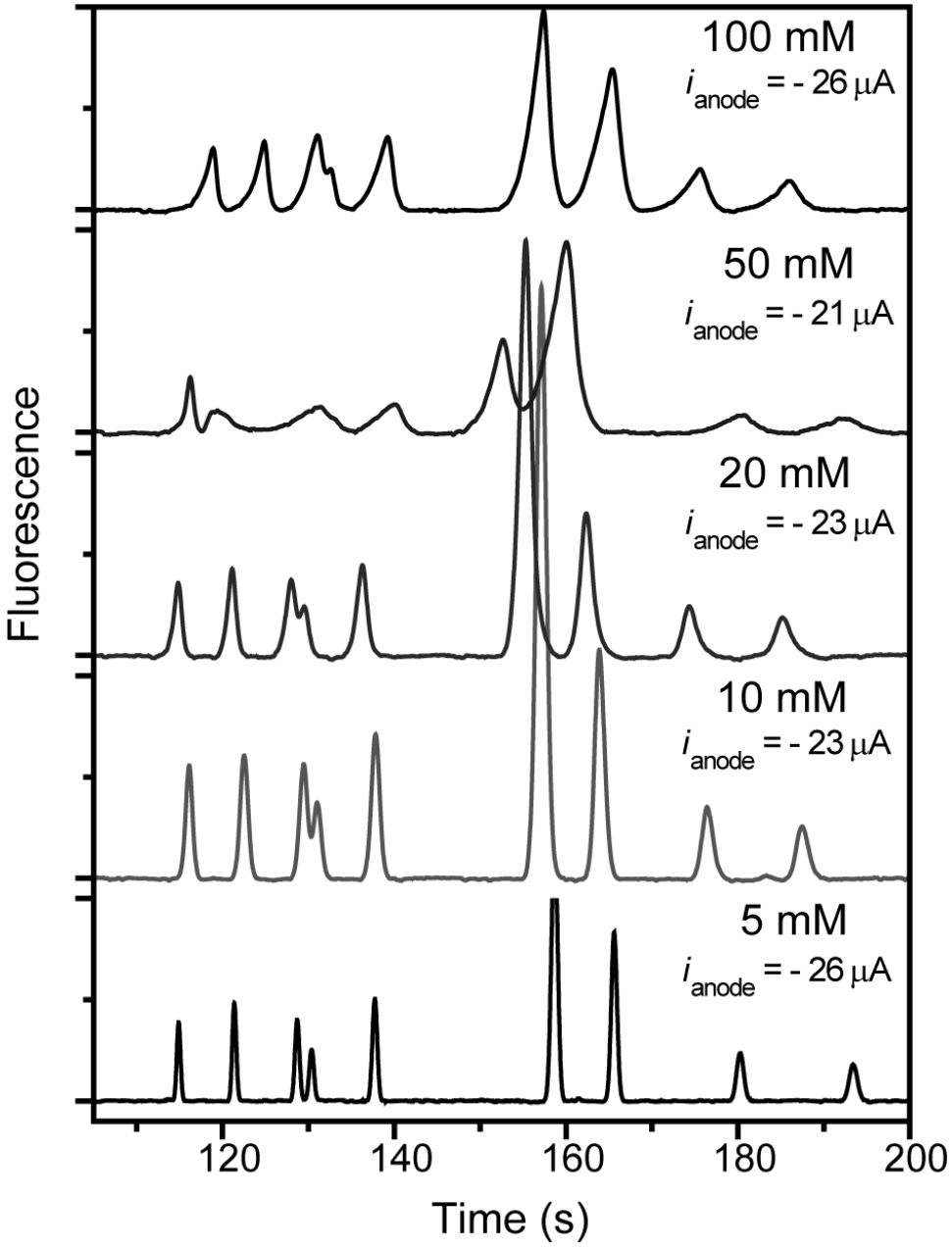

Figure D. 1 Electropherograms of an amino acid standard containing the indicated concentration of phosphate buffer in the sample.

All separations analyzed with 5 mM phosphate in the separation column.

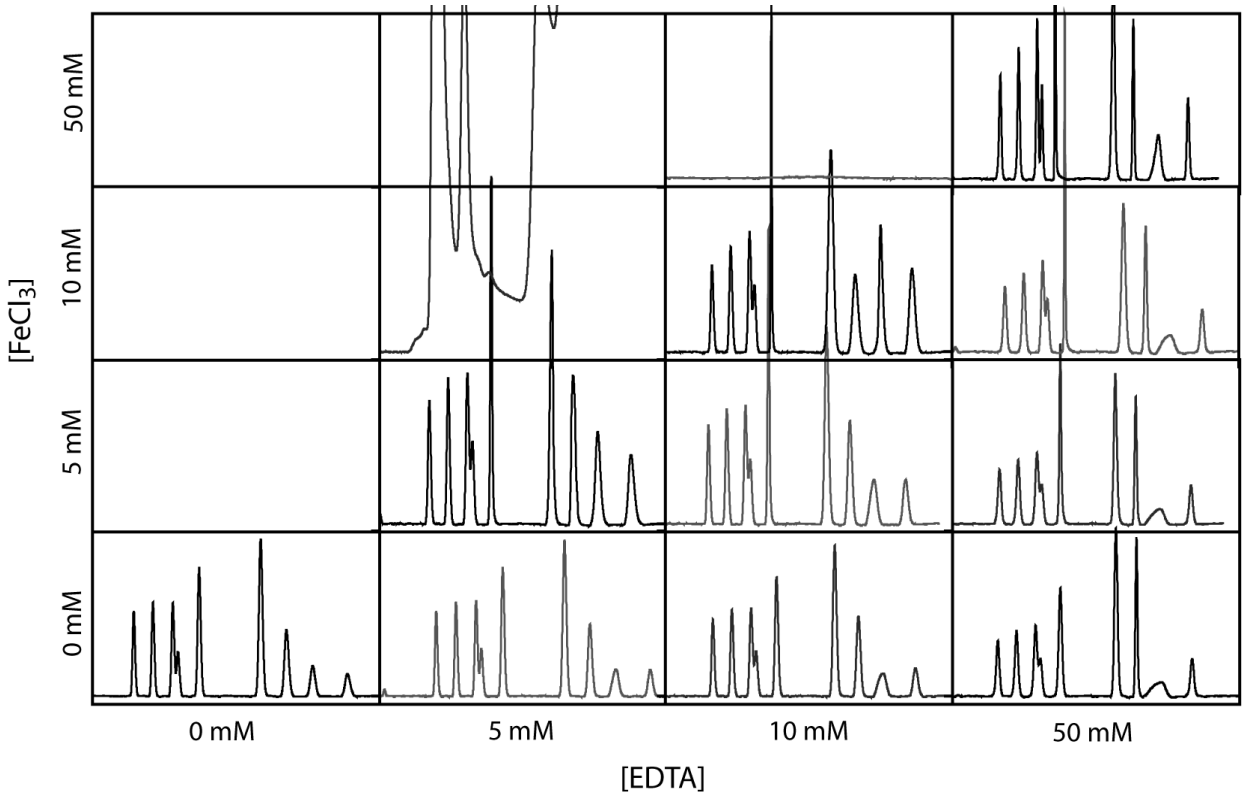

Figure D. 2. Electropherograms an amino standard containing various concentrations of EDTA and $FeCl_3$.

Sample and analysis buffer is 30 mM borate pH 9.5.

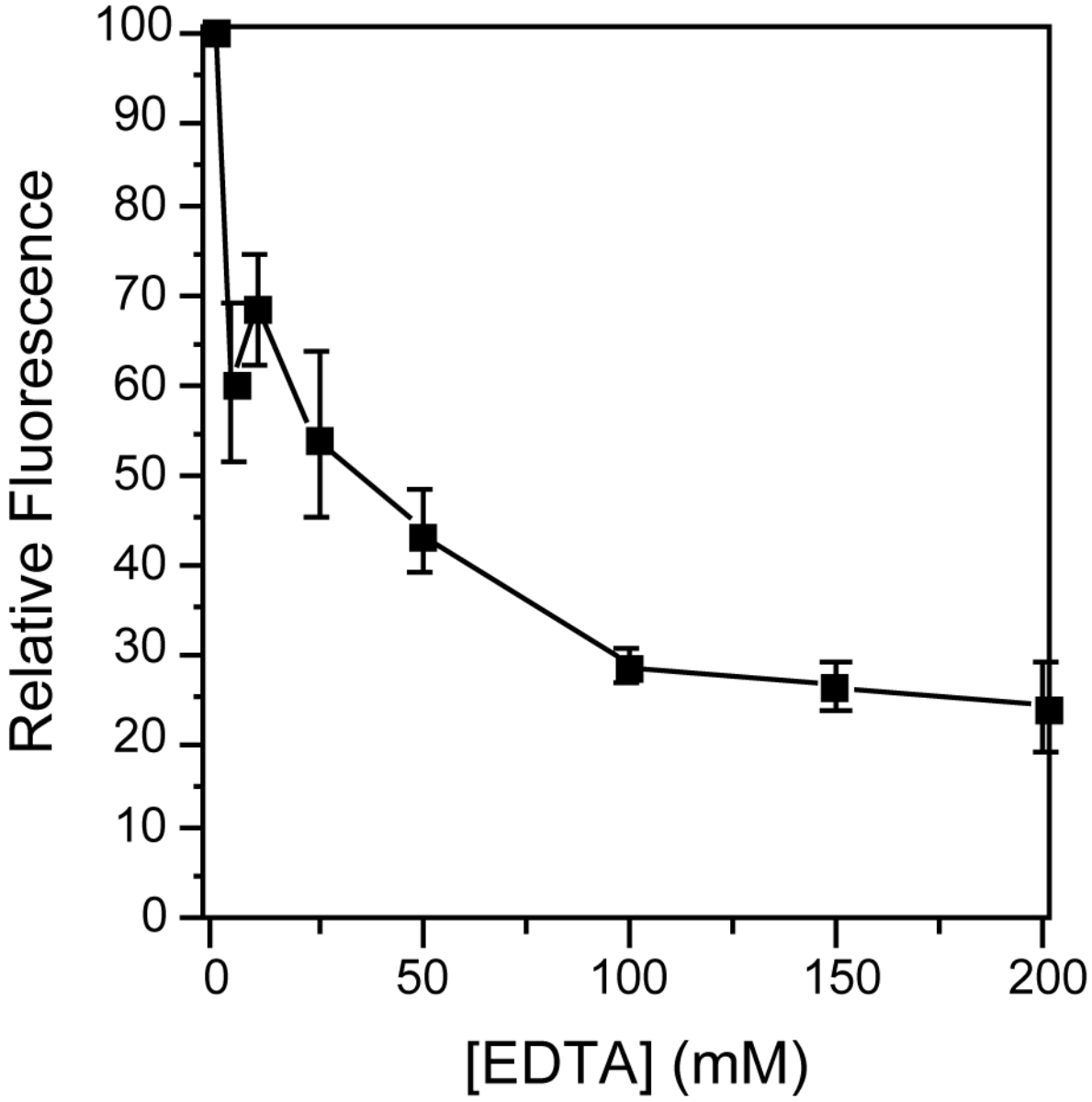

Figure D. 3. Effects of EDTA on fluorescamine labeling efficiency of glycine.

Labeling was performed in buffers containing 30 mM borate buffer, pH 9.5, and the indicated concentration of EDTA and 2.7 μM fluorescamine. Fluorescence was taken after a 10 minute reaction time, and shown as a percentage of the fluorescence of samples with no EDTA.

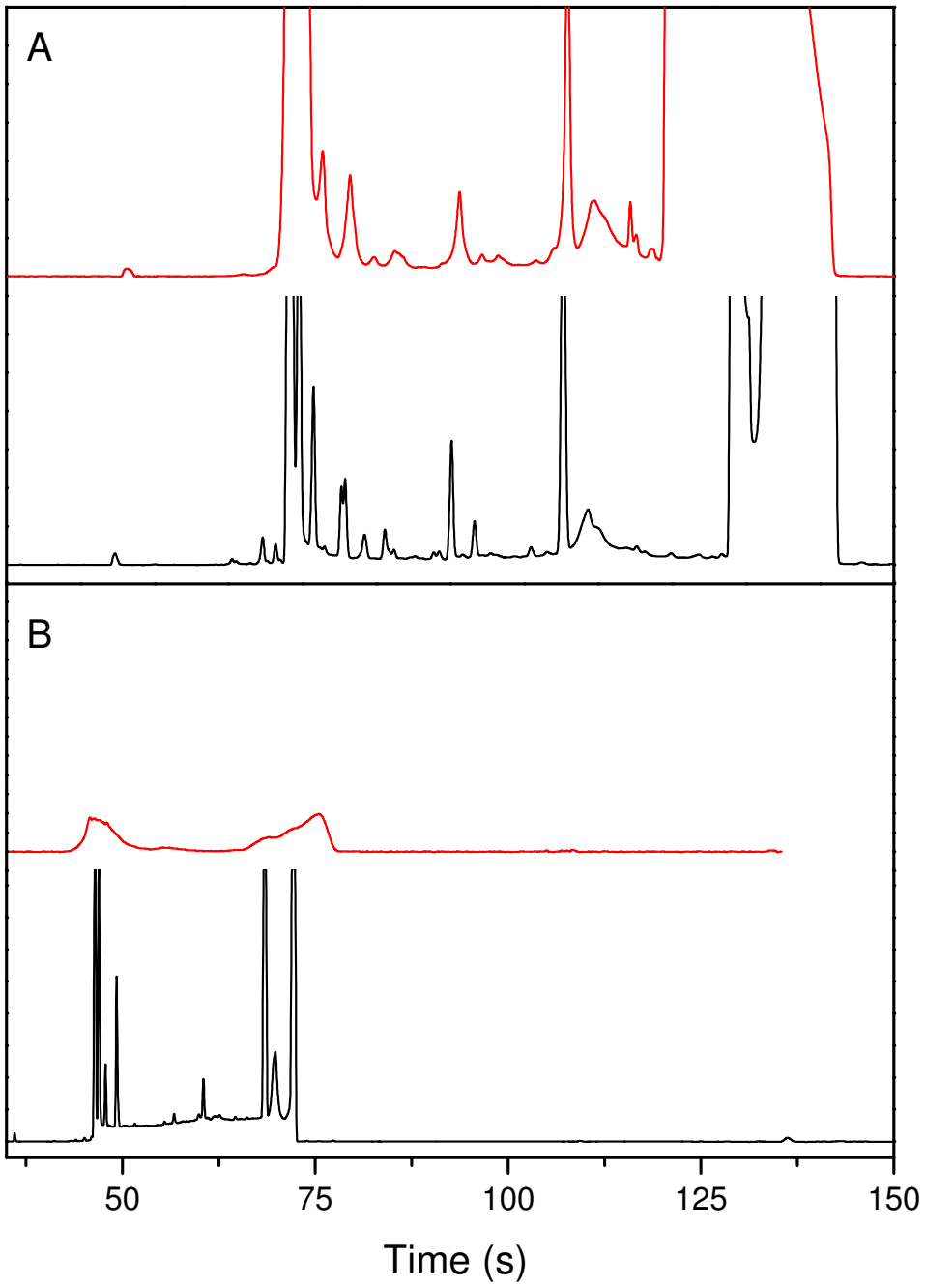

Figure D. 4. Electropherograms of Pacific Blue labeled Saline Valley sample SV07-4 (top, red) and its associated blank (bottom, black).

(A) Separation and labeling buffer are both 4 mM carbonate, pH 8.5. (B) Separation and labeling buffer are both 30 mM borate pH 9.5.

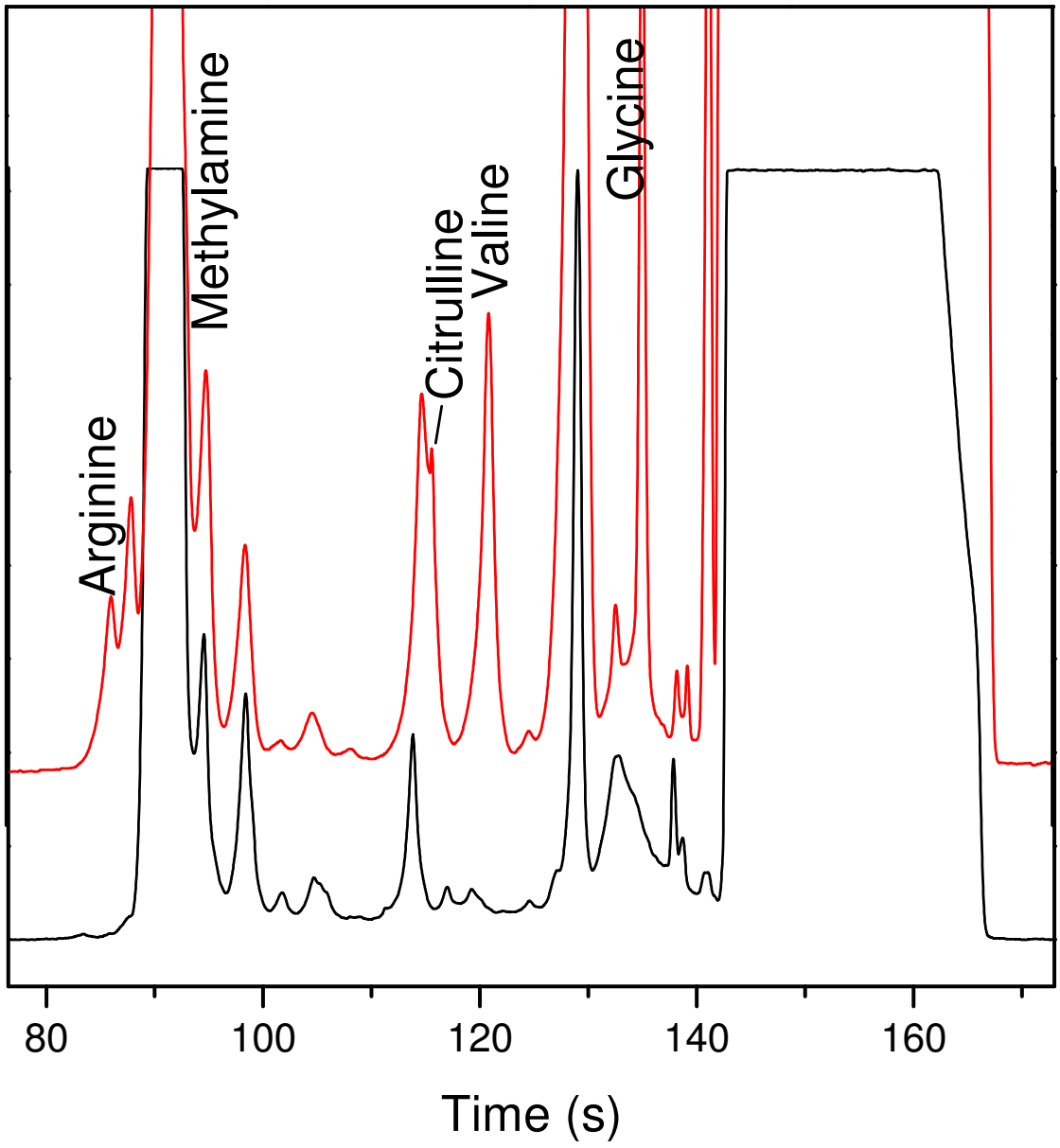

Figure D. 5. Electropherograms of Pacific Blue labeled Saline Valley sample SV07-4 (black, bottom) and Pacific Blue Saline Valley sample SV07-4 (red, top) spiked with arginine, methylamine, citrulline, valine, and glycine.

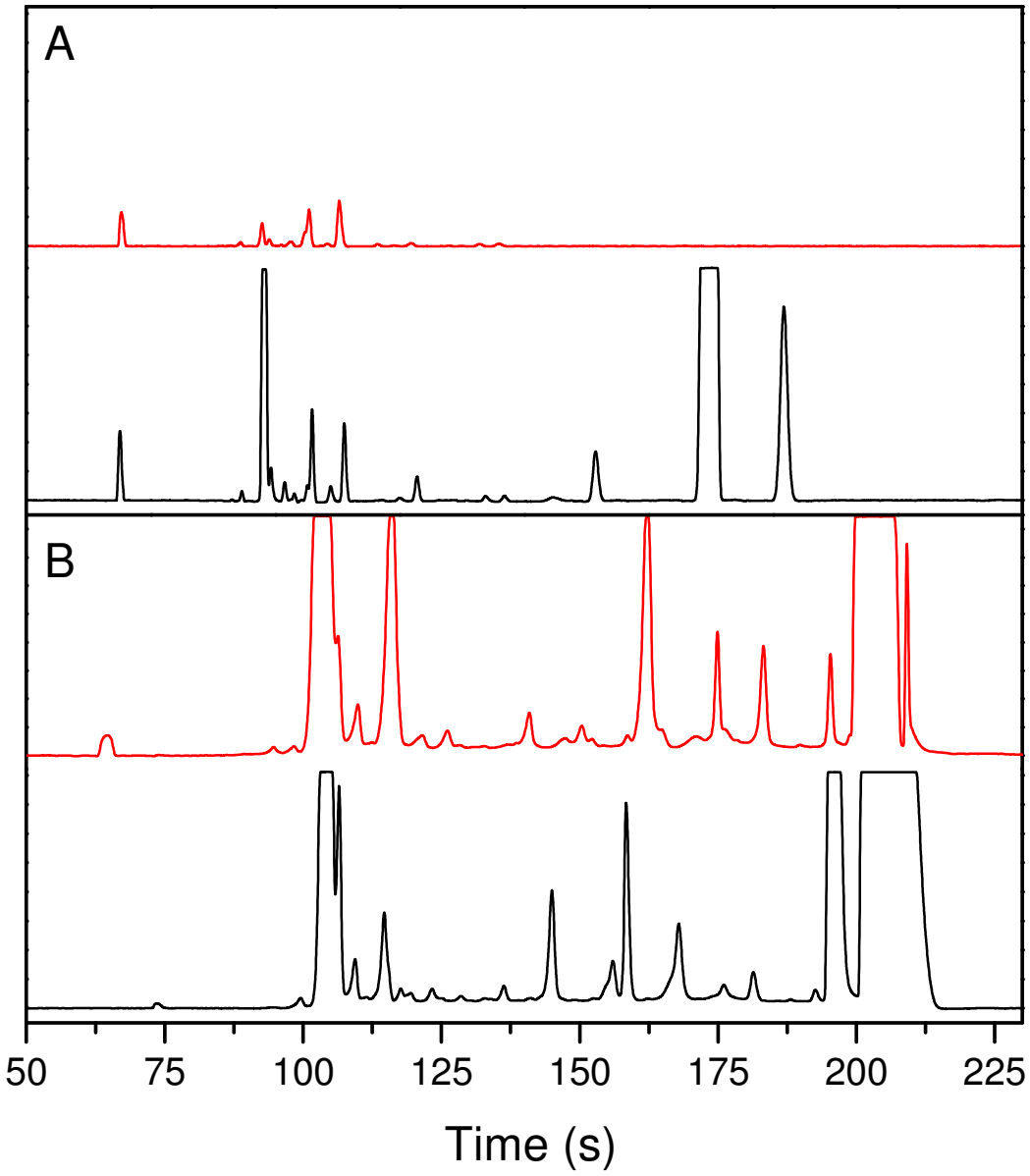

Figure D. 6. Electropherograms of Pacific Blue labeled Rio Tinto sample KF03-136 (top, red) and its associated procedural blank (bottom, black).

(A) Separation and labeling buffer are both 4 mM carbonate, pH 8.5. (B) Separation channel contains 30 mM borate, pH 9.5. The sample and blank were diluted with 30 mM borate before labeling, then brought to a final sample buffer composition of 30 mM borate, 50 mM EDTA for injection.

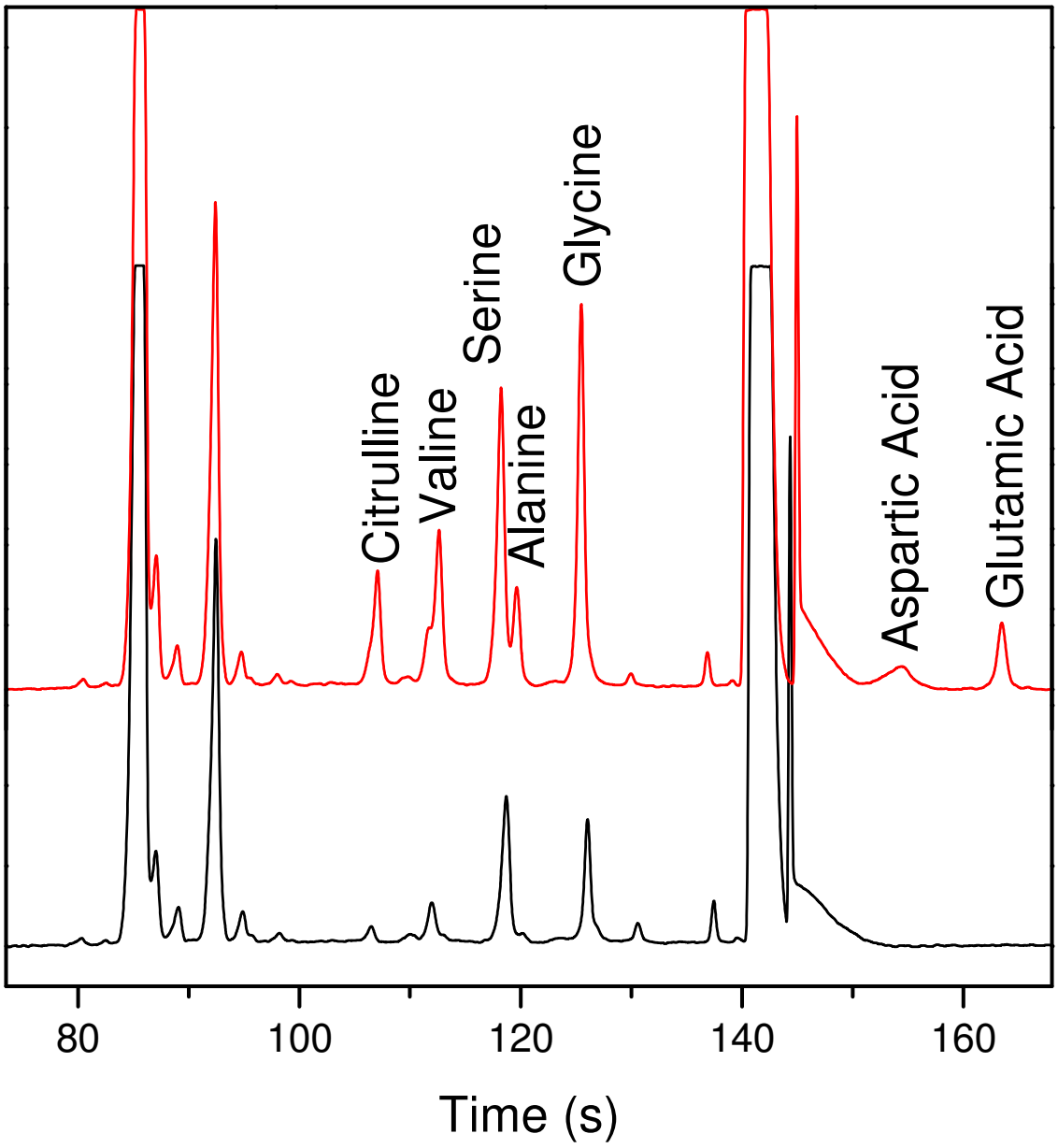

Figure D. 7. Electropherograms of Pacific Blue labeled Rio Tinto sample KF03-136 (black, bottom) and Pacific Blue Rio Tinto sample KF03-136 (red, top) spiked with citrulline, valine, serine, alanine, glycine, aspartic acid, and glutamic acid.

Appendix E: Supplemental Information for Chapter 4

Analysis of Carbonaceous Biomarkers with the Mars Organic Analyzer Microchip Capillary Electrophoresis System: Aldehydes and Ketones

E.1 Optimization of Cascade Blue Hydrazide Labeling of Aldehydes and Ketones

Scheme E.1 shows the acid catalyzed mechanism of hydrazone formation in the reaction of a hydrazide with an aldehyde or ketone. Electropherograms of the aldehyde and ketone standard labeled at pH ranging from 2 to 12 are shown in Figure E.1.

E.2 Limits of Detection

The limits of detection stated in the main text are presented in Table E.1.

E.3 Further Separation Characterization and Validation

The separation characteristics of peak efficiencies and resolutions between peaks are given in Table E.2.

Approximate peak capacities of the system were calculated using one of the most commonly used peak capacity equations:

$$n_c = \frac{t_2 - t_1}{4\bar{\sigma}R_s}$$

where n_c is the estimated peak capacity, t_2 is the elution time of the latest eluting peak, t_1 is the elution time of the "dead volume," $\bar{\sigma}$ is the average standard deviation of all peaks, and R_s is the desired resolution between peaks. For these calculations, we assume

$$\sigma = \frac{FWHM}{2\sqrt{2\ln 2}}$$

where FWHM is the full width at half maximum determined by fitting the peaks using PeakFit. We also take R_s to be one. The peak capacity that covers the largest separation range extends from the elution of the dead volume at approximately 32 s to the elution of α-ketoglutaric acid at approximately 184 s. However, there are only two ketones of interest that elute after the Cascade Blue peak at 125.5 s, leading us to discard this range for a peak capacity estimation. We estimate that between the elution of the dead volume and the elution of Cascade Blue $n_c \approx 109$. Of more interest to the wine analysis is the region between the elution of the aromatic aldehydes and ketones at 99.5 s and the elution of Cascade Blue, which has an estimated $n_c \approx 30$.

There is a minimal degree of run-to-run variability in the system. As a chip ages and accumulates ionic debris on the channel surface, separation times lengthen from approximately 120 s to over 200 s. Peak area does not appear to differ significantly between new chips and old chips. Work for this paper was done on new enough chips to provide separation times of 120 s to 180 s. There is also approximately a 5 % variation in peak area run-to-run due to human error in positioning the laser (~10 μm spot size) in the center of the channel (200 μm width) and variations in injection.

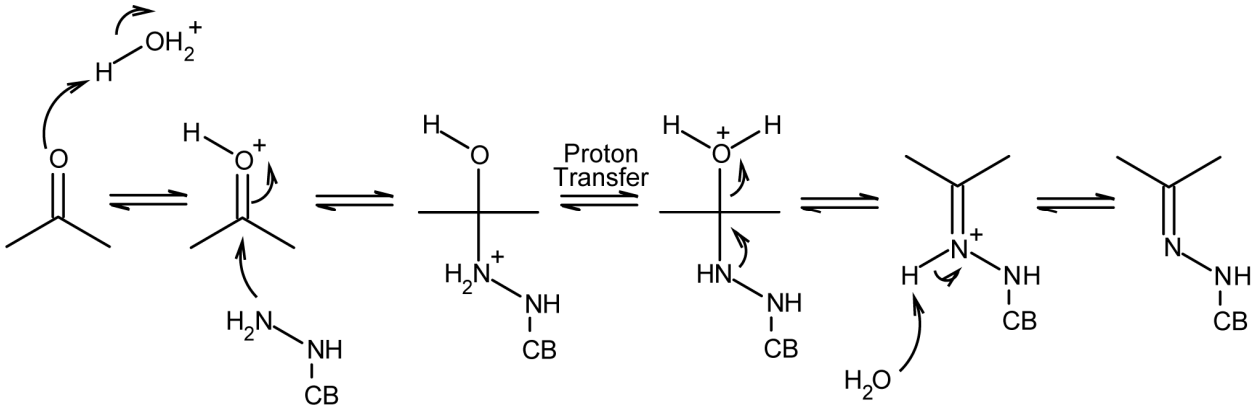

Scheme E. 1 Acid catalyzed mechanism of hydrazone formation

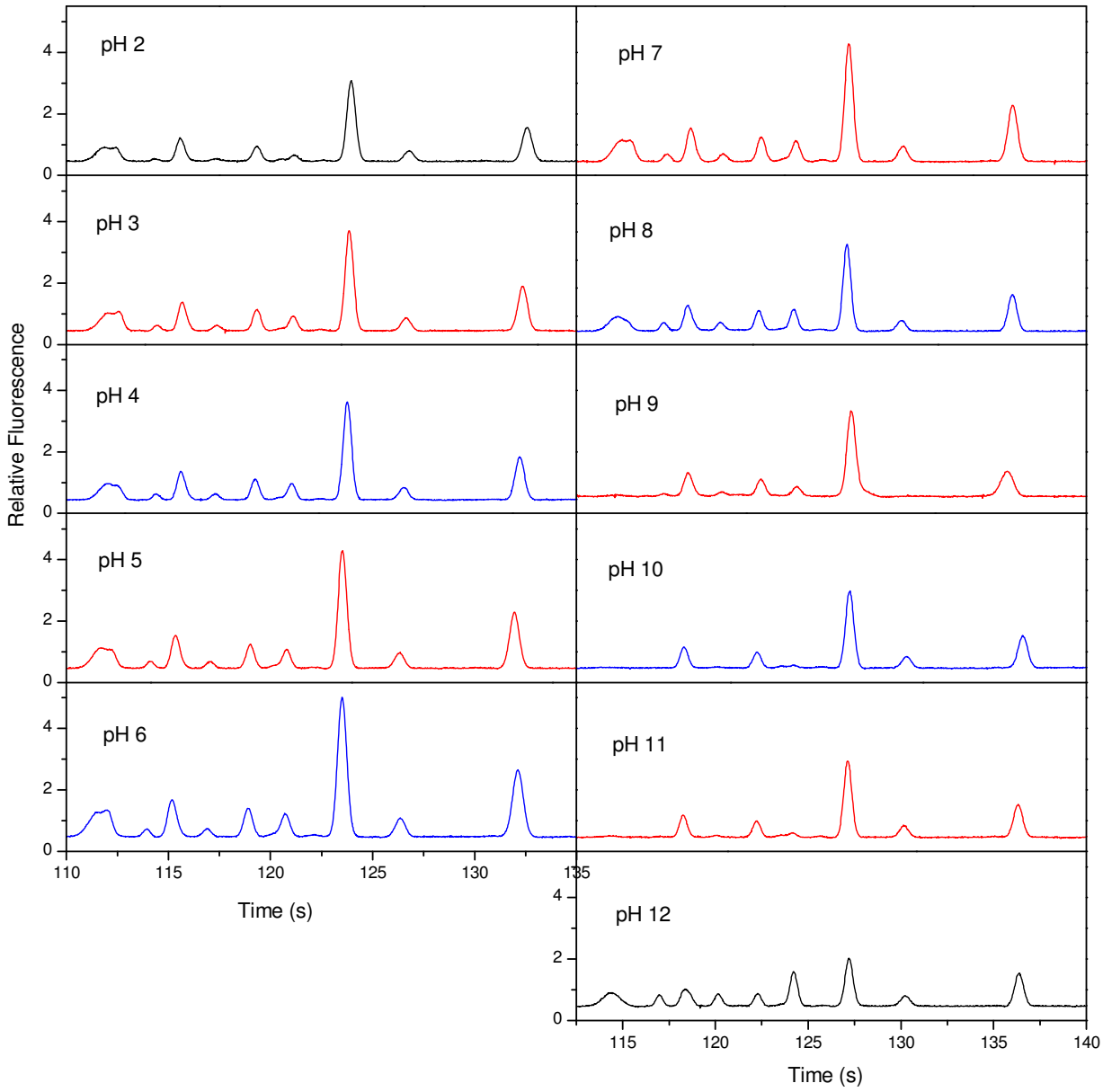

Figure E. 1. Electropherograms of the separation of the carbonyl standard labeled at pH's ranging from 3 to 12.

Standard was labeled with Cascade Blue hydrazide in 30 mM borate at the indicated pH, then diluted for analysis with 30 mM borate, pH 9.5. The pH was measured for bulk 30 mM borate with an error of 0.01 pH unit; however, upon dilution into labeling mixtures, the error likely increases, particularly for pH far from the borate pK_a.

Table E. 1. Aldehyde and ketone limits of detection

Ketone / Aldehyde	Limit of Detection[a]
Formaldehyde	70 ± 30 pM
Acetaldehyde	700 ± 200 pM
Acetone	5 ± 2 nM
Benzophenone	1.6 ± 0.6 µM

[a] LOD and uncertainty calculated from triplicate experiments at 12 concentrations.

Table E.2 Separation characteristics of ketones and aldehydes on the Mars Organic Analyzer.[a]

Peak	Aldehyde / Ketone	Theoretical Plates	Theoretical plates per meter	Resolution
1	p-Anisaldehyde Benzophenone	97,000	410,000	
2	3-Methyl-2-butanone	350,000	1,500,000	2.0
3	Butyraldehyde Diethylketone 3-Methyl-2-butanone	200,000	860,000	1.3
4	Methylethylketone	300,000	1,300,000	1.7
5	Butyraldehyde Methylethylketone Propionaldehyde	310,000	1,300,000	2.1
6	Acetone	320,000	1,300,000	2.0
7	Acetaldehyde	310,000	1,300,000	2.9
8	Acetaldehyde	300,000	1,300,000	2.9
9	Formaldehyde	270,000	1,200,000	5.4

[a] Separation shown in Figure 2 in Chapter 4.

E.4 Further Discussion of Fermented Beverage Analysis

The results of analysis of two wines not presented in the text, the Bears' Lair cabernet sauvignon and merlot, are presented in Table E.3.

Flor sherry yeast (named for the film, or flor, it develops on the surface of fermenting wine) operating under aerobic conditions oxidizes ethanol to acetaldehyde,[159] leading to its intensified concentration in the cream sherry studied.

The peak acetoin level of approximately 100 mg/L (1.1 mM)[159] decreases naturally (via reduction to the diol) by the end of fermentation to approximately 5-20 mg/L (50-230 μM);[159] all table wines studied are within this range except for the Bears' Lair cabernet sauvignon, which exhibits a slightly higher acetoin concentration (400 ± 100 μM).

Levels of other aldehydes and ketones observed in the fermented beverages studied correlate to the method of production and source of fermentable sugars. The table wines were the only fermented beverages examined to contain measurable levels of p-anisaldehyde and benzophenone. The table wines fermented from red grapes and the sake were the only fermented beverages to exhibit measurable levels of 3-methyl-2-butanone. Methylethylketone was only observed in wines fermented from red grapes and their skins, and presumably this species arises from the use of the skins of red grapes in fermentation.

Table E. 3 Selected aldehyde and ketone content of additional red table wines.

Ketone or Aldehyde	Wine	
	Bears' Lair Merlot	Bears' Lair Cabernet Sauvignon
Benzophenone / p-Anisaldehyde	11 ± 3 mM	10 ± 3 μM
3-Methyl-2-butanone	5 ± 1 μM	18 ± 4 μM
Acetoin	40 ± 10 μM	300 ± 60 μM
Methylethyl-ketone	4 ± 1 μM	29 ± 6 μM
Diacetyl	370 ± 80 μM	1.0 ± 0.2 mM
Formaldehyde	40 ± 10 nM	100 ± 20 nM

Appendix F: Supplemental Information for Chapter 5

Analysis of Carbonaceous Biomarkers with the Mars Organic Analyzer Microchip Capillary Electrophoresis System: Carboxylic Acids

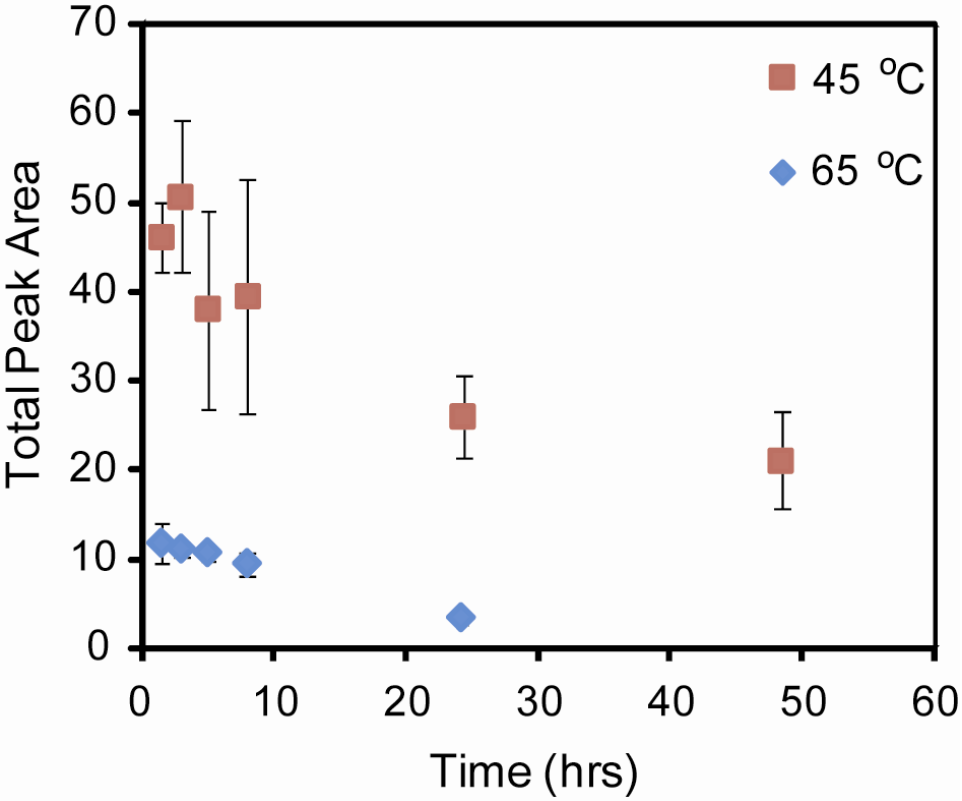

Figure F. 1. Dependence of the total peak area of a CB-labeled carboxylic acid standard on reaction time at (A) 45 °C and (B) 65 °C.

The standard contains 2.7 µM formic acid and heptanoic acid, 1.3 µM acetic acid, propionic acid, butyric acid, pentanoic acid, and hexanoic acid, and 4 µM octanoic acid. The standard was labeled with CB using EDC activation at pH 3, then diluted and analyzed with 30 mM borate, pH 9.5.

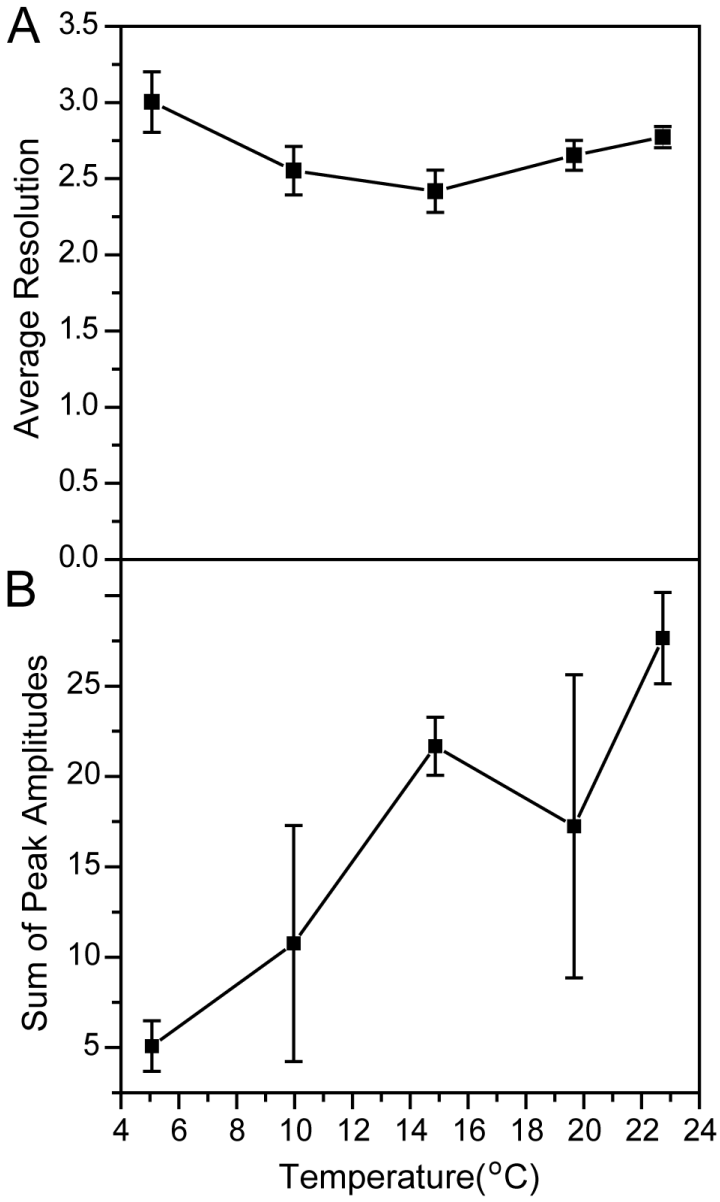

Figure F. 2. Separation temperature dependence of (A) average peak resolution and (B) total sum of peak amplitudes of a Cascade Blue standard containing eight aliphatic carboxylic acids.

The standard contains 2.7 μM formic acid and heptanoic acid, 1.3 μM acetic acid, propionic acid, butyric acid, pentanoic acid, and hexanoic acid, and 4 μM octanoic acid. The standard was labeled with CB using EDC activation at pH 3, then diluted and analyzed with 30 mM borate, pH 9.5.

Additional discussion of temperature effects on separation. Of note is the decrease in signal at decreased temperatures. Peaks also exhibited a significant increase in tailing as

temperatures declined. Precipitation of CB from aqueous solutions at reduced temperatures was observed visually in 10 mM bulk solutions, suggesting that the increase in tailing could be due to precipitation. The increase in tailing balances the decrease in diffusive band broadening at low temperatures, leading to temperature-independent peak resolution.

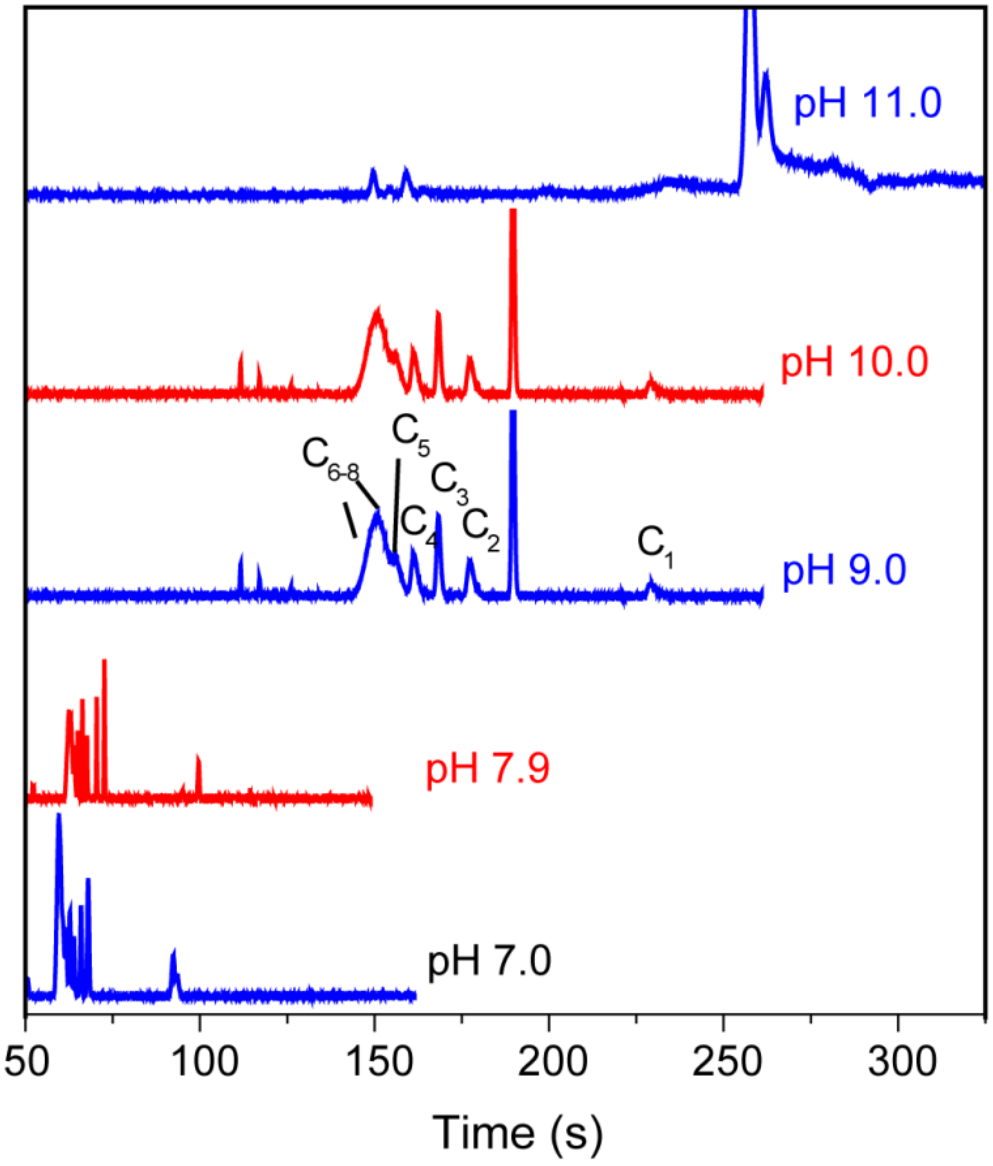

Figure F. 3. Electropherograms of a separation of a standard containing CB-labeled carboxylic acids at pH from 7 to 10.

The charge state of the CB sulfates changes from -3 to -2 at pH < 9, as evidenced by the decrease in elution time at pH 7 and 8. The standard contains 2.7 µM formic acid and heptanoic acid, 1.3 µM acetic acid, propionic acid, butyric acid, pentanoic acid, and hexanoic acid, and 4 µM octanoic acid. The standard was labeled with CB using EDC activation at pH 3, then diluted and analyzed with 30 mM borate, pH 9.5.

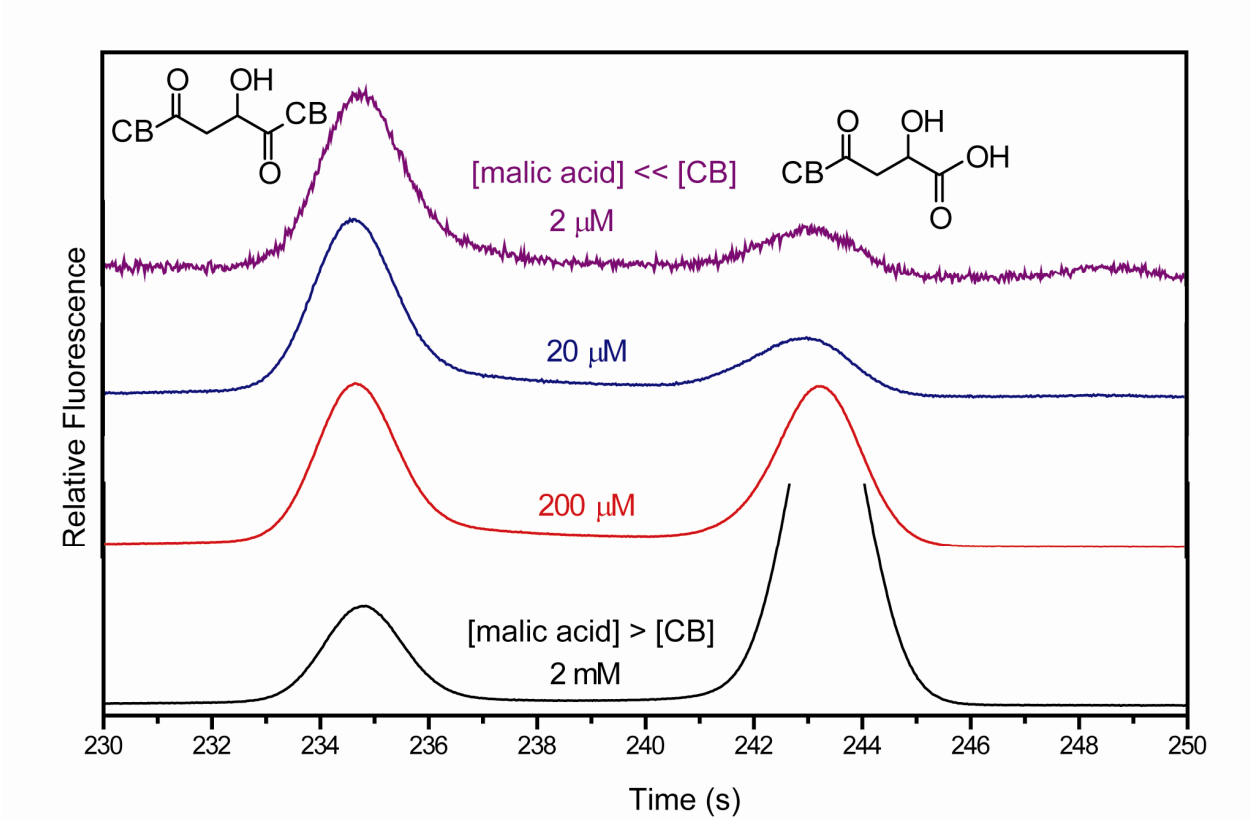

Figure F. 4. Malic acid peaks at several ratios of malic acid (MA) to Cascade Blue hydrazide dye (CB).

The CB concentration is kept constant at 300 μM. At high MA:CB, a single labeling reaction is expected to dominate over a double-labeling raction. At low MA:CB, double-labeling is expected to dominate over single-labeling. The peaks are assigned by examining the relative peak heights of the two malic acid peaks.

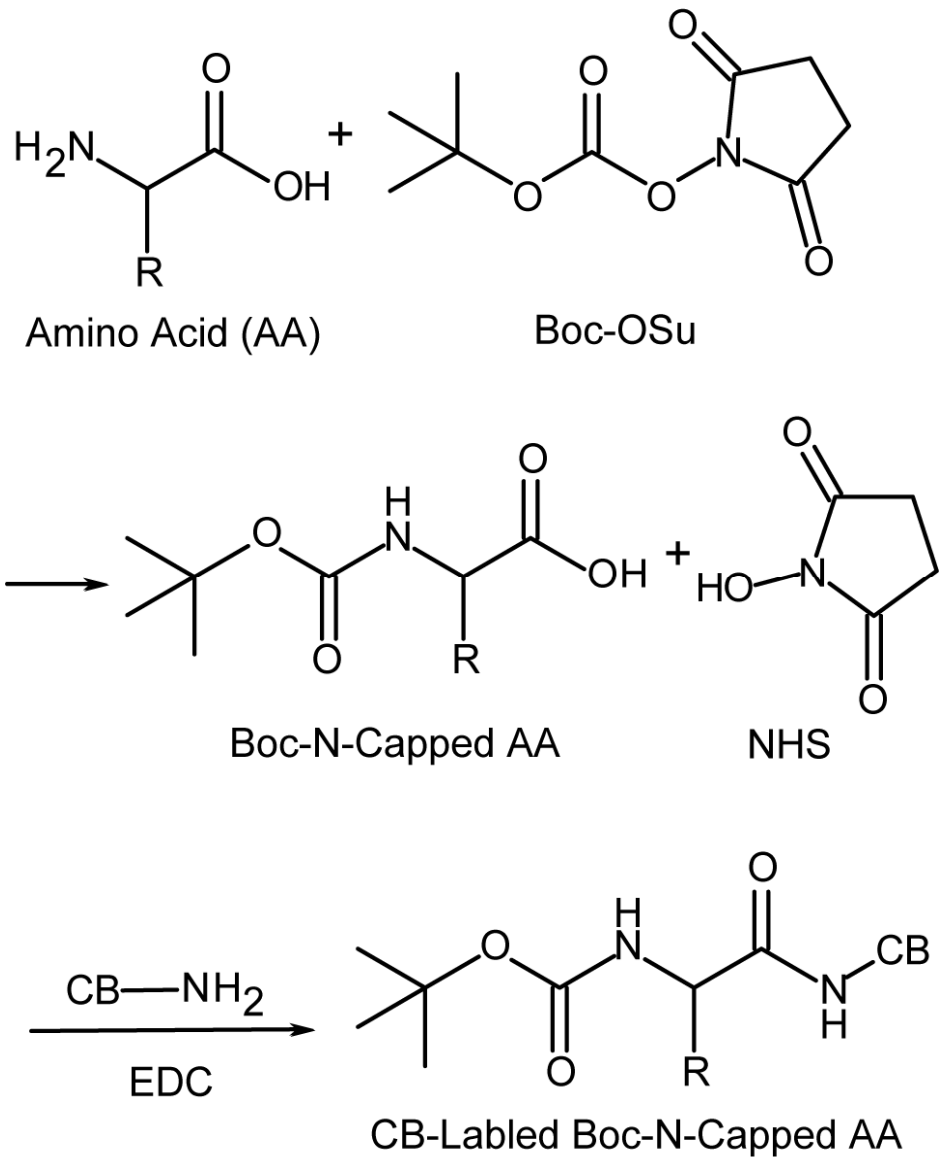

Scheme F. 1 BocOSu amine capping for amino acid labeling

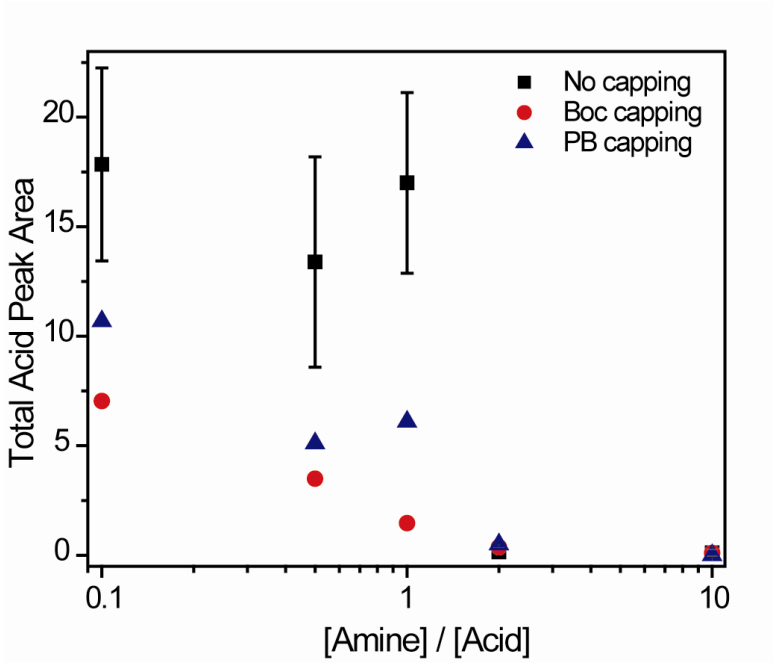

Figure F. 5. Dependence of acid peak area of a CB-labeled standard containing a mixture of carboxylic acids and amines at various ratios with no amine capping (black squares), with Boc-OSu capping of amino groups (red circles), and with capping of amino groups by Pacific Blue succinimidyl ester (blue triangles).

The standard contains 45 μM each formic acid, acetic acid, propionic acid, and butyric acid, and the indicated total concentration of methylamine and ethylamine (1:1). Capped experiments were performed by combining Boc-OSu or PB in DMSO with the standard; for uncapped experiments, DMSO was combined with the standard. Both standards were then labeled using EDC-activated CB labeling in 30 mM borate, pH 3, before dilution and analysis with 30 mM borate, pH 9.5, at 20 ^{o}C.

References

(1) *Planets and Life: The Emerging Science of Astrobiology*; Sullivan, I., Woodruff T.; Baross, J. A., Eds.; Cambridge University Press: New York, 2007.

(2) Kuttner, H. *Fury*; RosettaBooks LLC: New York, 1947.

(3) Heinlein, R. A. *Between Planets*; Charles Scribner's Sons: New York City, NY, 1951.

(4) Sonett, C. P. *Space Science Reviews* **1963**, *2*, 751.

(5) Leighton, R. B.; Murray, B. C.; Sharp, R. P.; Allen, J. D.; Sloan, R. K. *Science* **1965**, *149*, 627.

(6) Kasting, J. F. *Icarus* **1988**, *74*, 472.

(7) Strom, R. G.; Schaber, G. G.; Dawson, D. D. *J. Geophys. Res.* **1994**, *99*, 10899.

(8) Abelson, P. H. *Science* **1965**, *149*, 1179.

(9) Herr, K. C.; Pimentel, G. C. *Science* **1969**, *166*, 496.

(10) Fielder, G. *Nature* **1965**, *207*, 1381.

(11) Rasool, S. I.; Hogan, J. S.; Stewart, R. W.; Russell, L. H. *Journal of the Atmospheric Sciences* **1970**, *27*, 841.

(12) Klein, H. P. *J. Geophys. Res.* **1977**, *82*, 4677.

(13) Horowitz, N. H.; Hobby, G. L.; Hubbard, J. S. *J. Geophys. Res.* **1977**, *82*, 4659.

(14) Levin, G. V.; Straat, P. A. *J. Geophys. Res.* **1977**, *82*, 4663.

(15) Oyama, V. I.; Berdahl, B. J. *J. Geophys. Res.* **1977**, *82*, 4669.

(16) Oyama, V. I.; Berdahl, B. J.; Carle, G. C. *Nature* **1977**, *265*, 110.

(17) Biemann, K.; Oro, J.; Toulmin, P., III; Orgel, L. E.; Nier, A. O.; Anderson, D. M.; Simmonds, P. G.; Flory, D.; Diaz, A. V.; Rushneck, D. R.; Biller, J. A. *Science* **1976**, *194*, 72.

(18) Biemann, K.; Oro, J.; Toulmin, P., III; Orgel, L. E.; Nier, A. O.; Anderson, D. M.; Simmonds, P. G.; Flory, D.; Diaz, A. V.; Rushneck, D. R.; Biller, J. E.; Lafleur, A. L. *J. Geophys. Res.* **1977**, *82*.

(19) Rieder, R.; Economou, T.; Wanke, H.; Turkevich, A.; Crisp, J.; Bruckner, J.; Dreibus, G.; McSween, H. Y. *Science* **1997**, *278*, 1771.

(20) Klingelhöfer, G.; Morris, R. V.; Bernhardt, B.; Schröder, C.; Rodionov, D. S.; de Souza, P. A.; Yen, A.; Gellert, R.; Evlanov, E. N.; Zubkov, B.; Foh, J.; Bonnes, U.; Kankeleit, E.; Gütlich, P.; Ming, D. W.; Renz, F.; Wdowiak, T.; Squyres, S. W.; Arvidson, R. E. *Science* **2004**, *306*, 1740.

(21) Squyres, S. W.; Grotzinger, J. P.; Arvidson, R. E.; Bell, J. F.; Calvin, W.; Christensen, P. R.; Clark, B. C.; Crisp, J. A.; Farrand, W. H.; Herkenhoff, K. E.; Johnson, J. R.; Klingelhofer, G.; Knoll, A. H.; McLennan, S. M.; McSween, H. Y.; Morris, R. V.; Rice, J. W.; Rieder, R.; Soderblom, L. A. *Science* **2004**, *306*, 1709.

(22) Smith, P. H.; Tamppari, L. K.; Arvidson, R. E.; Bass, D.; Blaney, D.; Boynton, W. V.; Carswell, A.; Catling, D. C.; Clark, B. C.; Duck, T.; DeJong, E.; Fisher, D.; Goetz, W.; Gunnlaugsson, H. P.; Hecht, M. H.; Hipkin, V.; Hoffman, J.; Hviid, S. F.; Keller, H. U.; Kounaves, S. P.; Lange, C. F.; Lemmon, M. T.; Madsen, M. B.; Markiewicz, W. J.; Marshall, J.; McKay, C. P.; Mellon, M. T.; Ming, D. W.; Morris, R. V.; Pike, W. T.; Renno, N.; Staufer, U.; Stoker, C.; Taylor, P.; Whiteway, J. A.; Zent, A. P. *Science* **2009**, *325*, 58.

(23) Hecht, M. H.; Kounaves, S. P.; Quinn, R. C.; West, S. J.; Young, S. M. M.; Ming, D. W.; Catling, D. C.; Clark, B. C.; Boynton, W. V.; Hoffman, J.; DeFlores, L. P.; Gospodinova, K.; Kapit, J.; Smith, P. H. *Science* **2009**, *325*, 64.

(24) Levin, G. V. *Journal of Cosmology* **2010**, *5*, 920.

(25) Levin, G. V. *International Journal of Astrobiology* **2007**, *6*, 95.

(26) Benner, S. A.; Devine, K. G.; Matveeva, L. N.; Powell, D. H. *Proc. Natl. Acad. Sci. U. S. A.* **2000**, *97*, 2425.

(27) Levin, G. V.; Straat, P. A. *Icarus* **1981**, *45*, 494.

(28) Chaban, B.; Ng, S. Y. M.; Jarrell, K. F. *Canadian Journal of Microbiology* **2006**, *52*, 73.

(29) Cavicchioli, R. *Astrobiology* **2002**, *2*, 281.

(30) Whiteway, J. A.; Komguem, L.; Dickinson, C.; Cook, C.; Illnicki, M.; Seabrook, J.; Popovici, V.; Duck, T. J.; Davy, R.; Taylor, P. A.; Pathak, J.; Fisher, D.; Carswell, A. I.; Daly, M.; Hipkin, V.; Zent, A. P.; Hecht, M. H.; Wood, S. E.; Tamppari, L. K.; Renno, N.; Moores, J. E.; Lemmon, M. T.; Daerden, F.; Smith, P. H. *Science* **2009**, *325*, 68.

(31) Boynton, W. V.; Ming, D. W.; Kounaves, S. P.; Young, S. M. M.; Arvidson, R. E.; Hecht, M. H.; Hoffman, J.; Niles, P. B.; Hamara, D. K.; Quinn, R. C.; Smith, P. H.; Sutter, B.; Catling, D. C.; Morris, R. V. *Science* **2009**, *325*, 61.

(32) Marcy, G. W.; Butler, R. P.; Vogt, S. S.; Fischer, D. A. In *Bioastronomy 2002: Life among the Stars*; Norris, R. P., Stootman, F. H., Eds.; Astronomical Soc Pacific: San Francisco, 2004, p 11.

(33) Thomas, P. J.; Schubert, G. *Journal of Geophysical Research-Solid Earth and Planets* **1986**, *91*, D453.

(34) Pappalardo, R. T.; Belton, M. J. S.; Breneman, H. H.; Carr, M. H.; Chapman, C. R.; Collins, G. C.; Denk, T.; Fagents, S.; Geissler, P. E.; Giese, B.; Greeley, R.; Greenberg, R.; Head, J. W.; Helfenstein, P.; Hoppa, G.; Kadel, S. D.; Klaasen, K. P.; Klemaszewski, J. E.; Magee, K.; McEwen, A. S.; Moore, J. M.; Moore, W. B.; Neukum, G.; Phillips, C. B.; Prockter, L. M.; Schubert, G.; Senske, D. A.; Sullivan, R. J.; Tufts, B. R.; Turtle, E. P.; Wagner, R.; Williams, K. K. *J. Geophys. Res.* **1999**, *104*, 24015.

(35) Fagents, S. A. *J. Geophys. Res.-Planets* **2003**, *108*.

(36) Carlson, R. W.; Johnson, R. E.; Anderson, M. S. *Science* **1999**, *286*, 97.

(37) McCord, T. B.; Hansen, G. B.; Fanale, F. P.; Carlson, R. W.; Matson, D. L.; Johnson, T. V.; Smythe, W. D.; Crowley, J. K.; Martin, P. D.; Ocampo, A.; Hibbitts, C. A.; Granahan, J. C.; Team, N. *Science* **1998**, *280*, 1242.

(38) Anderson, J. D.; Schubert, G.; Jacobson, R. A.; Lau, E. L.; Moore, W. B.; Sjogren, W. L. *Science* **1998**, *281*, 2019.

(39) Baross, J. A.; Hoffman, S. E. *Origins of Life and Evolution of Biospheres* **1985**, *15*, 327.

(40) Schubert, G.; Anderson, J. D.; Travis, B. J.; Palguta, J. *Icarus* **2007**, *188*, 345.

(41) Pang, K. D.; Voge, C. C.; Rhoads, J. W.; Ajello, J. M. *J. Geophys. Res.* **1984**, *89*, 9459.

(42) Waite, J. H.; Combi, M. R.; Ip, W. H.; Cravens, T. E.; McNutt, R. L.; Kasprzak, W.; Yelle, R.; Luhmann, J.; Niemann, H.; Gell, D.; Magee, B.; Fletcher, G.; Lunine, J.; Tseng, W. L. *Science* **2006**, *311*, 1419.

(43) Rannou, P.; Montmessin, F.; Hourdin, F.; Lebonnois, S. *Science* **2006**, *311*, 201.

(44) Hayes, A.; Aharonson, O.; Callahan, P.; Elachi, C.; Gim, Y.; Kirk, R.; Lewis, K.; Lopes, R.; Lorenz, R.; Lunine, J.; Mitchell, K.; Mitri, G.; Stofan, E.; Wall, S. *Geophys. Res. Lett.* **2008**, *35*.

(45) Fortes, A. D.; Grindrod, P. M.; Trickett, S. K.; Vocadlo, L. *Icarus* **2007**, *188*, 139.

(46) McKay, C. P. *PLoS Biol* **2004**, *2*, e302.

(47) Sephton, M. A. *Natural Product Reports* **2002**, *19*, 292.

(48) Becker, L.; Popp, B.; Rust, T.; Bada, J. L. *Earth and Planetary Science Letters* **1999**, *167*, 71.

(49) Jull, A. J. T.; Courtney, C.; Jeffrey, D. A.; Beck, J. W. *Science* **1998**, *279*, 366.

(50) McKay, D. S.; Gibson, E. K., Jr.; Thomas-Keprta, K. L.; Vali, H.; Romanek, C. S.; Clemett, S. J.; Chillier, X. D. F.; Maechling, C. R.; Zare, R. N. *Science* **1996**, *273*, 924.

(51) Clemett, S. J.; Maechling, C. R.; Zare, R. N.; Swan, P. D.; Walker, R. M. *Science* **1993**, *262*, 721.

(52) Herbst, E. *Angewandte Chemie International Edition in English* **1990**, *29*, 595.

(53) Botta, O.; Bada, J. L. *Surv. Geophys.* **2002**, *23*, 411.

(54) Zolotov, M.; Shock, E. *J. Geophys. Res.* **1999**, *104*, 14033.

(55) Simoneit, B. R. T.; Lein, A. Y.; Peresypkin, V. I.; Osipov, G. A. *Geochimica et Cosmochimica Acta* **2004**, *68*, 2275.

(56) Bobbitt, D. R.; Reitsma, B. H.; Rougvie, A.; Yeung, E. S.; Aida, T.; Chen, Y.-Y.; Smith, B. F.; Squires, T. G.; Venier, C. G. *Fuel* **1985**, *64*, 114.

(57) Maga, J. A. *Journal of Agricultural and Food Chemistry* **1986**, *34*, 249.

(58) Kraft, J.; Hartung, A.; Lies, K.-H.; Schulze, J. *Journal of High Resolution Chromatography* **1982**, *5*, 489.

(59) Flynn, G. J. *Earth Moon Planets* **1996**, *72*, 469.

(60) Lu, Y.; Freeland, S. *Genome Biology* **2006**, *7*.

(61) Krause, E.; Bienert, M.; Schmieder, P.; Wenschuh, H. *Journal of the American Chemical Society* **2000**, *122*, 4865.

(62) Breslow, R.; Cheng, Z. L. *Proceedings of the National Academy of Sciences of the United States of America* **2009**, *106*, 9144.

(63) Cronin, J. R.; Pizzarello, S. *Science* **1997**, *275*, 951.

(64) Maddalena, R.; Russell, M.; Sullivan, D. P.; Apte, M. G. *Environ. Sci. Technol.* **2009**, *43*, 5626.

(65) Hollis, J. M.; Jewell, P. R.; Lovas, F. J.; Remijan, A.; Mollendal, H. *Astrophys. J.* **2004**, *610*, L21.

(66) Hutt, L. D.; Glavin, D. P.; Bada, J. L.; Mathies, R. A. *Analytical Chemistry* **1999**, *71*, 4000.

(67) Skelley, A. M.; Mathies, R. A. *J. Chromatogr. A* **2003**, *1021*, 191.

(68) Aubrey, A. D.; Chalmers, J. H.; Bada, J. L.; Grunthaner, F. J.; Amashukeli, X.; Willis, P.; Skelley, A. M.; Mathies, R. A.; Quinn, R. C.; Zent, A. P.; Ehrenfreund, P.; Amundson, R.; Glavin, D. P.; Botta, O.; Barron, L.; Blaney, D. L.; Clark, B. C.; Coleman, M.; Hofmann, B. A.; Josset, J. L.; Rettberg, P.; Ride, S.; Robert, F.; Sephton, M. A.; Yen, A. *Astrobiology* **2008**, *8*, 583.

(69) Chiesl, T. N.; Chu, W. K.; Stockton, A. M.; Amashukeli, X.; Grunthaner, F.; Mathies, R. A. *Anal. Chem.* **2009**, *81*, 2537.

(70) Vollhardt, K. P. C.; Schore, N. E. *Organic Chemistry, 2nd Ed.*; 2 ed.; W. H. Freeman and Company: New York, NY, 1994.

(71) Jiang, Z. J.; Smith, N. W.; Ferguson, P. D.; Taylor, M. R. *Journal of Separation Science* **2008**, *31*, 2774.

(72) Saito, Y.; Jinno, K.; Greibrokk, T. *Journal of Separation Science* **2004**, *27*, 1379.

(73) Schlotterbeck, G.; Ross, A.; Hochstrasser, R.; Senn, H.; Kuhn, T.; Marek, D.; Schett, O. *Analytical Chemistry* **2002**, *74*, 4464.

(74) *Handbook of Capillary Electrophoresis*; 2 ed.; Landers, J. P., Ed.; CRC Press, 1997.

(75) Brown, R. S.; Luong, J. H. T.; Szolar, O. H. J.; Halasz, A.; Hawari, J. *Analytical Chemistry* **1996**, *68*, 287.

(76) Szolar, O. H. J.; Brown, R. S.; Luong, J. H. T. *Analytical Chemistry* **1995**, *67*, 3004.

(77) Nguyen, A. L.; Luong, J. H. T. *Electrophoresis* **1997**, *18*, 247.

(78) Nguyen, A.-L.; Luong, J. H. T. *Analytical Chemistry* **1997**, *69*, 1726.

(79) Kaneta, T.; Yamashita, T.; Imasaka, T. *Analytica Chimica Acta* **1995**, *299*, 371.

(80) do Rosário, P. M. Á.; Nogueira, J. M. F. *Electrophoresis* **2006**, *27*, 4694.

(81) Skelley, A. M.; Aubrey, A. D.; Willis, P. A.; Amashukeli, X.; Ehrenfreund, P.; Bada, J. L.; Grunthaner, F. J.; Mathies, R. A. *J. Geophys. Res. - Biogeosciences* **2007**, *112*, G04S11.

(82) Terabe, S.; Otsuka, K.; Nishi, H. *Journal of Chromatography A* **1994**, *666*, 295.

(83) De Bernardo, S.; Weigele, M.; Toome, V.; Manhart, K.; Leimgruber, W.; Böhlen, P.; Stein, S.; Udenfriend, S. *Archives of Biochemistry and Biophysics* **1974**, *163*, 390.

(84) Brechtel, R.; Hohmann, W.; Rudiger, H.; Watzig, H. *J. Chroma. A* **1995**, *716*, 97.

(85) Reyes, D. R.; Iossifidis, D.; Auroux, P. A.; Manz, A. *Analytical Chemistry* **2002**, *74*, 2623.

(86) Terry, S. C.; Jerman, J. H.; Angell, J. B. *Electron Devices, IEEE Transactions on* **1979**, *26*, 1880.

(87) Manz, A.; Harrison, D. J.; Verpoorte, E. M. J.; Fettinger, J. C.; Paulus, A.; Lüdi, H.; Widmer, H. M. *Journal of Chromatography A* **1992**, *593*, 253.

(88) Yeung, S. H. I.; Liu, P.; Del Bueno, N.; Greenspoon, S. A.; Mathies, R. A. *Analytical Chemistry* **2009**, *81*, 210.

(89) Zarrin, F.; Dovichi, N. J. *Analytical Chemistry* **1985**, *57*, 2690.

(90) Liu, C. N.; Toriello, N. M.; Mathies, R. A. *Analytical Chemistry* **2006**, *78*, 5474.

(91) Benhabib, M.; Chiesl, T. N.; Stockton, A. M.; Scherer, J. R.; Mathies, R. A. *Anal. Chem.* **2010**, *82*, 2372.

(92) Benhabib, M., University of California, Berkeley, 2009.

(93) Liu, P.; Seo, T. S.; Beyor, N.; Shin, K. J.; Scherer, J. R.; Mathies, R. A. *Analytical Chemistry* **2007**, *79*, 1881.

(94) Paegel, B. M.; Grover, W. H.; Skelley, A. M.; Mathies, R. A.; Joyce, G. F. *Analytical Chemistry* **2006**, *78*, 7522.

(95) Jensen, E. C.; Bhat, B. P.; Mathies, R. A. *Lab Chip* **2010**, *10*, 685.

(96) Douglas, E. S.; Hsiao, S. C.; Onoe, H.; Bertozzi, C. R.; Francis, M. B.; Mathies, R. A. *Lab Chip* **2009**, *9*, 2010.

(97) Beyor, N.; Yi, L. N.; Seo, T. S.; Mathies, R. A. *Analytical Chemistry* **2009**, *81*, 3523.

(98) Thaitrong, N.; Toriello, N. M.; Del Bueno, N.; Mathies, R. A. *Analytical Chemistry* **2009**, *81*, 1371.

(99) Toriello, N. M.; Liu, C. N.; Blazej, R. G.; Thaitrong, N.; Mathies, R. A. *Analytical Chemistry* **2007**, *79*, 8549.

(100) Liu, P.; Mathies, R. A. *Trends Biotechnol.* **2009**, *27*, 572.

(101) Zeng, Y.; Novak, R.; Shuga, J.; Smith, M. T.; Mathies, R. A. *Analytical Chemistry* **2010**, *82*, 3183.

(102) Grover, W. H.; Skelley, A. M.; Liu, C. N.; Lagally, E. T.; Mathies, R. A. *Sens. Actuator B-Chem.* **2003**, *89*, 315.

(103) Skelley, A. M.; Scherer, J. R.; Aubrey, A. D.; Grover, W. H.; Ivester, R. H. C.; Ehrenfreund, P.; Grunthaner, F. J.; Bada, J. L.; Mathies, R. A. *Proc. Natl. Acad. Sci. U. S. A.* **2005**, *102*, 1041.

(104) Jensen, E. C.; Chiesl, T.; Stockton, A. M.; Bera, A.; Mathies, R. *Sensors and Actuators* **2011**, *In preparation*.

(105) Jensen, E. C.; Zheng, C. G.; Kim, J.; Mathies, R. *Journal of Laboratory Automation* **2010**, *In press*.

(106) Skelley, A. M.; Cleaves, H. J.; Jayarajah, C. N.; Bada, J. L.; Mathies, R. A. *Astrobiology* **2006**, *6*, 824.

(107) Lee, S. *Oil Shale Technology*; CRC Press: Boca Raton, FL, 1990.

(108) Obana, H.; Hori, S.; Kashimoto, T. *Bull. Environm. Contam. Toxicol.* **1981**, *26*, 613.

(109) Song, G.-Q.; Peng, Z.-L.; Lin, J.-M. *Journal of Separation Science* **2006**, *29*, 2065.

(110) Grundl, T. J.; Aldstadt, J. H.; Harb, J. G.; St. Germain, R. W.; Schweitzer, R. C. *Environ. Sci. Technol.* **2003**, *37*, 1189.

(111) Considine, T.; Robbat Jr, A. *Environ. Sci. Technol.* **2008**, *42*, 1213.

(112) Mao, C.; McGill, K. E.; Tucker, S. A. *Journal of Separation Science* **2004**, *27*, 991.

(113) Kminek, G.; Bada, J. L. *Earth and Planetary Science Letters* **2006**, *245*, 1.

(114) Magenheim, A. J.; Gieskes, J. M. *Geochimica et Cosmochimica Acta* **1992**, *56*, 2329.

(115) Amashukeli, X.; Pelletier, C. C.; Kirby, J. P.; Grunthaner, F. J. *Journal of Geophysical Research-Biogeosciences* **2007**, *112*.

(116) Glavin, D. P.; Bada, J. L. *Analytical Chemistry* **1998**, *70*, 3119.

(117) Kminek, G.; Bada, J. L.; Botta, O.; Glavin, D. P.; Grunthaner, F. *Planetary and space science* **2000**, *48*, 1087.

(118) Navarro-Gonzalez, R.; Navarro, K. F.; de la Rosa, J.; Iniguez, E.; Molina, P.; Miranda, L. D.; Morales, P.; Cienfuegos, E.; Coll, P.; Raulin, F.; Amils, R.; McKay, C. P. *Proceedings of the National Academy of Sciences of the United States of America* **2006**, *103*, 16089.

(119) McKay, C. P.; Friedmann, E. I.; Gomez-Silva, B.; Caceres-Villanueva, L.; Andersen, D. T.; Landheim, R. *Astrobiology* **2003**, *3*, 393.

(120) Dick, S. J. *Endeavour* **2006**, *30*, 71.

(121) Bada, J. L.; Sephton, M. A.; Ehrenfreund, P.; Mathies, R. A.; Skelley, A. M.; Grunthaner, F. J.; Zent, A. P.; Quinn, R. C.; Josset, J. L.; Robert, F.; Botta, O.; Glavin, D. P. *Astron. Geophys.* **2005**, *46*, 26.

(122) Ehrenfreund, P.; Glavin, D. P.; Botta, O.; Cooper, G.; Bada, J. L. *Proceedings of the National Academy of Sciences of the United States of America* **2001**, *98*, 2138.

(123) Glavin, D. P.; Dworkin, J. P.; Sandford, S. A. *Meteorit. Planet. Sci.* **2008**, *43*, 399.

(124) Malin, M. C.; Edgett, K. S. *Science* **2000**, *288*, 2330.

(125) Jakosky, B. M.; Farmer, C. B. *Journal of Geophysical Research* **1982**, *87*, 2999.

(126) Baker, V. R.; Strom, R. G.; Gulick, V. C.; Kargel, J. S.; Komatsu, G.; Kale, V. S. *Nature* **1991**, *352*, 589.

(127) Clifford, S. M. *J. Geophys. Res.-Planets* **1993**, *98*, 10973.

(128) ten Kate, I. L.; Garry, J. R. C.; Peeters, Z.; Quinn, R.; Foing, B.; Ehrenfreund, P. *Meteorit. Planet. Sci.* **2005**, *40*, 1185.

(129) Thorsen, T.; Maerkl, S. J.; Quake, S. R. *Science* **2002**, *298*, 580.

(130) Easley, C. J.; Karlinsey, J. M.; Bienvenue, J. M.; Legendre, L. A.; Roper, M. G.; Feldman, S. H.; Hughes, M. A.; Hewlett, E. L.; Merkel, T. J.; Ferrance, J. P.; Landers, J. P. *Proceedings of the National Academy of Sciences of the United States of America* **2006**, *103*, 19272.

(131) Harrison, D. J.; Fluri, K.; Seiler, K.; Fan, Z. H.; Effenhauser, C. S.; Manz, A. *Science* **1993**, *261*, 895.

(132) Culbertson, C. T.; Jacobson, S. C.; Ramsey, J. M. *Analytical Chemistry* **2000**, *72*, 5814.

(133) Culbertson, C. T.; Tugnawat, Y.; Meyer, A. R.; Roman, G. T.; Ramsey, J. M.; Gonda, S. R. *Analytical Chemistry* **2005**, *77*, 7933.

(134) Skelley, A. M.; Mathies, R. A. *Journal of Chromatography A* **2006**, *1132*, 304.

(135) Jayarajah, C. N.; Skelley, A. M.; Fortner, A. D.; Mathies, R. A. *Analytical Chemistry* **2007**, *79*, 8162.

(136) Paegel, B. M.; Hutt, L. D.; Simpson, P. C.; Mathies, R. A. *Analytical Chemistry* **2000**, *72*, 3030.

(137) Glavin, D.; Brinkerhoff, W.; Dworkin, J.; Eigenbrode, J.; Franz, H.; Mahaffy, P.; Stern, J.; Allamondola, L.; Blake, D.; Sandford, S.; Amashukeli, X.; Fisher, A.; Grunthaner, F.; Fries, M.; Steele, A.; Aubrey, A.; Bada, J.; Chiesl, T.; Mathies, R.; Bish, D.; Chipera, S.; Corrigan, C. In *Astrobiology Science Conference, 2008*; Astrobiology: Santa Clara, CA, 2008; Vol. 8, p 297.

(138) Stockton, A. M.; Chiesl, T. N.; Scherer, J. R.; Mathies, R. A. *Anal. Chem.* **2009**, *81*, 790.

(139) Sun, W. C.; Gee, K. R.; Haugland, R. P. *Bioorg. Med. Chem. Lett.* **1998**, *8*, 3107.

(140) Khaledi, M. G. *Journal of Chromatography A* **1997**, *780*, 3.

(141) Muijselaar, P. G.; Otsuka, K.; Terabe, S. *Journal of Chromatography A* **1997**, *780*, 41.

(142) Aebersold, R. H.; Leavitt, J.; Saavedra, R. A.; Hood, L. E.; Kent, S. B. H. *Proceedings of the National Academy of Sciences of the United States of America* **1987**, *84*, 6970.

(143) Kvenvold.K; Lawless, J.; Pering, K.; Peterson, E.; Flores, J.; Ponnampe.C; Kaplan, I. R.; Moore, C. *Nature* **1970**, *228*, 923.

(144) Cronin, J. R.; Gandy, W. E.; Pizzarello, S. *J. Mol. Evol.* **1981**, *17*, 265.

(145) Ewing, S. A.; Michalski, G.; Thiemens, M.; Quinn, R. C.; Macalady, J. L.; Kohl, S.; Wankel, S. D.; Kendall, C.; McKay, C. P.; Amundson, R. *Global Biogeochemical Cycles* **2007**, *21*, GB3009.

(146) Cronin, J. R.; Pizzarello, S.; Epstein, S.; Krishnamurthy, R. V. *Geochimica et Cosmochimica Acta* **1993**, *57*, 4745.

(147) Bada, J. L.; Cronin, J. R.; Ho, M. S.; Kvenvolden, K. A.; Lawless, J. G.; Miller, S. L.; Oro, J.; Steinberg, S. *Nature* **1983**, *301*, 494.

(148) Botta, O.; Glavin, D. P.; Kminek, G.; Bada, J. L. *Origins of Life and Evolution of Biospheres* **2002**, *32*, 143.

(149) Lester, E. D.; Satomi, M.; Ponce, A. *Soil Biol. Biochem.* **2007**, *39*, 704.

(150) Zent, A. P.; McKay, C. P. *Icarus* **1994**, *108*, 146.

(151) Glavin, D. P.; Schubert, M.; Botta, O.; Kminek, G.; Bada, J. L. *Earth Planet. Sci. Lett.* **2001**, *185*, 1.

(152) Bada, J. L.; McDonald, G. D. *Icarus* **1995**, *114*, 139.

(153) Schubert, B. A.; Lowenstein, T. K.; Timofeeff, M. N. *Astrobiology* **2009**, *9*, 467.

(154) Lowenstein, T. K. In *McGraw Hill 2008 Yearbook of Science and Technology*; McGraw-Hill: 2007, p 13.

(155) Fernandez-Remolar, D. C.; Morris, R. V.; Gruener, J. E.; Amils, R.; Knoll, A. H. *Earth and Planetary Science Letters* **2005**, *240*, 149.

(156) Zettler, L. A. A.; Gomez, F.; Zettler, E.; Keenan, B. G.; Amils, R.; Sogin, M. L. *Nature* **2002**, *417*, 137.

(157) Zuckerman, B.; Buhl, D.; Palmer, P.; Snyder, L. W. *Astrophys. J.* **1970**, *160*, 485.

(158) Prat, G.; Adan, A.; Sanchez-Turet, M. *Hum. Psychopharmacol.-Clin. Exp.* **2009**, *24*, 259.

(159) Margalit, Y. *Concepts in Wine Chemistry*; 2 ed.; The Wine Appreciation Guild: South San Francisco, 2004.

(160) Wang, B. B.; Wang, J.; Zhou, S. R.; Tan, S. N.; He, X.; Yang, Z.; Xie, Y. C.; Li, S.; Zheng, C. G.; Ma, X. *J. Neurol. Sci.* **2008**, *268*, 172.

(161) Zhang, L. P.; Tang, X. J.; Rothman, N.; Vermeulen, R.; Ji, Z. Y.; Shen, M.; Qiu, C. Y.; Guo, W. H.; Liu, S. W.; Reiss, B.; Freeman, L. B.; Ge, Y. C.; Hubbard, A. E.; Hua, M.; Blair, A.; Galvan, N.; Ruan, X. L.; Alter, B. P.; Xin, K. X.; Li, S. H.; Moore, L. E.; Kim, S.; Xie, Y. X.; Hayes, R. B.; Azuma, M.; Hauptmann, M.; Xiong, J.; Stewart, P.; Li, L. Y.; Rappaport, S. M.; Huang, H. L.; Fraumeni, J. F.; Smith, M. T.; Lan, Q. *Cancer Epidemiol. Biomarkers Prev.* **2010**, *19*, 80.

(162) Stockton, A. M.; Chiesl, T. N.; Lowenstein, T. K.; Amashukeli, X.; Grunthaner, F.; Mathies, R. *Astrobiology* **2009**, *9*, 823.

(163) Peters, G. H.; Abbey, W.; Bearman, G. H.; Mungas, G. S.; Smith, J. A.; Anderson, R. C.; Douglas, S.; Beegle, L. W. *Icarus* **2008**, *197*, 470.

(164) Allen, C. C.; Jager, K. M.; Morris, R. V.; Lindstrom, D. J.; Lindstrom, M. M.; Lockwood, J. P. *Eos Trans. Am. Geophys. Union* **1998**, *79*, 405.

(165) Rathore, A. S.; Horváth, C. *Electrophoresis* **1997**, *18*, 2935.

(166) Moore, A. W.; Jorgenson, J. W. *Analytical Chemistry* **1995**, *67*, 3464.

(167) Liu, S.-Q.; Pilone, G. J. *Int. J. Food Sci. Tech.* **2000**, *35*, 49.

(168) Elias, R. J.; Laurie, V. F.; Ebeler, S. E.; Wong, J. W.; Waterhouse, A. L. *Anal. Chim. Acta* **2008**, *626*, 104.

(169) Environmental Protection Agency (EPA), U. S. *The Class V Underground Injection Control Study*, Office of Ground Water and Drinking Water (4601), 1999.

(170) In *Guidelines for drinking-water quality*; World Health Organization: Geneva, 1996.

(171) Gable, R. S. *Addiction* **2004**, *99*, 686.

(172) *National Tap Water Quality Database*, Environmental Working Group, 2005.

(173) Zuckerma.B; Ball, J. A.; Gottlieb, C. A. *Astrophys. J.* **1971**, *163*, L41.

(174) Mehringer, D. M.; Snyder, L. E.; Miao, Y. T. *Astrophys. J.* **1997**, *480*, L71.

(175) Rinsland, C. P.; Boone, C. D.; Bernath, P. F.; Mahieu, E.; Zander, R.; Dufour, G.; Clerbaux, C.; Turquety, S.; Chiou, L.; McConnell, J. C.; Neary, L.; Kaminski, J. W. *Geophys. Res. Lett.* **2006**, *33*, L23804.

(176) Stockton, A. M.; Tjin, C. C.; Huang, G. L.; Benhabib, M.; Chiesl, T. N.; Mathies, R. A. *Electrophoresis* **2010**, *31*, 3642.

(177) Klampfl, C. W. *Electrophoresis* **2007**, *28*, 3362.

(178) Galli, V.; Garcia, A.; Saavedra, L.; Barbas, C. *Electrophoresis* **2003**, *24*, 1951.

(179) Baena, B.; Cifuentes, A.; Barbas, C. *Electrophoresis* **2005**, *26*, 2622.

(180) Mato, I.; Huidobro, J. F.; Simal-Lozano, J.; Sancho, M. T. *Crit. Rev. Anal. Chem.* **2006**, *36*, 3.

(181) Mato, I.; Suarez-Luque, S.; Huidobro, J. F. *Food Res. Int.* **2005**, *38*, 1175.

(182) Du, X.-L.; Zhang, H.-S.; Deng, Y.-H.; Wang, H. *Journal of Chromatography A* **2008**, *1178*, 92.

(183) Nozaki, S. *Chem. Lett.* **1997**, 1.

(184) Lepper, K.; McKeever, S. W. S. *Icarus* **2000**, *144*, 295.

(185) Thompson, J. M. *Journal of Volcanology and Geothermal Research* **1985**, *25*, 81.

(186) Mahaffy, P. *Space Science Reviews* **2008**, *135*, 255.

(187) Buch, A.; Sternberg, R.; Szopa, C.; Freissinet, C.; Garnier, C.; Bekri, E. J.; Rodier, C.; Navarro-González, R.; Raulin, F.; Cabane, M.; Stambouli, M.; Glavin, D. P.; Mahaffy, P. R. *Advances in Space Research* **2009**, *43*, 143.

(188) Stockton, A. M.; Chandra Tjin, C.; Huang, G. L.; Benhabib, M.; Chiesl, T.; Mathies, R. *Electrophoresis* **2010**, *In press.*

(189) Stockton, A. M.; Chandra Tjin, C.; Chiesl, T.; Mathies, R. *Electrophoresis* **2010**, *In preparation.*

(190) Whitesides, G. M. *Nature* **2006**, *442*, 368.

(191) Mansur, E. A.; Ye, M. X.; Wang, Y. D.; Dai, Y. Y. *Chin. J. Chem. Eng.* **2008**, *16*, 503.

(192) Willis, P. A.; Hunt, B. D.; White, V. E.; Lee, M. C.; Ikeda, M.; Bae, S.; Pelletier, M. J.; Grunthaner, F. J. *Lab Chip* **2007**, *7*, 1469.

(193) Moini, M.; Schultz, C. L.; Mahmood, H. *Analytical Chemistry* **2003**, *75*, 6282.

(194) *Electrospray Ionization Mass Spectrometry: Fundamentals, Instrumentation, and Applications*; Cole, R. B., Ed.; John Wiley & Sons, 1997.

(195) Wilm, M.; Mann, M. *Analytical Chemistry* **1996**, *68*, 1.

(196) Yan, C.; Dadoo, R.; Zhao, H.; Zare, R. N.; Rakestraw, D. J. *Analytical Chemistry* **1995**, *67*, 2026.

(197) Fintschenko, Y.; Choi, W.-Y.; Ngola, S. M.; Shepodd, T. J. *Fresenius J. Anal. Chem.* **2001**, *371*, 174.

(198) Yu, C.; Svec, F.; Fréchet, J. M. J. *Electrophoresis* **2000**, *21*, 120.

(199) Ericson, C.; Holm, J.; Ericson, T.; Hjertén, S. *Analytical Chemistry* **1999**, *72*, 81.

(200) Watson, M. W. L.; Mudrik, J. M.; Wheeler, A. R. *Analytical Chemistry* **2009**, *81*, 3851.

(201) Throckmorton, D. J.; Shepodd, T. J.; Singh, A. K. *Analytical Chemistry* **2002**, *74*, 784.

(202) Chiesl, T. N.; Stockton, A. M.; Huang, G. L.; Chandra Tjin, C.; Turkia, H.; Paasikallio, T.; Pitkänen, J.-P.; Mathies, R. *Journal of Chromatography, B* **2011**, *In preparation.*

(203) Levin, G. V.; Straat, P. A. *Journal of Theoretical Biology* **1981**, *91*, 41.

(204) Quinn, D. *Ishmael*; Bantam / Turner Books: New York, NY, 1992.

(205) Diamond, J. *Guns, Germs, and Steel*; W. W. Norton: New York, NY, 1997.